Dark matter detection and detectability: paradigm confirmation or shift?

May 2nd 2018

Debate 4: the origins of the Galactic Center Excess

Shunsaku Horiuchi (Virginia Tech), Tim Linden (Ohio State)

Contents

1. **Introduction and Background**

2. **Observations indicate pulsars produce the Excess - Data Driven**
   Insights from new analyses
3. **Astrophysical Sources Do Not Explain the Excess - Data Driven**
   Difficulties interpreting new results within the astrophysical context

4. **Dark Matter Explanations are better than astrophysical explanations**
   Do recent results favor the dark matter hypothesis?
5. **Astrophysical Explanations are better than dark matter explanations**
   Do recent results favor the astrophysics hypothesis?

6. **Future directions**

1. INTRODUCTION & BACKGROUND TO THE GALACTIC CENTER EXCESS

Galactic Center Excess (GCE)

From the Galactic Center out to mid-latitudes

Goodenough & Hooper (2009)
Vitale & Morselli (2009)
Hooper & Goodenough (2011)
Hooper & Linden (2011)
Boyarsky et al (2011)
Abazajian & Kaplinghat (2012)
Gordon & Macias (2013)
Hooper & Slatyer (2013)
Huang et al (2013)
Macias & Gordon (2014)
Abazajian et al (2014, 2015)
Calore et al (2014)
Zhou et al (2014)
Daylan et al (2014)
Selig et al (2015)
Huang et al (2015)
Gaggero et al (2015)
Carlson et al (2015, 2016)
Yand & Aharonian (2016)
Horiuchi et al (2016)
Lee et al (2016)
Bartels et al (2016)
Linden et al (2016)
Ackermann et al (2017)
Ajello et al (2017)
Macias et al (2017)
Bartels et al (2017)
…

(not a complete list)

Method
Found by morphological template fitting

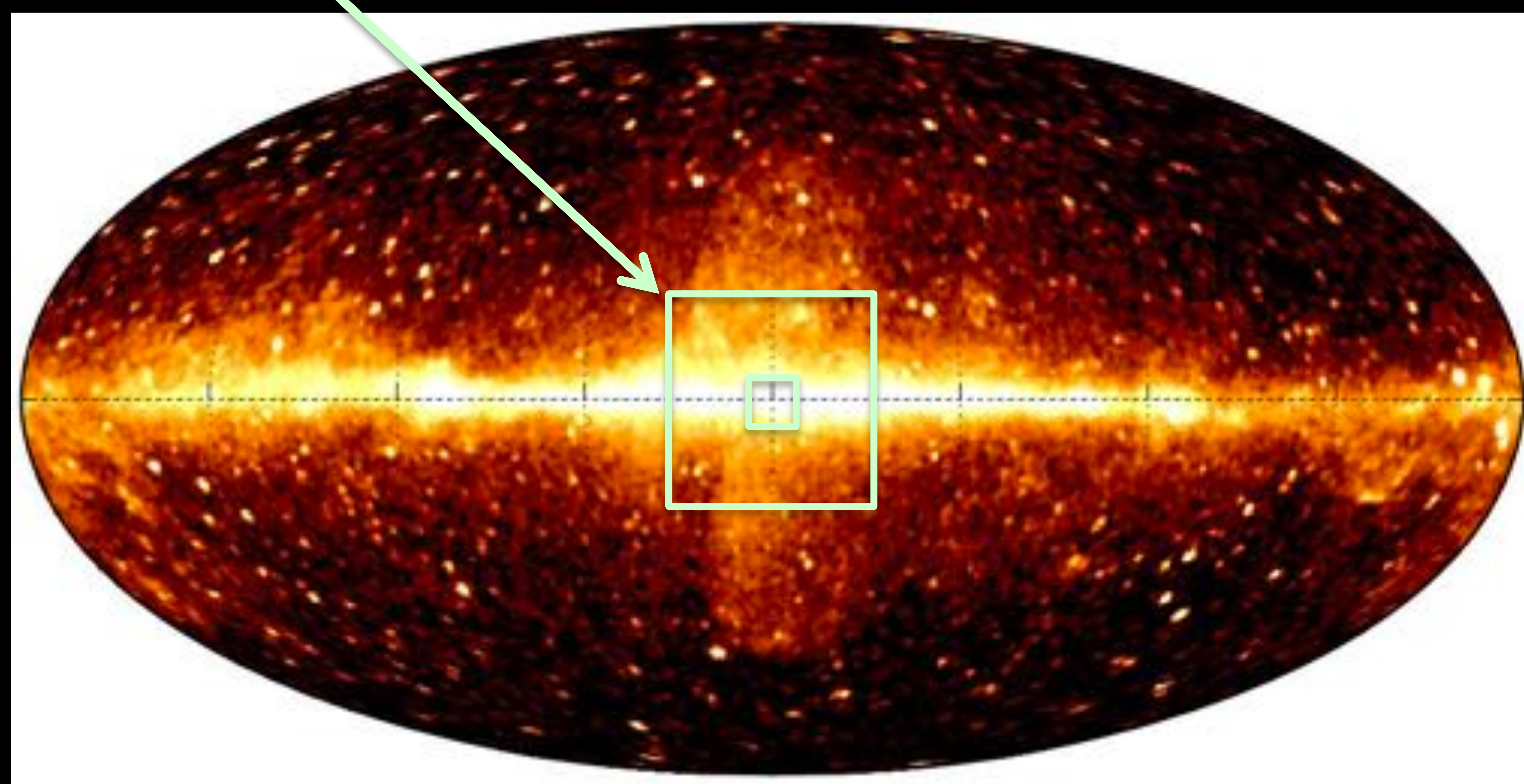

Fermi (2017)

Modeling strategy: template fitting

Data

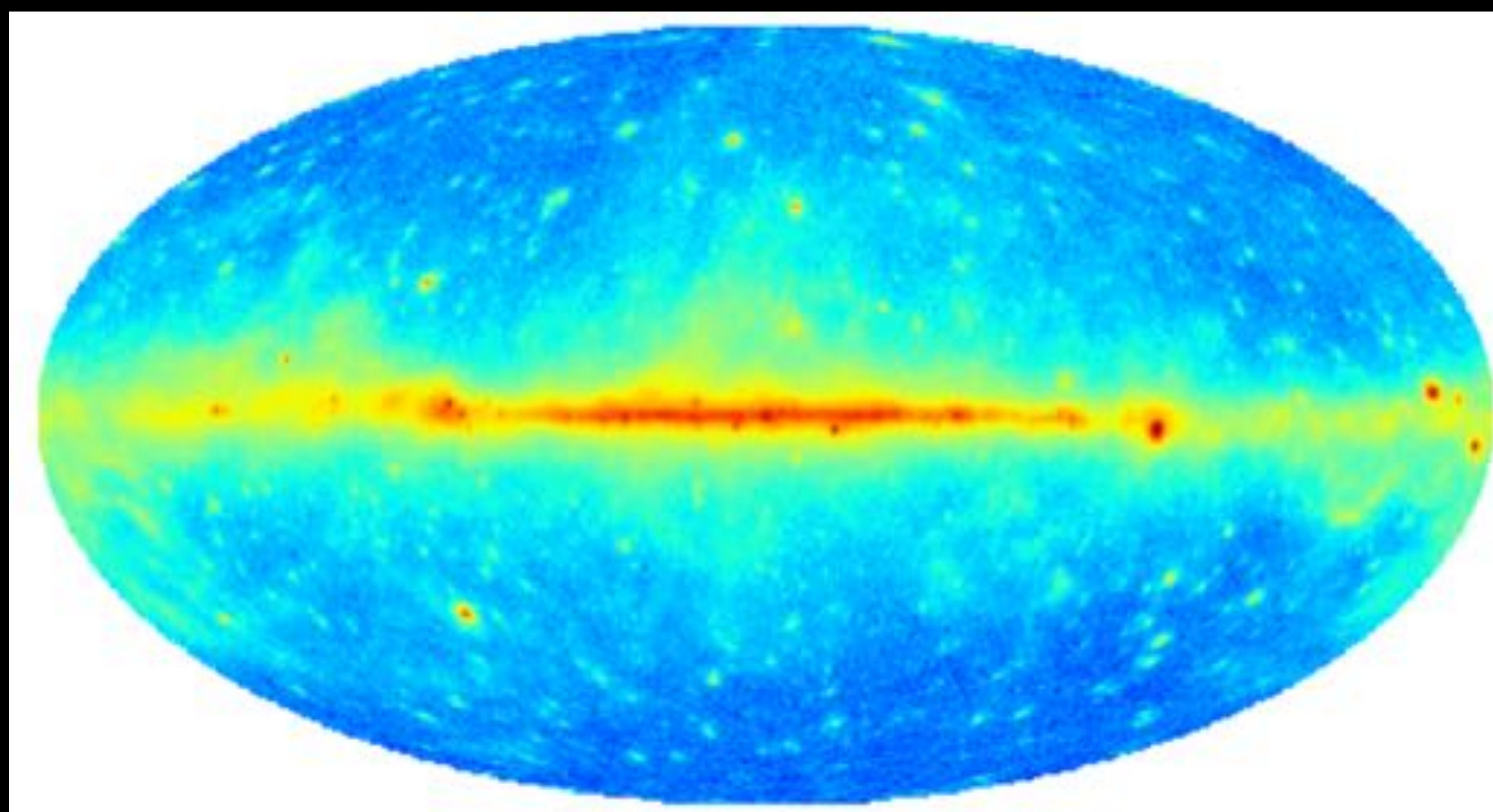

=

Galactic diffuse emission

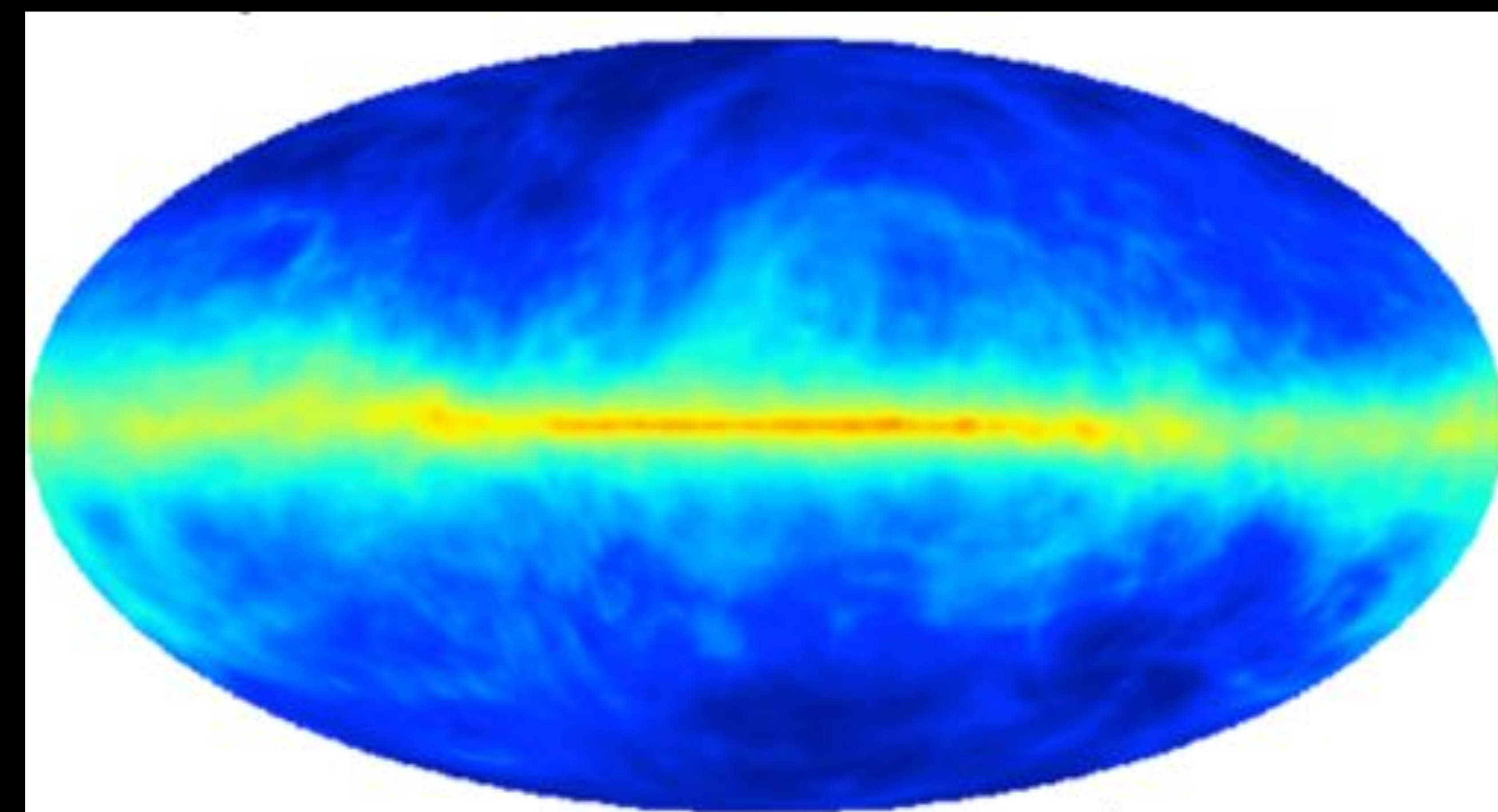

+

Known sources

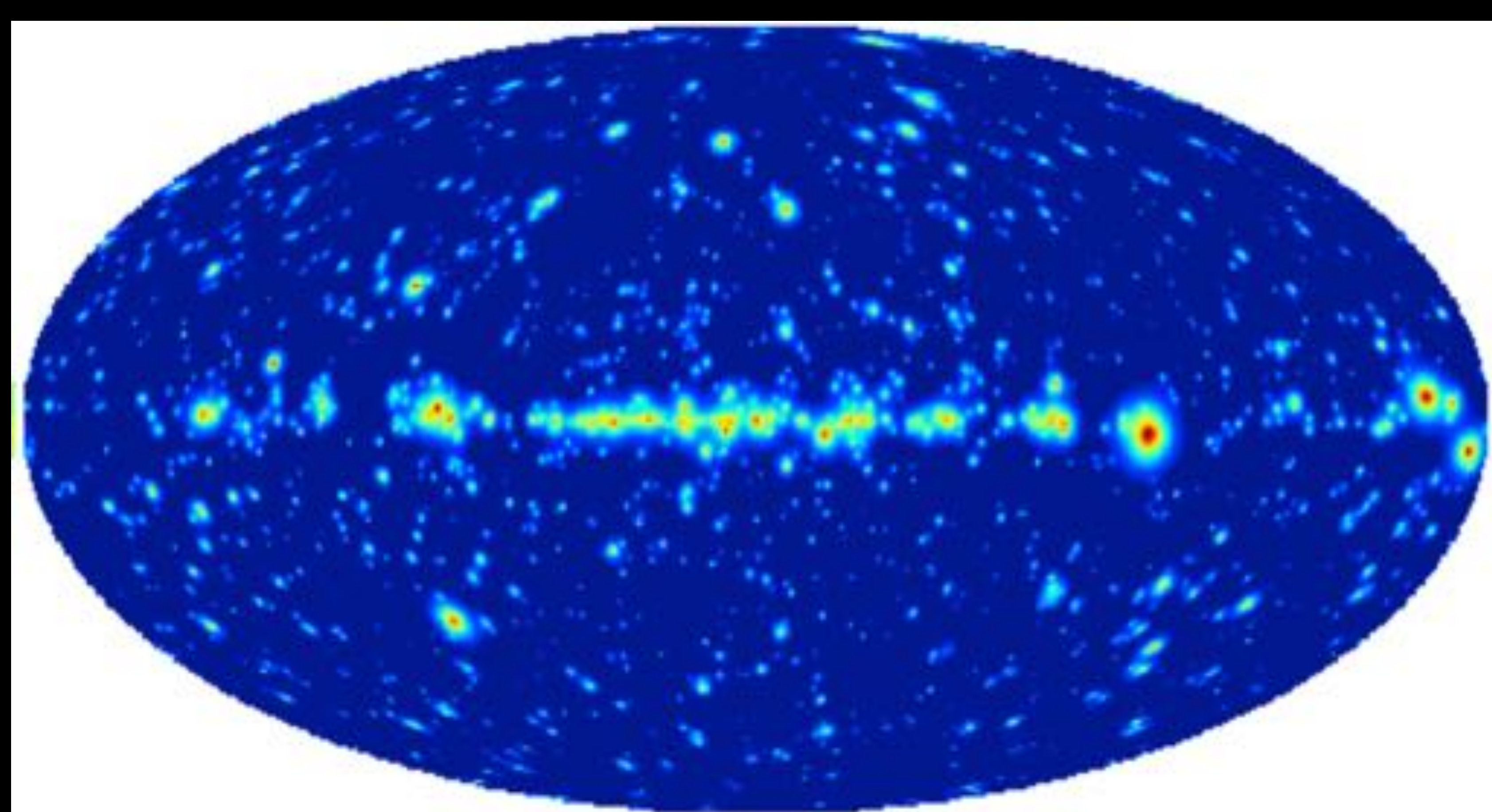

+

New sources, e.g., dark matter

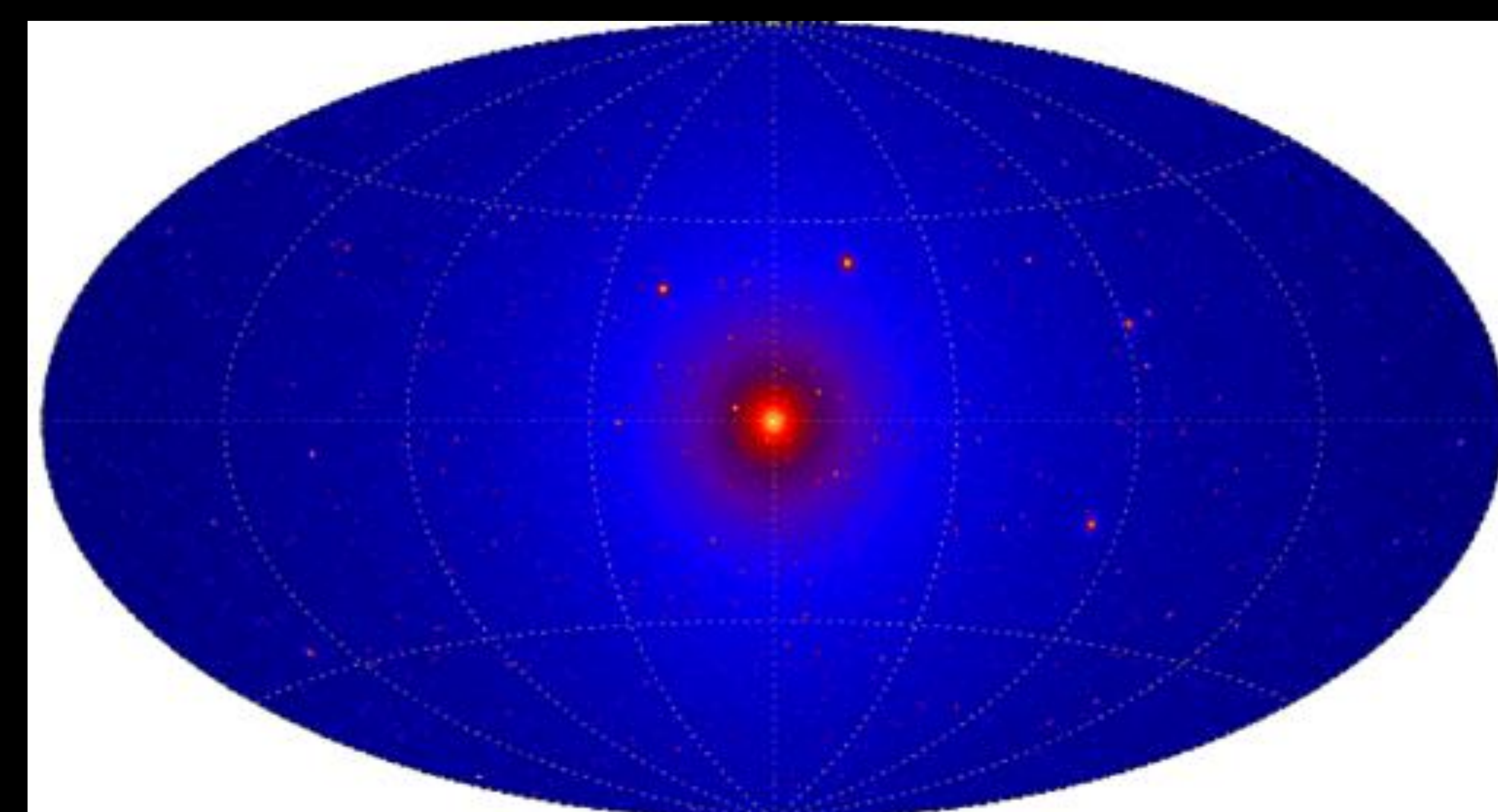

Galactic Diffuse Emission

Decay of neutron pions

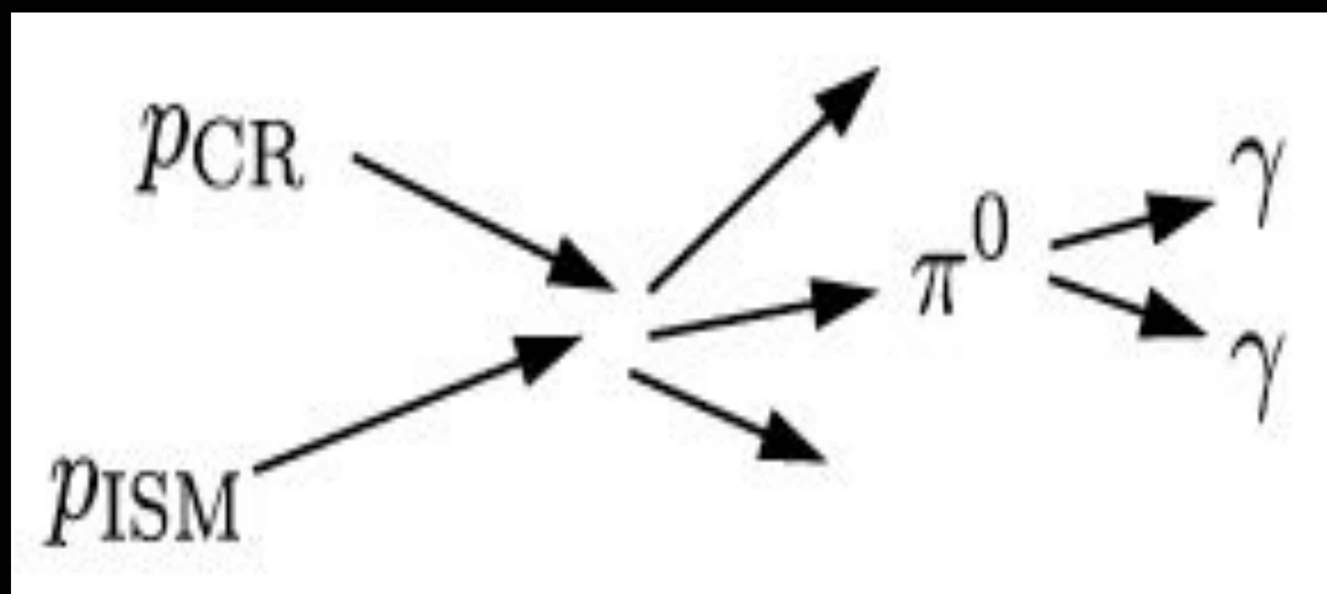

Bremsstrahlung

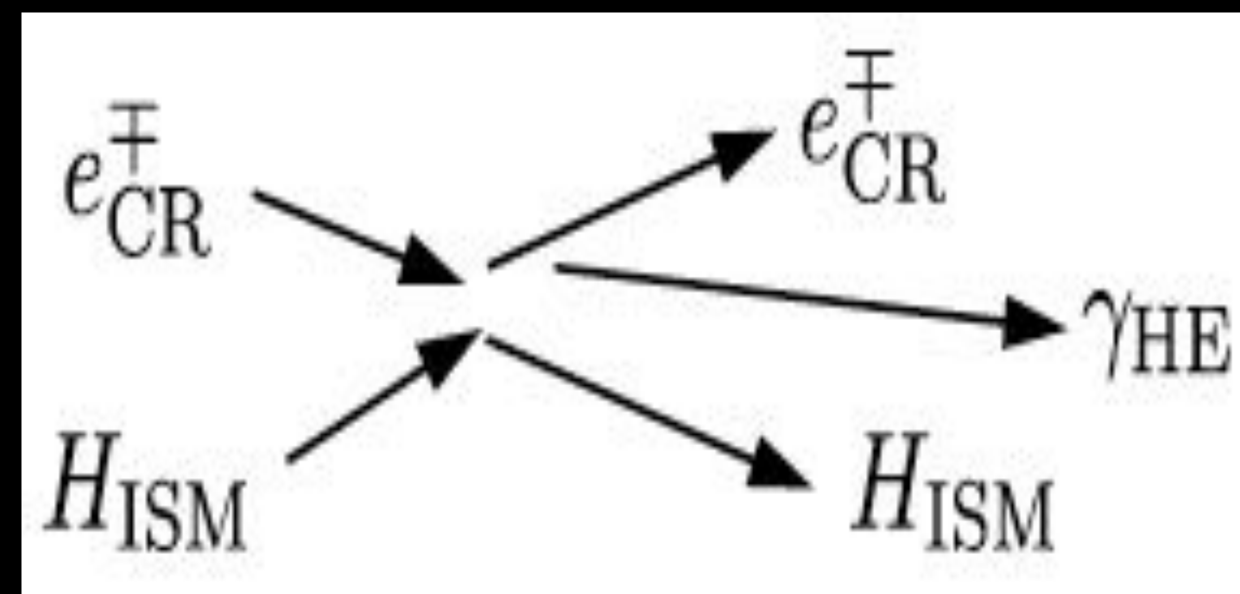

Inverse Compton

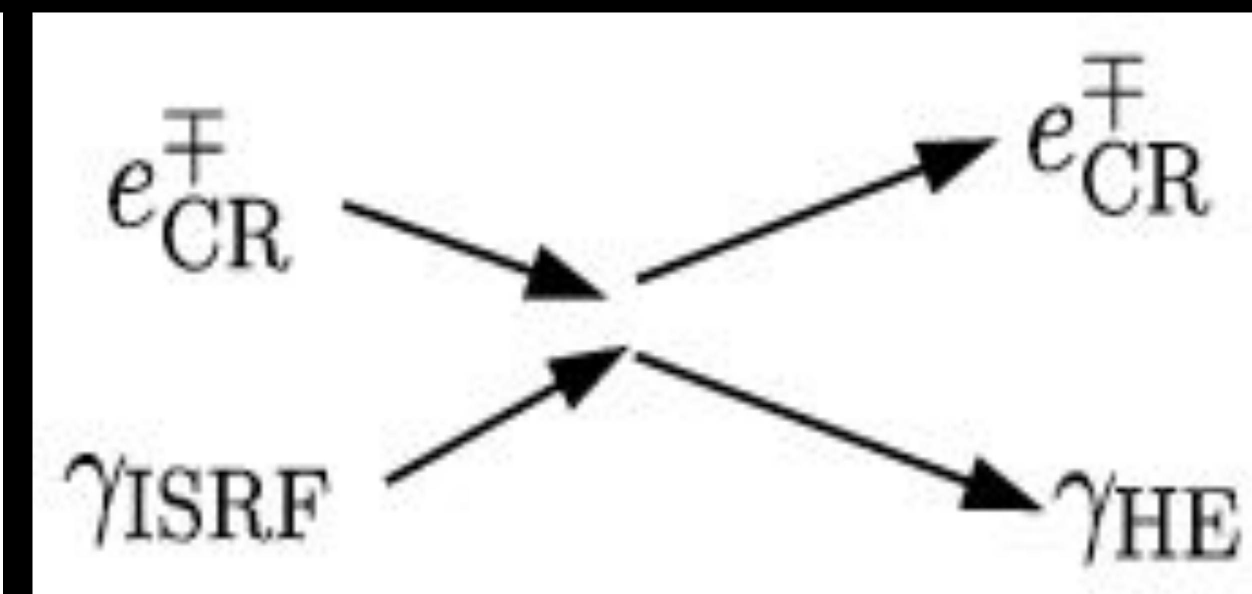

Simulations

Numerically solve the diffusion equation, e.g., Galprop

- ✓ Allows physical parameter choices
- ✓ Can be tuned to the Galactic Center
- ✗ Many parameters not well known
- ✗ Still missing some physics
- ✗ Still poor resolution

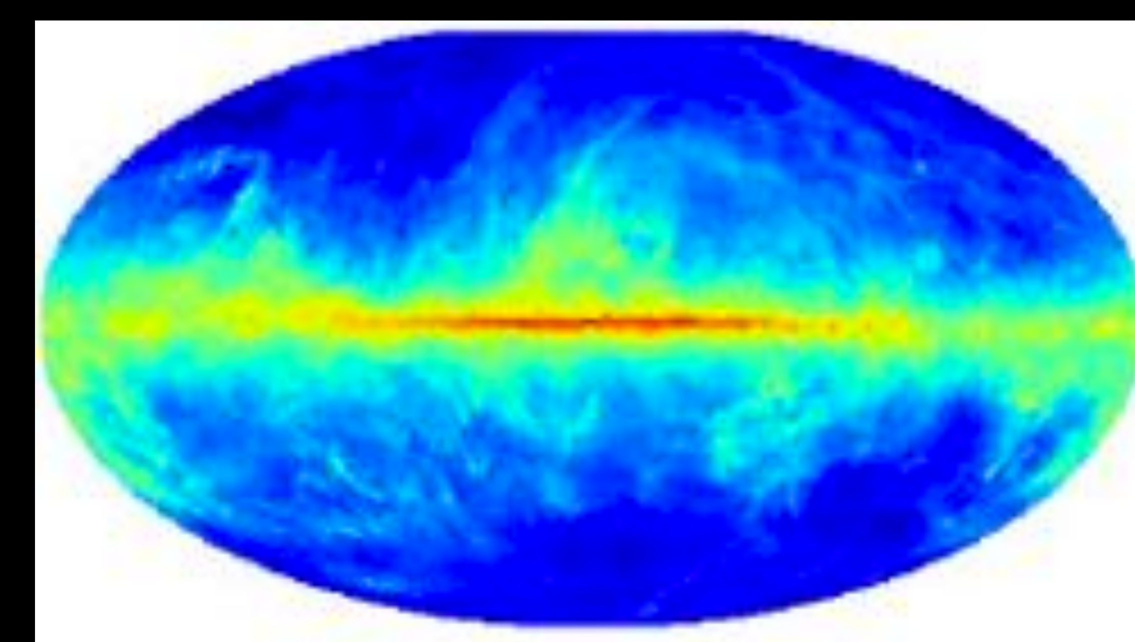

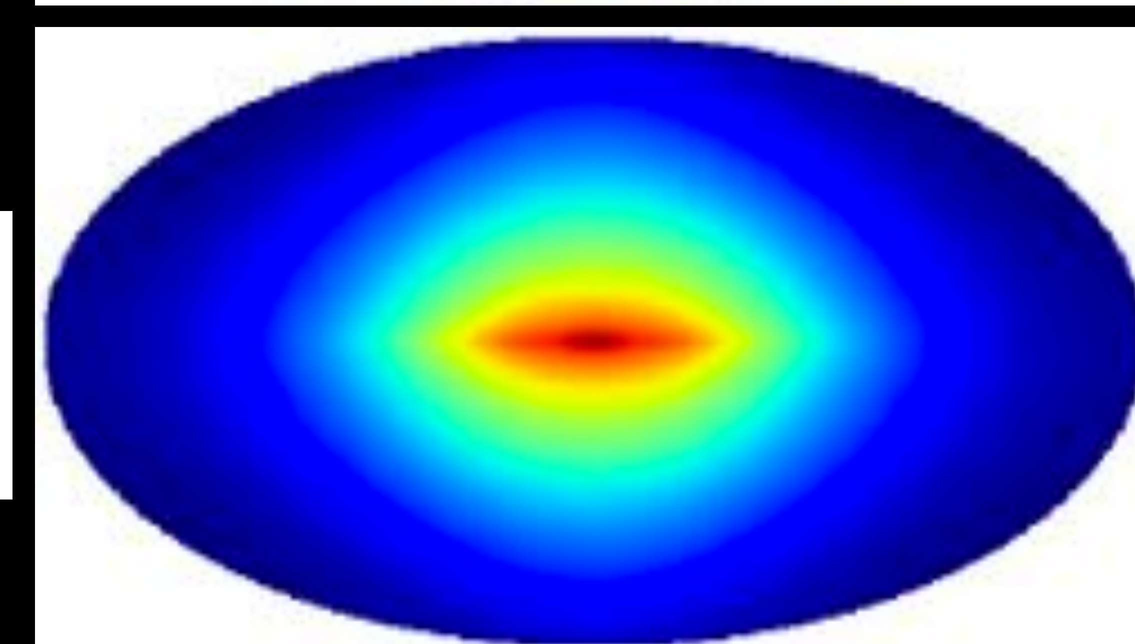

$$\frac{\partial\psi}{\partial t} = q(\vec{r},p) + \vec{\nabla}\cdot(D_{xx}\vec{\nabla}\psi - \vec{V}\psi) + \frac{\partial}{\partial p}p^2 D_{pp}\frac{\partial}{\partial p}\frac{1}{p^2}\psi - \frac{\partial}{\partial p}\left[\dot{p}\psi - \frac{p}{3}(\vec{\nabla}\cdot\vec{V})\psi\right] - \frac{1}{\tau_f}\psi - \frac{1}{\tau_r}\psi$$

e.g., Galprop; Moskalenko & Strong (1998)

Galactic Diffuse Emission

Decay of neutron pions

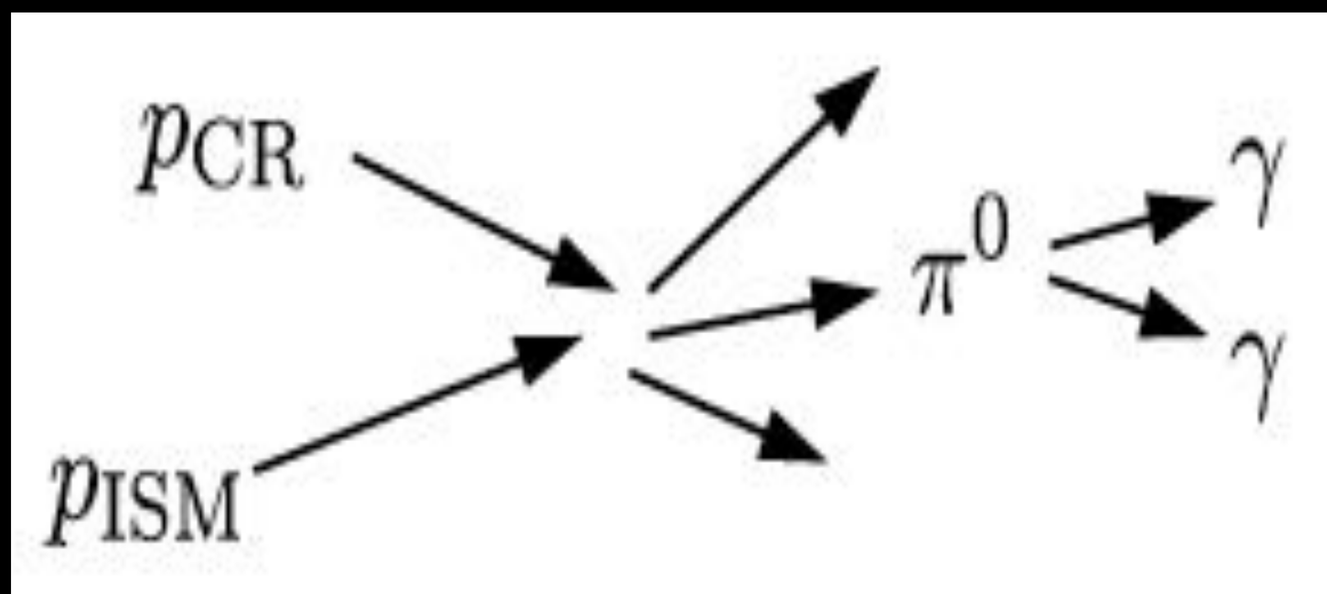

Bremsstrahlung

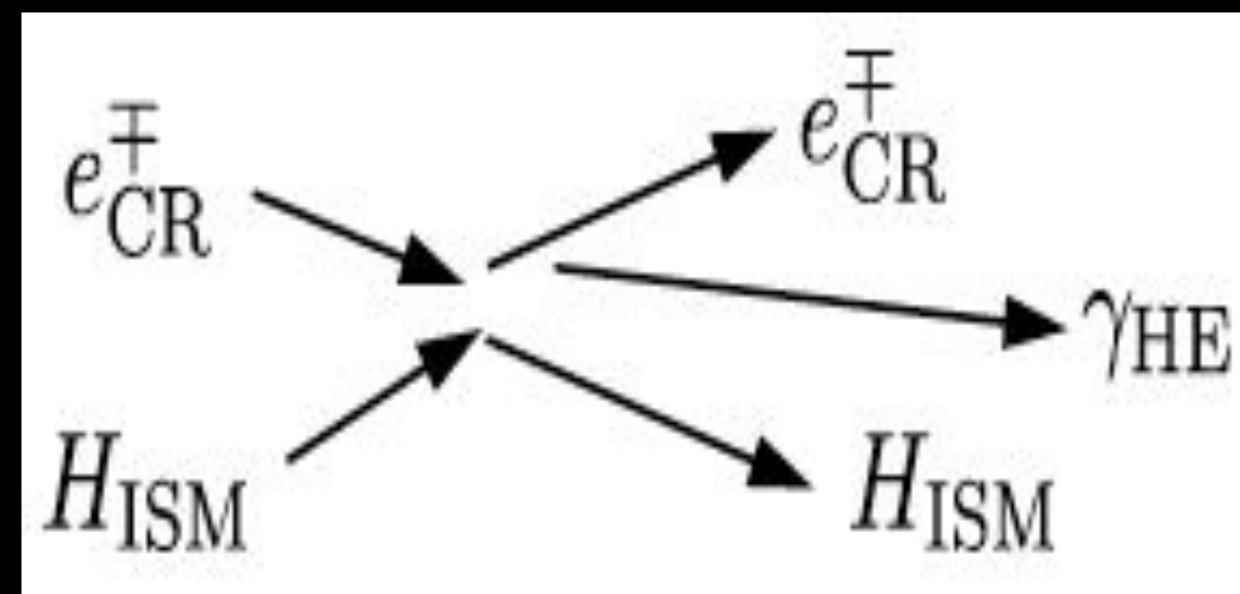

Inverse Compton

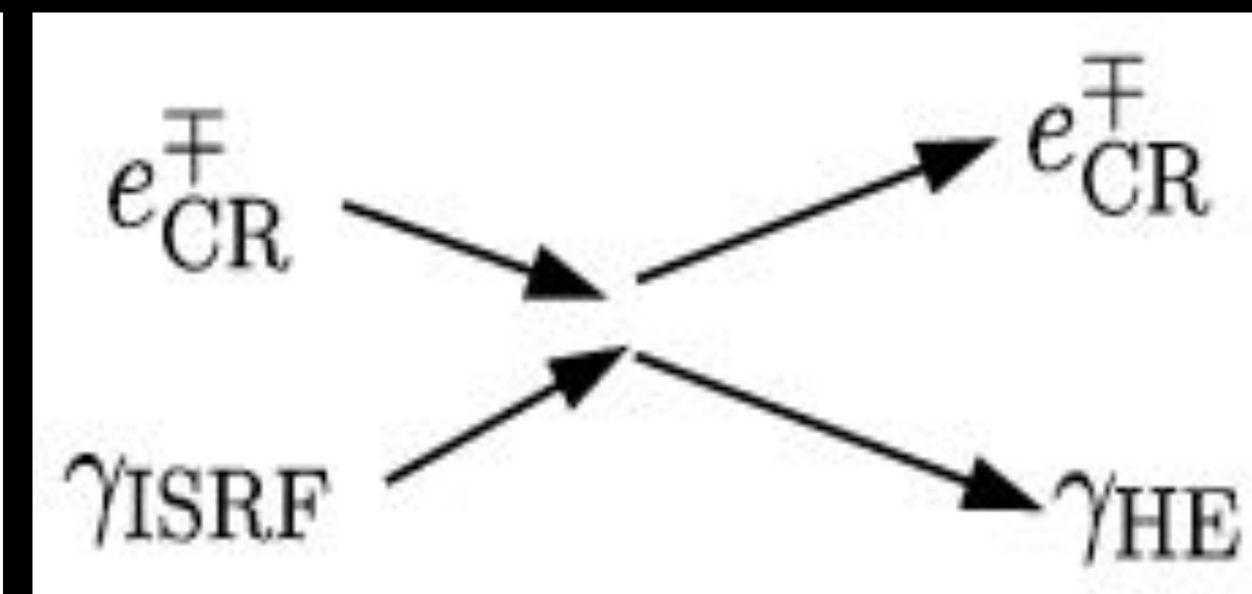

Fermi diffuse map

Built for all-sky, starting with many templates split into annuli

- ✓ Simple (hard work already done!)
- ✓ Accounts for some cosmic-ray injection and propagation variations (via annuli)
- ✗ Somewhat of a black box for user
- ✗ Fixed to (usually) older data
- ✗ Construction not dedicated for the Galactic Center

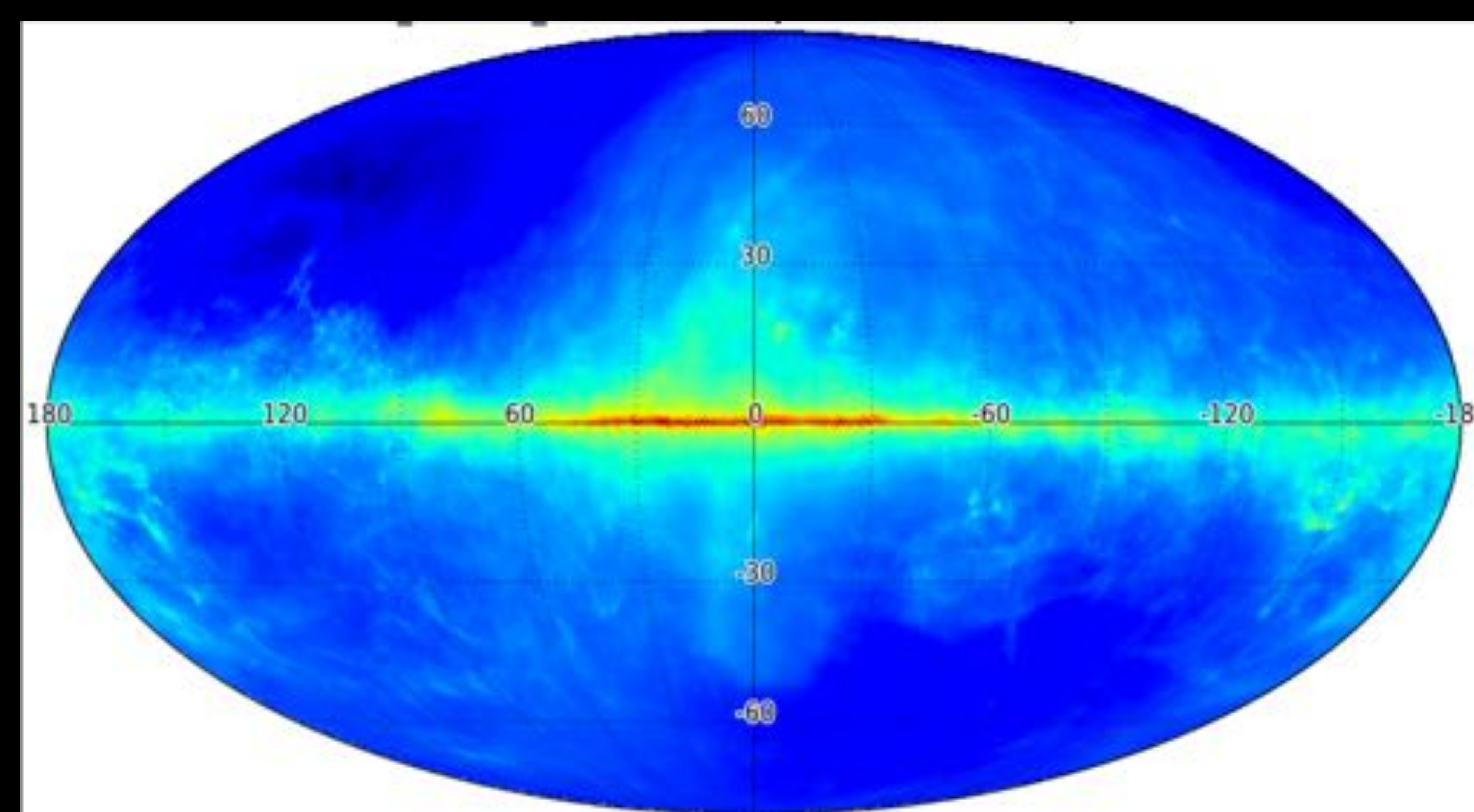

Acero et al (2016)

Source templates

Known source template
List of known point and extended sources, e.g., Sgr A*, Fermi bubbles, loop I

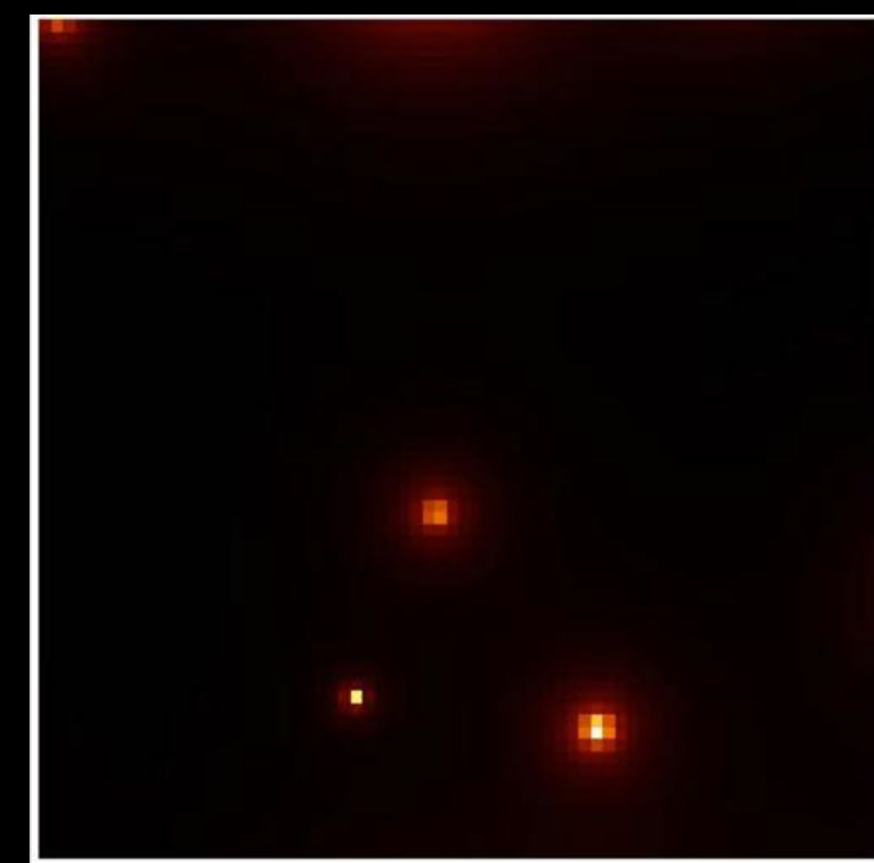

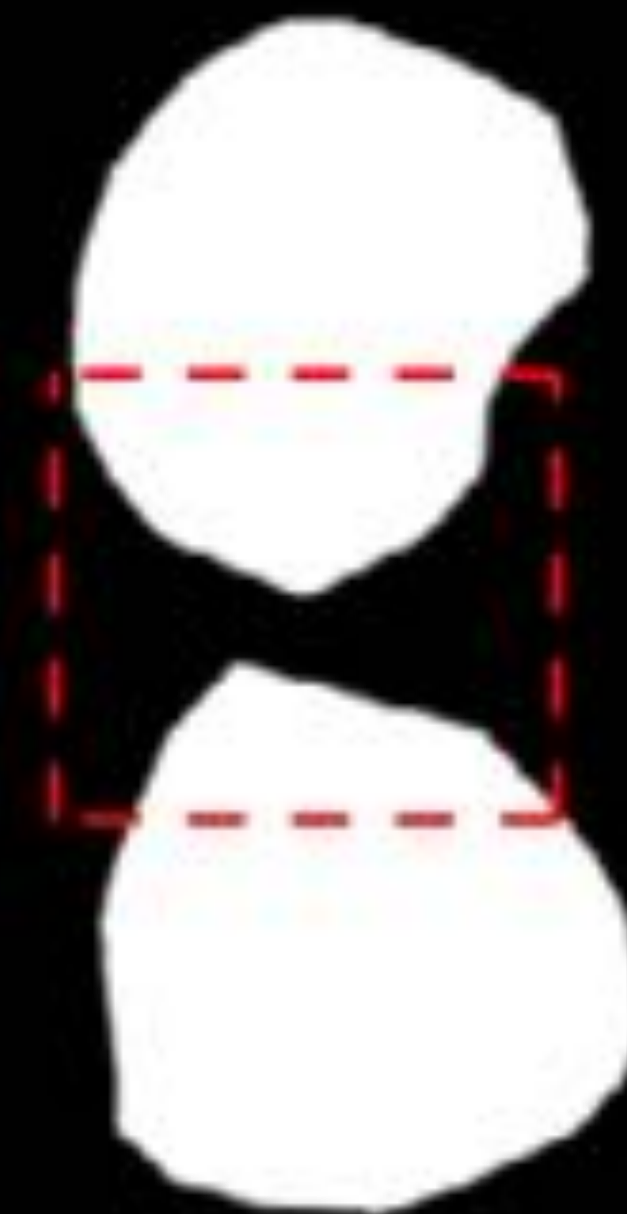

New physics template
"generalized" NFW-squared template, which allows for cosmological simulation info with parameterized contraction effects

$$\rho \propto \left(\frac{r}{r_s}\right)^{-\gamma} \left(1 + \frac{r}{r_s}\right)^{-3+\gamma}$$

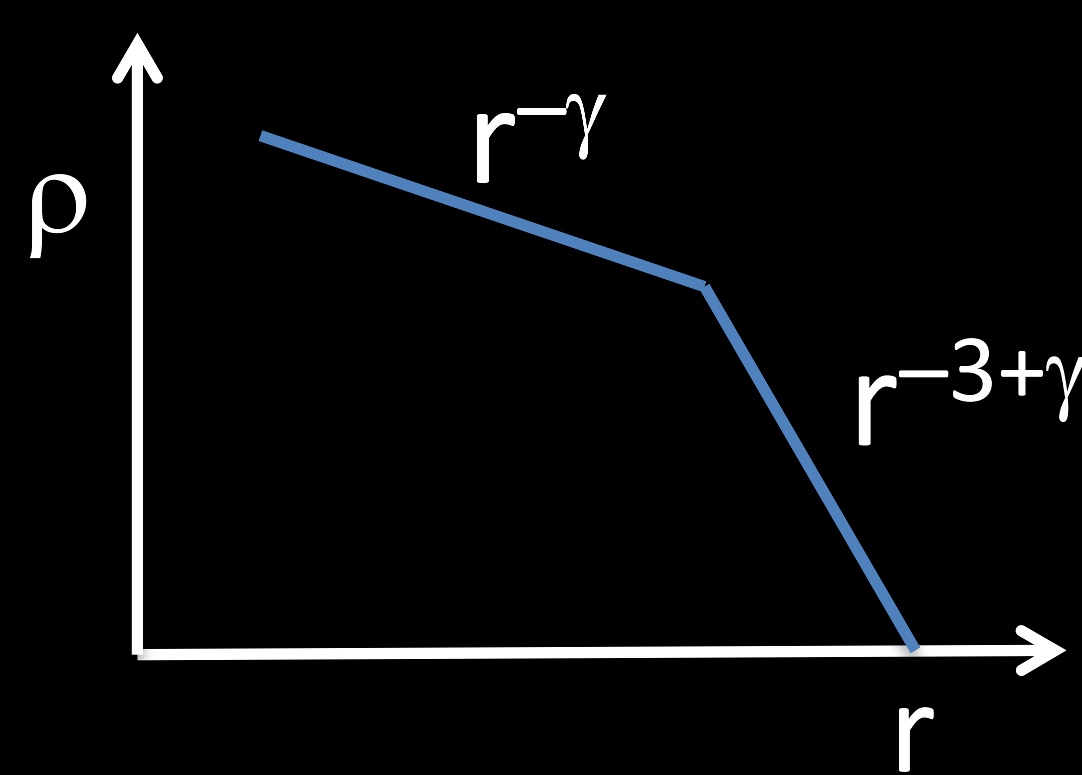

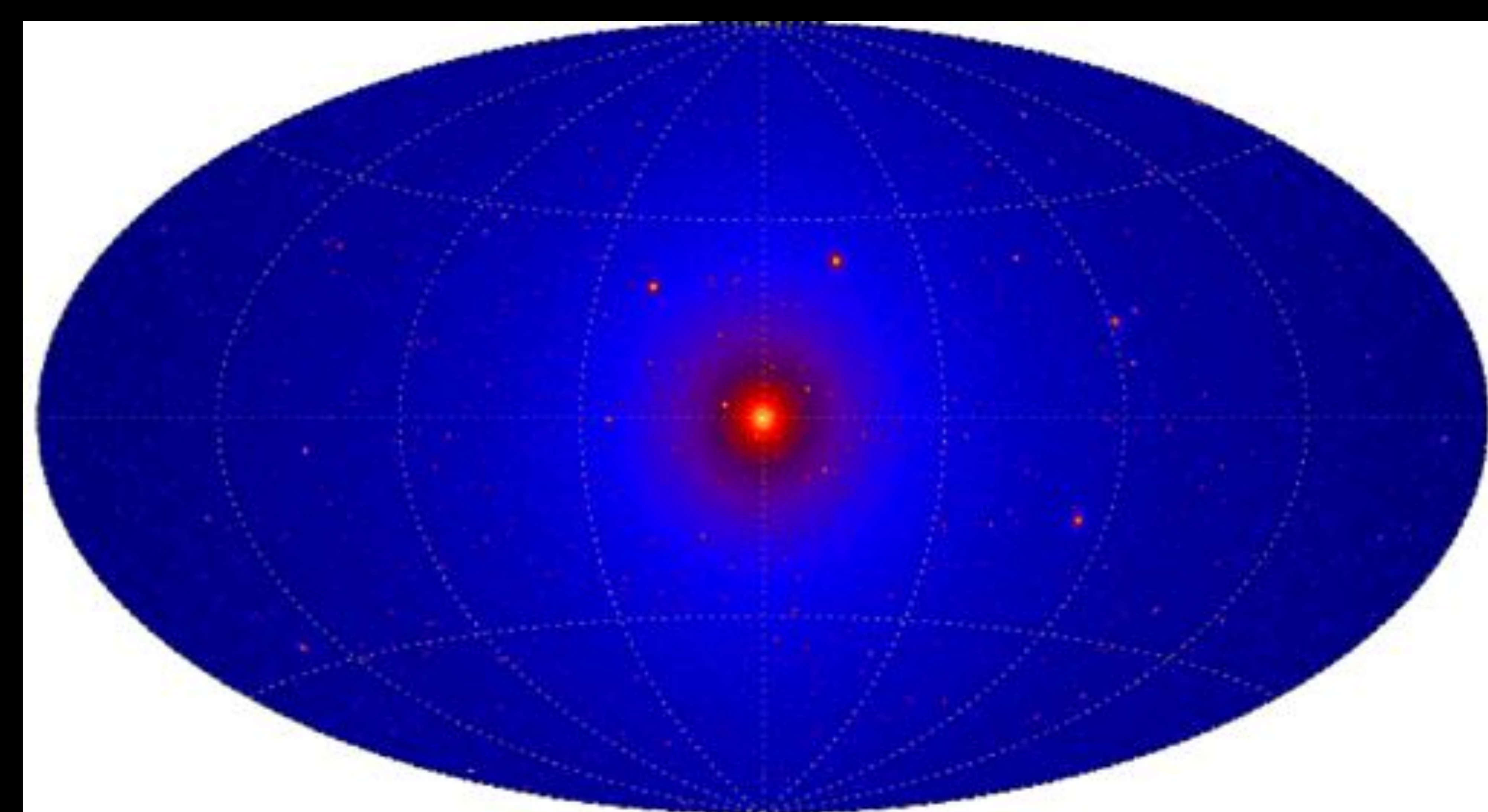

Results

Gordon & Macias (2013)

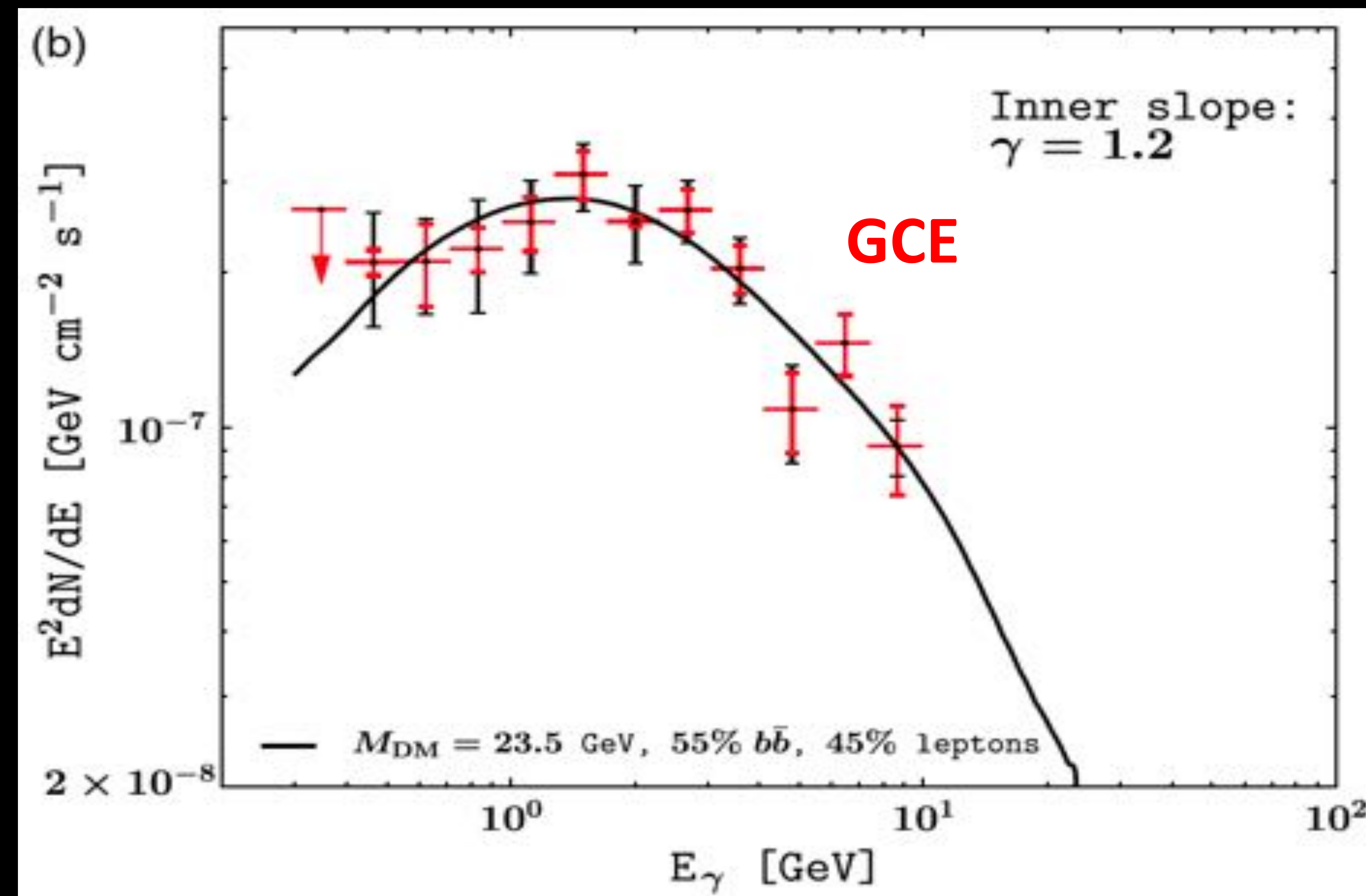

The dark matter template is detected in excess wrt to

- Galactic diffuse models
- Gamma-ray emission from Sgr A*
- Other catalog & new point sources

Main features:

- Spectrum peaks at a ~GeV
- Peak flux ~$10^{-(6\text{-}7)}$ GeV cm^{-2} s^{-1}
- Gamma-ray luminosity is ~10^{36}–10^{37} erg/s
- Spatial morphology ~$r^{-2.4}$

Significance

Statistical significance is ~20–60σ depending on the data and templates used.

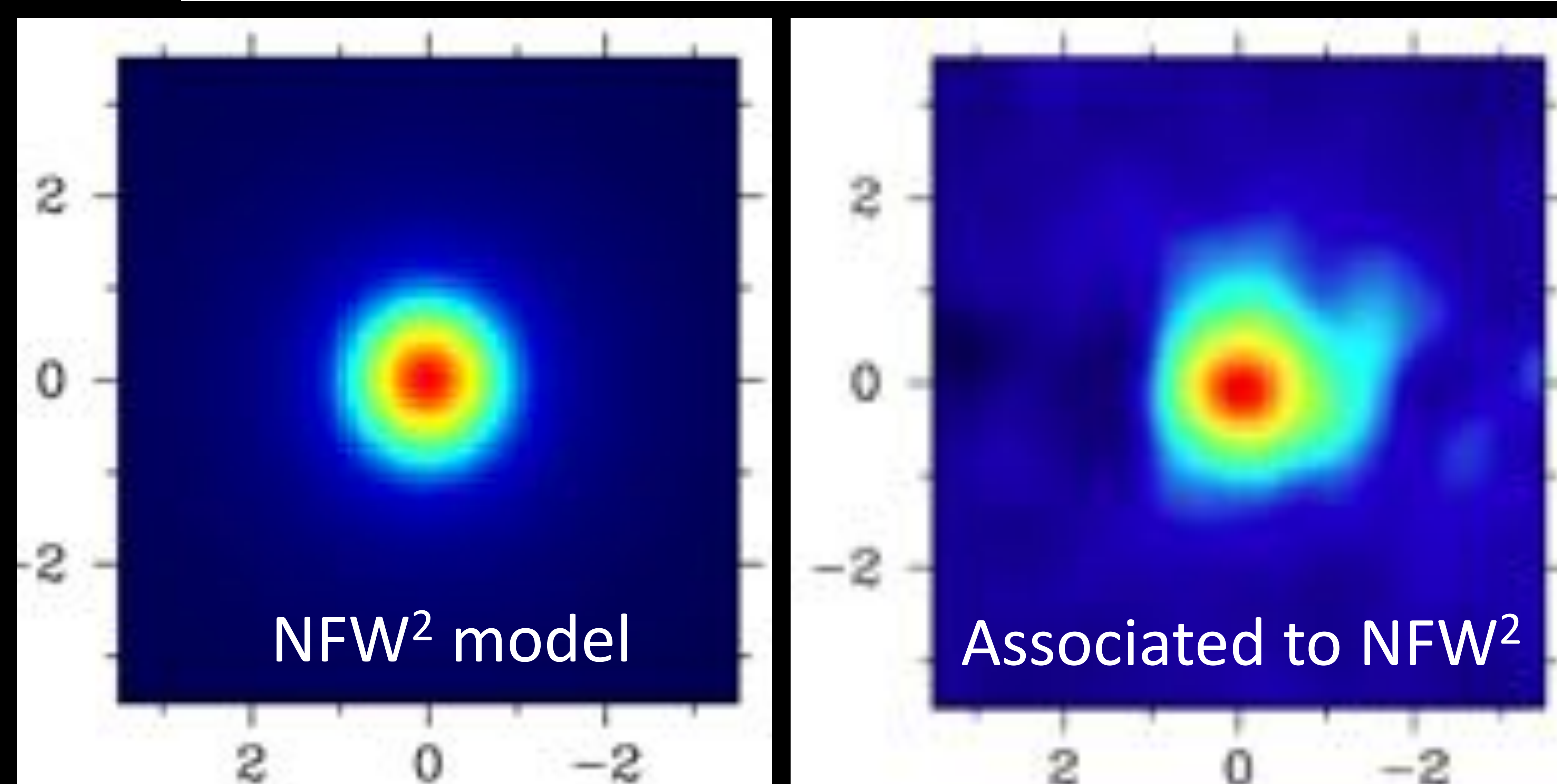

Abazajian & Kaplinghat (2012)

Background model uncertainties

More relevant is systematic uncertainty.

Dedicated diffuse models
Calibrated by the Fermi collaboration for Galactic Center analysis

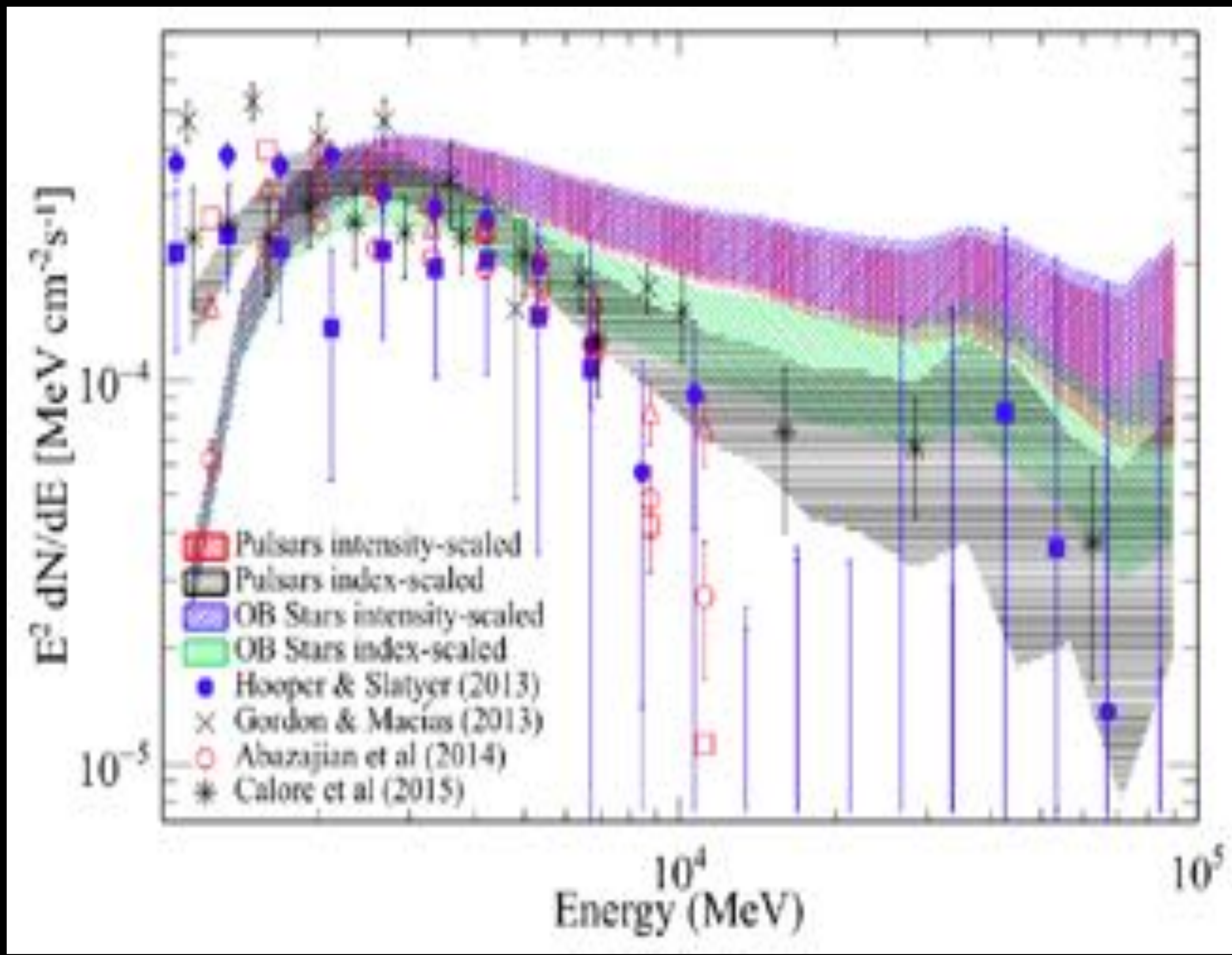

Fermi (2016)

Galprop models
Scan range of parameters of diffusion, B-fields, ISRF, cosmic-ray injection, etc…

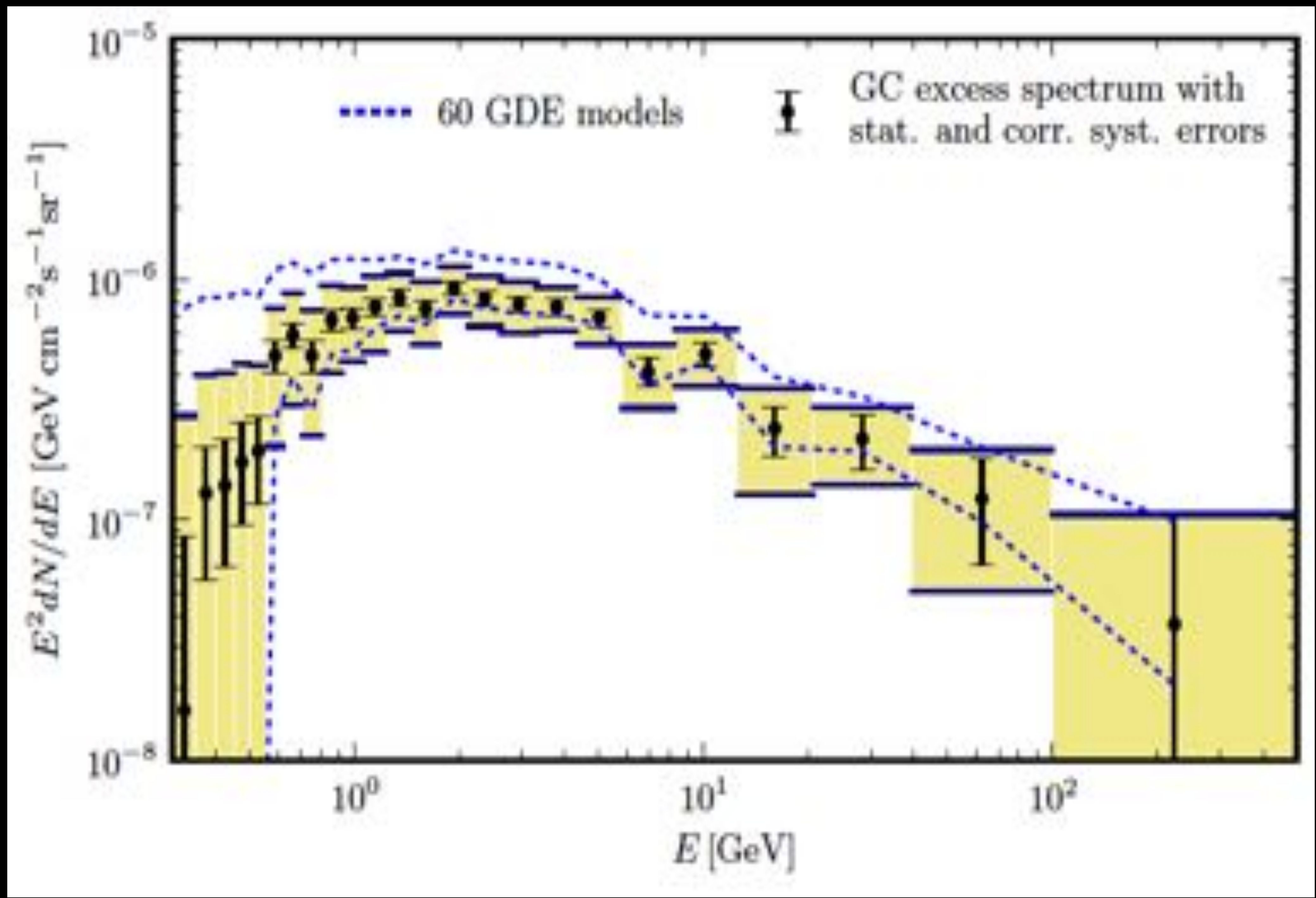

Calore et al (2015)

➔ Despite efforts, the excess remains

Dark Matter

Dark matter can explain the observations
Annihilation of thermally produced WIMPs explains the spectrum and morphology well

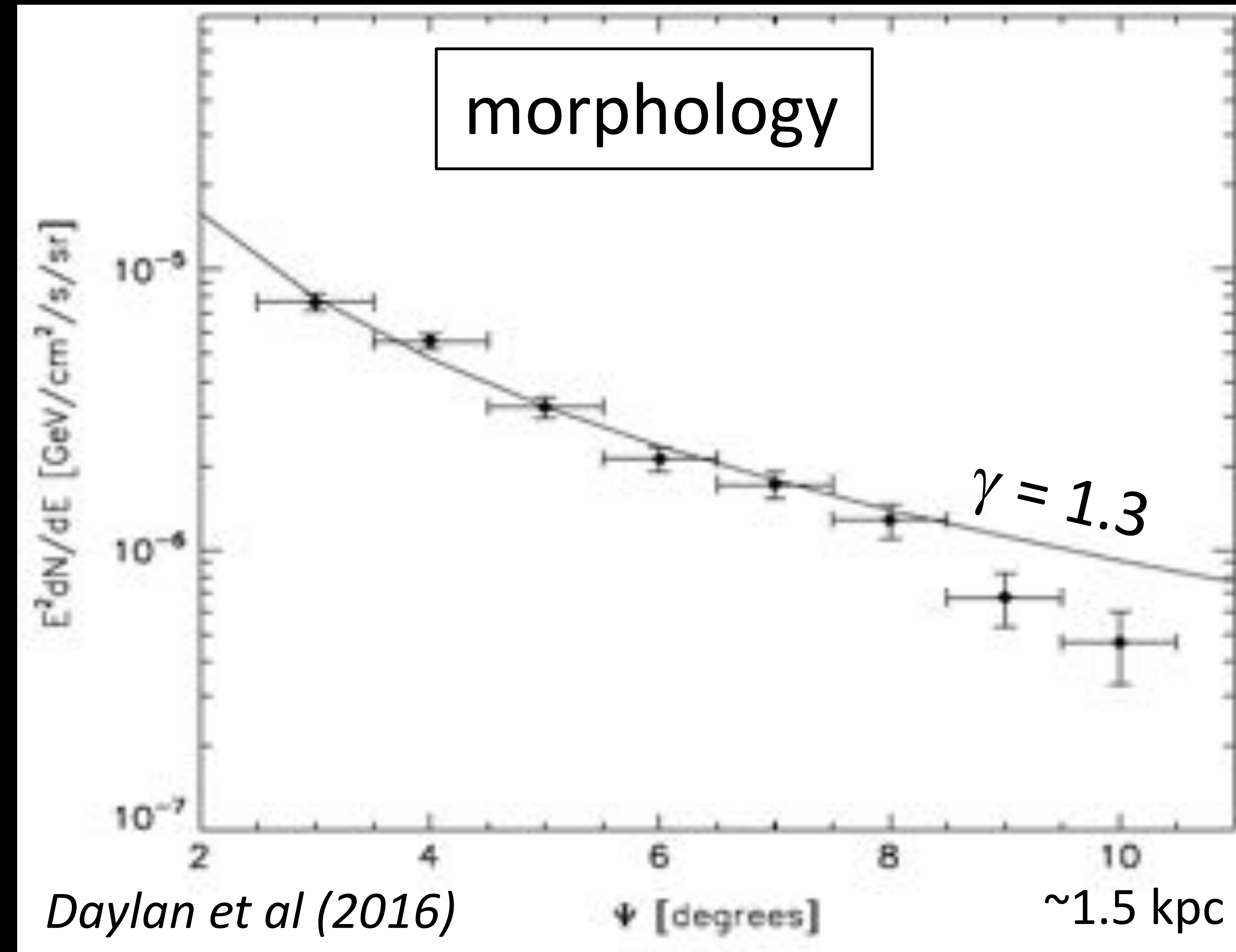

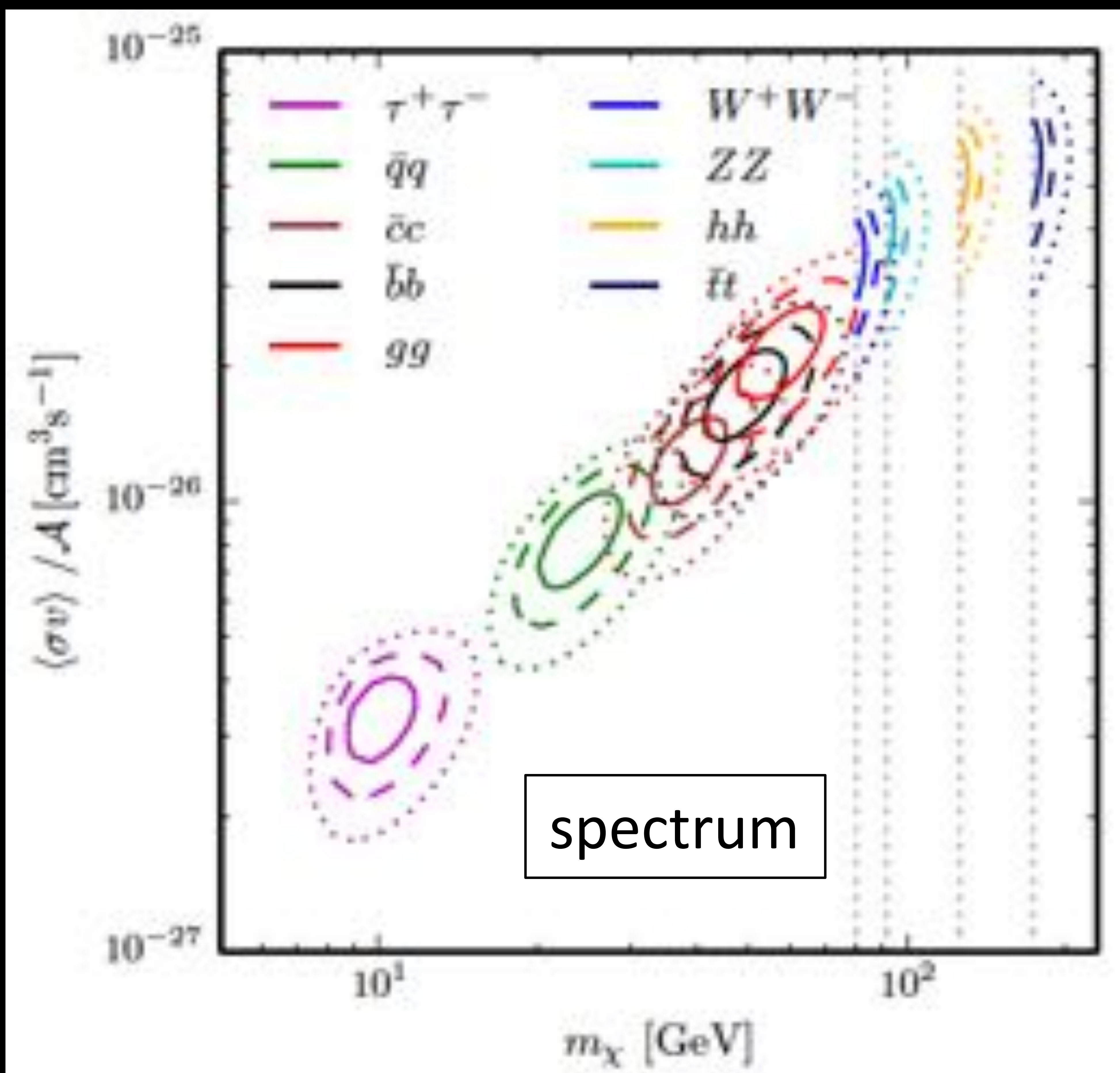

Calore et al (2014)

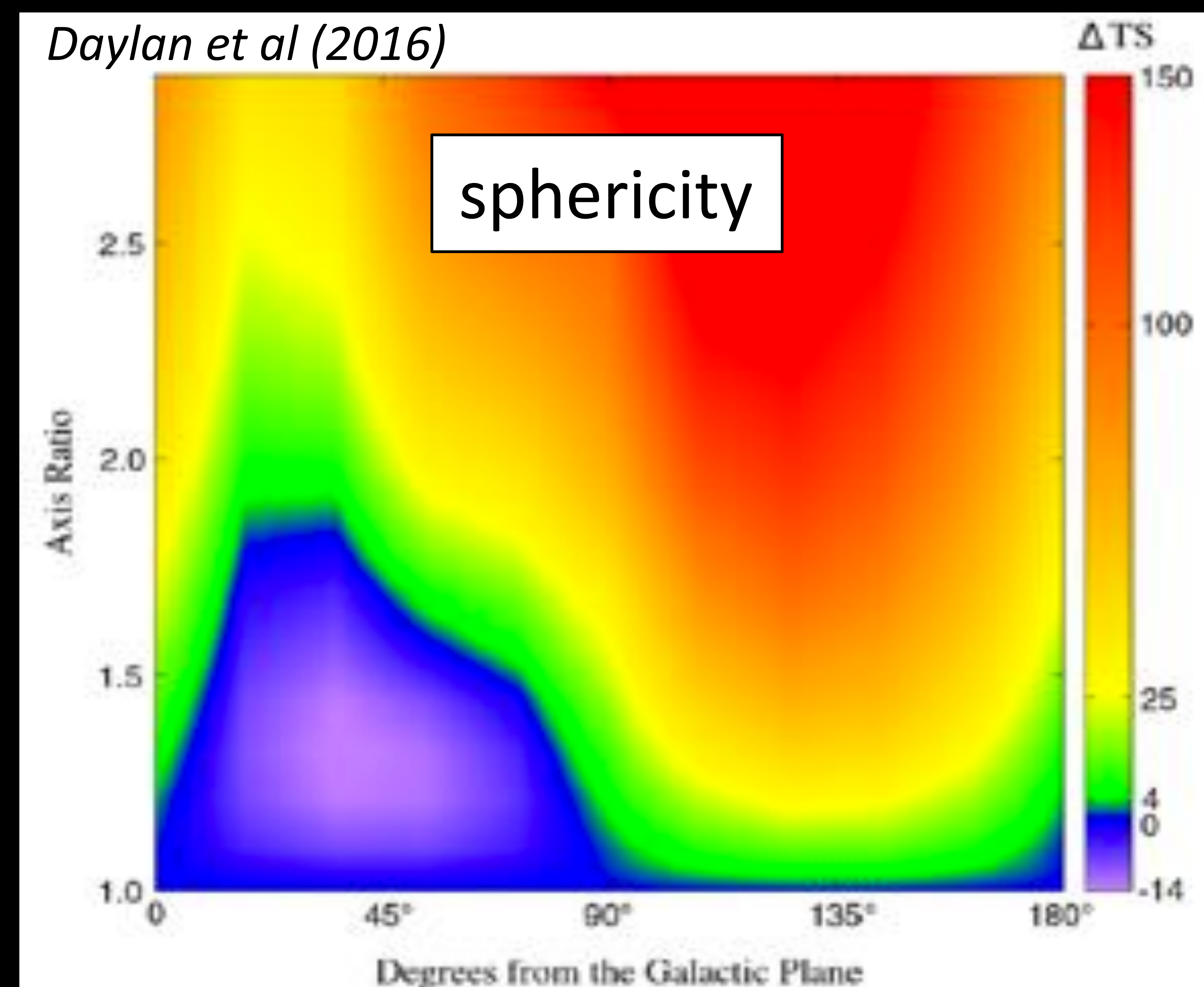

1. **Spectral similarity of pulsars and the GCE**
2. **Photon count statistics support sub-threshold point sources**
3. **Spatial morphology support GCE is connected to old stellar population**

2. OBSERVATIONS INDICATE PULSARS PRODUCE THE EXCESS - DATA DRIVEN

Spectral similarity with millisecond pulsars

Millisecond pulsars

- Millisecond pulsars are gamma-ray sources with similar spectra to the GCE.
- *O*(5,000) needed in the Galactic Center

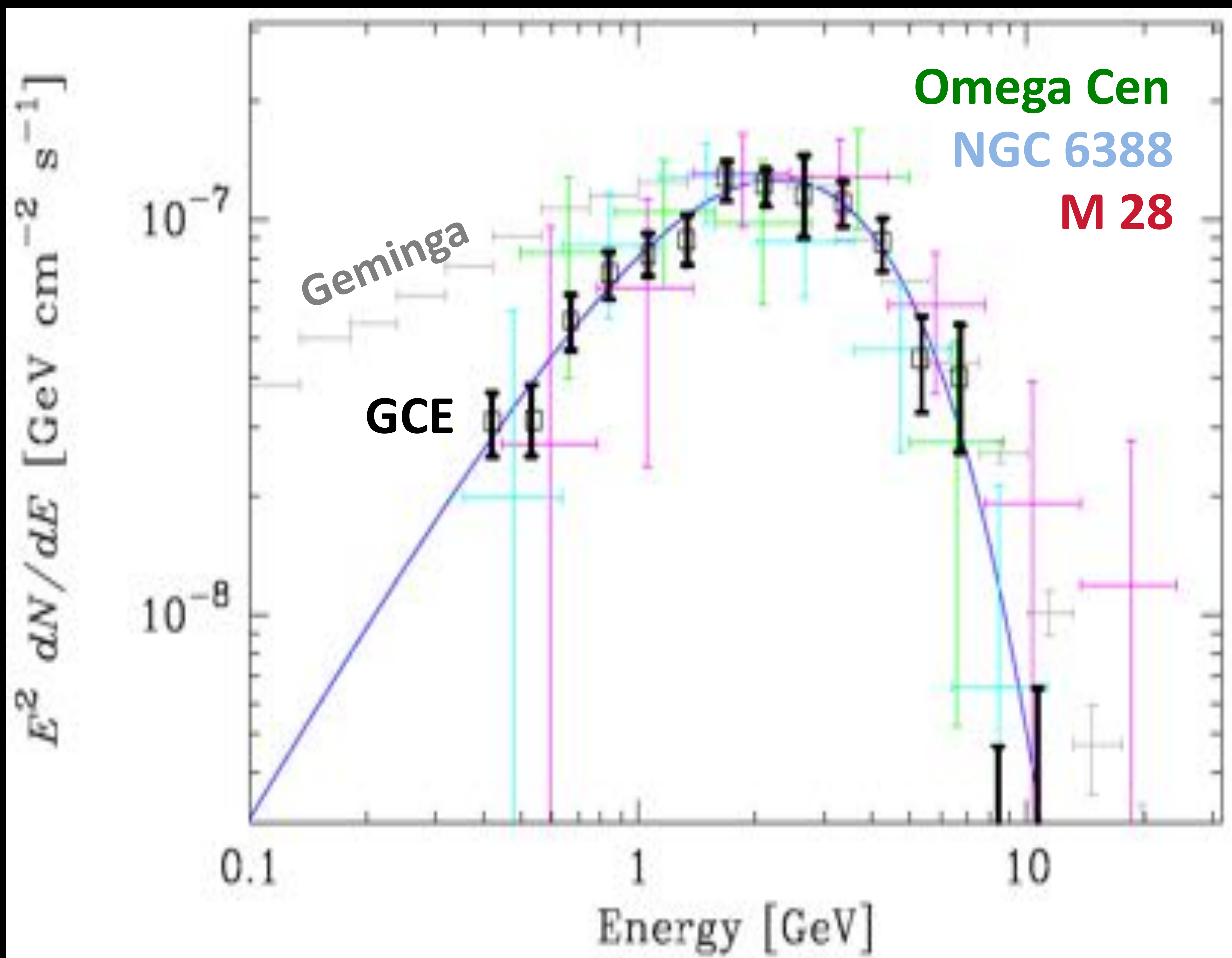

Abazajian (2011)

Globular clusters detected in gamma rays

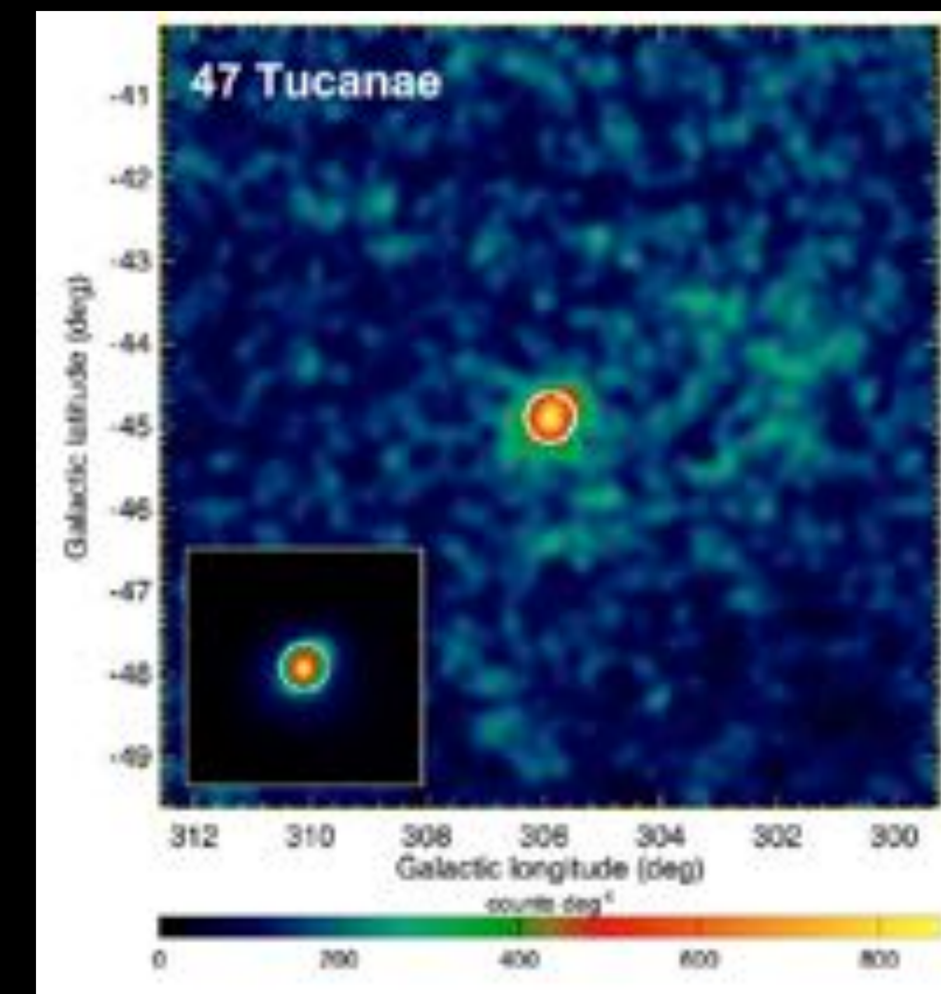

Fermi (2010)

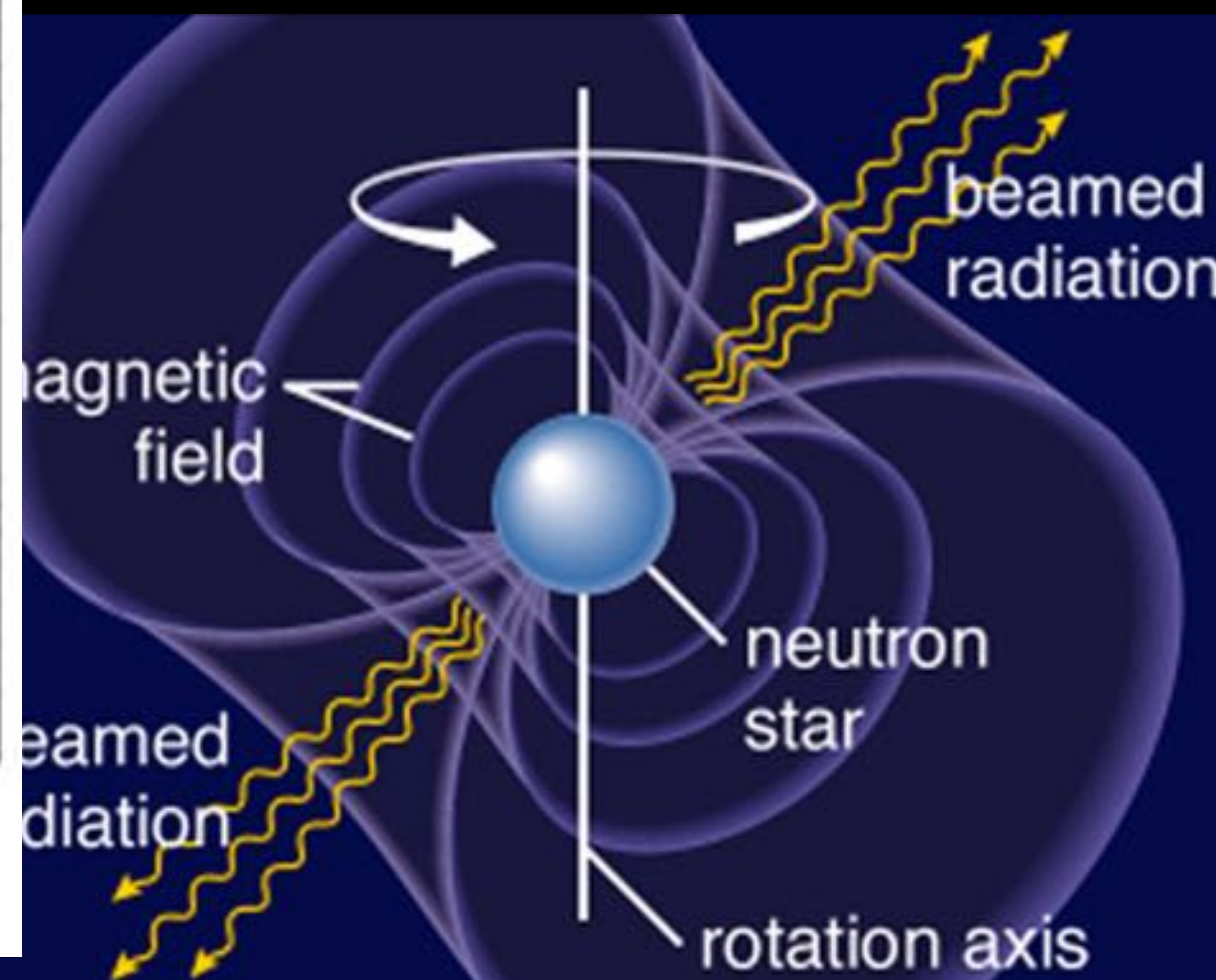

point source vs diffuse source

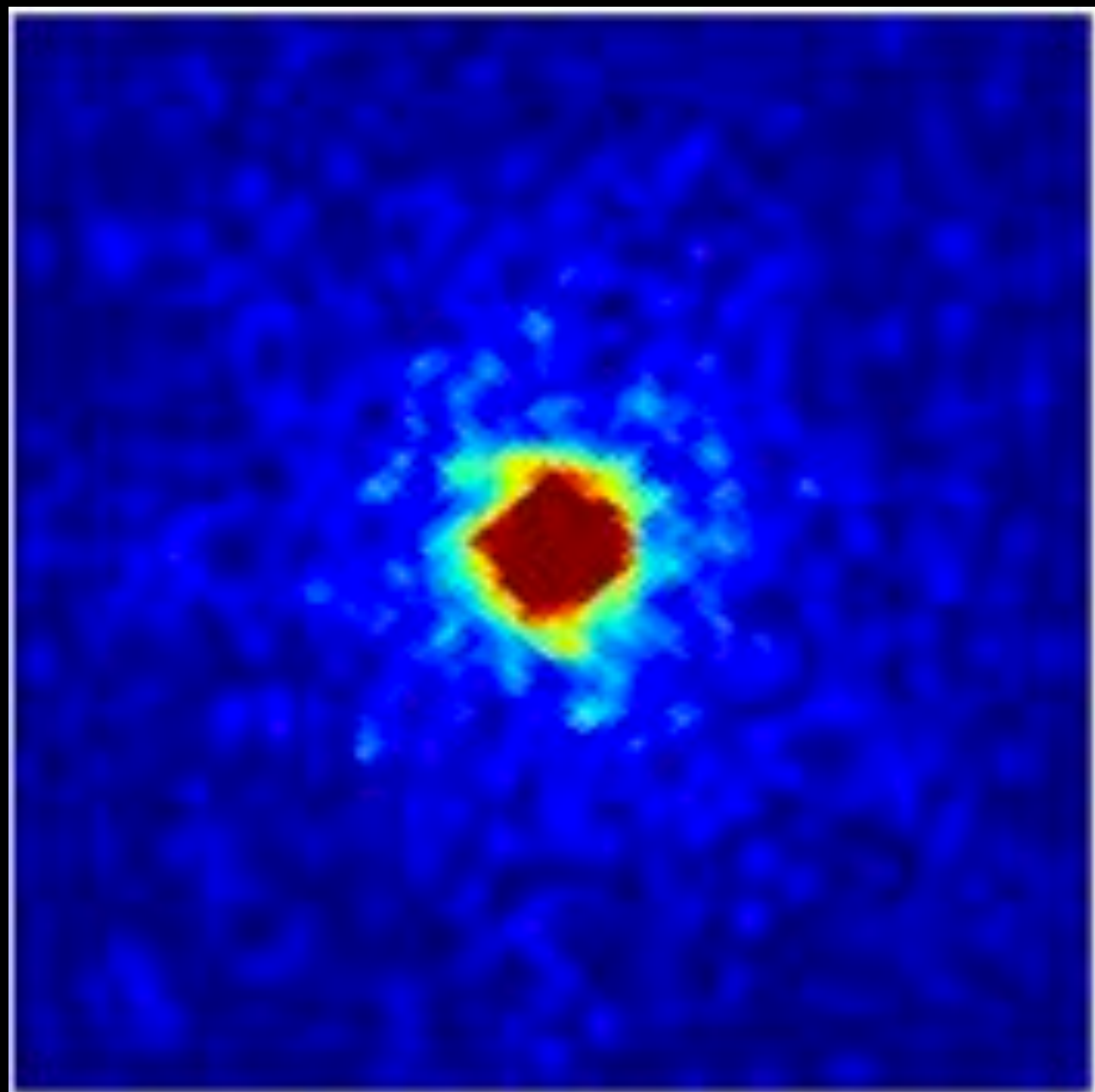

vs

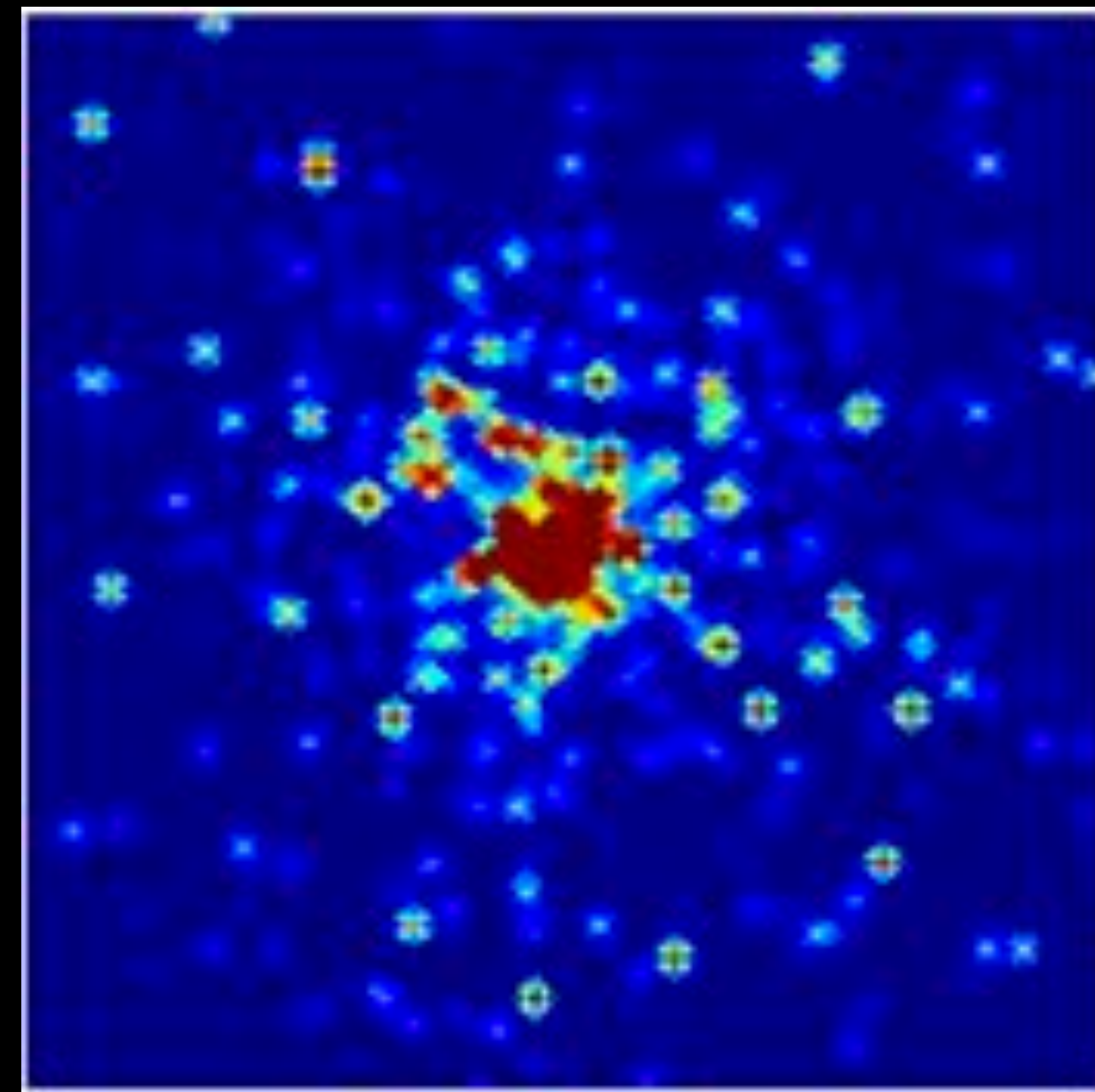

Lee et al (2016)

point source vs diffuse source

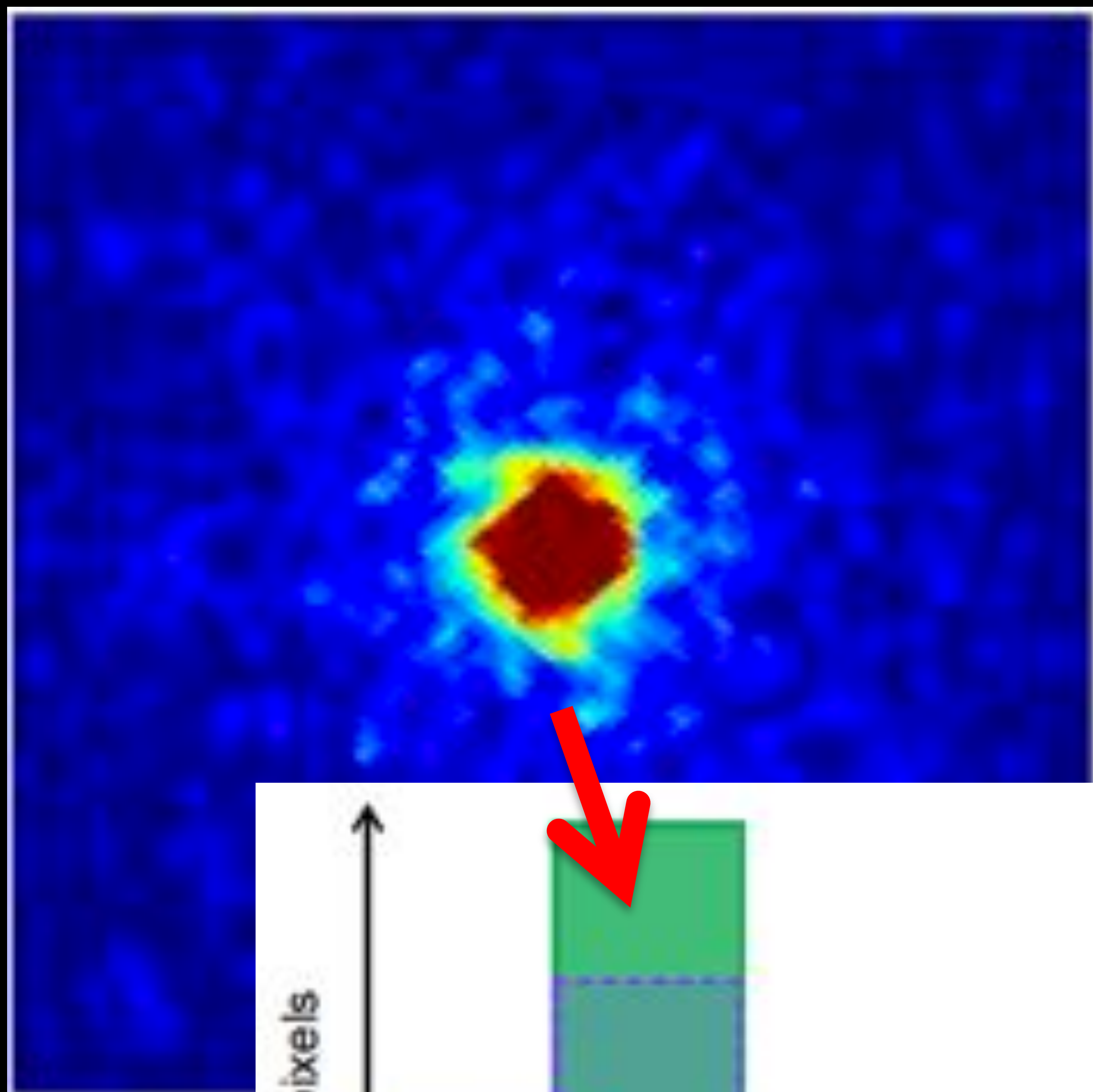

vs

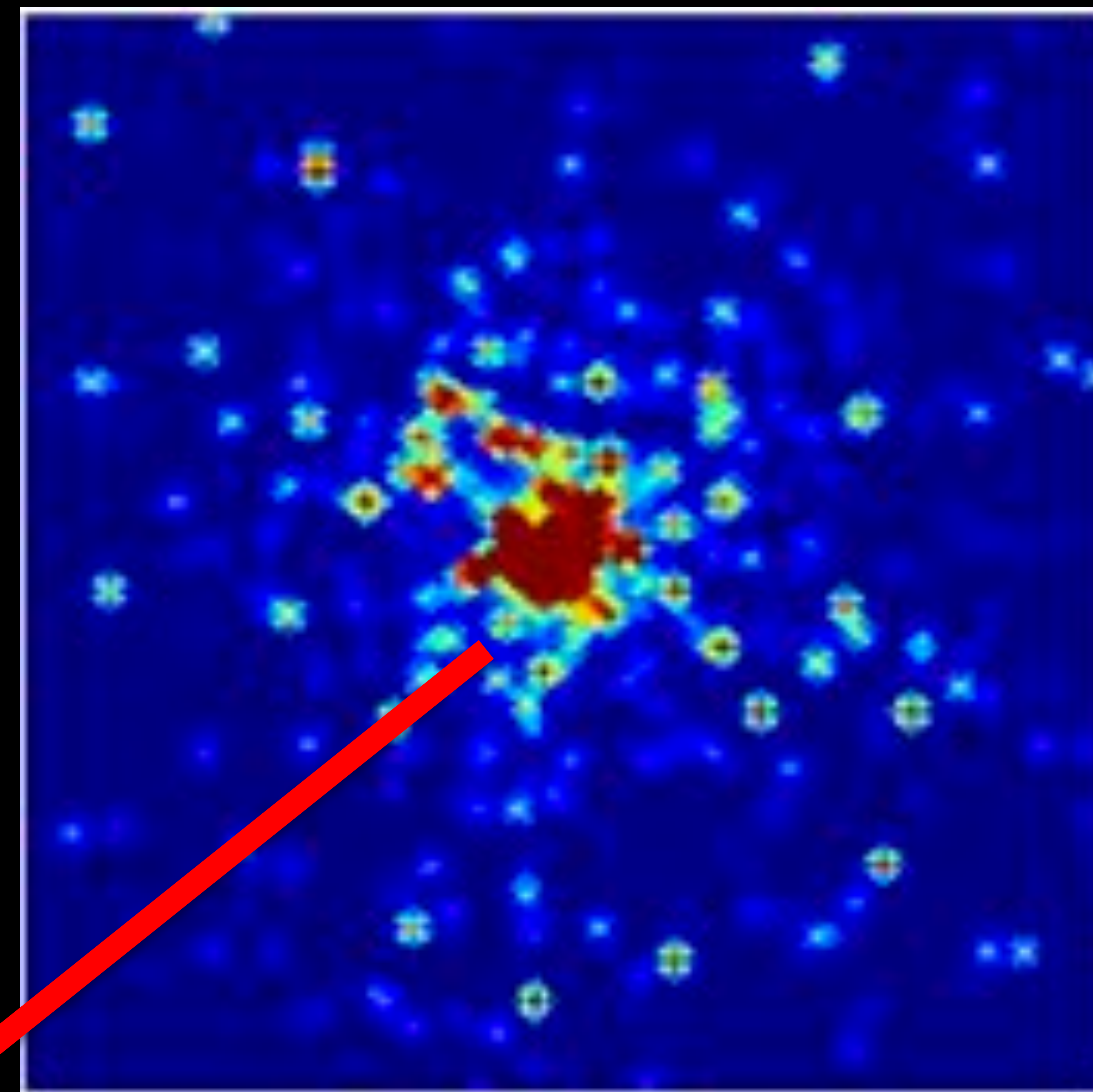

Lee et al (2016)

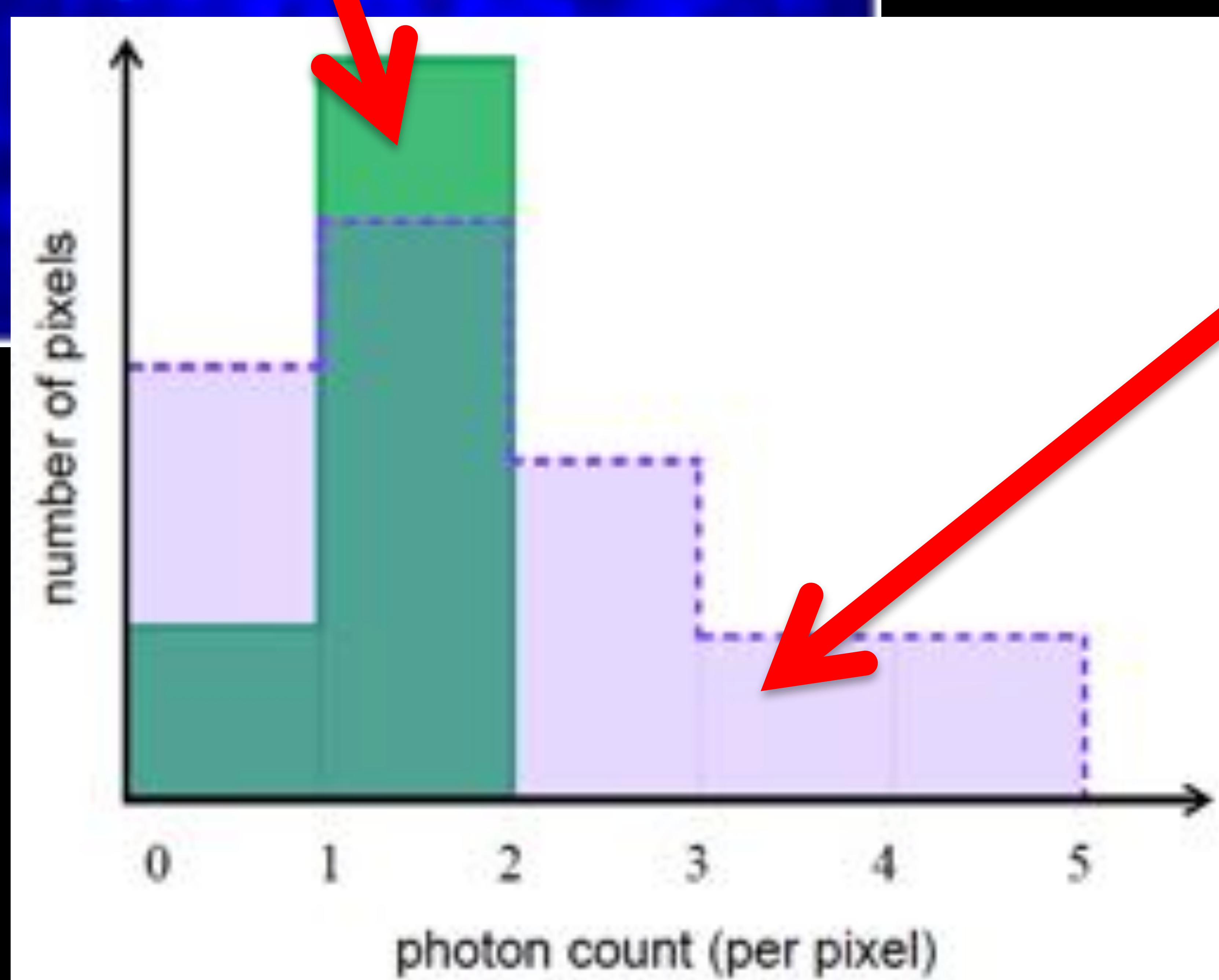

Look for peaks on top of Poisson noise

Bartels et al (2016)

data

c.f. P(D) distribution in X-ray astronomy (Malyshev & Hogg 2011)

Photon count distribution fit procedure

Non-Poissonian fit *Lee et al (2016)*

Fit the photon counts distribution in < 30 deg

$p_k^{(p)}$: probability of finding k photons in pixel p

Smooth emission: follows Poisson statistics, Galactic diffuse, bubbles, isotropic, NFW-DM

$$p_k^{(p)} = \lambda^k e^{-\lambda}/k!$$

λ: Sum of templates

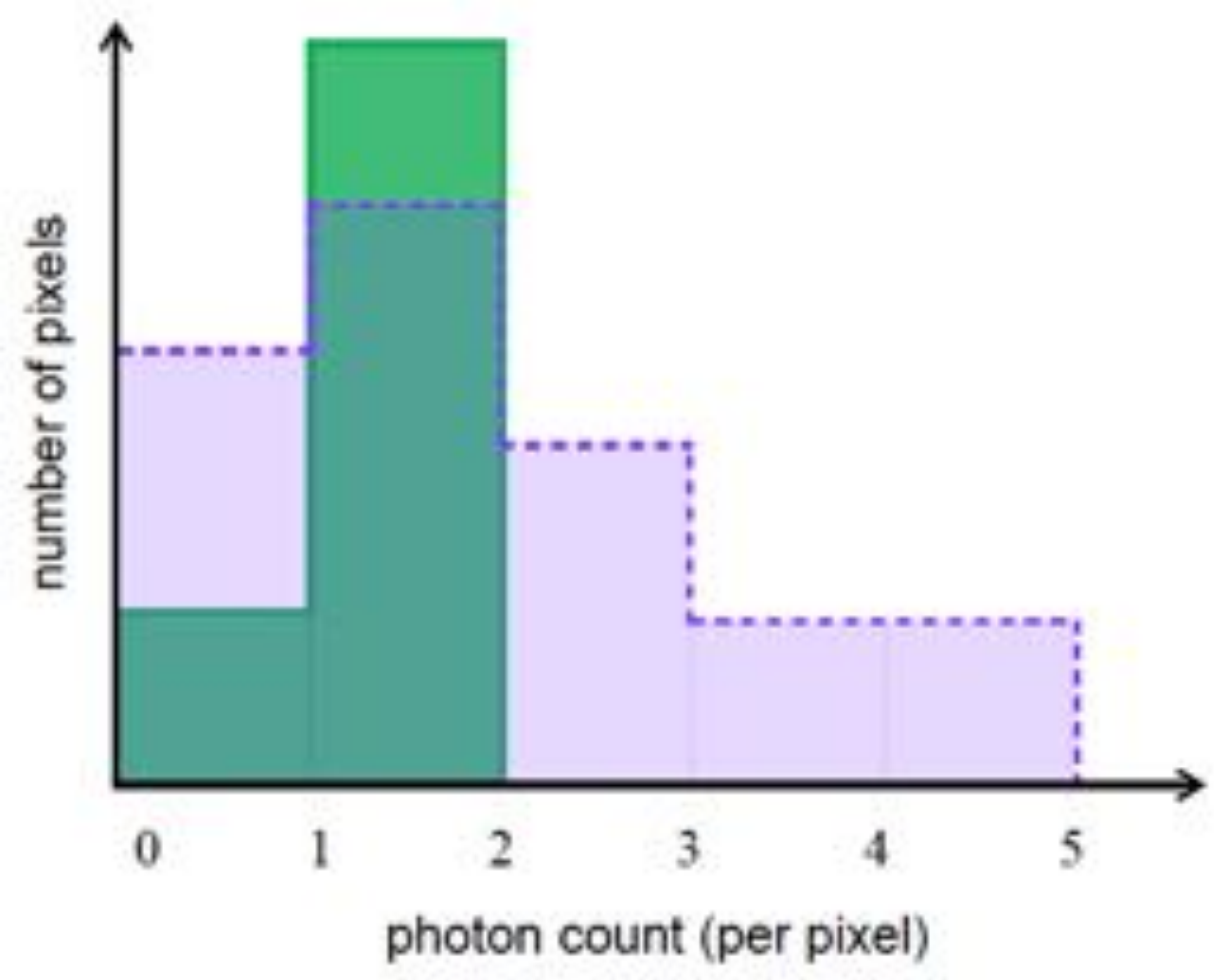

Unresolved point source: follows Non-Poissonian statistics

Source count:

$$\frac{dN^{(p)}}{dF} = A^p \begin{cases} \left(\frac{F}{F_b}\right)^{-n_1}, & F \geq F_b \\ \left(\frac{F}{F_b}\right)^{-n_2}, & F < F_b \end{cases}$$

Where A^p follows the spatial morphology:

- Disk-PS
- NFW-PS
- Extragalactic-PS

Photon count distribution fit result

- NFW-PS contributes ~8.7% of photons, while NFW-DM is consistent with 0%
- Bayes factor 10^6 for NFW-PS compared to without
- If NFW-PS is not added, the NFW-DM absorbs the excess
- The diffuse emission normalization stays within 1% of high latitude values.

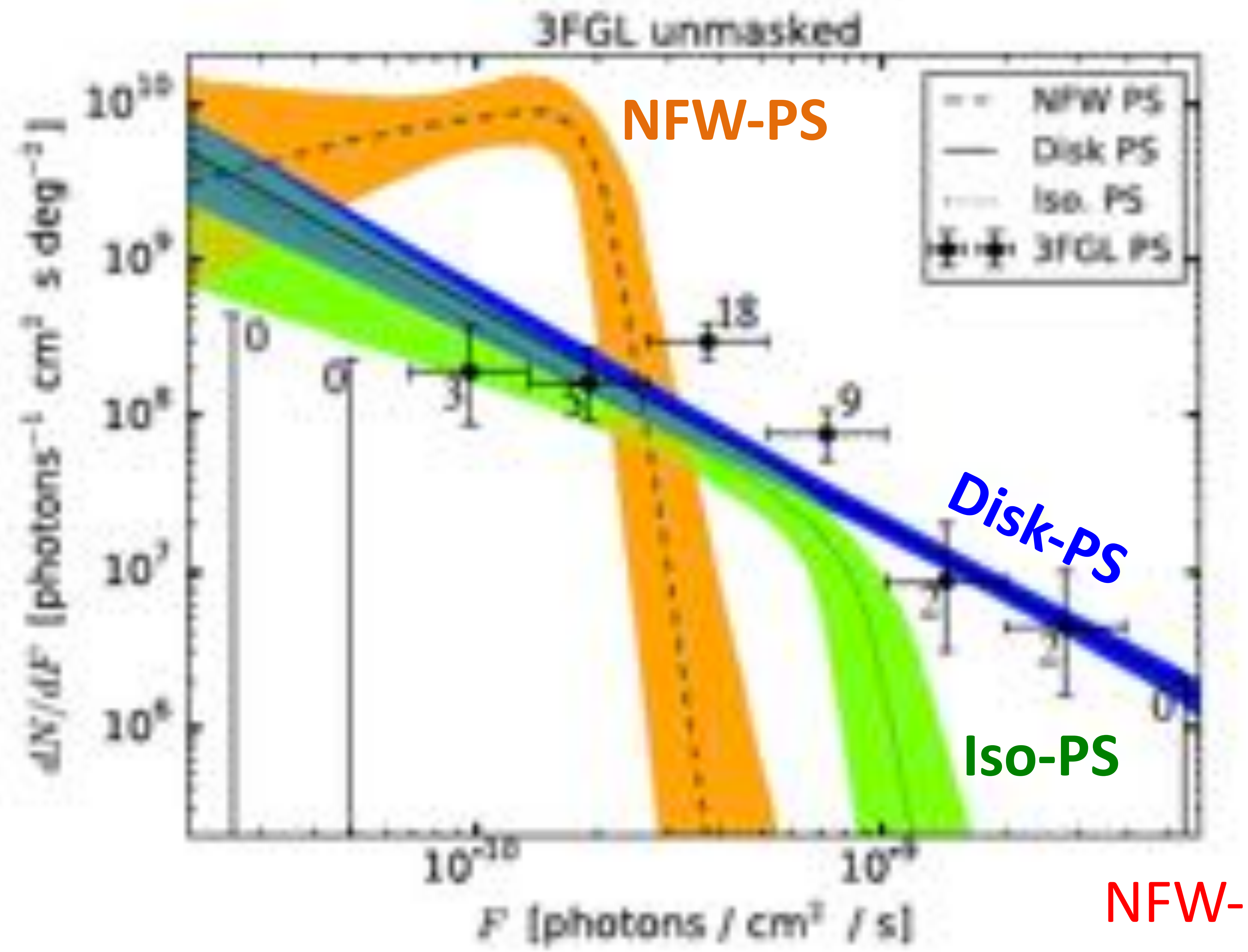

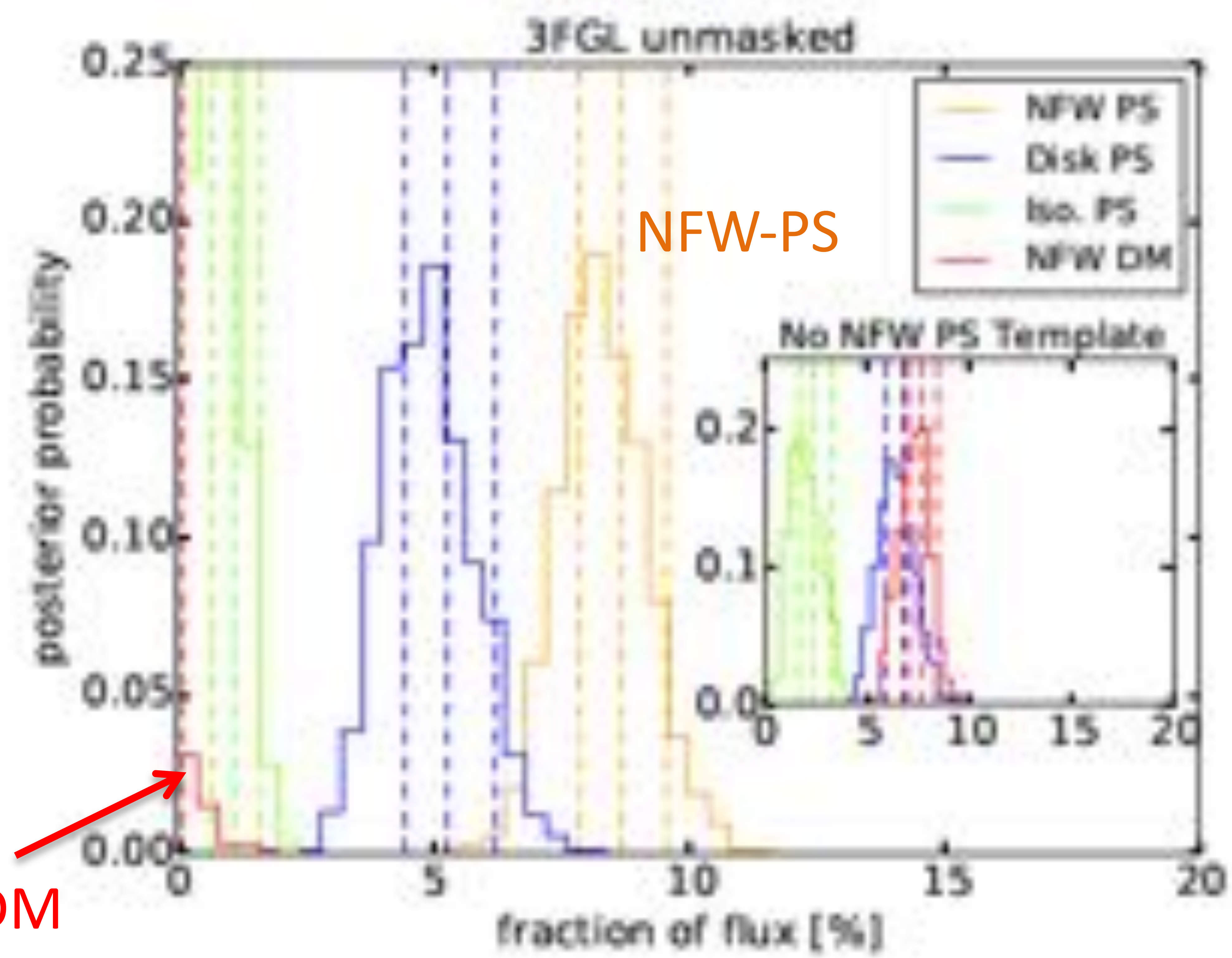

➔ Strong preference for sub-threshold point sources following the NFW morphology over a diffuse NFW (dark matter) source

Lee et al (2016)

Photon count distribution fit result

- NFW-PS contributes ~8.7% of photons, while NFW-DM is consistent with 0%
- Bayes factor 10^6 for NFW-PS compared to without
- If NFW-PS is not added, the NFW-DM absorbs the excess
- The diffuse emission normalization stays within 1% of high latitude values.

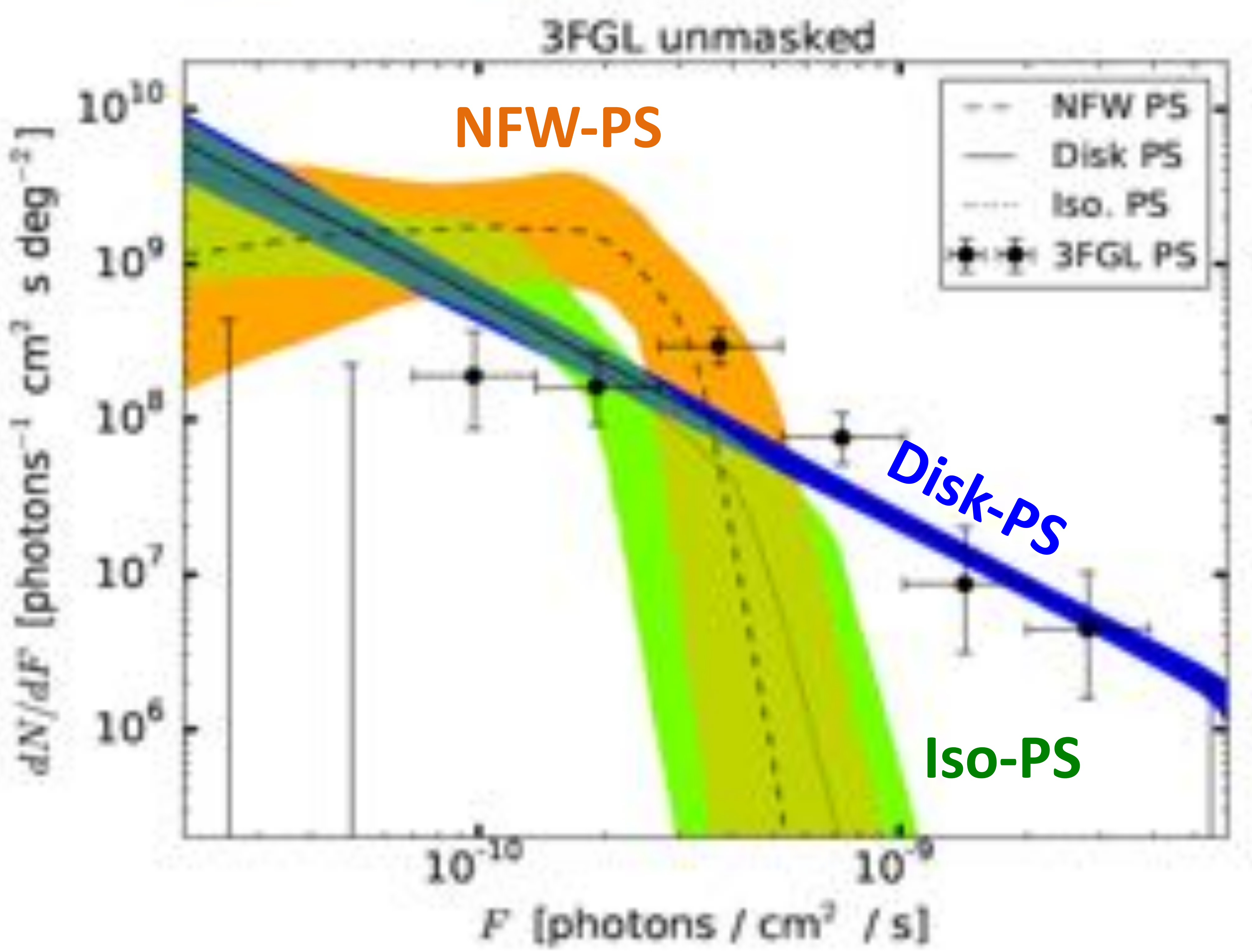

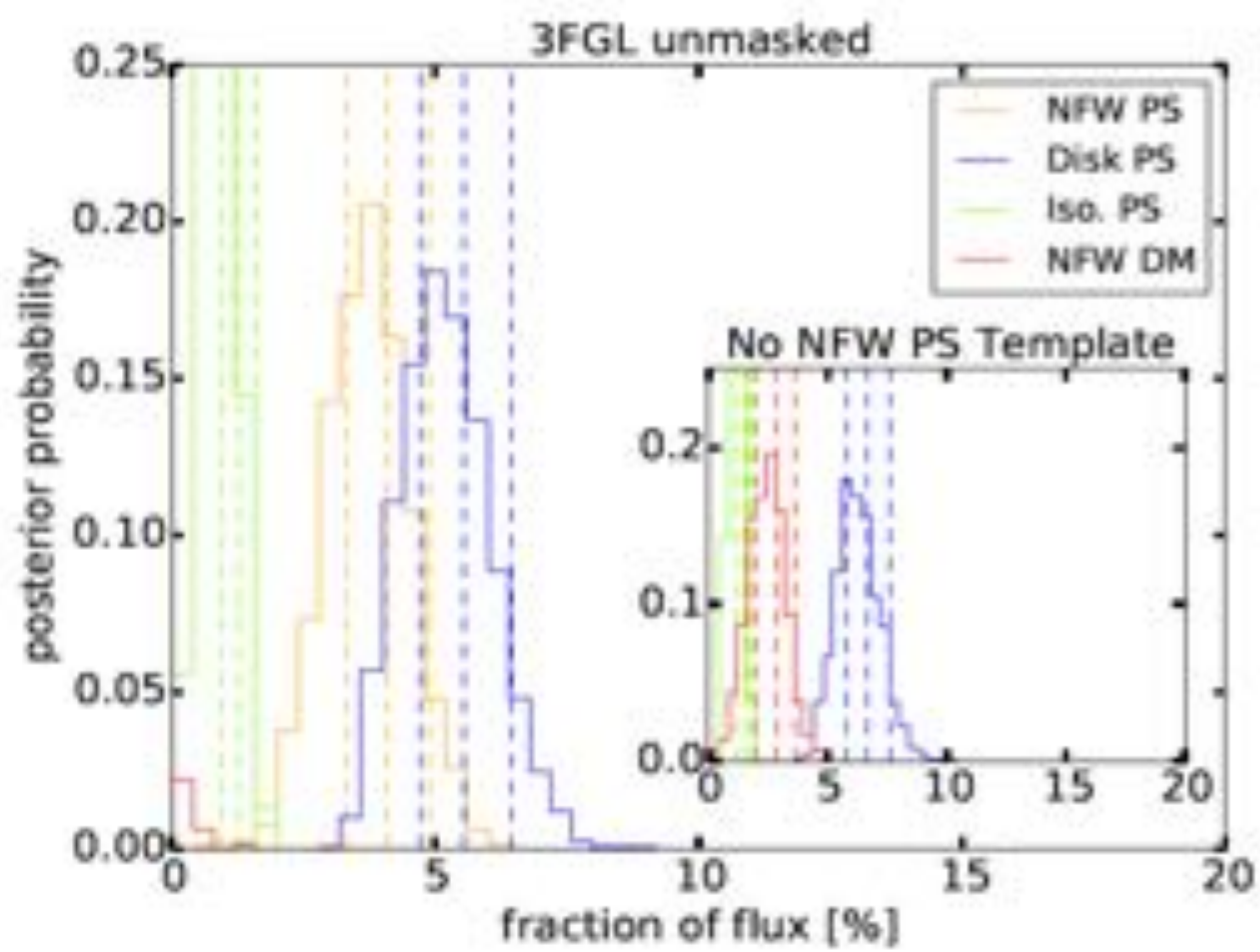

Lee et al (2016)

➔ Strong preference for sub-threshold point sources following the NFW morphology over a diffuse NFW (dark matter) source

Same conclusions with a wavelet method

Wavelet analysis

1. Convolve with a Mexican hat kernel to identify peaks in high signal-to-noise.
2. Model distribution of peaks in SNR and angular rings

➔ Fit better by sub-threshold MSP sources than diffuse

Truly diffuse (=DM)

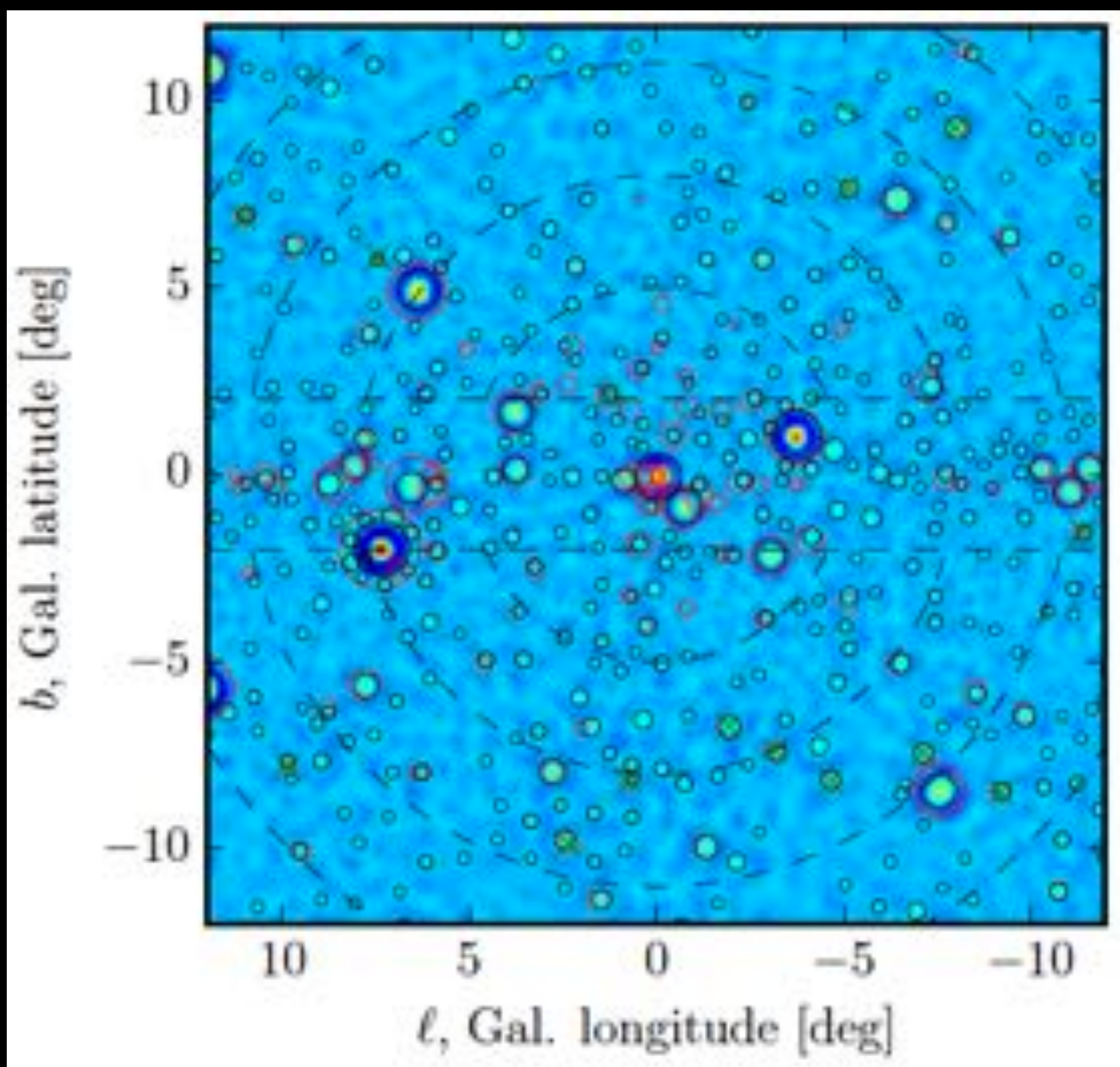

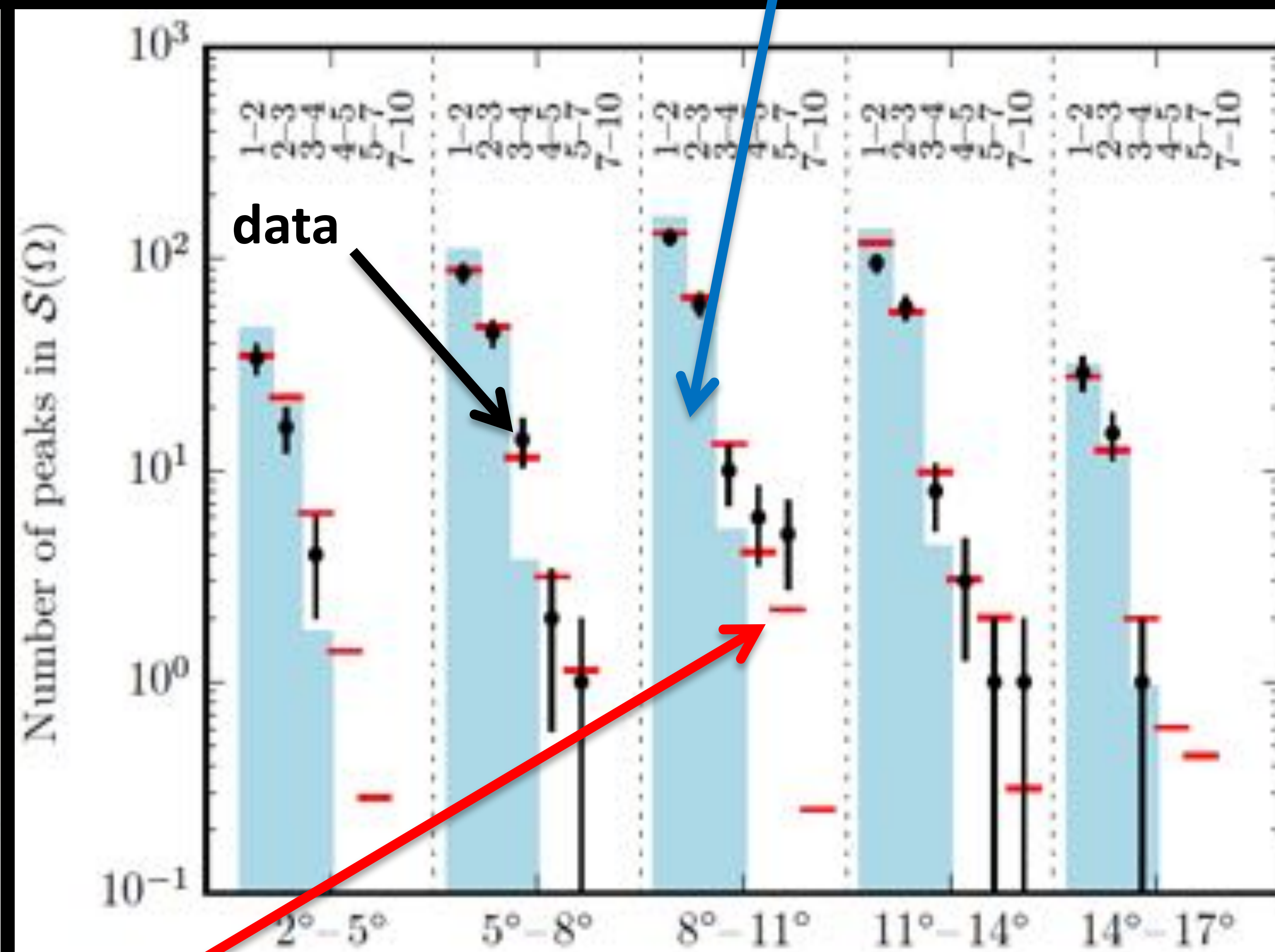

Bartels et al (2016)

Point sources (=MSP)

$$\frac{dN}{dL}\Big|_{L\leq L_{\max}} \propto L^{-1.5}$$

spherical symmetry vs bulge shape

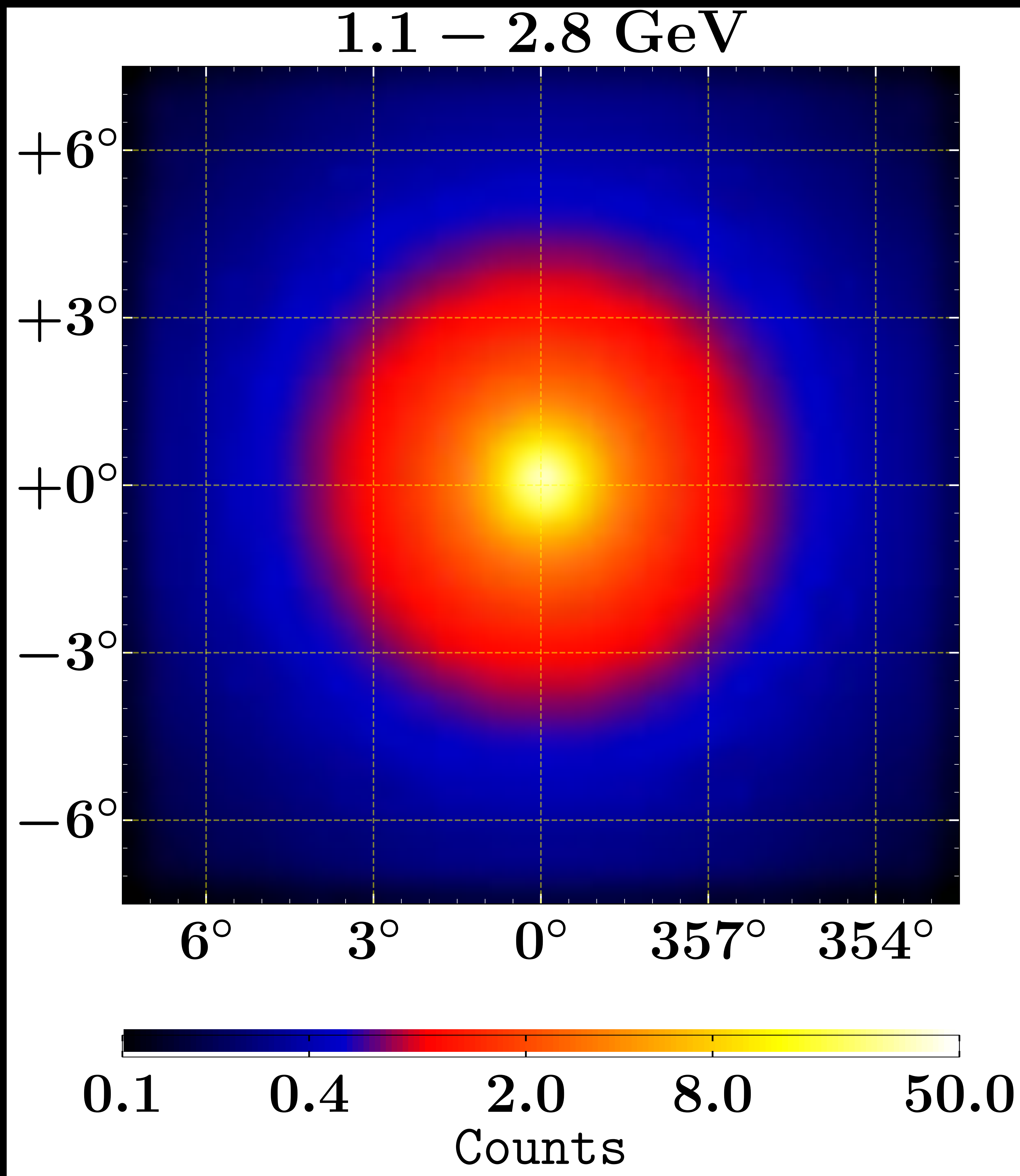

vs

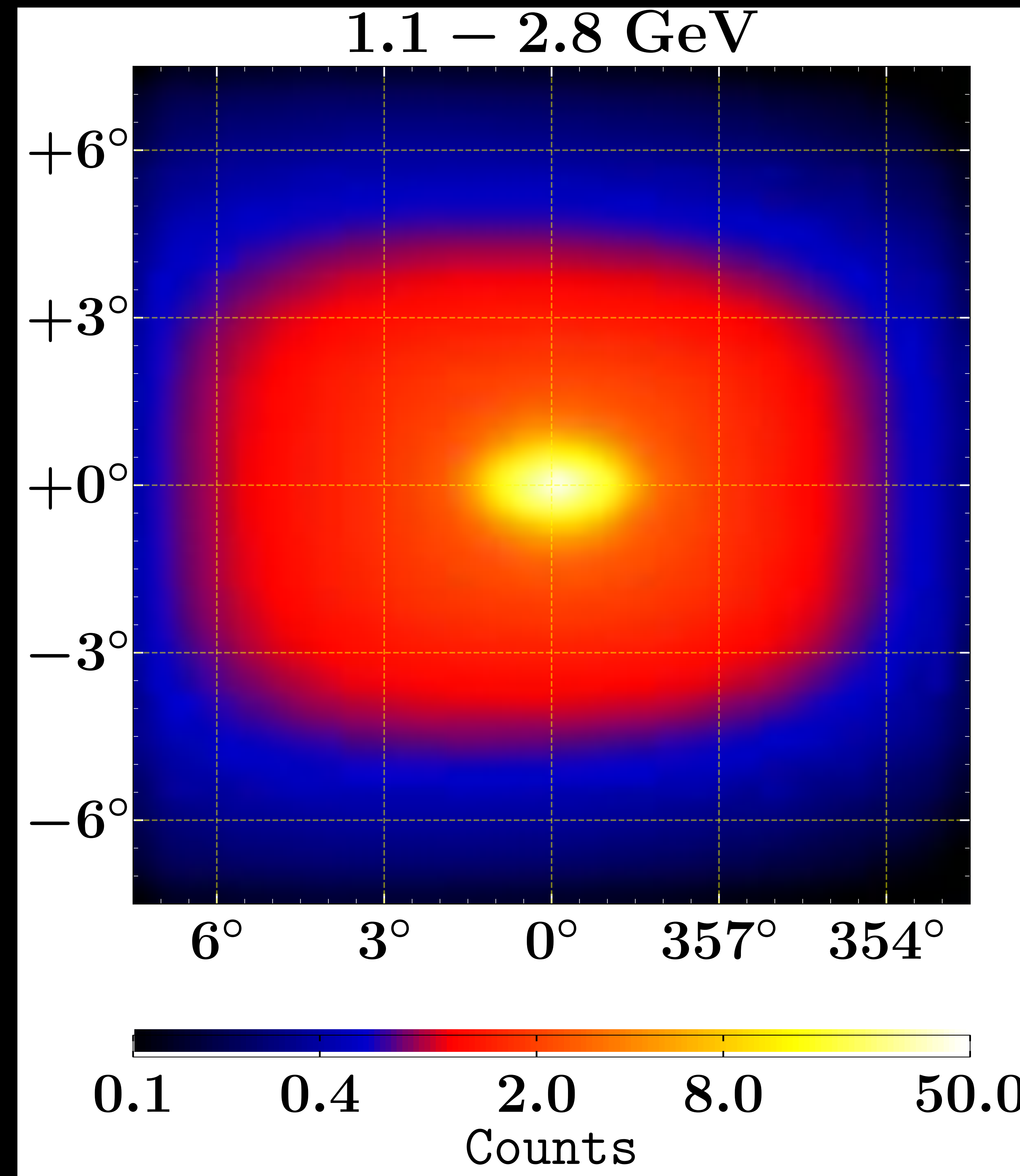

The Galactic Bulge

Nuclear Bulge: central stellar cluster + disk

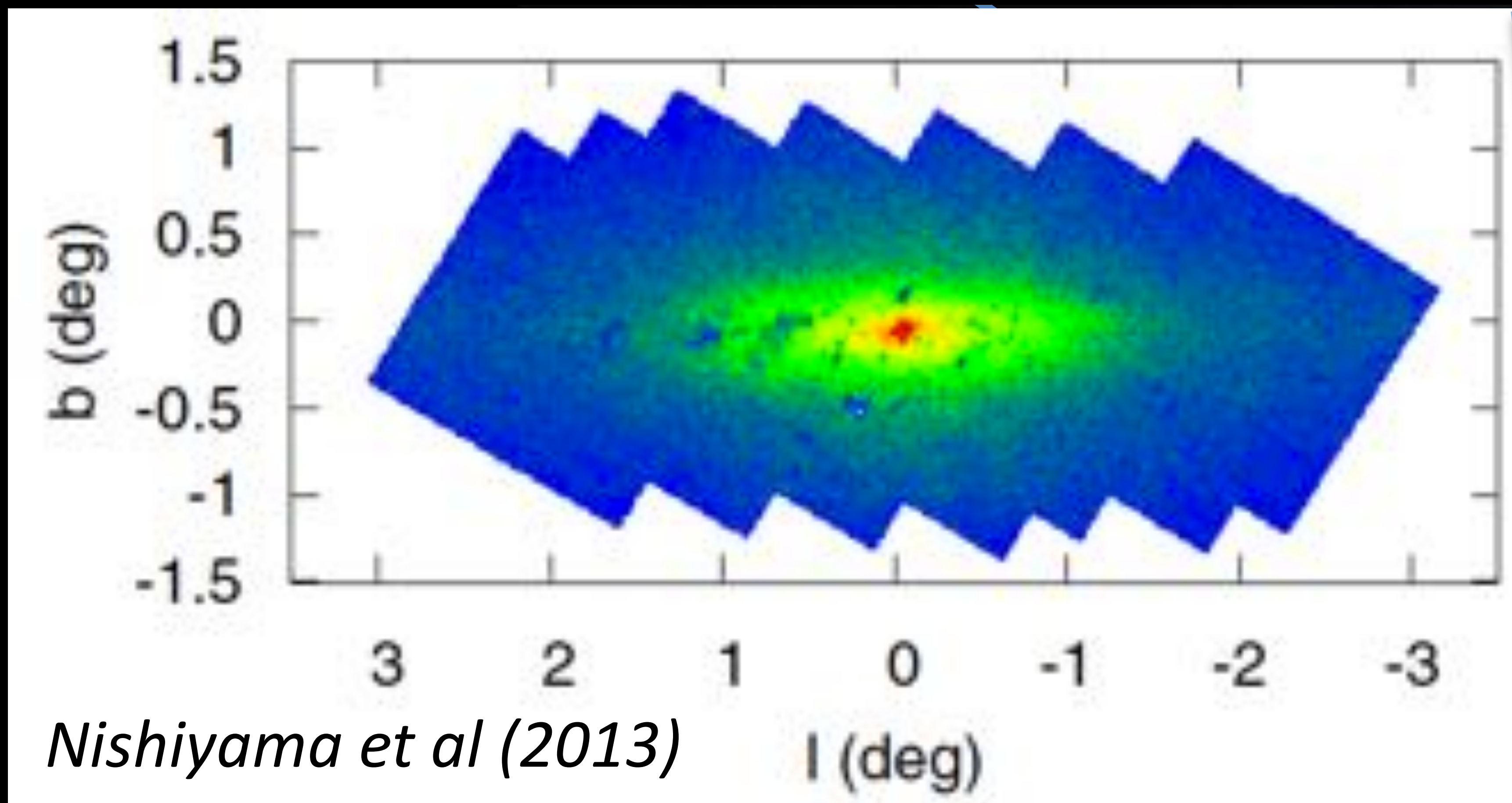

Nishiyama et al (2013)

The boxy bulge:
rectangle, not symmetric

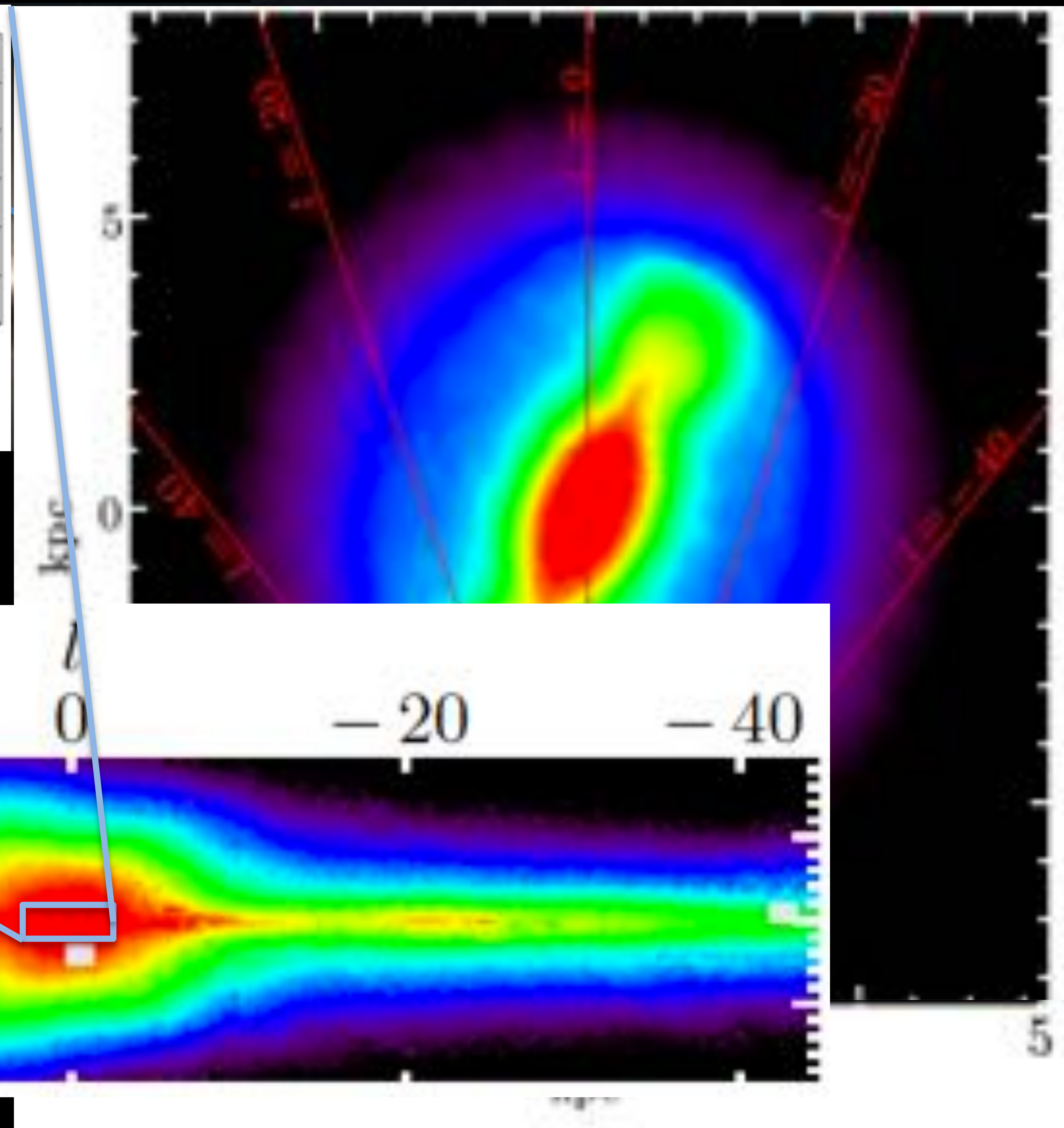

Side view

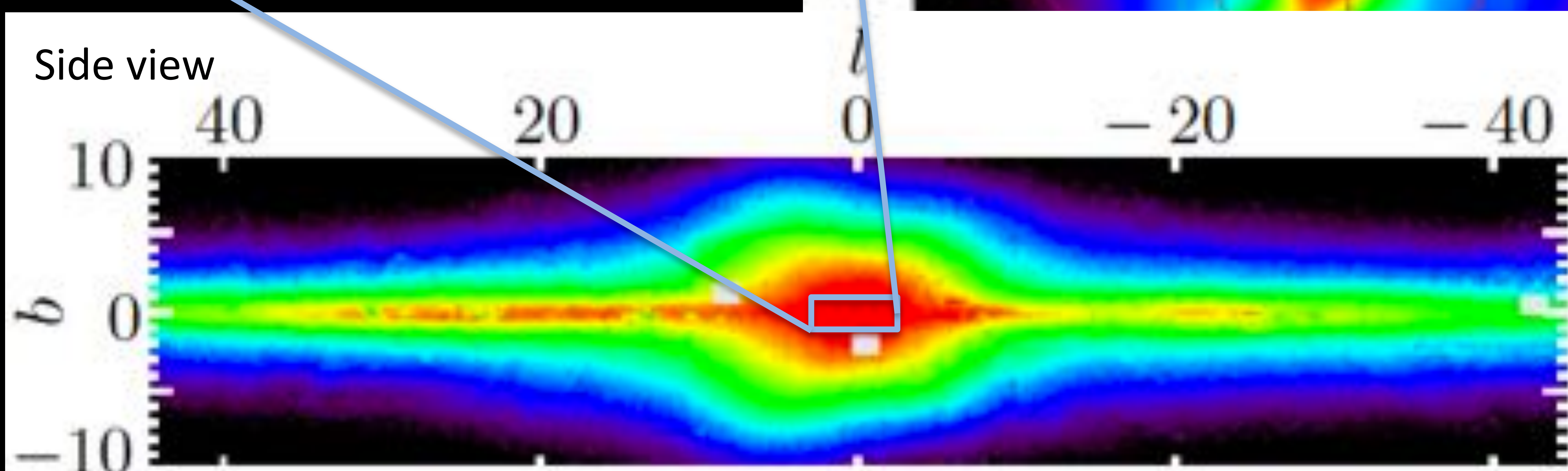

Bland-Hawthorn & Gerhard (2017)

Define a base model

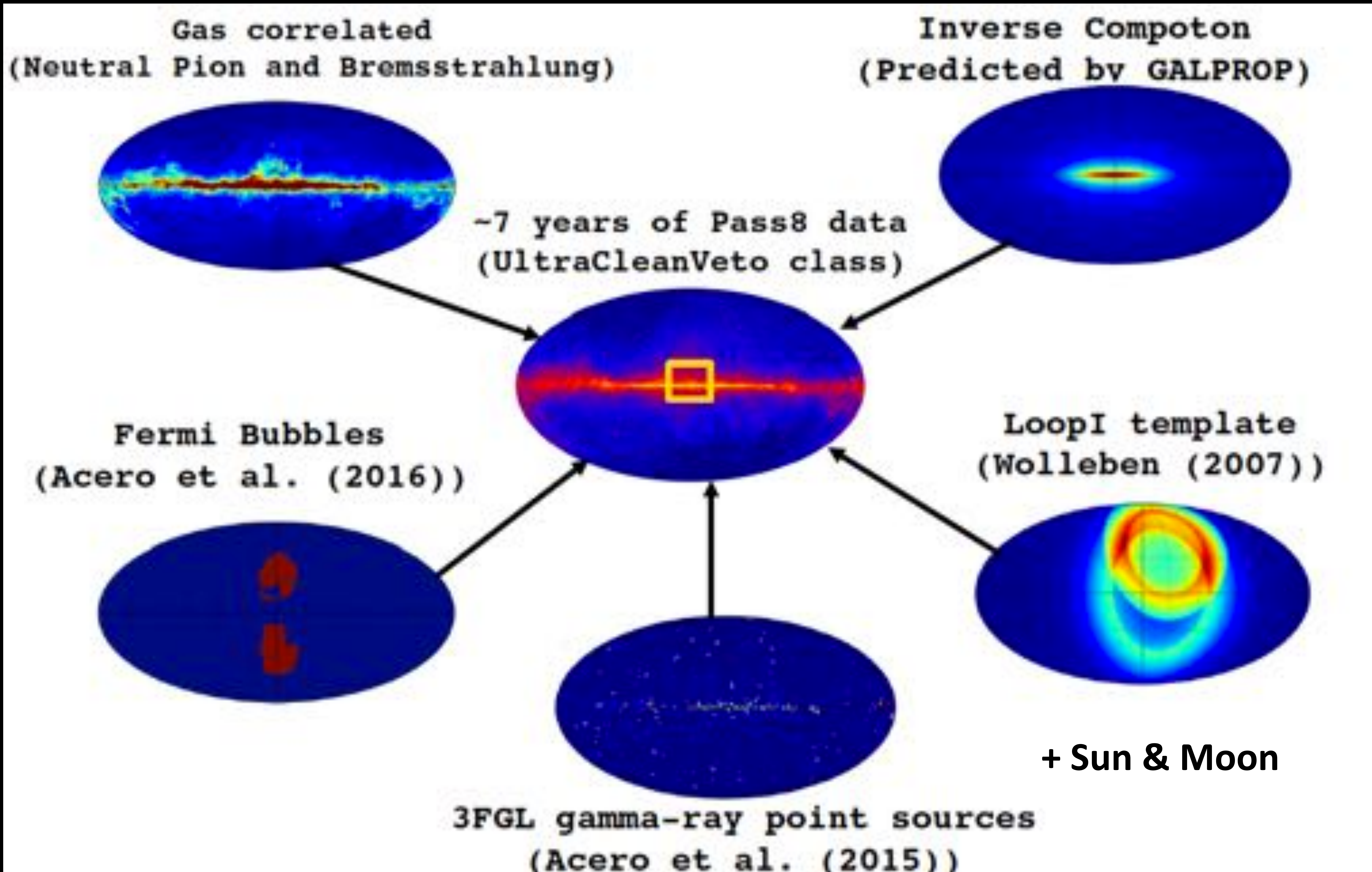

+ Sun & Moon

Add new components systematically

Gas + IC + 3FGL + Loop I + Sun & Moon

Base	Source	$\log(\mathcal{L}_{\rm Base})$	$\log(\mathcal{L}_{\rm Base+Source})$	$\rm TS_{Source}$	σ	Number of source parameters
baseline	FB	-172461.4	-172422.3	78	6.9	19
baseline	NFW-s	-172461.4	-172265.3	392	18.4	19
baseline	Boxy bulge	-172461.4	-172238.7	445	19.7	19
baseline	X-bulge	-172461.4	-172224.1	475	20.5	19
baseline	NFW	-172461.4	-172167.9	587	23.0	19
baseline	NB	-172461.4	-171991.8	939	29.5	19
baseline	NP	-172461.4	-169804.1	5315	55.7	64×19
baseline+NP	FB	-169804.1	-169773.6	61	5.8	19
baseline+NP	NB	-169804.1	-169697.2	214	13.0	19
baseline+NP	Boxy bulge	-169804.1	-169663.7	281	15.3	19
baseline+NP	NFW	-169804.1	-169623.3	362	17.6	19
baseline+NP	X-bulge	-169804.1	-169616.2	376	18.0	19
baseline+NP+Boxy bulge	NFW	-169663.7	-169598.2	131	9.7	19
baseline+NP+Boxy bulge	NB	-169663.7	-169566.0	195	12.4	19
baseline+NP+Boxy bulge+NB	NFW	-169566.0	-169553.3	25	2.7	19
baseline+NP+Boxy bulge+NFW	NB	-169598.2	-169553.3	90	7.6	19
baseline+NP+NFW	Boxy bulge+NB	-169623.3	-169553.0	140	10.0	2×19
baseline+NP+NFW	X-bulge+NB	-169623.3	-169531.0	185	10.8	2×19
baseline+NP+NB	X-bulge	-169697.2	-169542.0	310	16.1	19
baseline+NP+NB	Boxy bulge	-169697.2	-169566.0	262	14.6	19
baseline+NP+NB	NFW	-169697.2	-169599.0	197	12.4	19
baseline+NP+NB+NFW	X-bulge	-169598.9	-169531.0	136	9.9	19
baseline+NP+X-bulge+NB	NFW	-169542.0	-169531.0	22	2.4	19

➔ **NFW detected at low significance when bulge is included**

Macias et al (2018)

Add new components systematically

Gas + IC + 3FGL + Loop I + Sun & Moon

Base	Source	$\log(\mathcal{L}_{\rm Base})$	$\log(\mathcal{L}_{\rm Base+Source})$	$TS_{\rm Source}$	σ	Number of source parameters
baseline	FB	-172461.4	-172422.3	78	6.9	19
baseline	NFW-s	-172461.4	-172265.3	392	18.4	19
baseline	Boxy bulge	-172461.4	-172238.7	445	19.7	19
baseline	X-bulge	-172461.4	-172224.1	475	20.5	19
baseline	NFW	-172461.4	-172167.9	587	23.0	19
baseline	NB	-172461.4	-171991.8	939	29.5	19
baseline	NP	-172461.4	-169804.1	5315	55.7	64×19
baseline+NP	FB	-169804.1	-169773.6	61	5.8	19
baseline+NP	NB	-169804.1	-169697.2	214	13.0	19
baseline+NP	Boxy bulge	-169804.1	-169663.7	281	15.3	19
baseline+NP	NFW	-169804.1	-169623.3	362	17.6	19
baseline+NP	X-bulge	-169804.1	-169616.2	376	18.0	19
baseline+NP+Boxy bulge	NFW	-169663.7	-169598.2	131	9.7	19
baseline+NP+Boxy bulge	NB	-169663.7	-169566.0	195	12.4	19
baseline+NP+Boxy bulge+NB	NFW	-169566.0	-169553.3	25	2.7	19
baseline+NP+Boxy bulge+NFW	NB	-169598.2	-169553.3	90	7.6	19
baseline+NP+NFW	Boxy bulge+NB	-169623.3	-169553.0	140	10.0	2×19
baseline+NP+NFW	X-bulge+NB	-169623.3	-169531.0	185	10.8	2×19
baseline+NP+NB	X-bulge	-169697.2	-169542.0	310	16.1	19
baseline+NP+NB	Boxy bulge	-169697.2	-169566.0	262	14.6	19
baseline+NP+NB	NFW	-169697.2	-169599.0	197	12.4	19
baseline+NP+NB+NFW	X-bulge	-169598.9	-169531.0	136	9.9	19
baseline+NP+X-bulge+NB	NFW	-169542.0	-169531.0	22	2.4	19

→ **NFW detected at low significance when bulge is included**

Macias et al (2018)

Systematics

Gas maps: using the gas maps used by the Fermi Diffuse models yield the same conclusions

Point sources: using none or the 2FIG point source catalog yield the same conclusions

Base	Source	$\log(\mathcal{L}_{\rm Base})$	$\log(\mathcal{L}_{\rm Base+Source})$	$\rm TS_{Source}$	σ	Number of source parameters
baseline+NB+Boxy	NFW	-172005.9	-171999.0	13.8	1.4	19
baseline+NFW	NB+Boxy	-172167.9	-171999.0	337.8	18.3	2 × 19
baseline*	NFW	-173565.0	-172929.2	1272	34.6	19
baseline*+NFW	NB+Boxy	-172929.2	-172533.0	792.4	28.2	2 × 19
baseline*+NB+Boxy	NFW	-172547.4	-172533.0	28.8	3.0	19
baseline	2FIG	-172461.4	-170710.5	3501	37.3	81 × 19
baseline+2FIG	Boxy	-170710.5	-170536.3	348.4	18.7	19
baseline+2FIG	NFW	-170710.5	-170484.6	452	19.9	19
baseline+2FIG	NB	-170710.5	-170470.5	480	20.6	19
baseline+2FIG+NB	NFW	-170470.5	-170387.8	165	11.1	19
baseline+2FIG+NB	Boxy	-170470.5	-170317.2	306.6	17.5	19
baseline+2FIG+NB+Boxy	NFW	-170317.2	-170313.5	7.4	0.5	19

Galactic plane mask: using a |b| < 1 deg mask yields the same conclusions

baseline	NFW	-430824.6	-430696.9	255	14.4	19
baseline	Boxy	-430824.6	-430626.1	397	18.5	19
baseline	NP	-430824.6	-430189.9	1269	35.6	22 × 19
baseline+NP	NFW	-430189.9	-430097.0	186	12.0	19
baseline+NP	Boxy	-430189.9	-430035.8	308	16.1	19
baseline+NP+Boxy	NFW	-430035.8	-430026.3	19	2.0	19

Bulge preferred over spherical symmetry

Bulge over NFW²

When a bulge model is included, the detection of NFW² falls ($\sigma < 3$) while bulge significance is $\sigma > 10$.

This is robust to

- Point sources used
- Diffuse emission models used
- Galactic mask

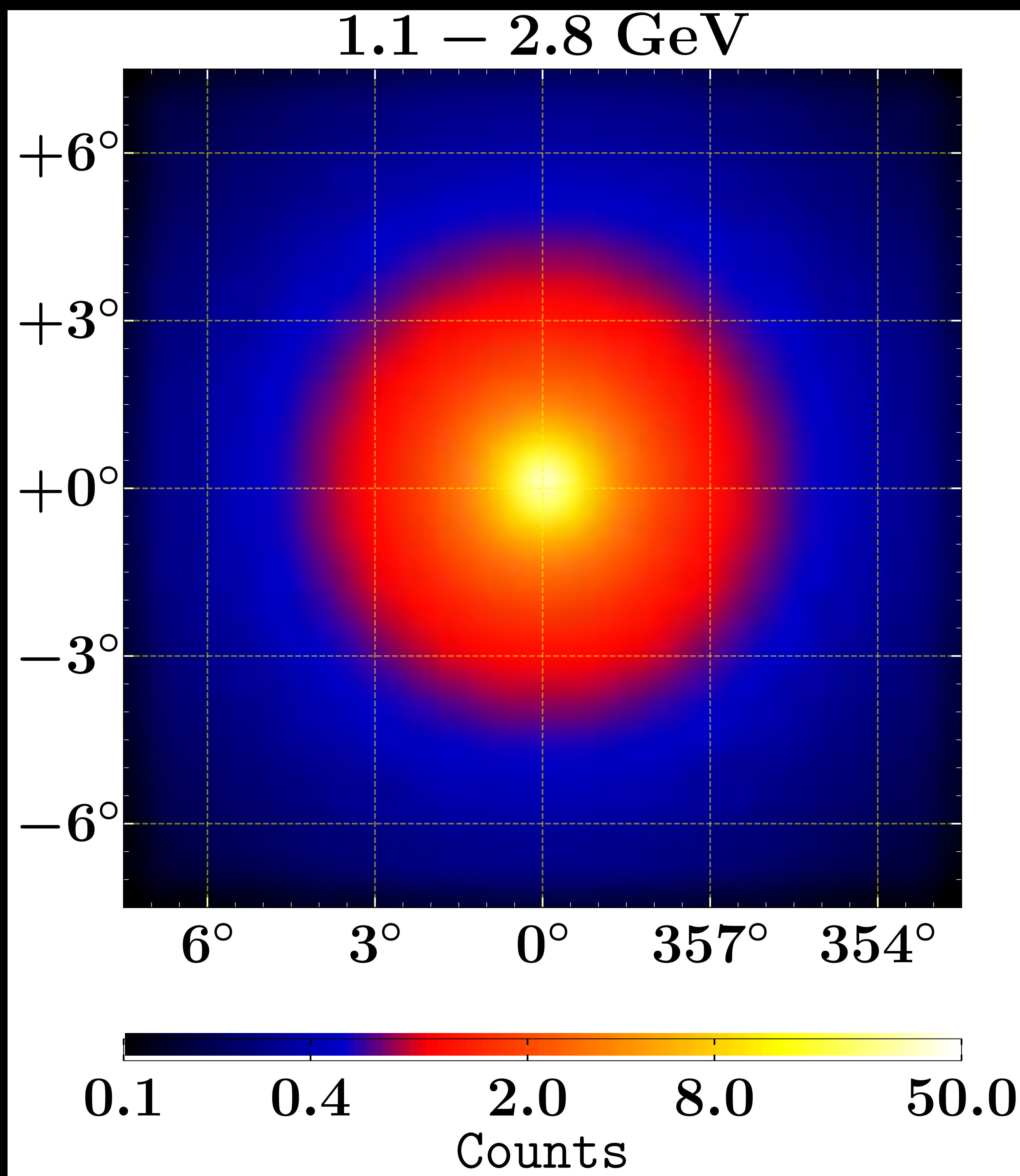

<<

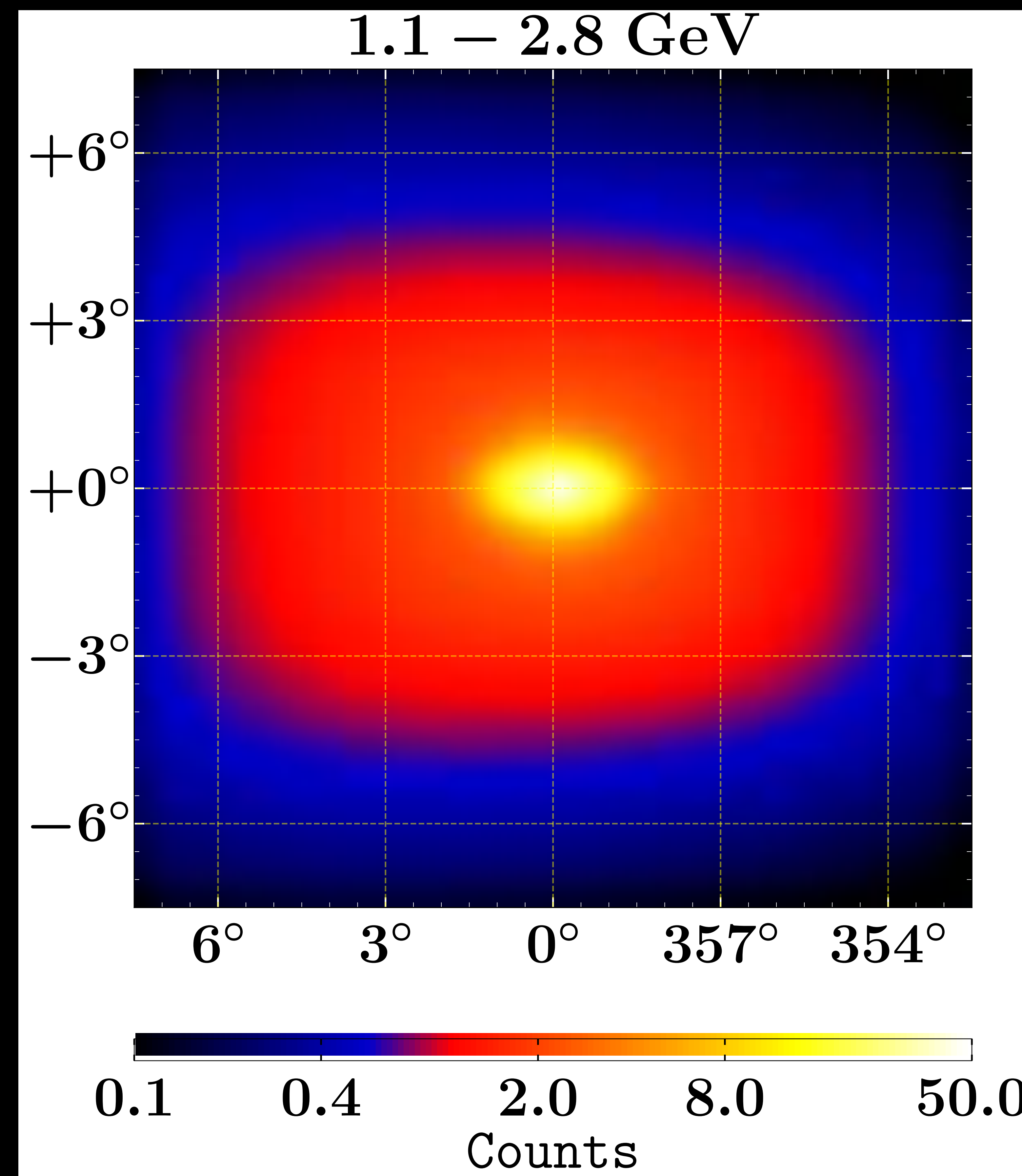

SkyFACT : a hybrid approach

SkyFACT = **Sky F**actorization with **A**daptive **C**onstrained **T**emplates
Hybrid method to study diffuse gamma rays that combines adaptive spatial-spectral template regression and image reconstruction.

Storm et al (2017)

$$\phi_{pb} = \sum_k T_p^{(k)} \tau_p^{(k)} \cdot S_b^{(k)} \sigma_b^{(k)} \cdot \nu^{(k)}$$

Modulated by nuisance parameters τ, σ, ν

Spatial template   Spectral template

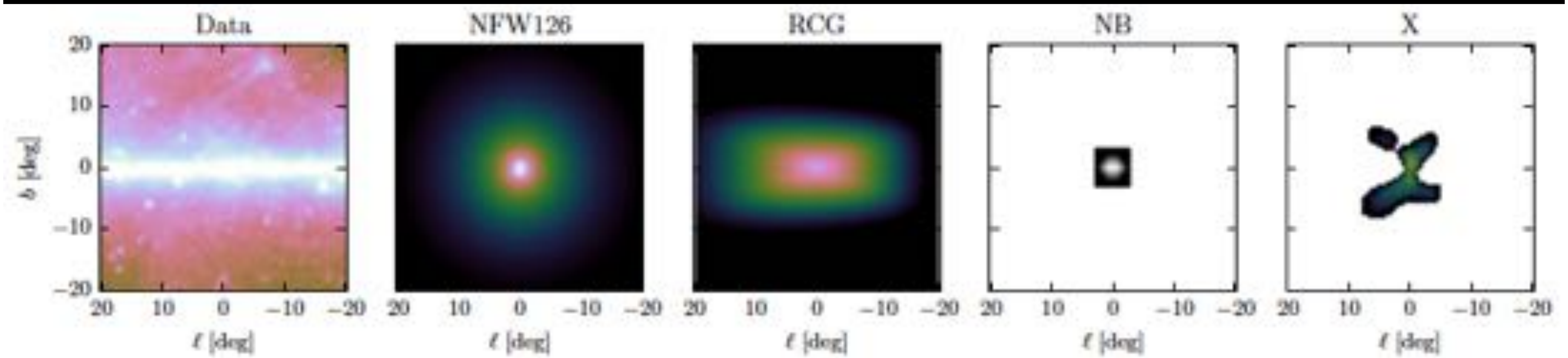

Bartels et al (2017)

Same conclusions from SkyFACT analysis

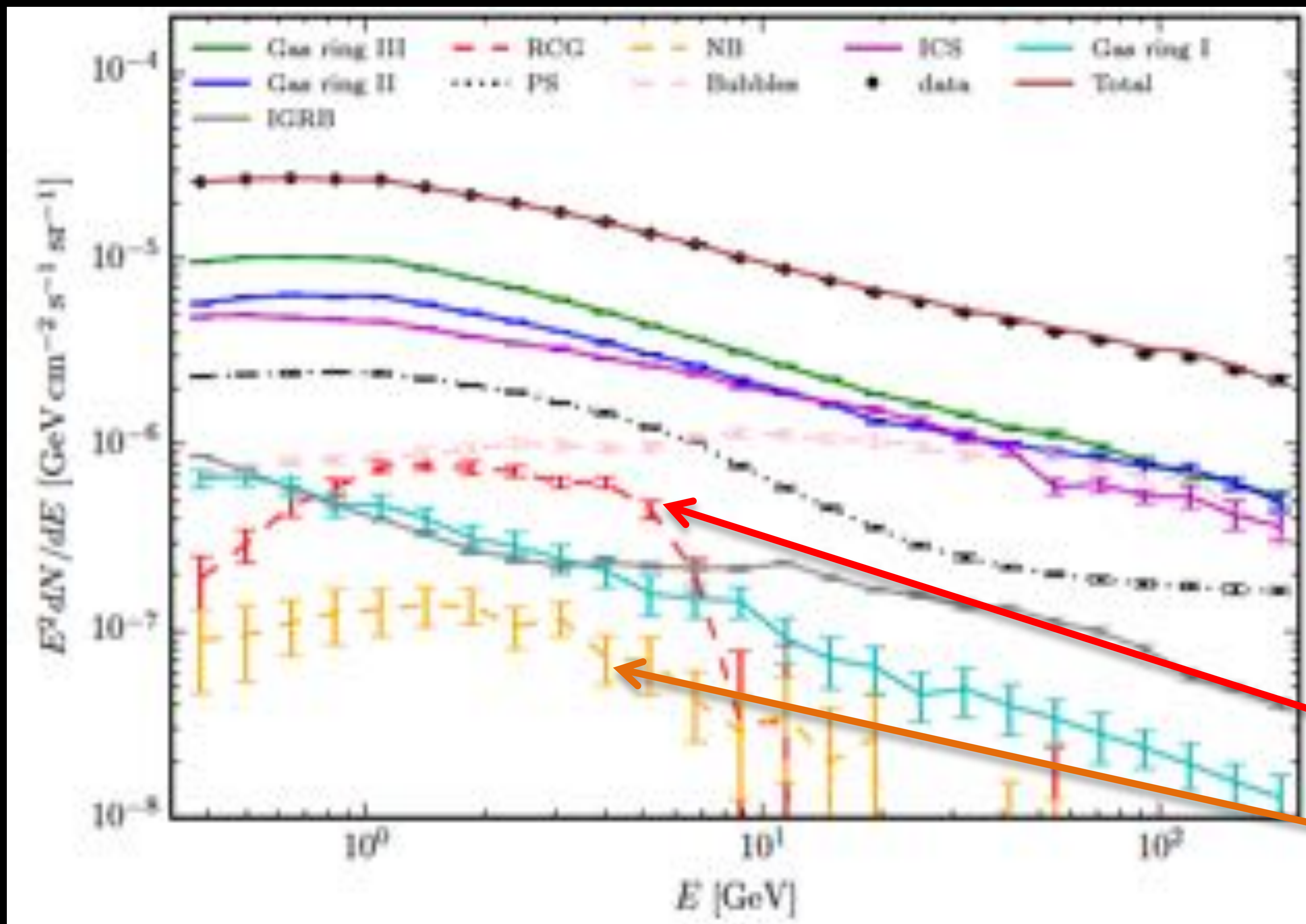

Fit in central 40x180 degrees, which facilitates the fitting of gas template rings (x3) and provides leverage to disentangle components.

Regularization by modulation parameters account for small-scale model inaccuracies.

Boxy bulge

Nuclear bulge

We demonstrated that the stellar bulge model provides a significantly better fit ($> 10\sigma$) to the data than the DM-emission related Einasto or contracted NFW profiles. Hence the GCE appears to simply trace stellar mass in the bulge, not the dark matter density squared (although the actual DM profile is sufficiently uncertain that this possibility cannot be entirely excluded). What

Bartels et al (2017)

1. Spectral information
2. Photon count statistics
3. Spatial morphology

Motivate sub-threshold sources connected to the stars of the bulge

…but how do astrophysical explanations fare?

Observations Do Not Indicate that Pulsars Produce the Galactic Center Excess

Tim Linden

CCAPP Postdoctoral Fellow
Center for Cosmology and Astro-Particle Physics
The Ohio State University

CCAPP
The Ohio State University

Observations Do Not Indicate that Pulsars Produce the Galactic Center Excess

1.) Difficulties in observing sub-threshold point sources.

2.) Issues in the 2FIG Catalog

2.) Peculiarities in the derived population.

3.) Alternative results from wavelet analyses

Observations Do Not Indicate that Pulsars Produce the Galactic Center Excess

1.) Different background models lead to different answers:

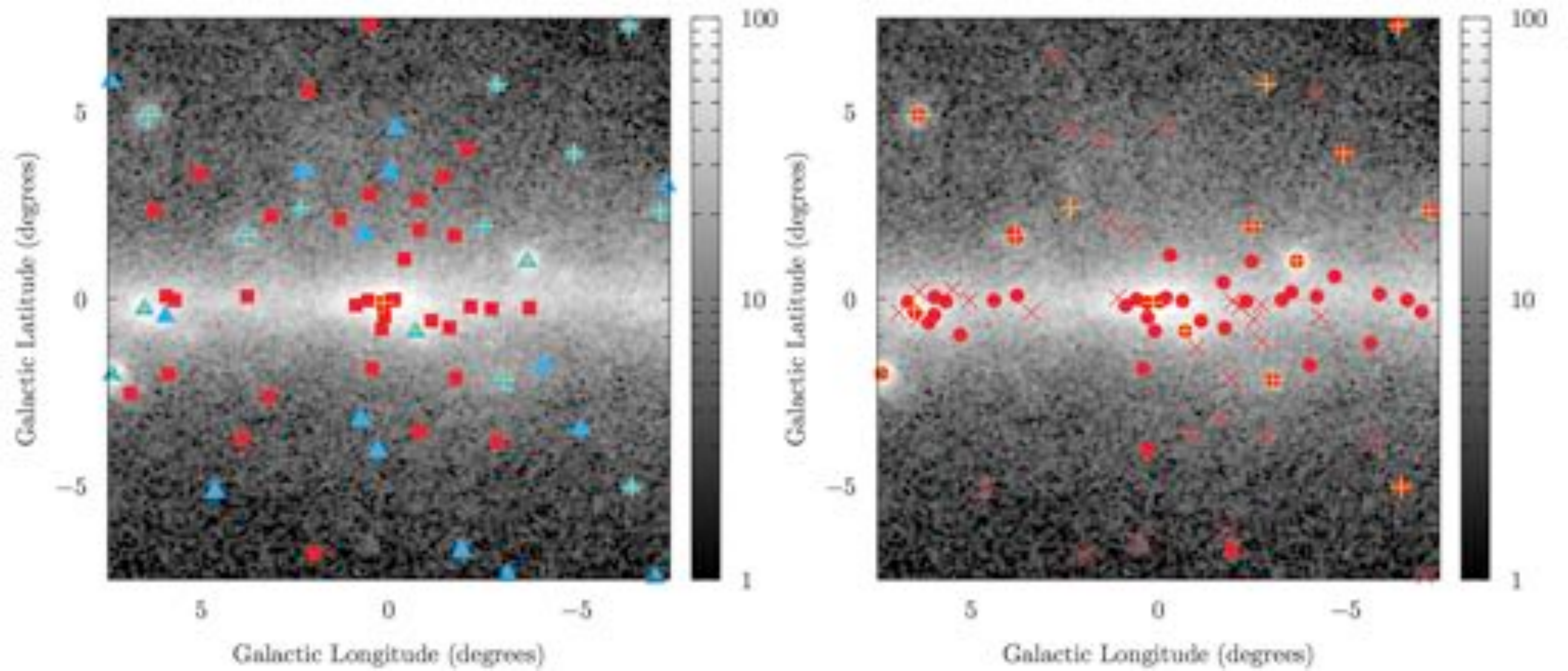

Fermi-LAT Collaboration (2015; 1511.02938)

Observations Do Not Indicate that Pulsars Produce the Galactic Center Excess

1.) Different background models lead to different answers:

White circles and squares show PS that are detected at more than 7σ in one catalog, but not detected in the other.

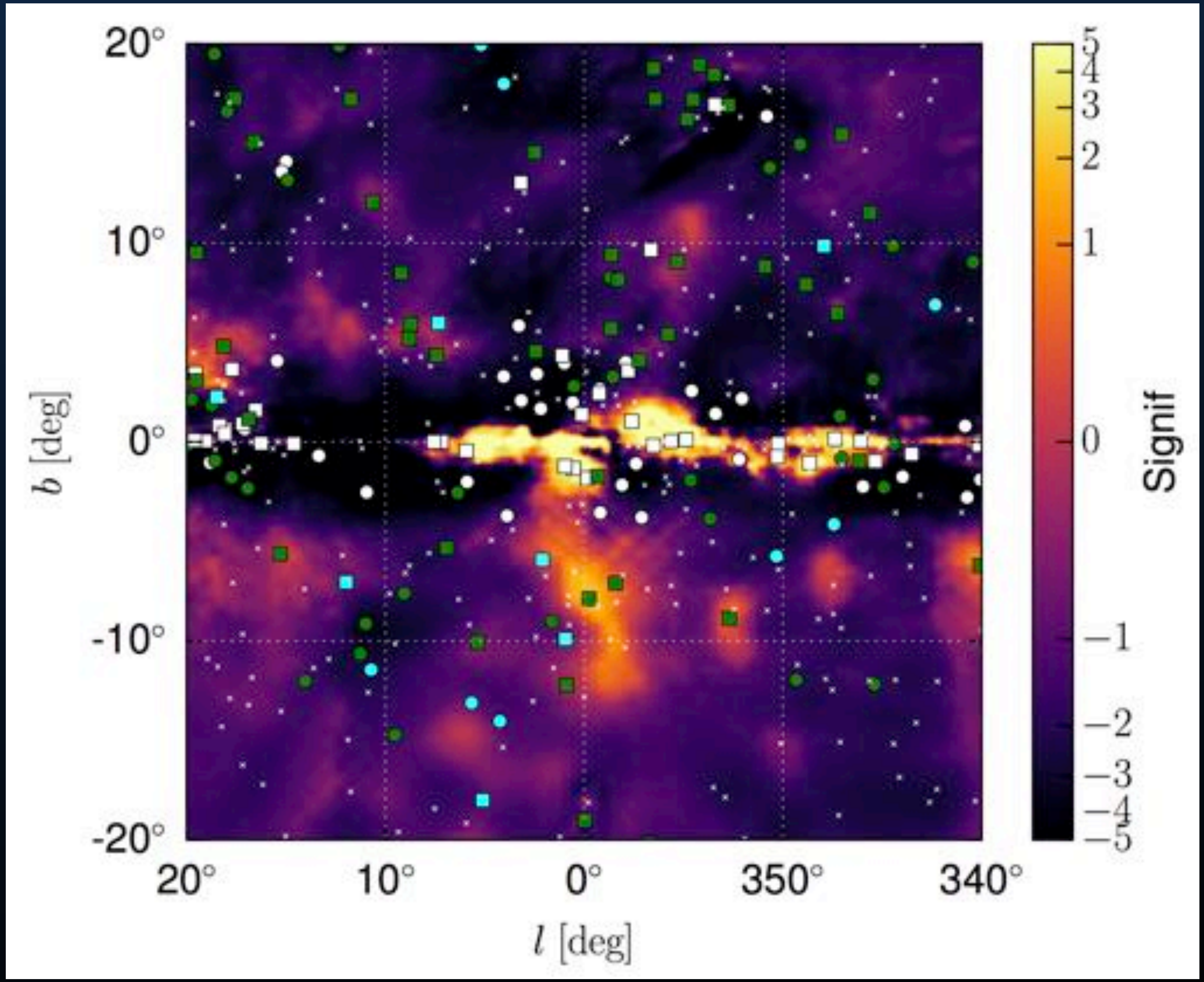

Fermi-LAT Collaboration (2017; 1705.00009)

Observations Do Not Indicate that Pulsars Produce the Galactic Center Excess

Not just statistics - also different global morphologies.

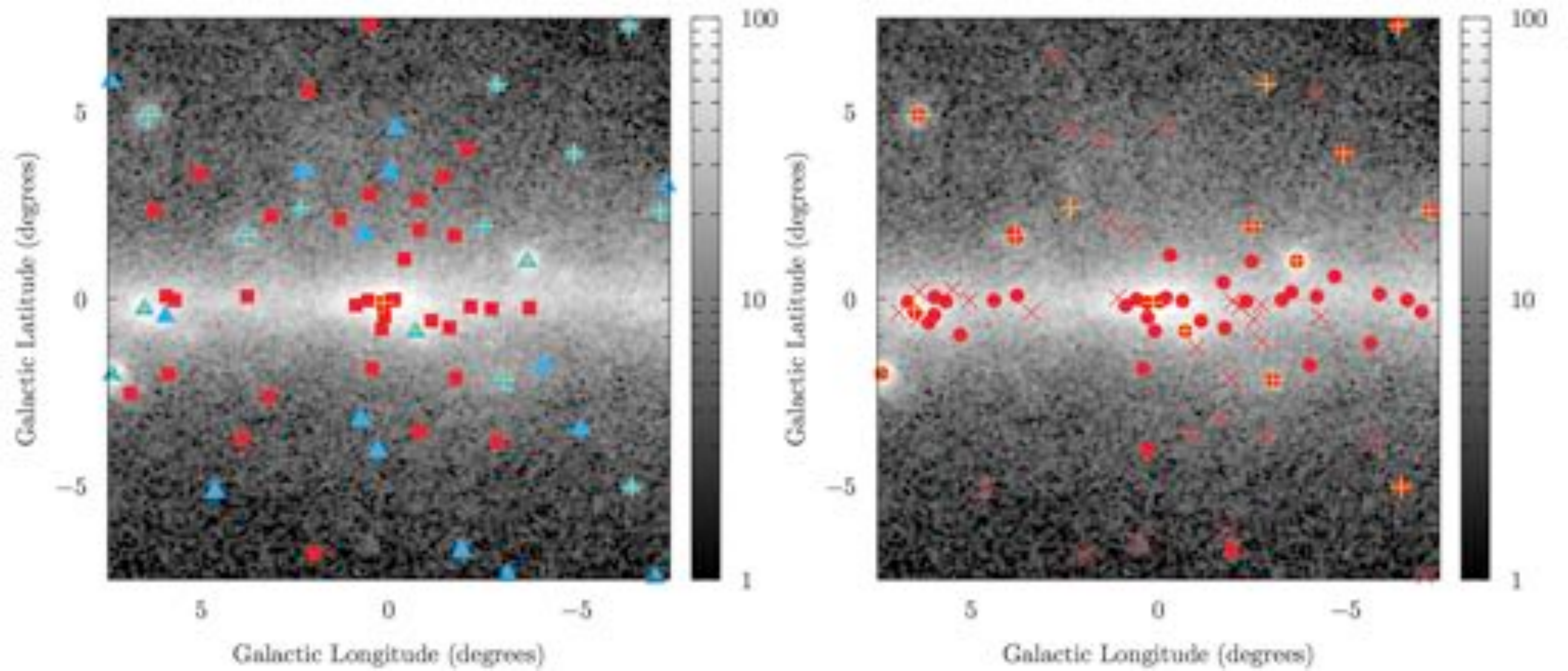

Fermi-LAT Collaboration (2015; 1511.02938)

Observations Do Not Indicate that Pulsars Produce the Galactic Center Excess

Moreover - none of these maps is close to "correct"

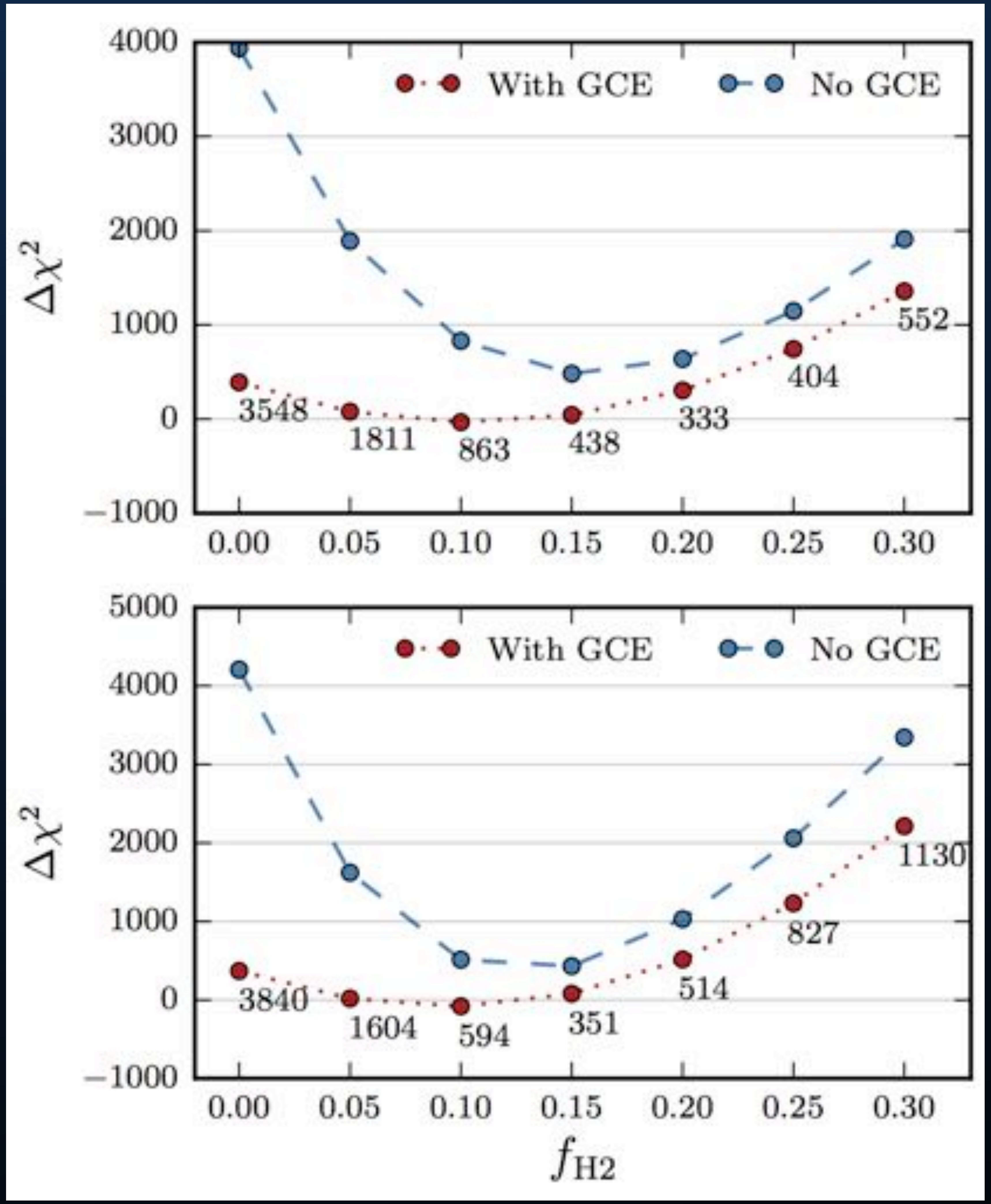

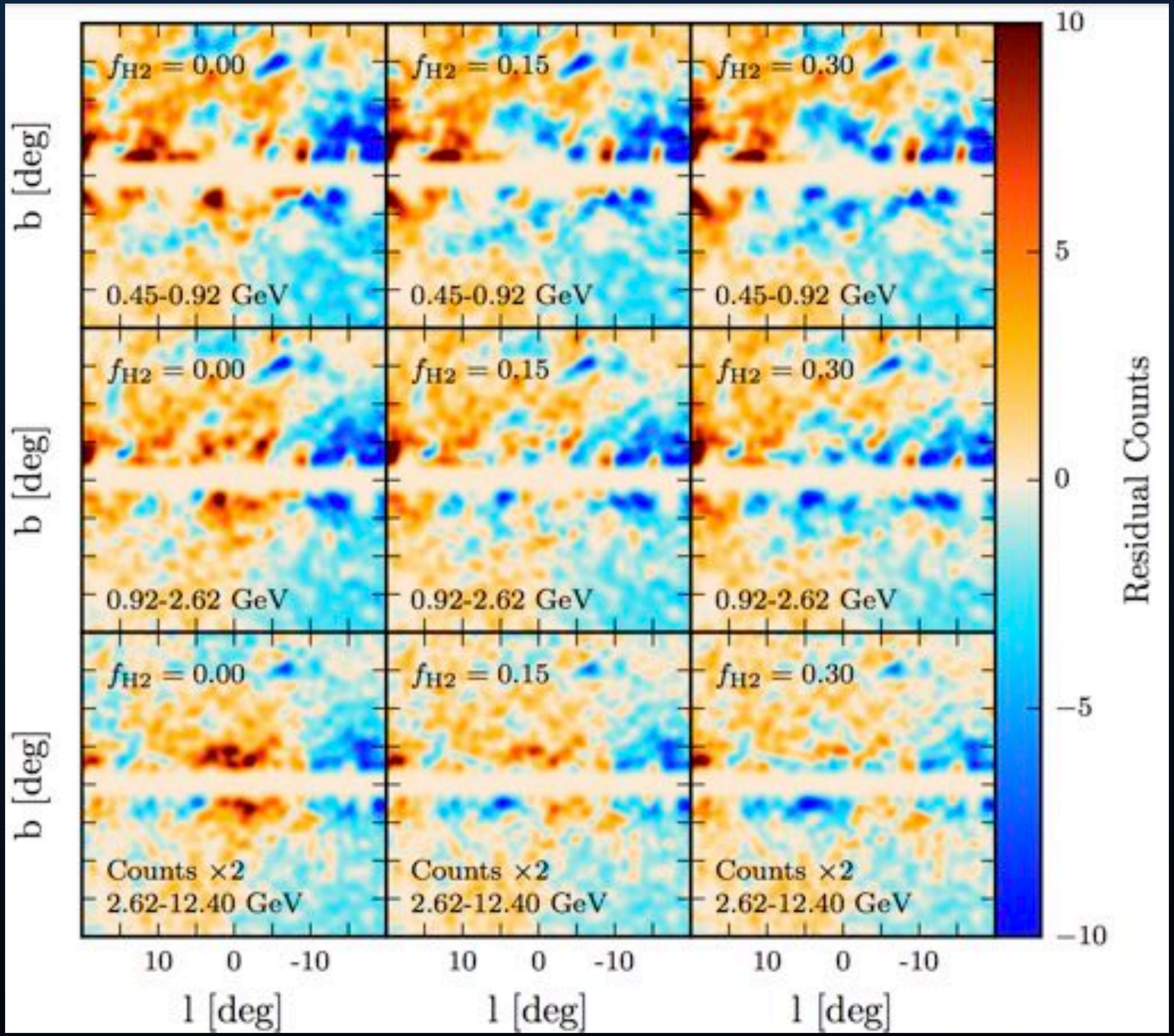

Carlson, TL & Profumo (2016; 1603.06584)

NPTF and Wavelet Analyses

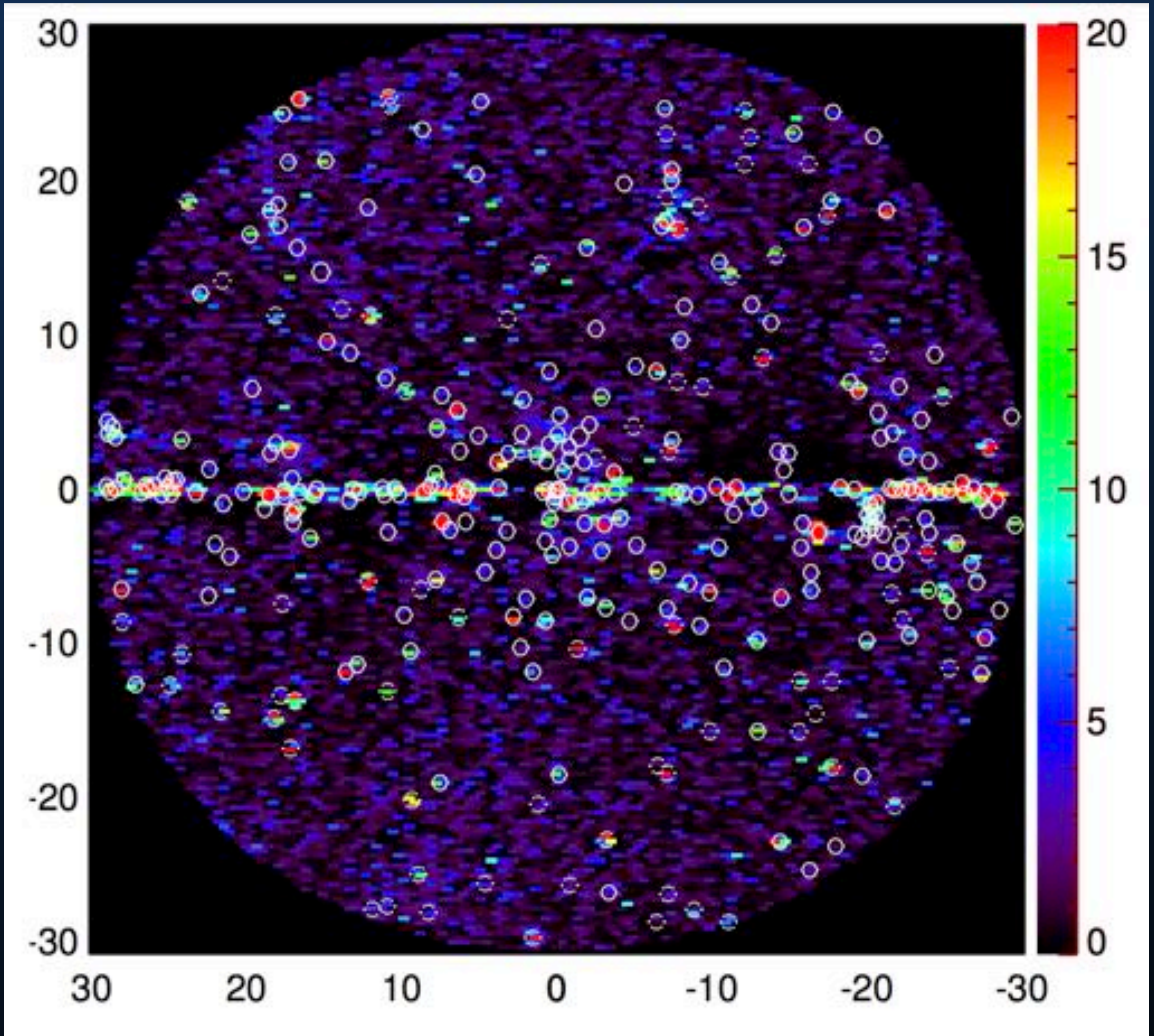

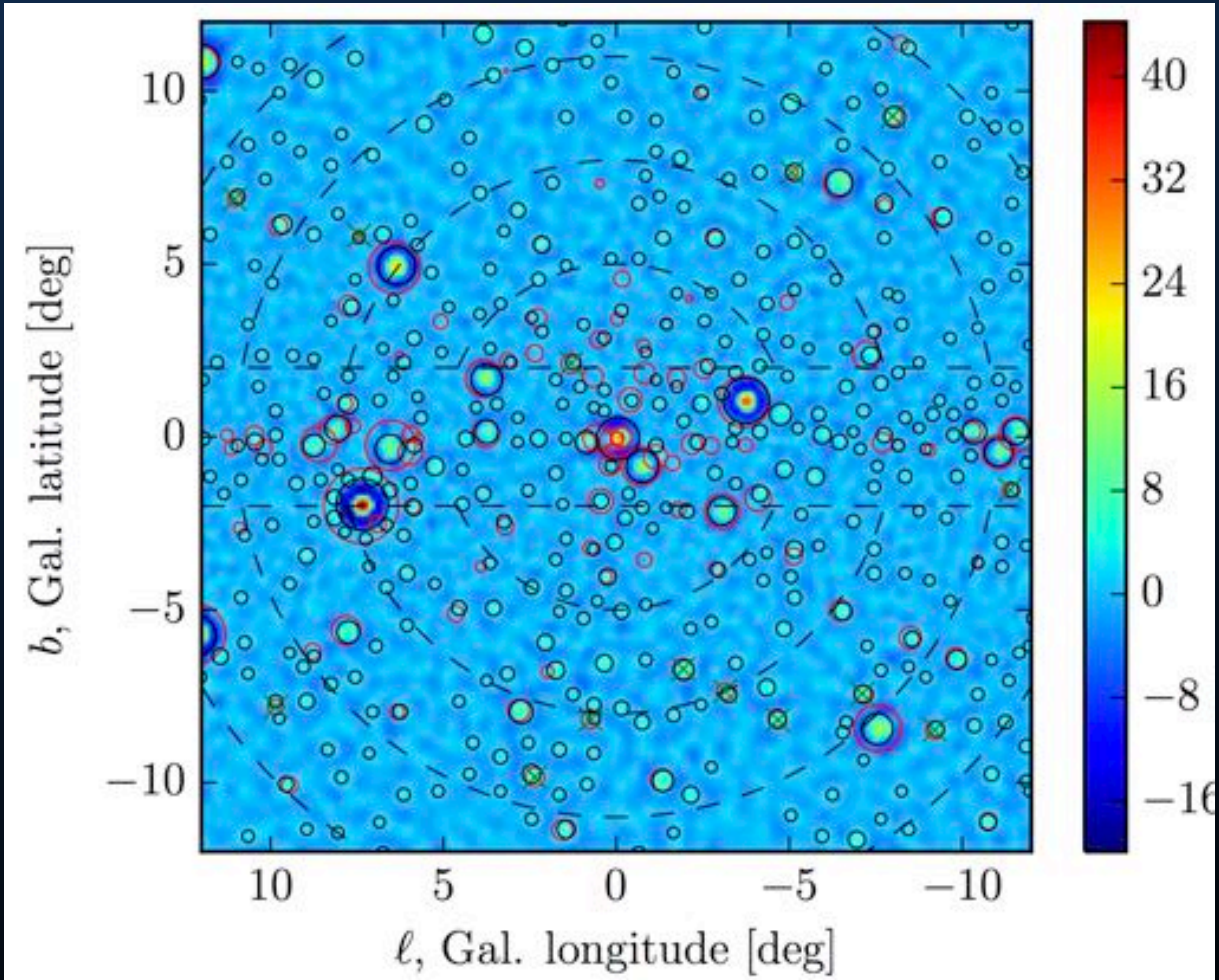

Lee et al. (2016; 1506.05124)

Bartels et al. (2016; 1506.05104)

Wavelets Compared to the Full Residual

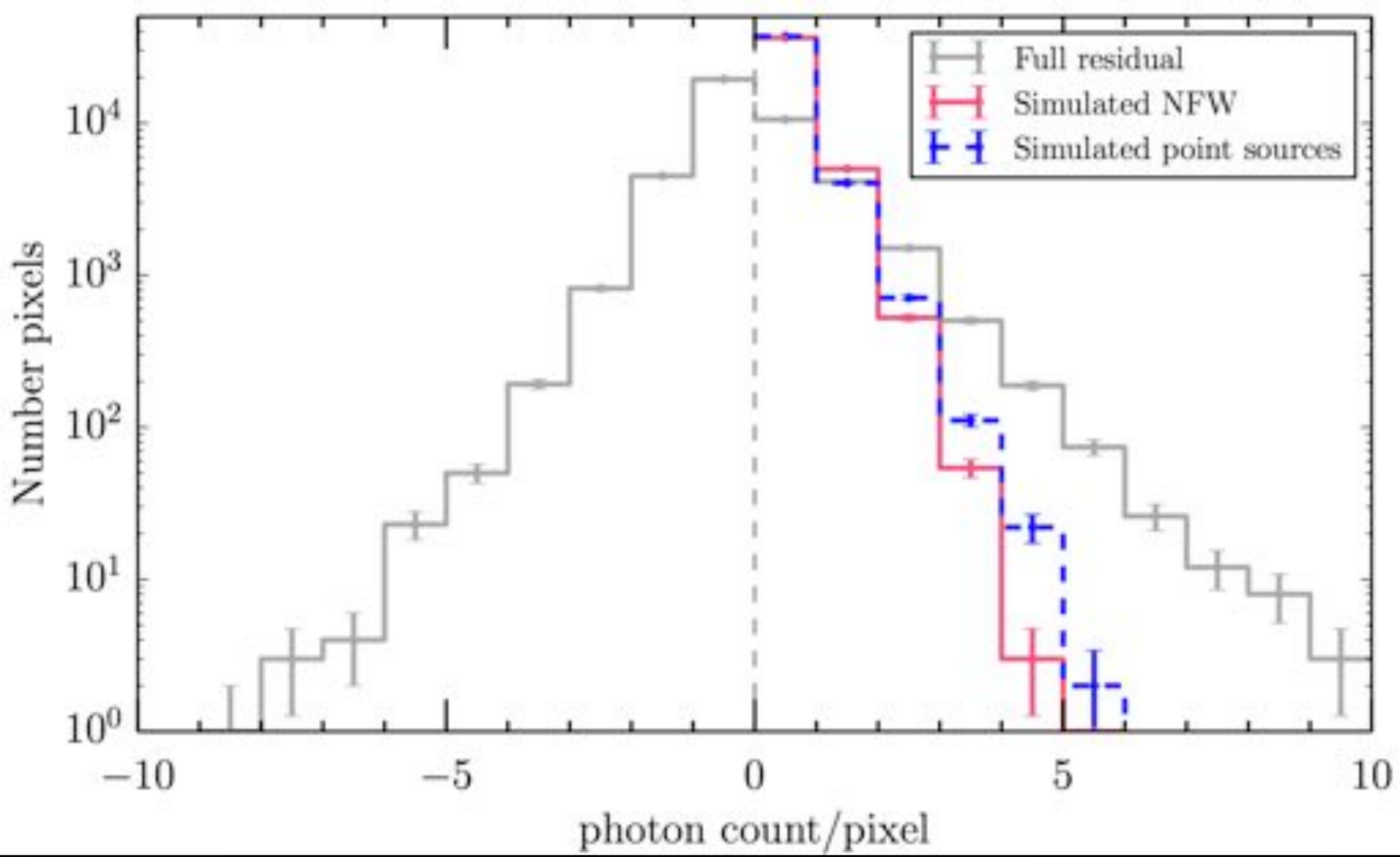

NPTF and Wavelet Analyses

A new wavelet analysis splits the GCE region into several ROIs, where the wavelet components operate independently.

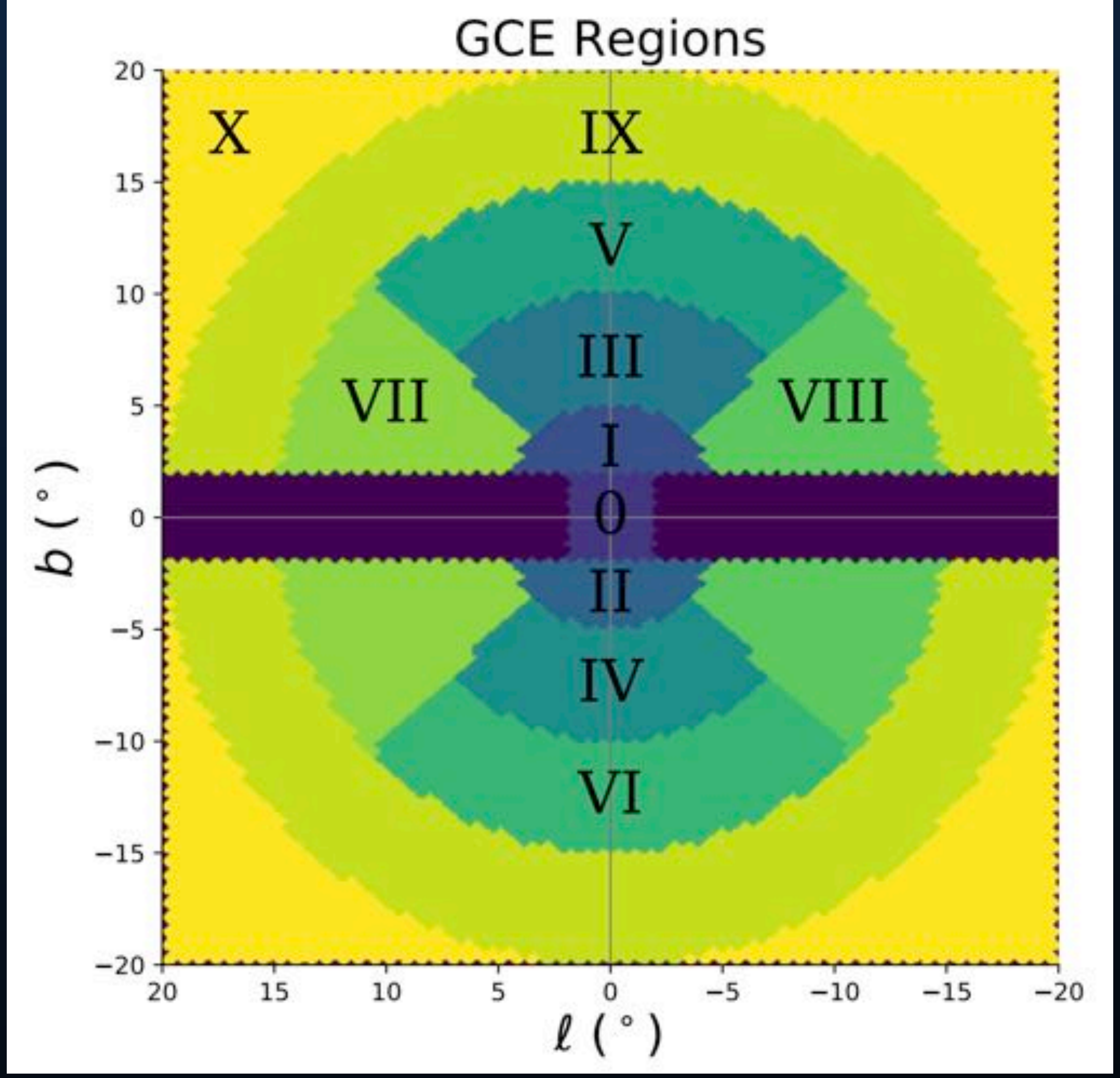

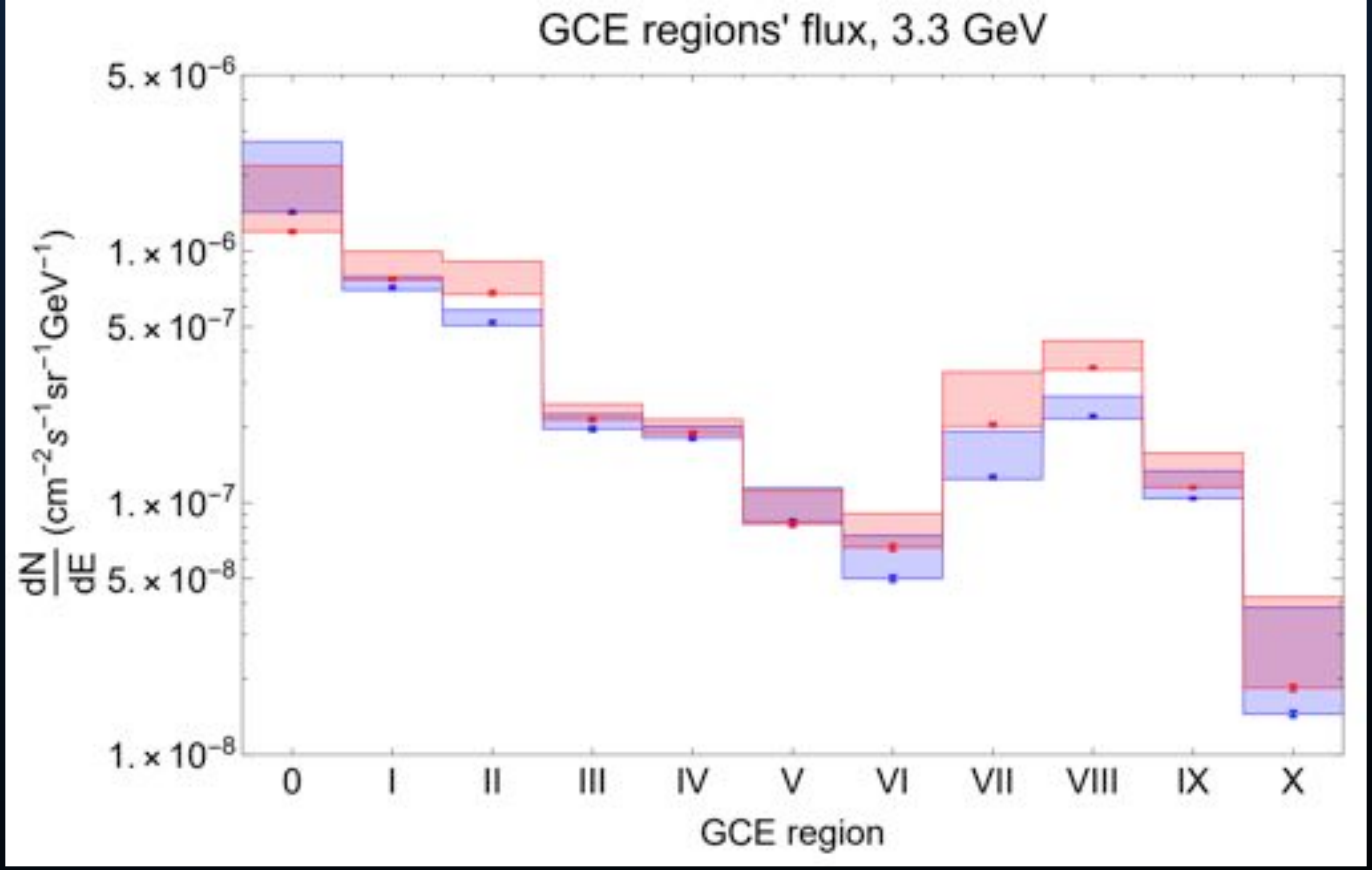

Balaji et al. (1803.01952)

NPTF and Wavelet Analyses

Blue (total power in GCE), Red (power in GCE at scales larger than 4º.

Significant negative point source power near the Galactic plane.

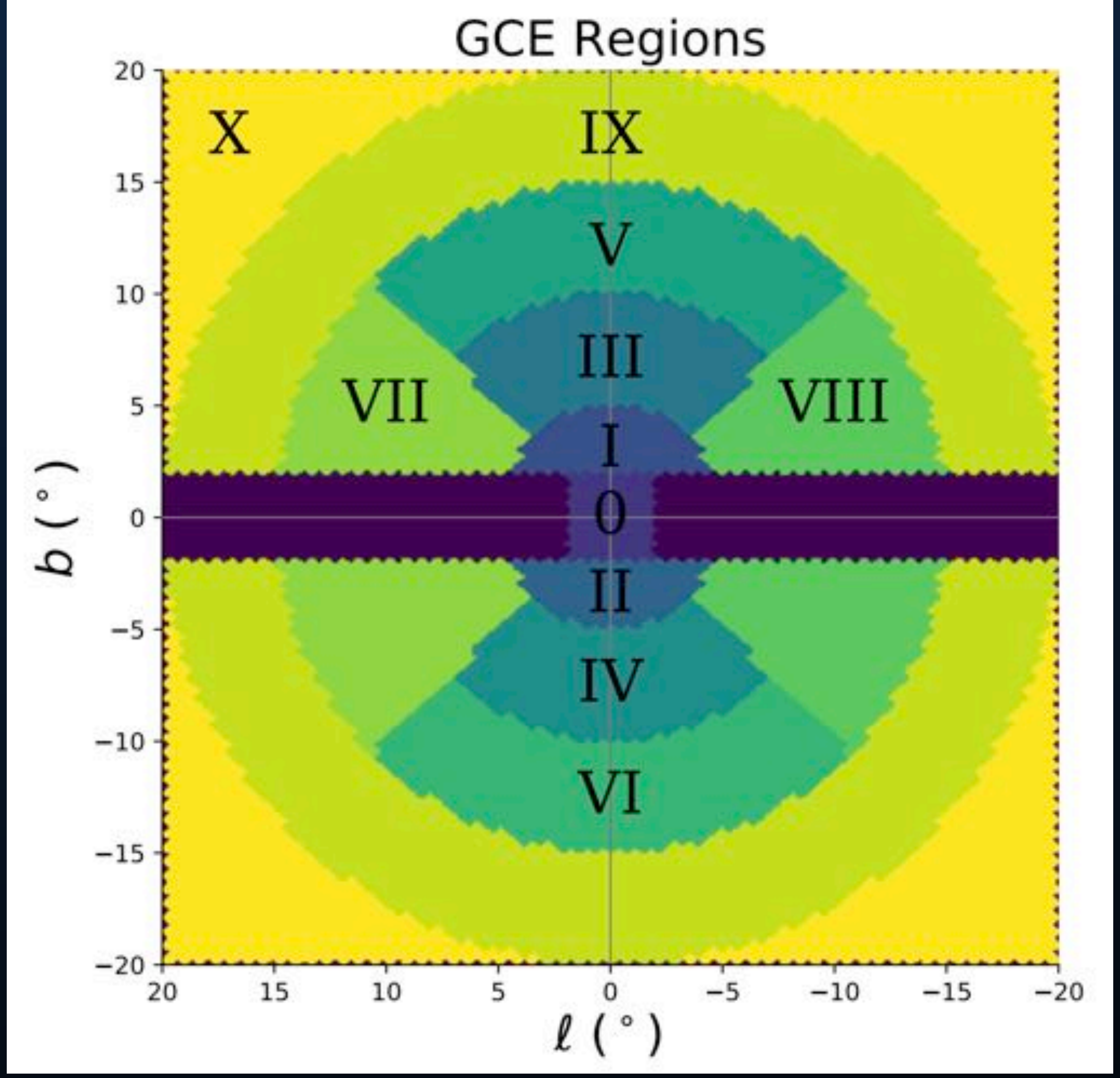

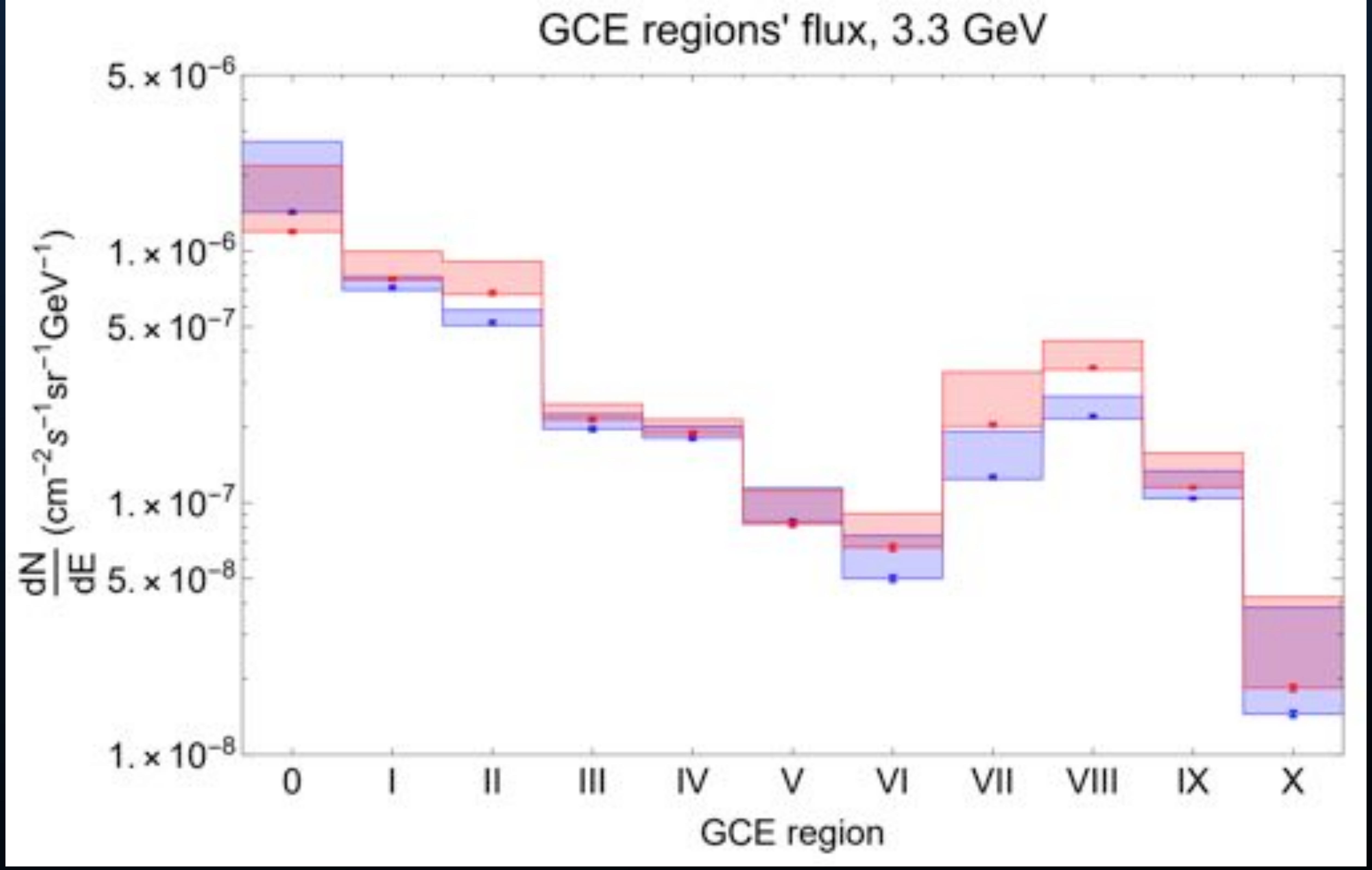

Balaji et al. (1803.01952)

NPTF and Wavelet Analyses

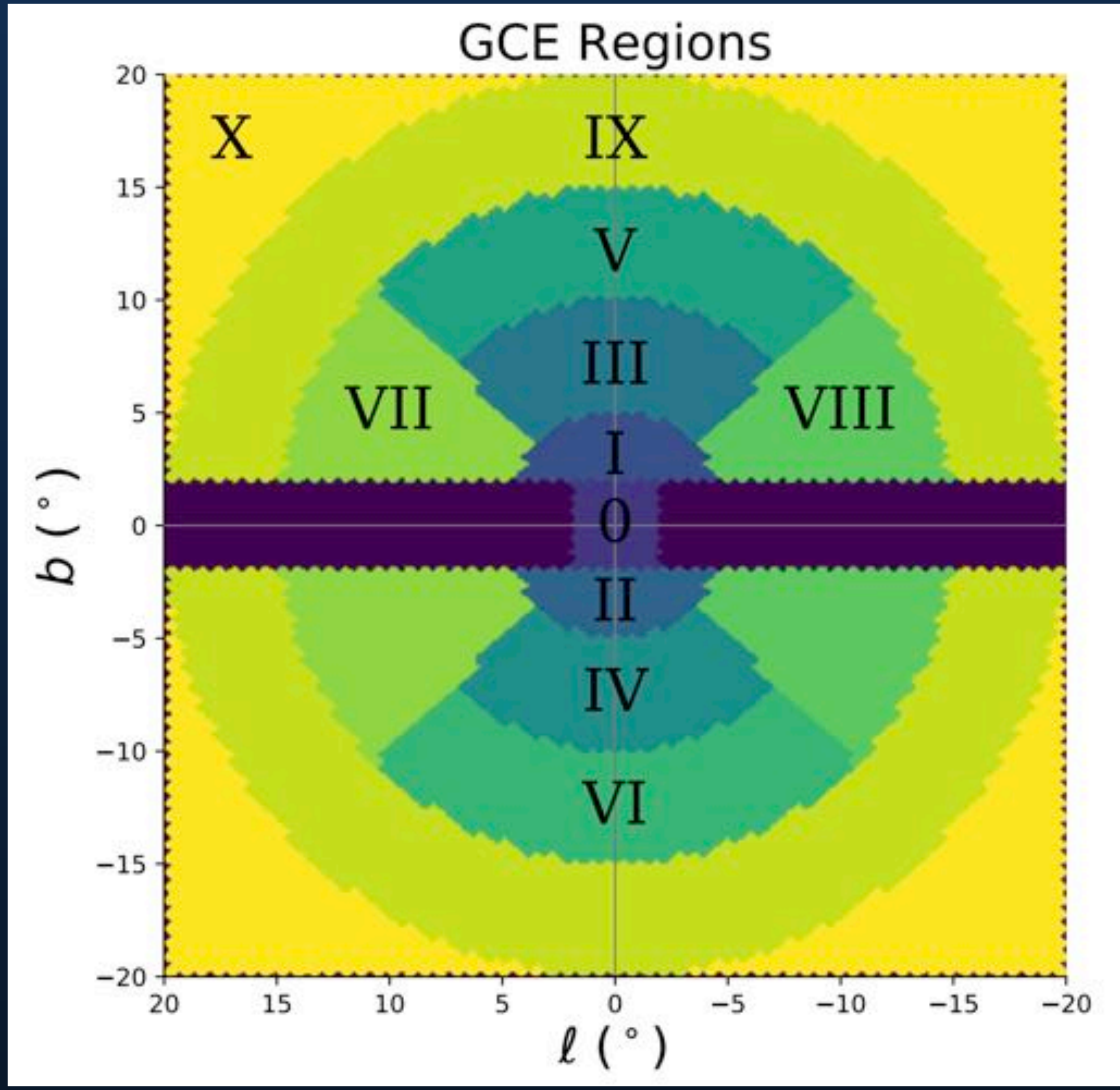

Regions VII and VIII are the easiest to understand and compare to, since they are removed from the center, far from the Bubbles, and in these parts of the sky point sources from the Galactic disk are expected to be relatively most dominant. At 1.5 GeV and above, in these two regions we find that ∼30–50% of the total ($1 \leq j \leq 9$) emission is in the first two wavelet scales, and moreover the first two wavelet scales contribute *negatively*. There are 1.2 3FGL point sources per deg^2 on average in these two windows. This is still higher than the average of 1.02 3FGL point sources per deg^2 along the two stripes of $2° \leq |b| \leq 5°$ extending at all longitudes: Regions VII and VIII are rich in detected point sources. Only Regions II and VI have a similar ∼ 30% of their emission in the first two wavelet scales, which is also negative. The magnitude and the sign of this small scale contribution is intriguing. The negative sign in the first two wavelet levels for the regions near the Galactic center and Galactic disk means that unphysical flux has been imparted to the templates on small angular scales at intermediate angular distances from the Galactic center. This is suggestive either of mismodelled bremsstrahlung and pion emission or the inclusion of spurious point sources near the galactic center. We note that Region 0 does not suffer from a similarly large negative contribution at small angular scales. This may be an indication of the large positive contribution from the GCE, or an issue with the procedure to determine the point-source maps.

Balaji et al. (1803.01952)

NPTF and Wavelet Analyses

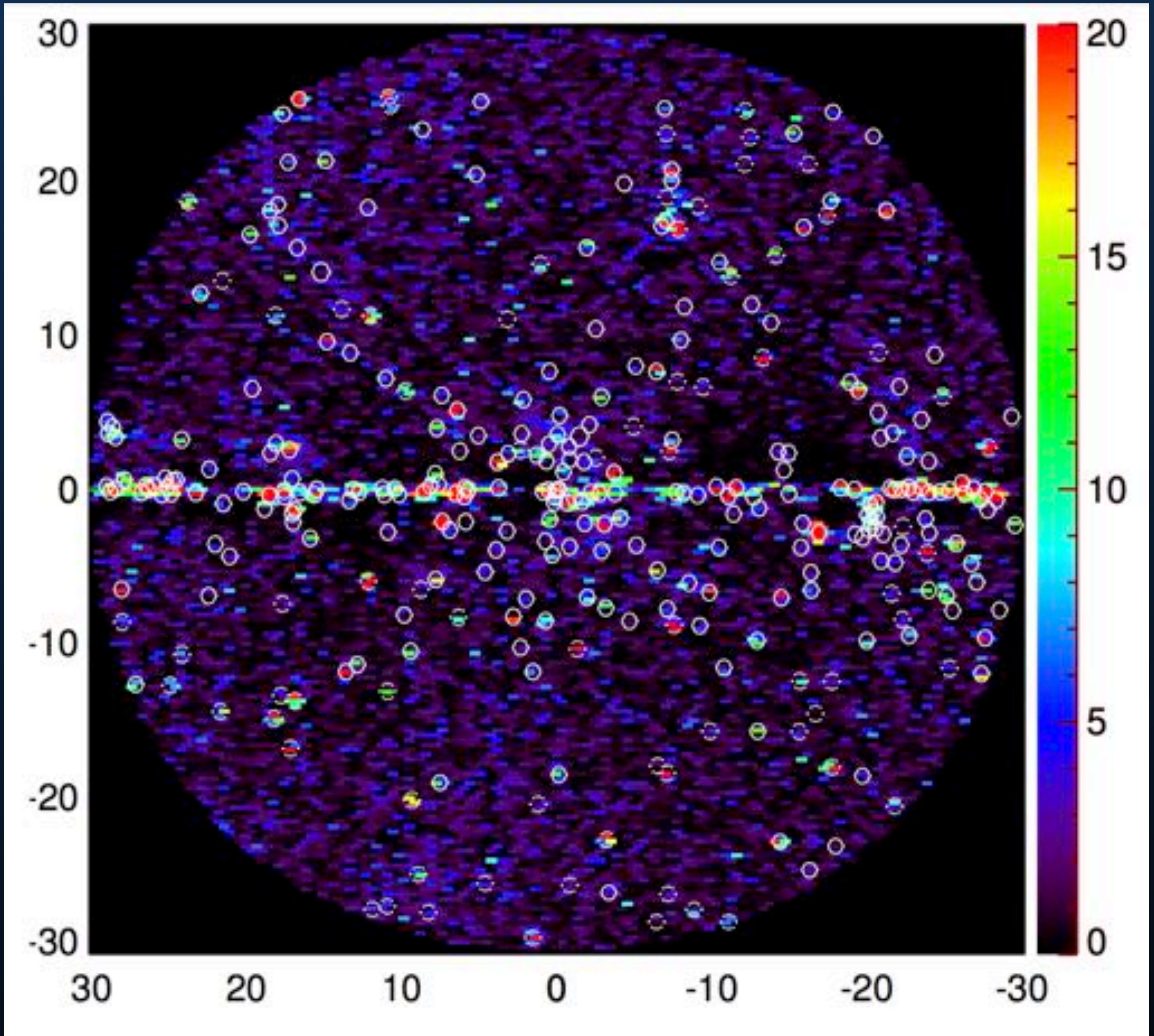

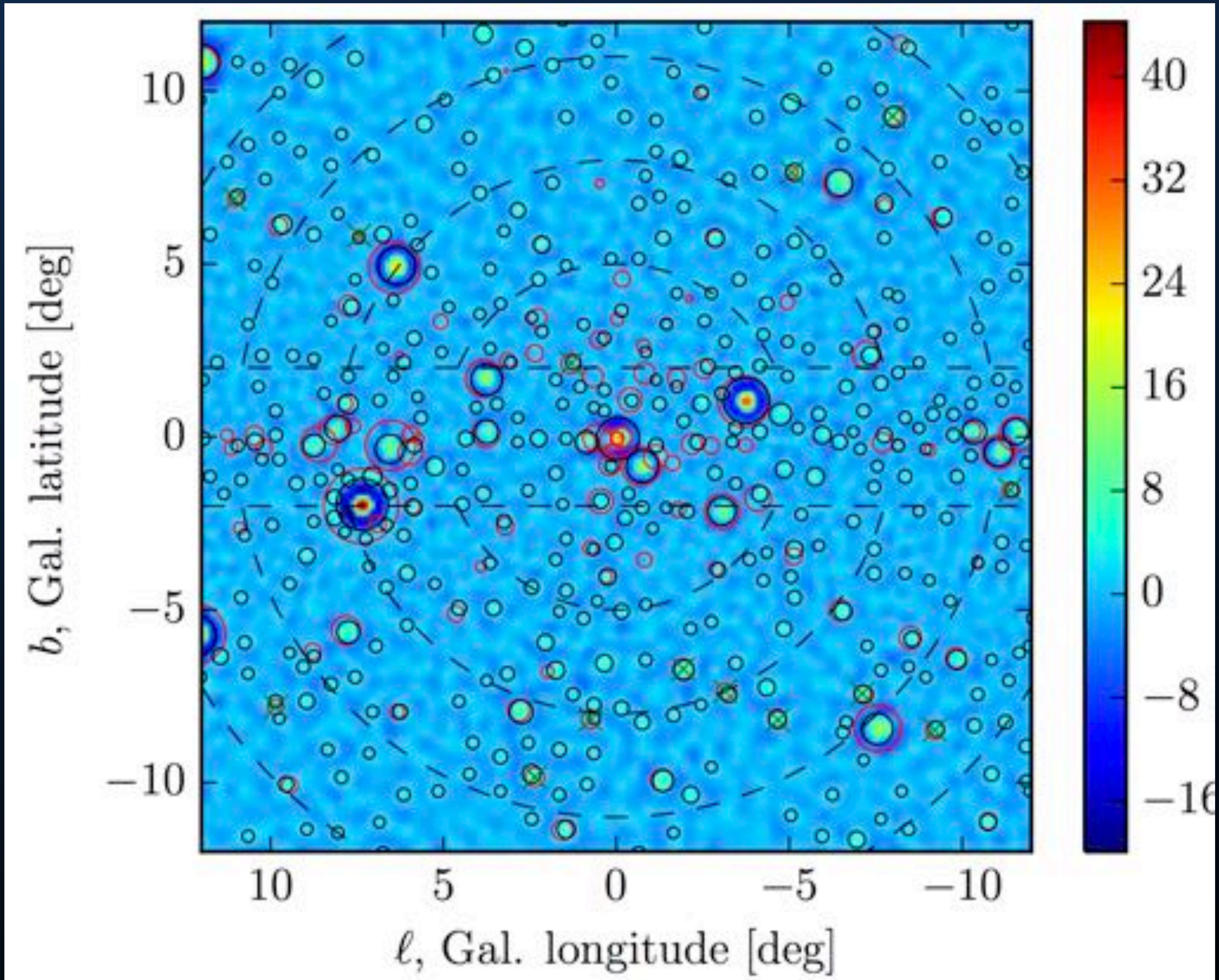

Lee et al. (2016; 1506.05124)

Bartels et al. (2016; 1506.05104)

NPTF and Wavelet Analyses

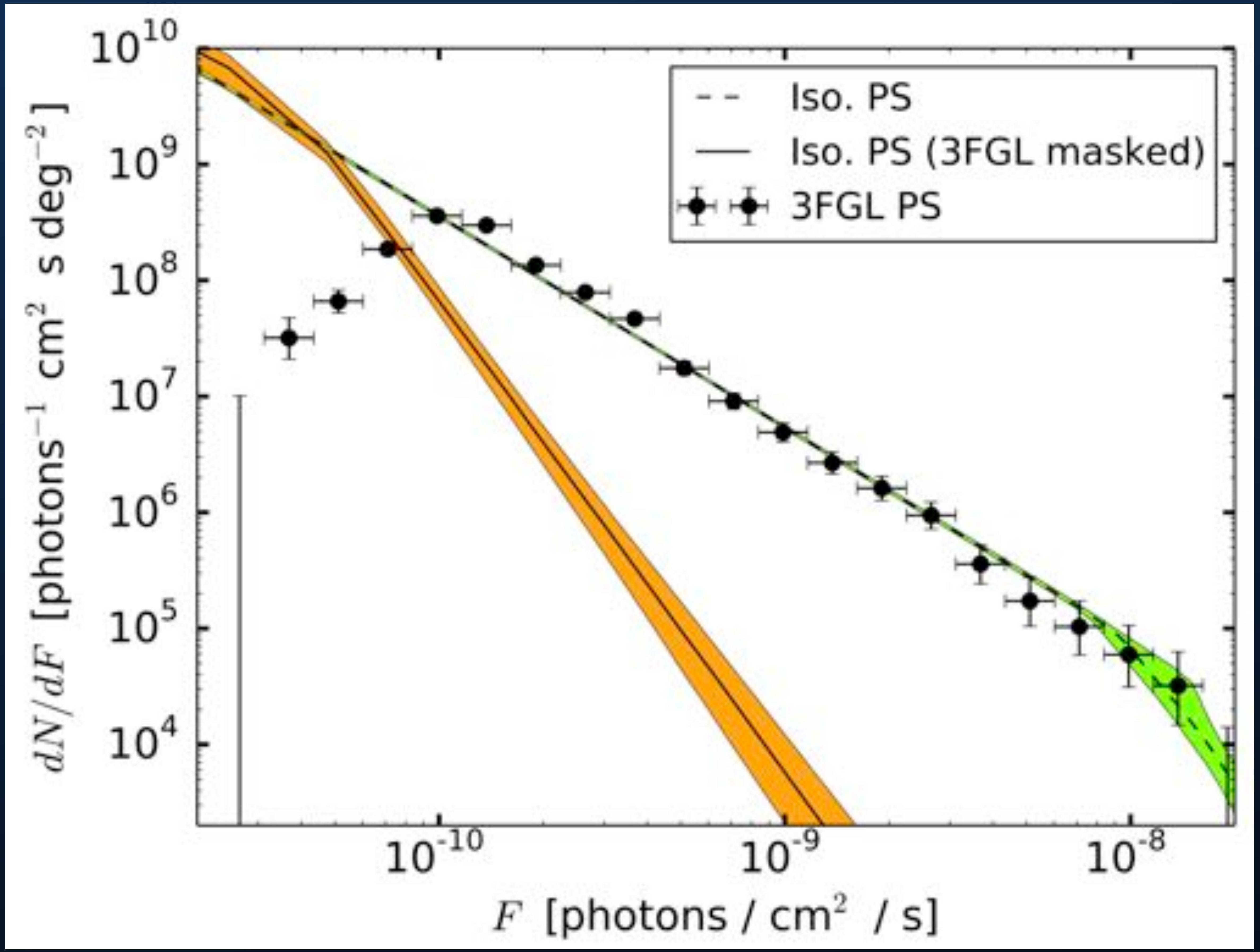

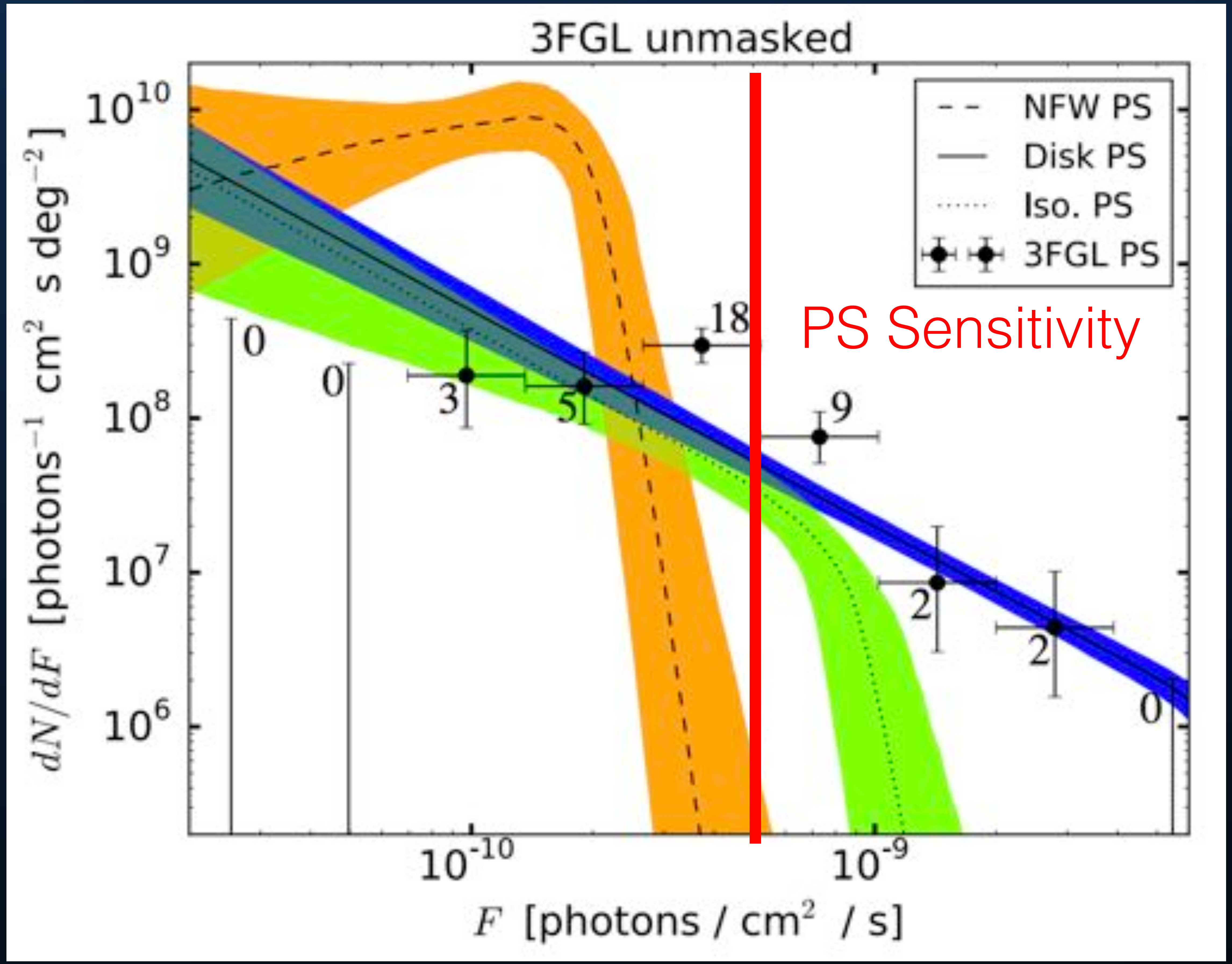

The luminosity distribution of sub-threshold point-sources favored by these models is odd.

Lee et al. (2016; 1506.05124)

A Bulge Component

Macias et al. (2018; 1611.06644)

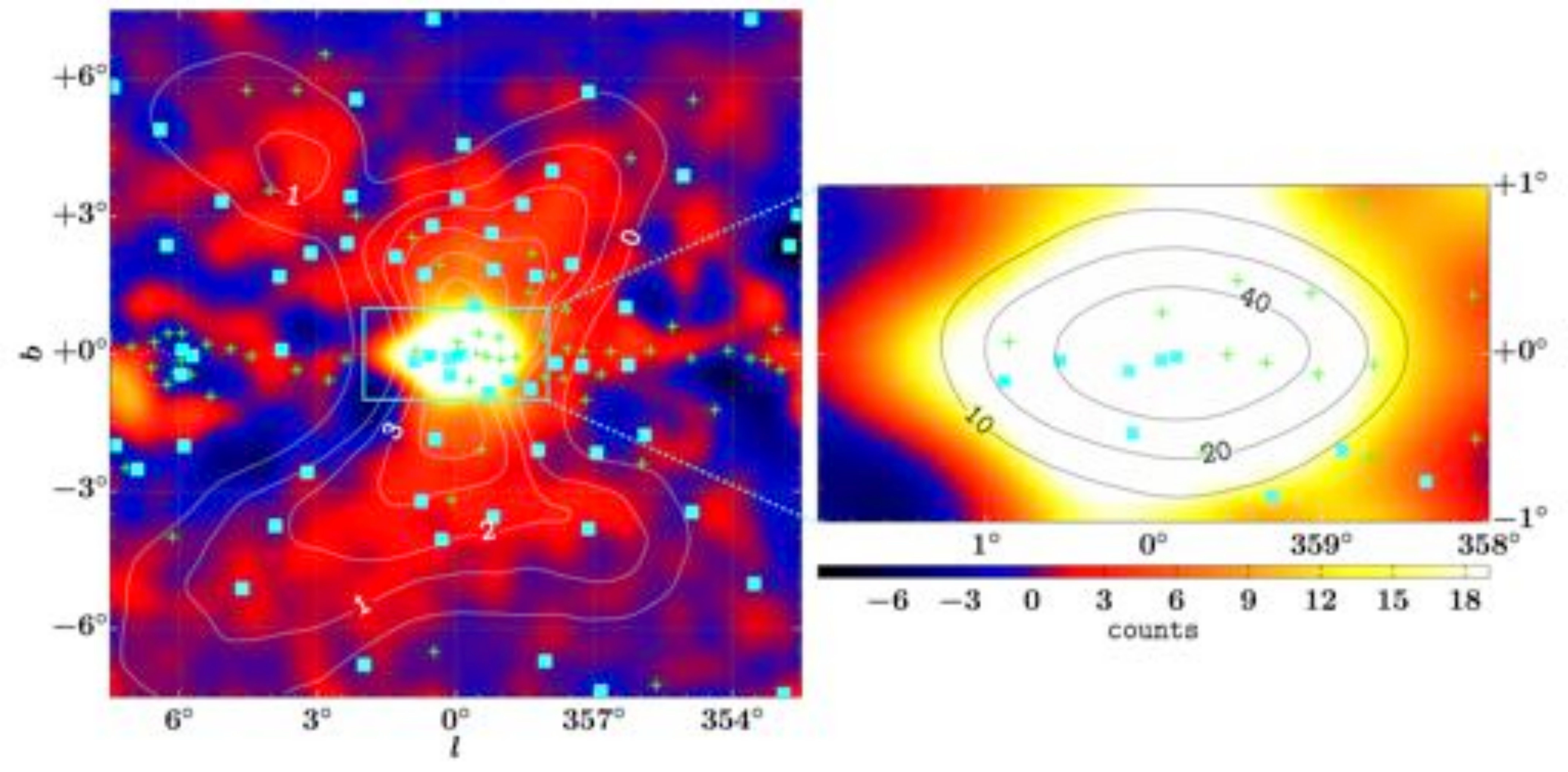

The distribution of point sources can also affect the properties of the resulting diffuse emission model.

A Bulge Component

Macias et al. (2018; 1611.06644)

Linden (2015; 1509.02928)

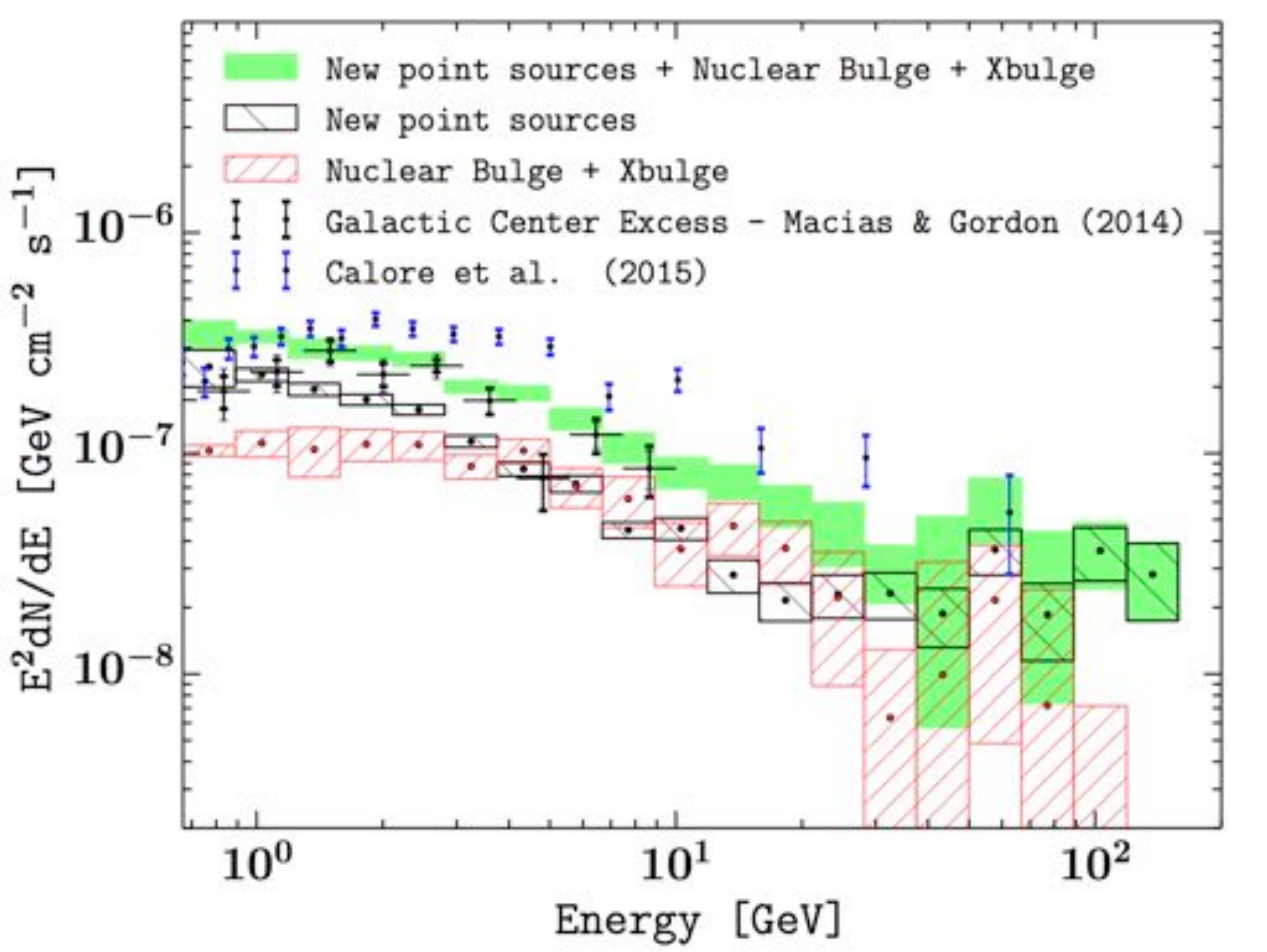

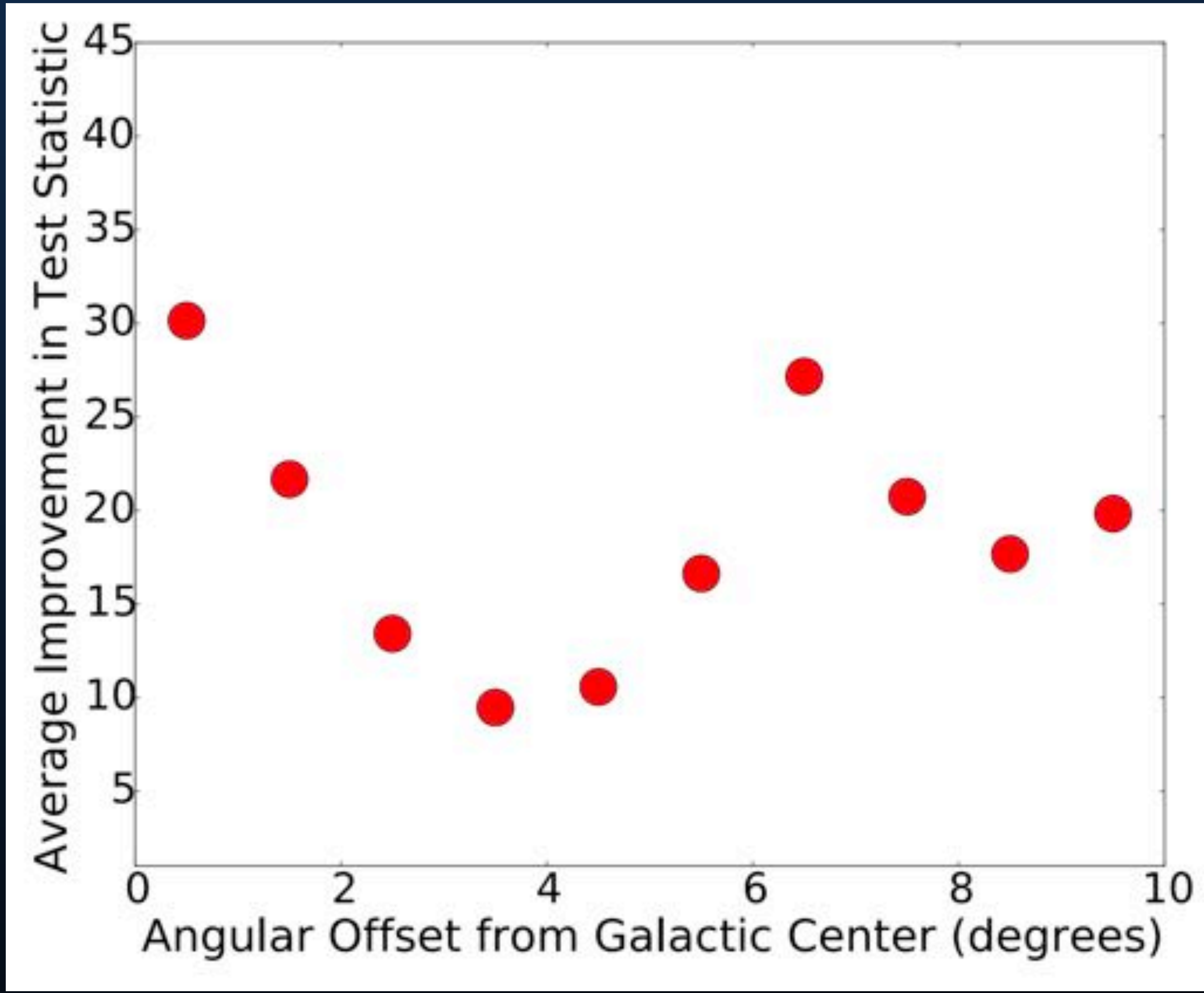

These new point sources are comparably bright to the data.

It is very likely that many of these sources are spurious.

A Bulge Component

Macias et al. (2018; 1611.06644)

Base	Source	$\log(\mathcal{L}_{\rm Base})$	$\log(\mathcal{L}_{\rm Base+Source})$	$\rm TS_{Source}$	σ	Number of source parameters
baseline	FB	-172461.4	-172422.3	78	6.9	19
baseline	NFW-s	-172461.4	-172265.3	392	18.4	19
baseline	X-bulge	-172461.4	-172224.1	475	20.5	19
baseline	NFW	-172461.4	-172167.9	587	23.0	19
baseline	NB	-172461.4	-171991.8	939	29.5	19
baseline	NP	-172461.4	-169804.1	5315	55.7	64×19
baseline+NP	FB	-169804.1	-169773.6	61	5.8	19
baseline+NP	NB	-169804.1	-169697.2	214	13.0	19
baseline+NP	NFW	-169804.1	-169623.3	362	17.6	19
baseline+NP	X-bulge	-169804.1	-169616.2	376	18.0	19
baseline+NP+X-bulge	NFW	-169616.2	-169568.4	96	7.9	19
baseline+NP+X-bulge	NB	-169616.2	-169542.0	148	10.4	19
baseline+NP+X-bulge+NB	NFW	-169542.0	-169531.0	22	2.4	19
baseline+NP+X-bulge+NB	FB	-169542.0	-169525.5	33	3.5	19
baseline+NP+NB	X-bulge	-169697.2	-169542.0	310	16.1	19
baseline+NP+NFW	X-bulge+NB	-169623.3	-169531.0	185	10.8	2×19
baseline+NP+NFW+NB	X-bulge	-169598.9	-169531.0	136	9.9	19

A Bulge Component - Low Energy Fits

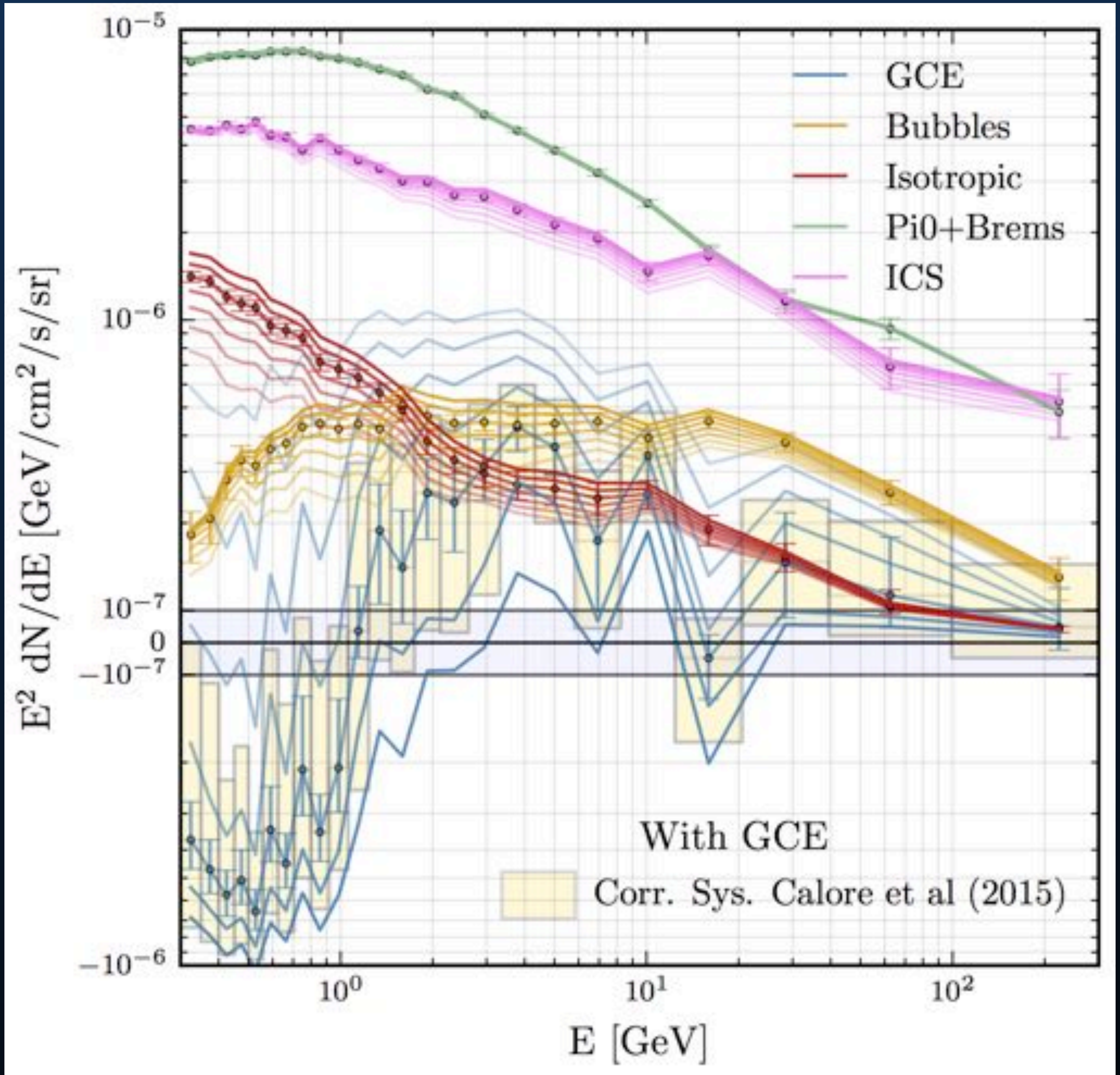

Carlson et al. (2016; 1603.06584)

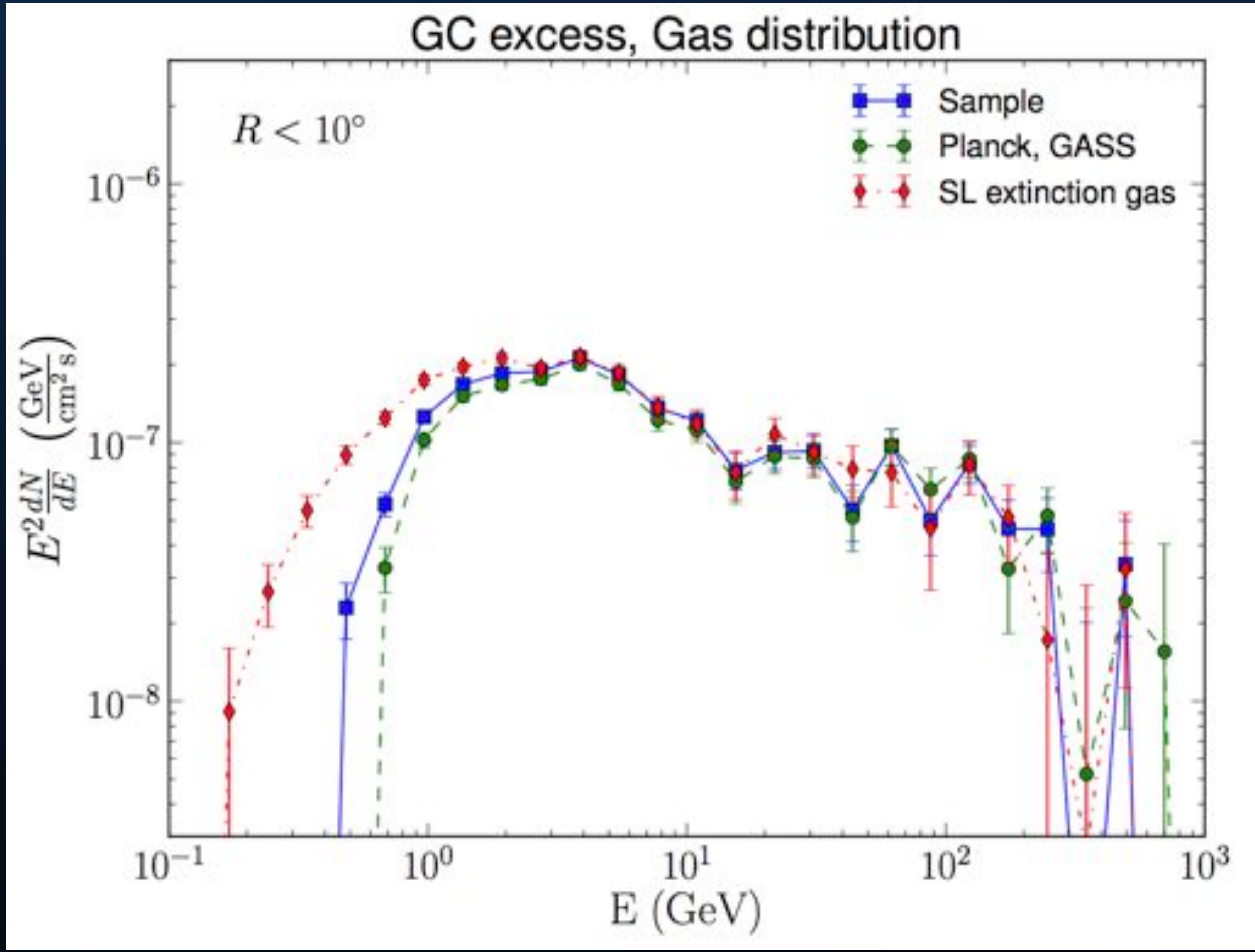

Fermi-LAT Collaboration (2017; 1704.03910)

Emission Outside of the Bulge

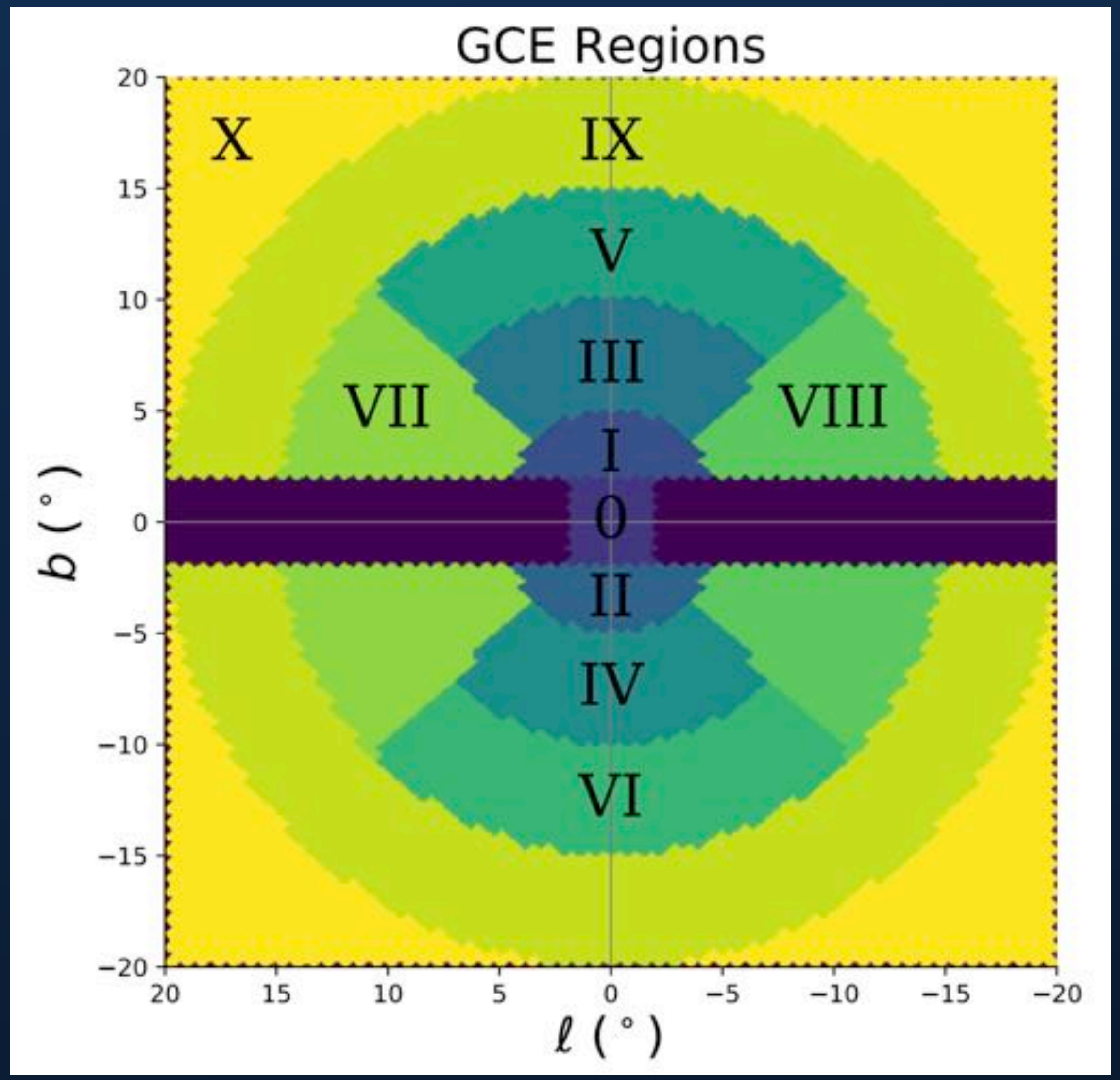

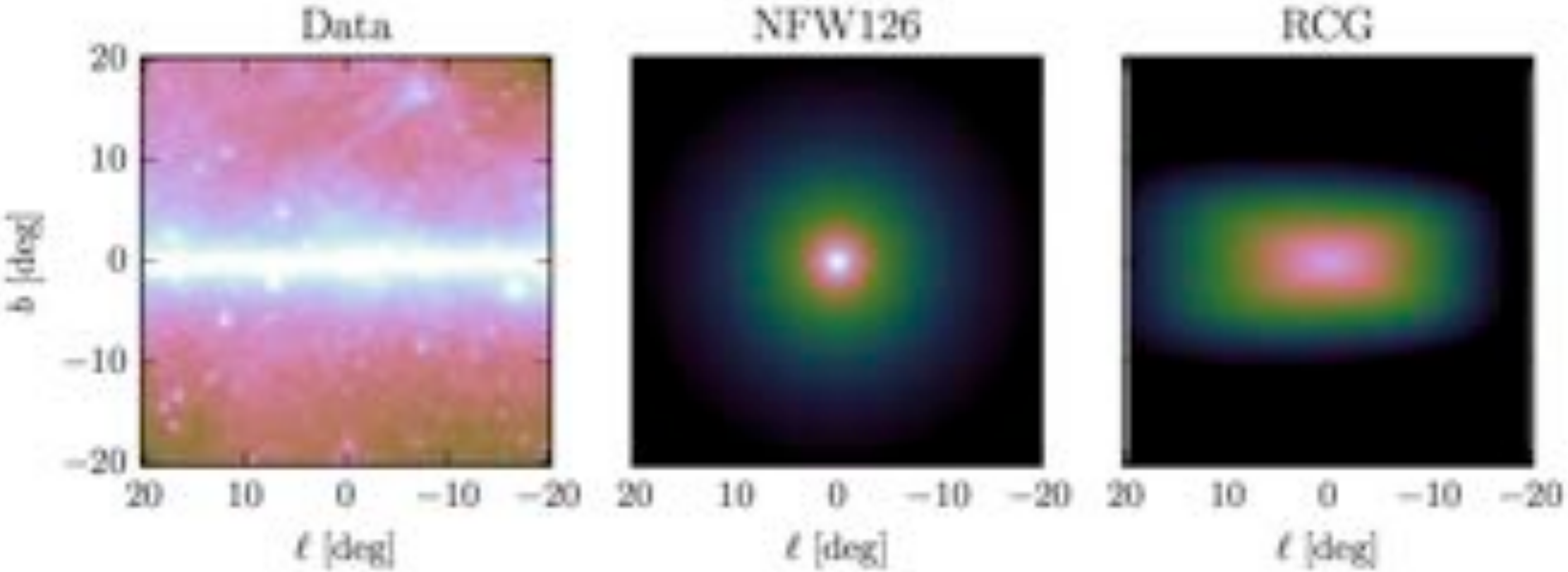

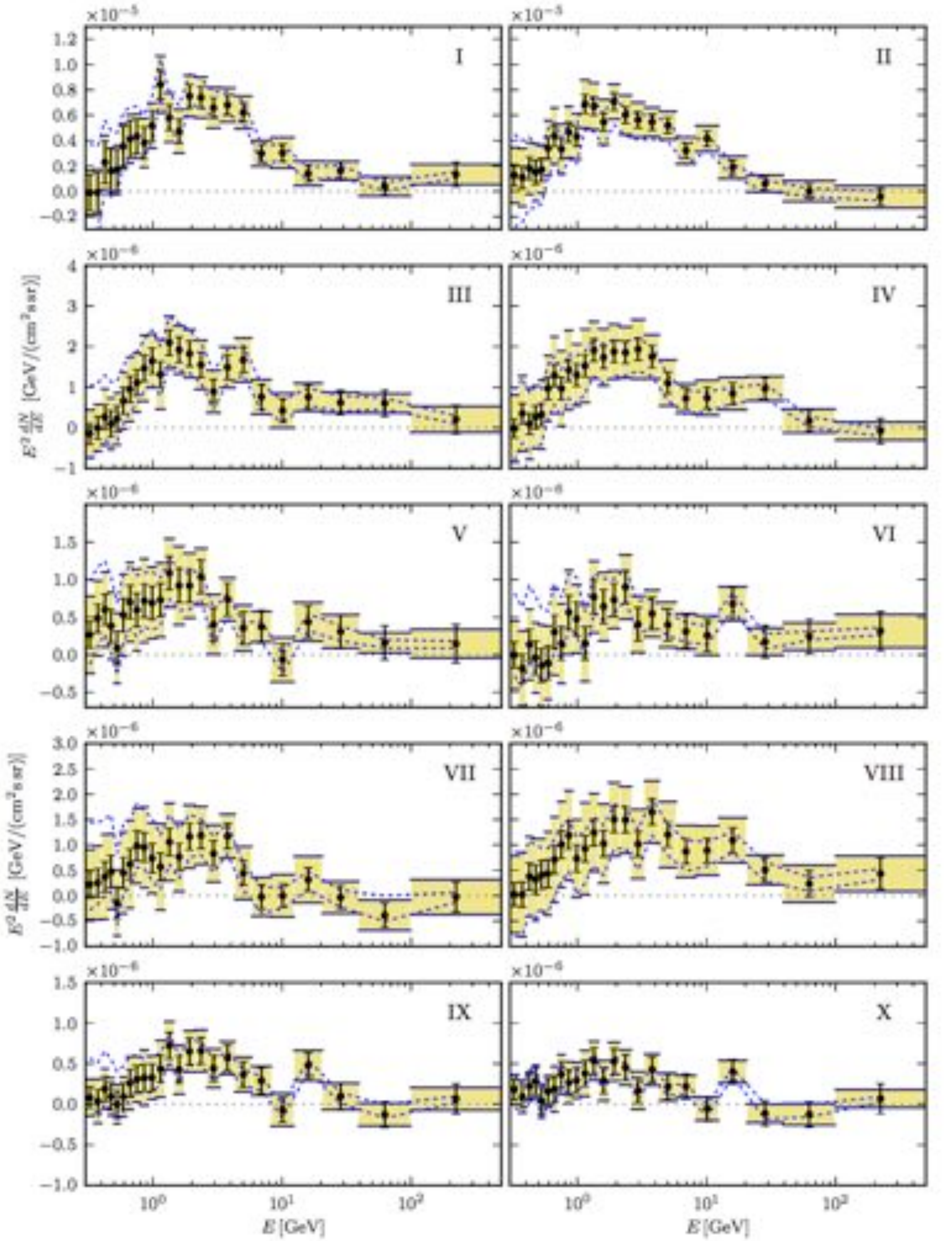

2FIG Catalog

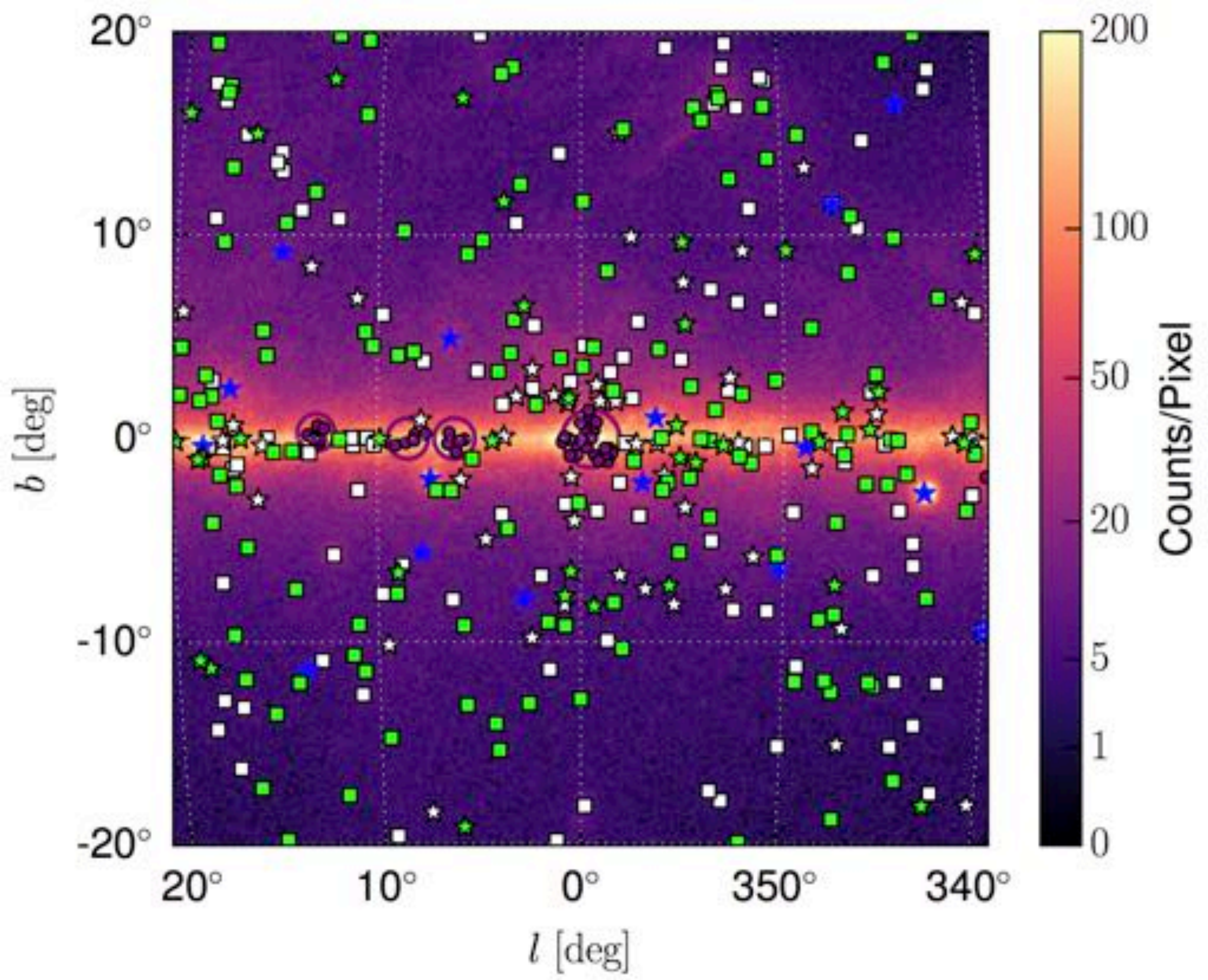

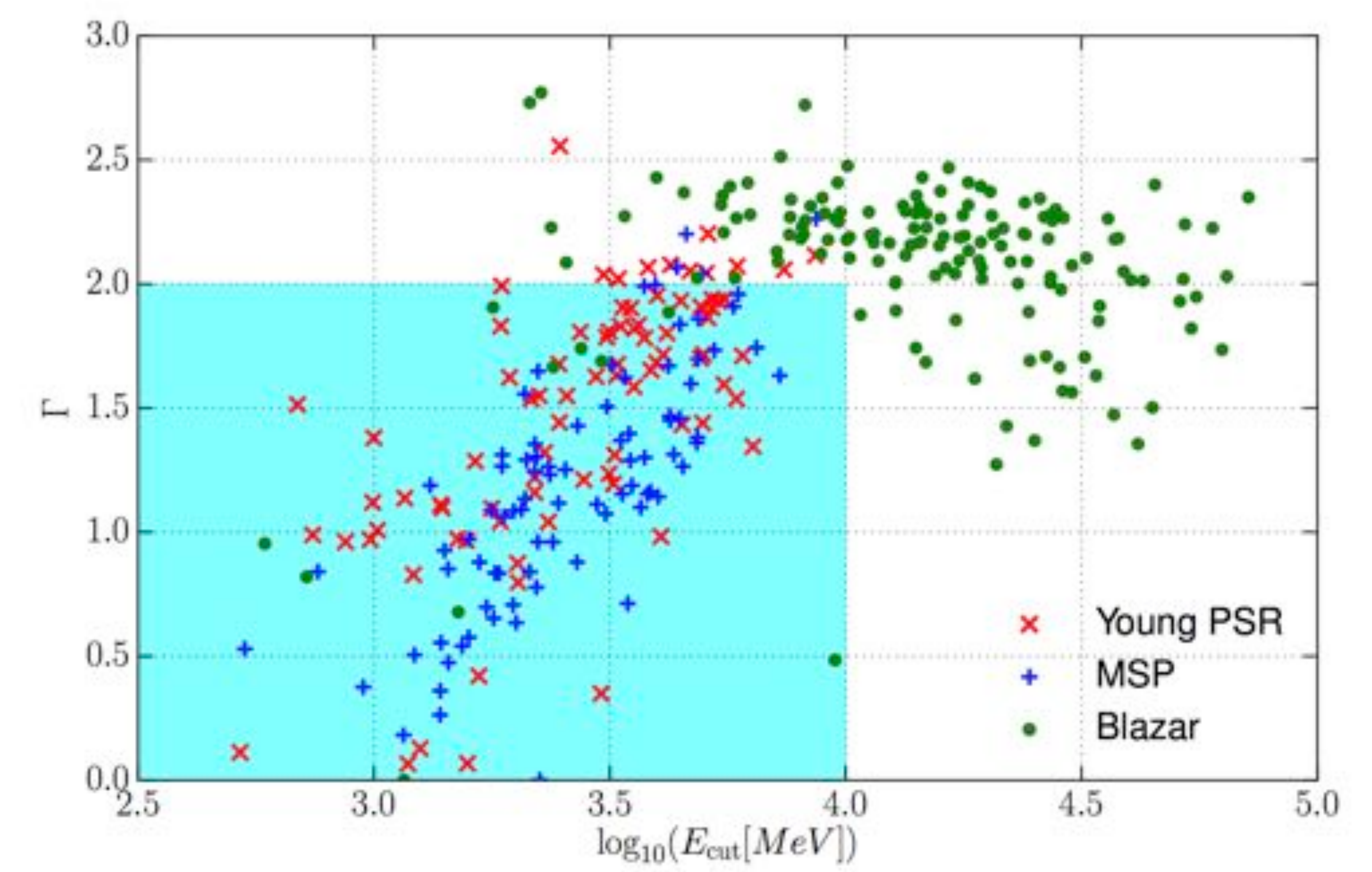

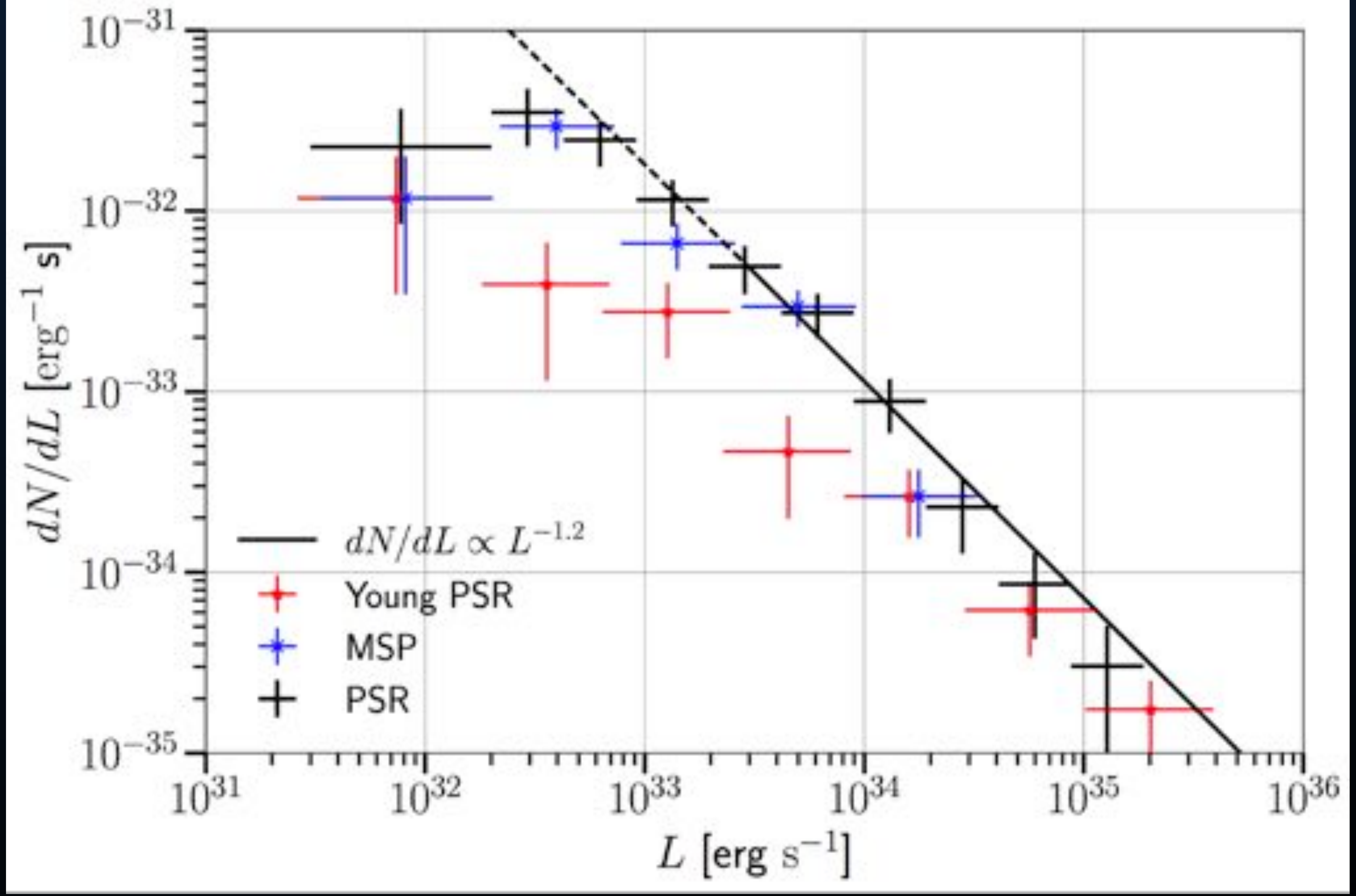

Fermi-LAT collaboration unveiled a new analysis that claimed a detection of these pulsars at >7σ.

Fermi-LAT Collaboration (2017; 1705.00009)

2FIG Catalog

	Alternate IEM						Official IEM					
A	$N_{\rm disk}$	z_0[kpc]	β	$N_{\rm bulge}$	α	TS	$N_{\rm disk}$	z_0[kpc]	β	$N_{\rm bulge}$	α	TS
1	23500^{+5500}_{-5000}	$0.63^{+0.14}_{-0.14}$	$1.35^{+0.07}_{-0.07}$	0	$\cdots$	0	22500^{+5200}_{-4800}	$0.71^{+0.16}_{-0.16}$	$1.34^{+0.07}_{-0.07}$	0	$\cdots$	0
2	3740^{+1030}_{-940}	$0.66^{+0.14}_{-0.14}$	$1.23^{+0.06}_{-0.06}$	1580^{+330}_{-270}	2.60	60	3560^{+980}_{-870}	$0.72^{+0.17}_{-0.17}$	$1.24^{+0.06}_{-0.06}$	1330^{+270}_{-210}	2.60	63
3	3960^{+1070}_{-970}	$0.70^{+0.16}_{-0.16}$	$1.24^{+0.07}_{-0.07}$	1660^{+350}_{-300}	$2.55^{+0.24}_{-0.24}$	65	3610^{+1010}_{-930}	$0.75^{+0.18}_{-0.18}$	$1.25^{+0.07}_{-0.07}$	1370^{+280}_{-220}	$2.57^{+0.23}_{-0.23}$	69
B	$N_{\rm disk}$	z_0[kpc]	β	$N_{\rm bulge}$	α	TS	$N_{\rm disk}$	z_0[kpc]	β	$N_{\rm bulge}$	α	TS
1	25600^{+5900}_{-5200}	$0.72^{+0.22}_{-0.22}$	$1.37^{+0.13}_{-0.13}$	0	$\cdots$	0	24500^{+5700}_{-5000}	$0.76^{+0.23}_{-0.23}$	$1.33^{+0.14}_{-0.14}$	0	$\cdots$	0
2	4670^{+1350}_{-1230}	$0.69^{+0.21}_{-0.21}$	$1.25^{+0.12}_{-0.12}$	1380^{+370}_{-310}	2.60	53	3710^{+1270}_{-1150}	$0.75^{+0.23}_{-0.23}$	$1.26^{+0.12}_{-0.12}$	1310^{+350}_{-290}	2.60	54
3	4360^{+1370}_{-1180}	$0.68^{+0.20}_{-0.20}$	$1.24^{+0.11}_{-0.11}$	1430^{+380}_{-320}	$2.57^{+0.27}_{-0.27}$	58	3660^{+1210}_{-1110}	$0.73^{+0.22}_{-0.22}$	$1.25^{+0.12}_{-0.12}$	1350^{+330}_{-300}	$2.65^{+0.28}_{-0.28}$	59

Table 2
Results from the maximum likelihood fits to the number of observed PSR candidates.

Note. — Best fit and 1σ uncertainty for $N_{\rm disk}$, z_0, β, $N_{\rm bulge}$ and α and TS with respect to the null hypothesis (first row) for the Alt. (left block) and Off. IEM (right block) and first (top block with pixel size 3.3°) and second (bottom with pixel size 6.0°) setup of spatial and energy flux bins (see the text for further details on the binning).

The fit is improved substantially with the addition of GC pulsars.

Lee et al. (2016; 1506.05124)

2FIG Catalog

We re-analyzed the Fermi-LAT data, and found very different results.

An error was subsequently found in the Fermi-LAT analysis.

$L_{\rm min} = 10^{32}$ erg/s

N_D	z_0[kpc]	β	N_B	α	TS
$(1.21^{+0.44}_{-0.35})\times10^5$	$0.19^{+0.07}_{-0.05}$	$2.08^{+0.10}_{-0.09}$	0	···	0
$(1.07^{+0.45}_{-0.33})\times10^5$	$0.13^{+0.06}_{-0.04}$	$2.15^{+0.12}_{-0.10}$	$(5.14^{+5.50}_{-2.62})\times10^5$	2.60	8.1

$L_{\rm min} = 10^{33}$ erg/s

N_D	z_0[kpc]	β	N_B	α	TS
$(1.24^{+0.36}_{-0.29})\times10^4$	$0.32^{+0.08}_{-0.06}$	$2.10^{+0.13}_{-0.13}$	0	···	0
$(1.02^{+0.40}_{-0.29})\times10^4$	$0.23^{+0.09}_{-0.06}$	$2.20^{+0.17}_{-0.14}$	$(4.57^{+3.95}_{-2.07})\times10^3$	2.6	10.1

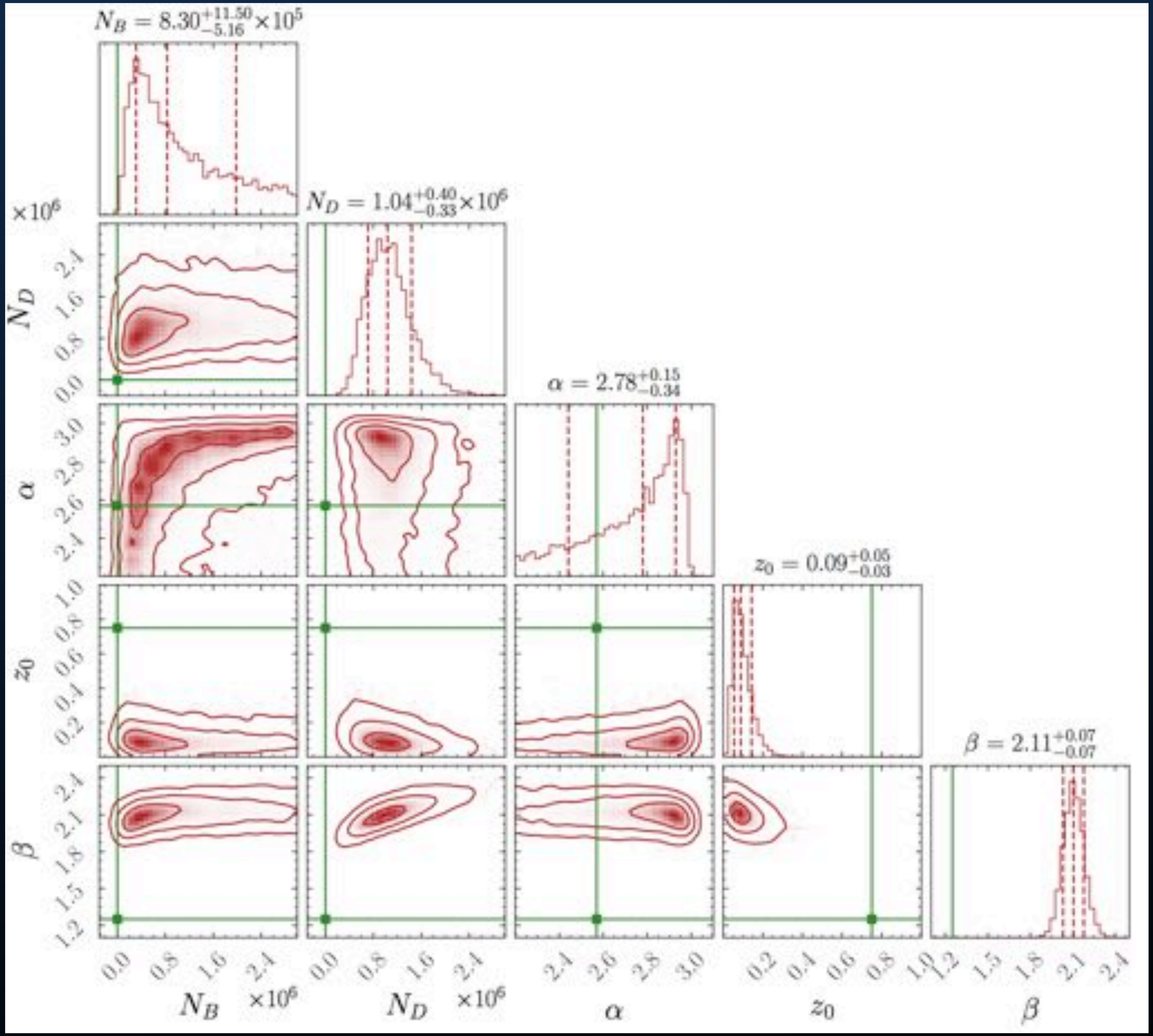

Bartels et al. (2018; 1710.10266)

Pulsar Spectra

Pulsar spectra do not spectrally match the GeV excess at low-energies

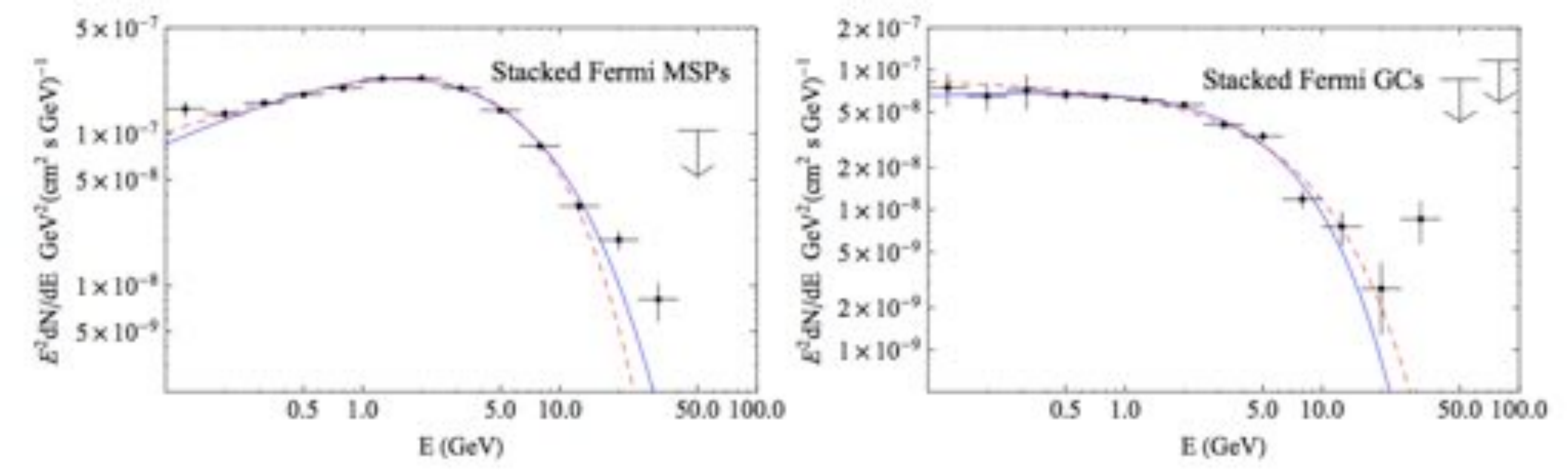

Cholis et al. (2014; 1407.5583)

Pulsar Spectra

Pulsar spectra do not spectrally match the GeV excess at low-energies

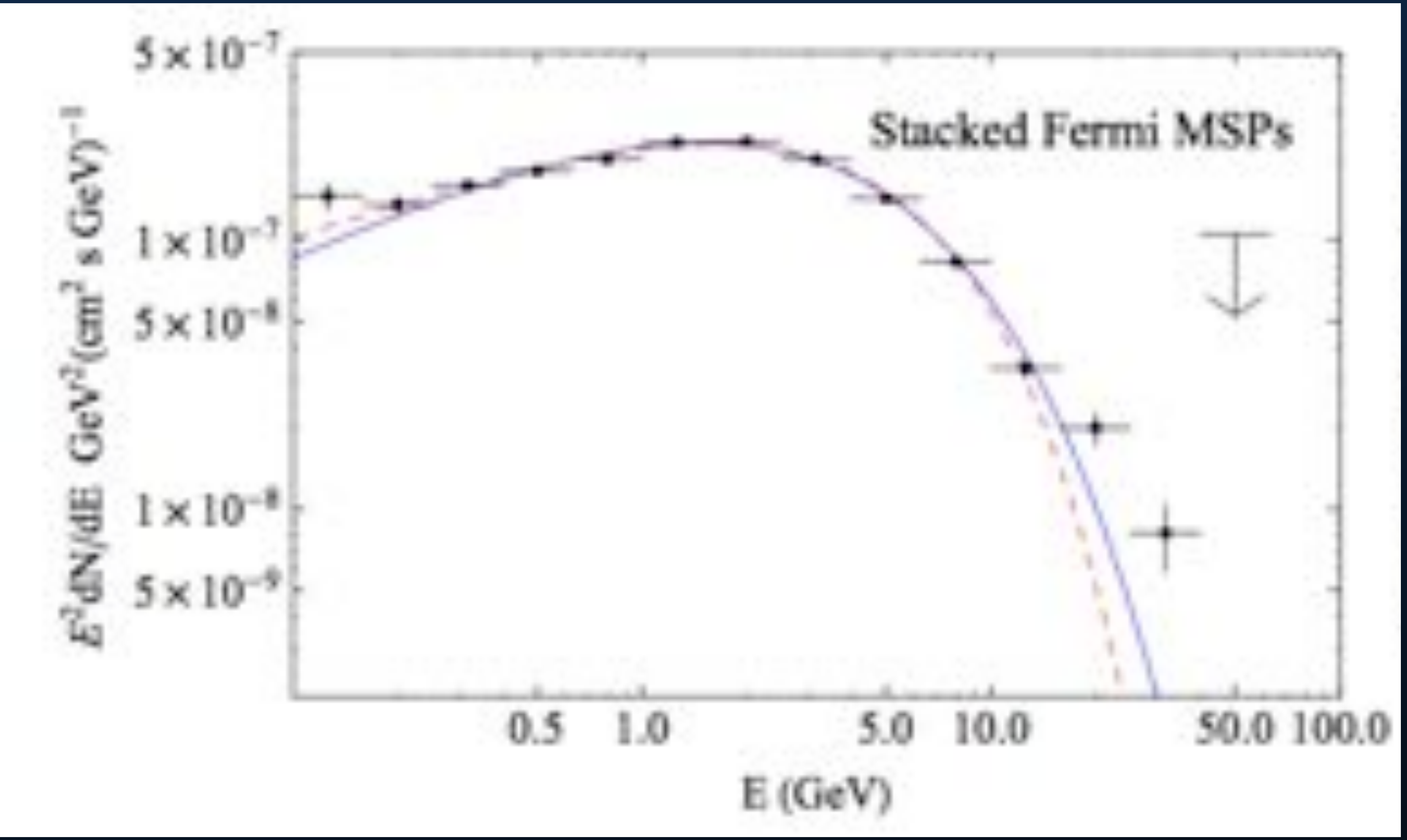

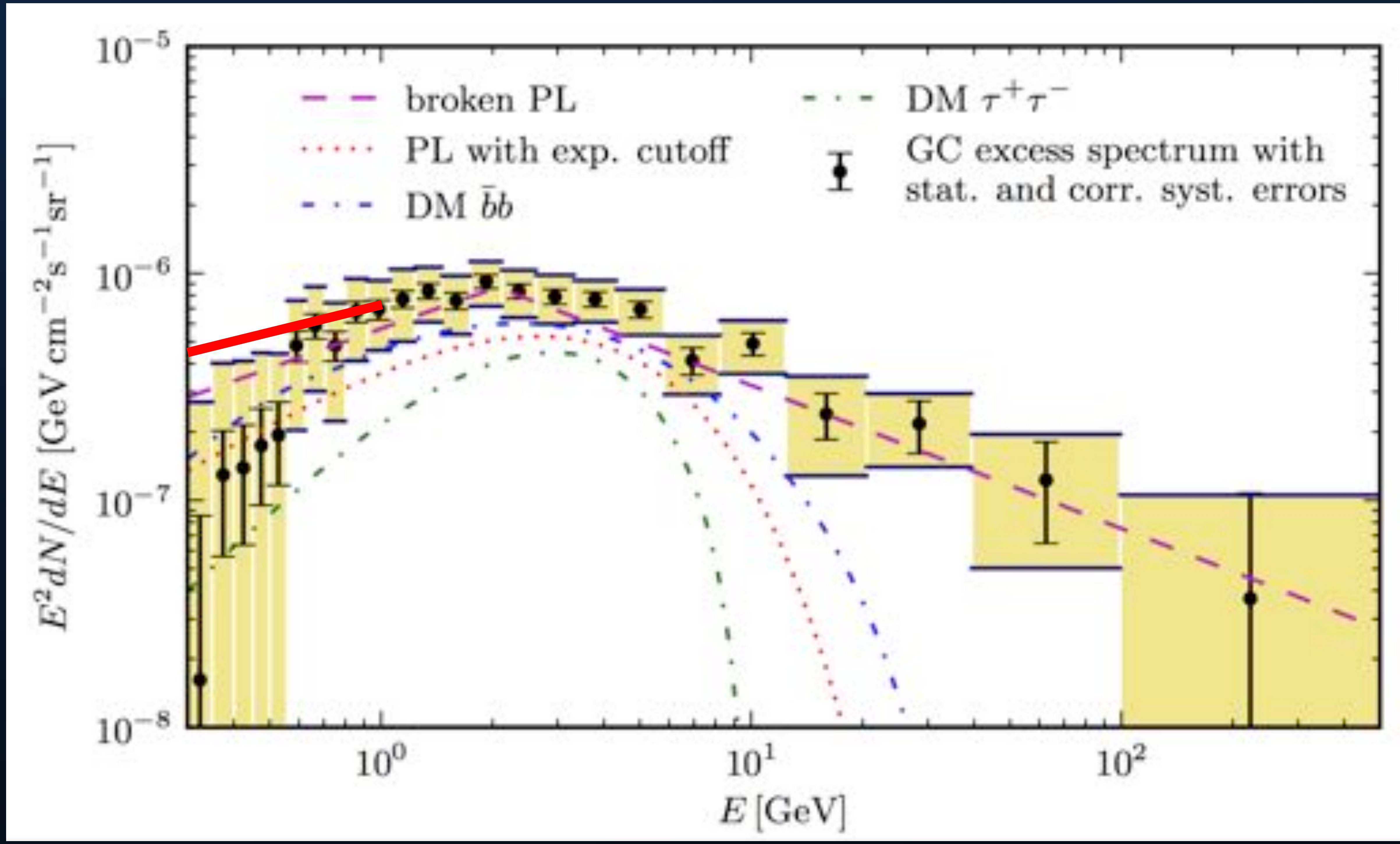

Cholis et al. (2014; 1407.5583)

Calore et al. (2015; 1409.0042)

Pulsar Spectra

Models that change the diffuse emission to better fit the observed data usually produce a harder spectrum at low-energies.

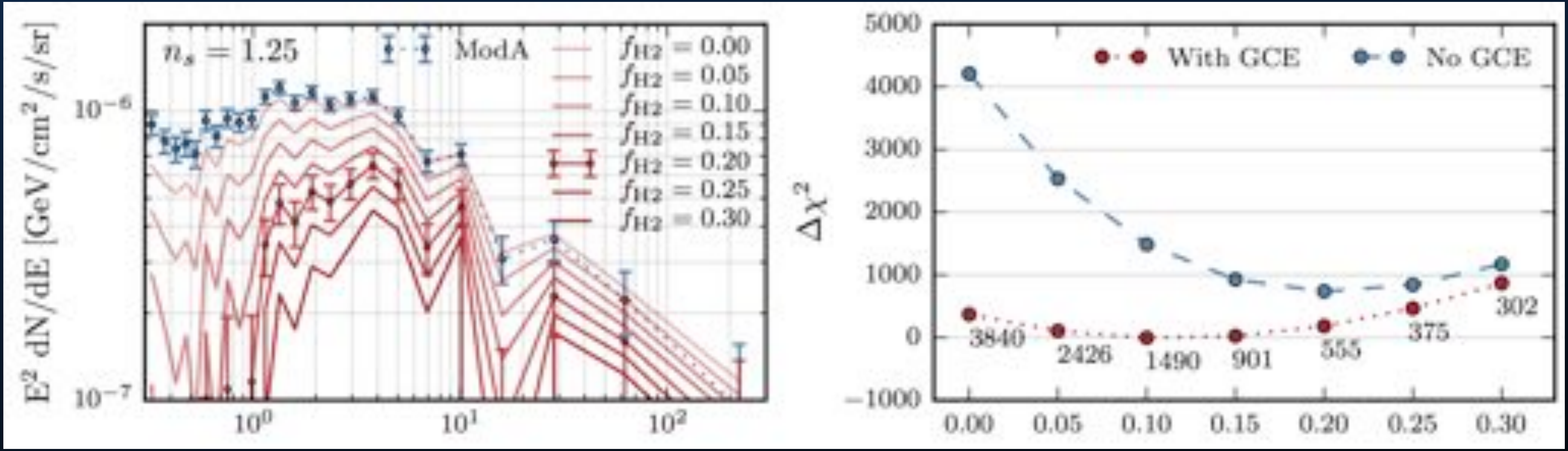

Carlson et al. (2016; 1603.06584)

Pulsar Morphology

Portail et al. (2016; 1608.07954)

Models of the Galactic bulge show that it is significantly aspherical and does not extend to extremely high latitudes.

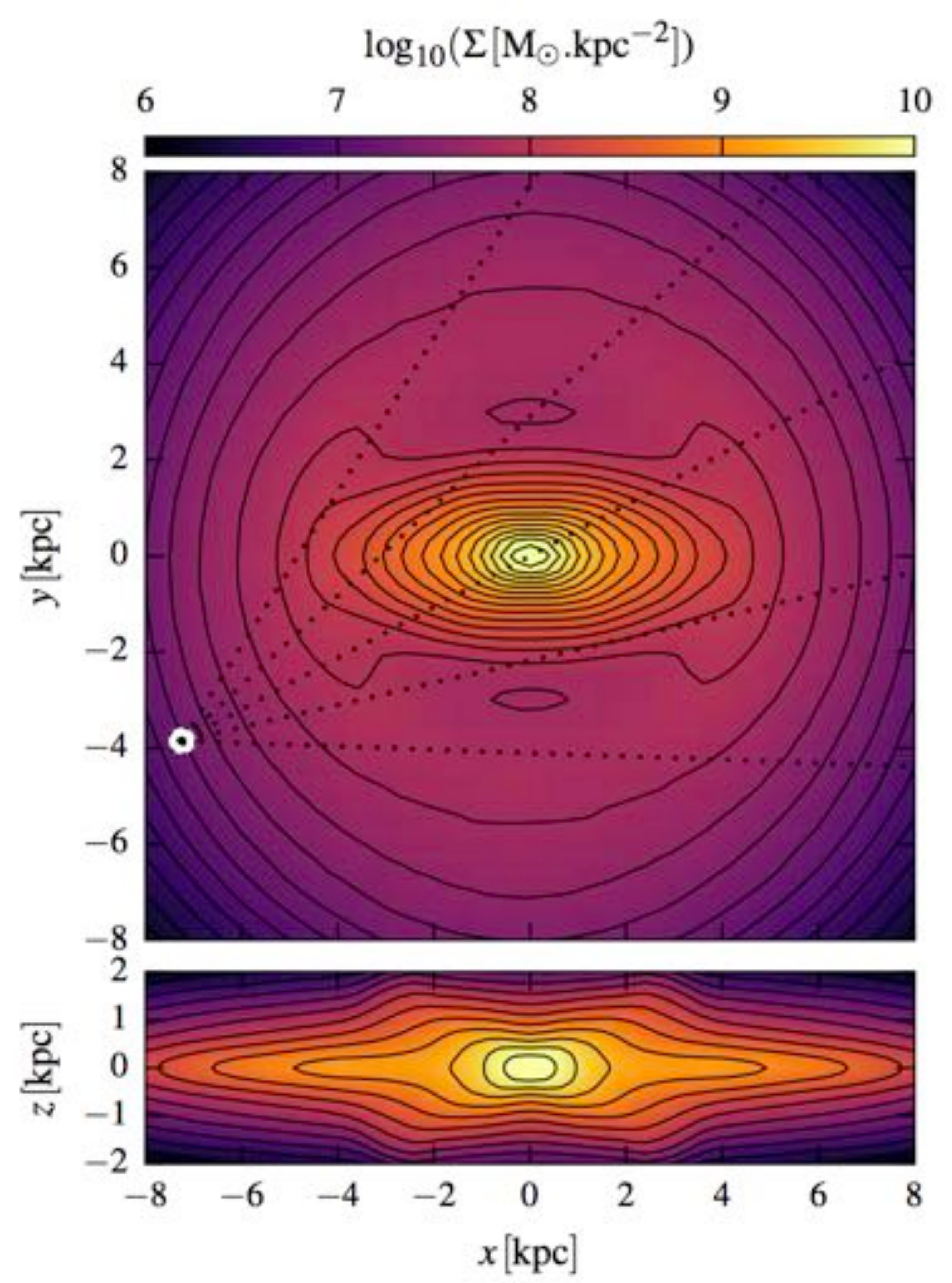

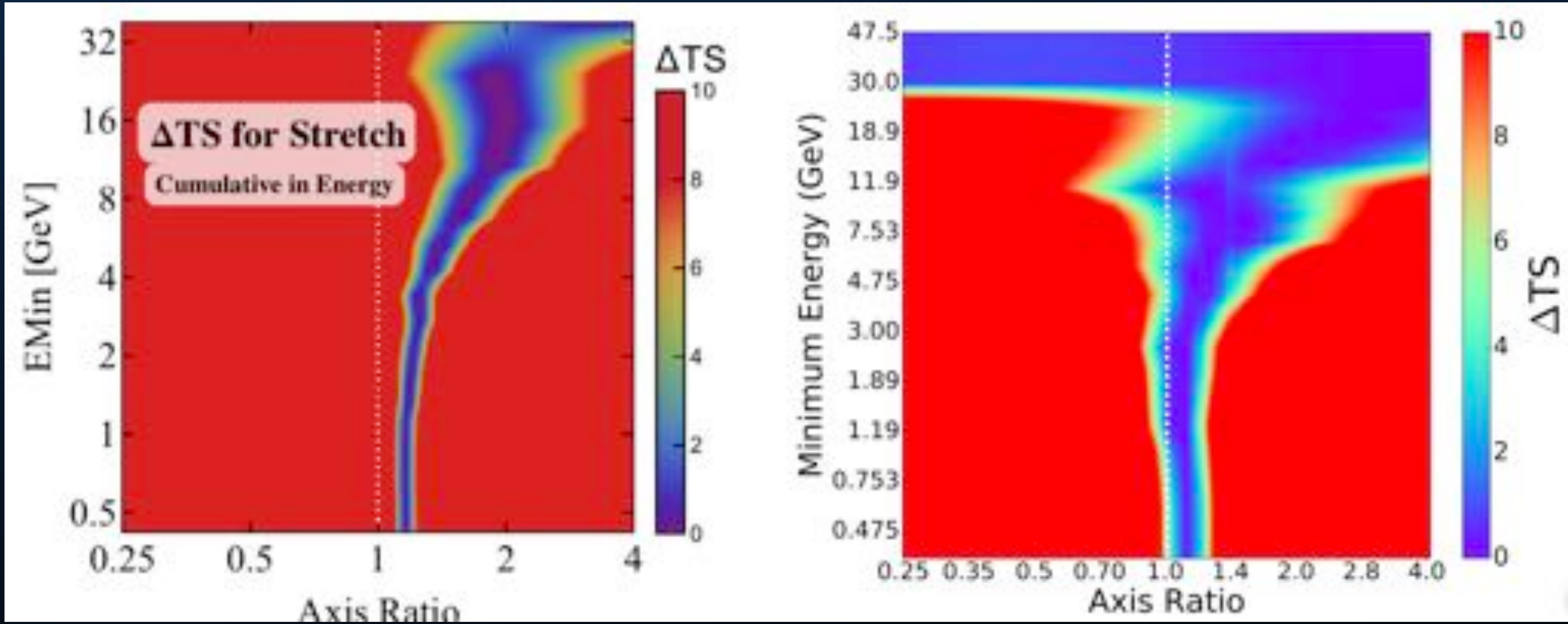

Linden et al. (2016; 1604.01026)

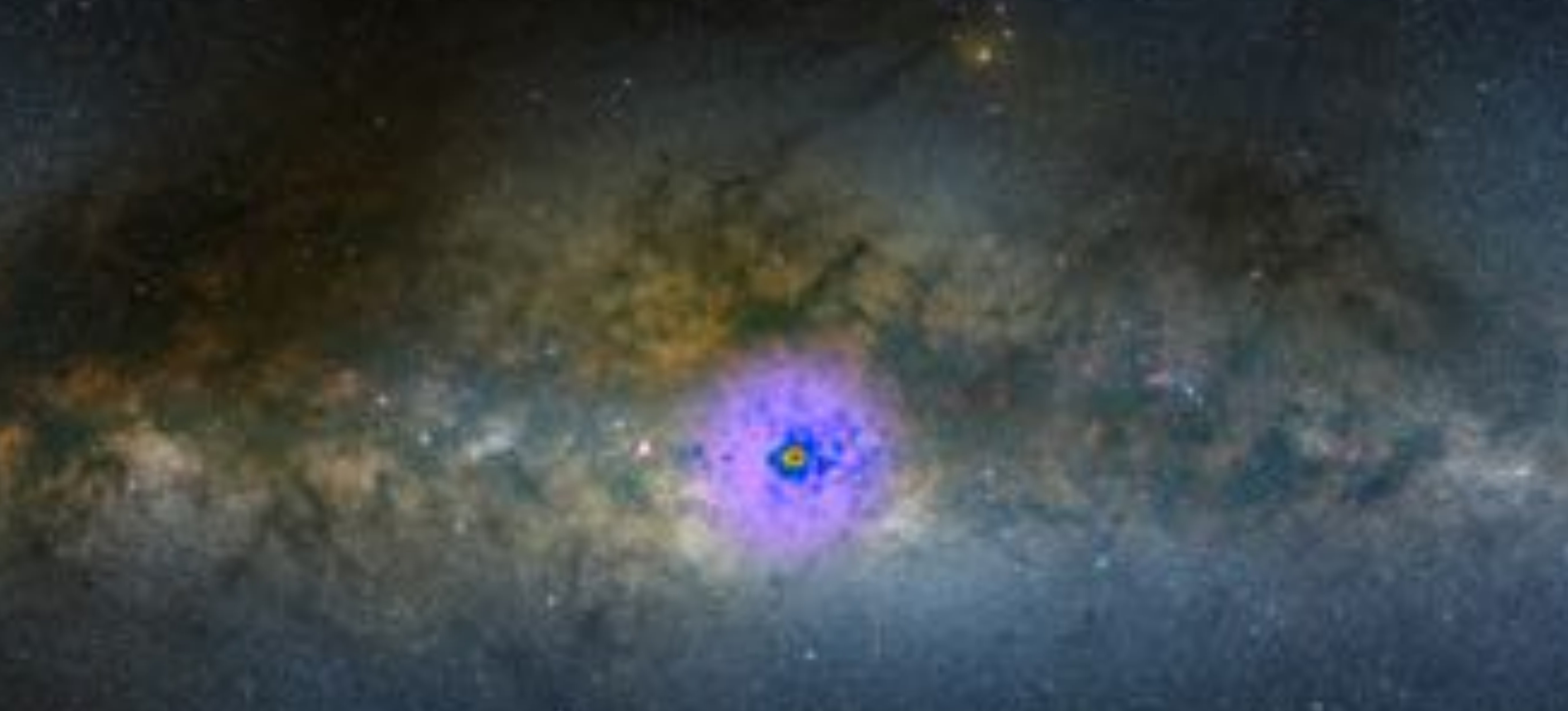

Dark Matter Explanations are Better than Astrophysical Explanations

Tim Linden

CCAPP Postdoctoral Fellow
Center for Cosmology and Astro-Particle Physics
The Ohio State University

Dark Matter Explanations are Better than Pulsar Explanations

1.) Difficulties in building a pulsar model

2.) Difficulties in building diffuse models

3.) Dark Matter Fits to the gamma-ray data

The Expected MSP Population

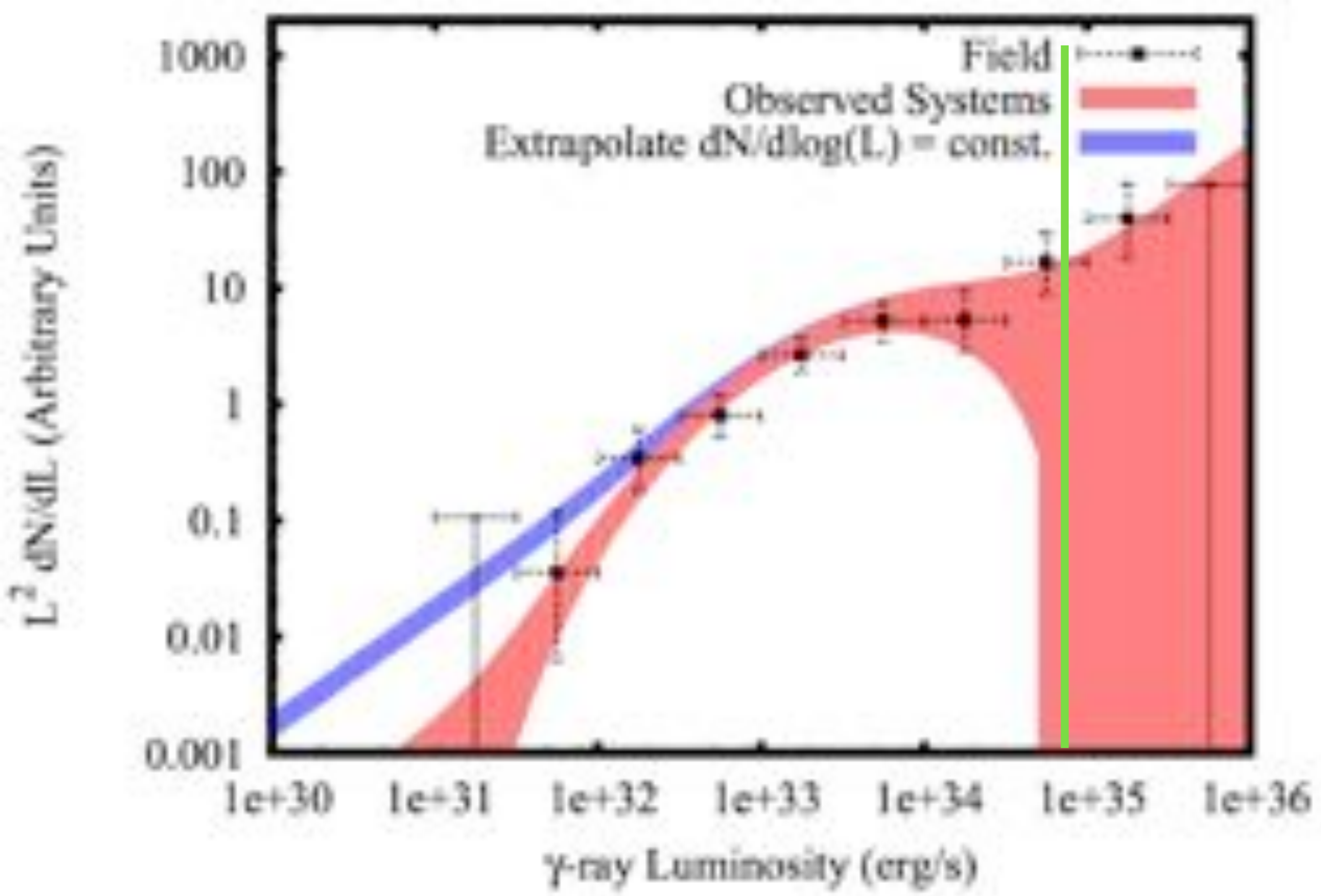

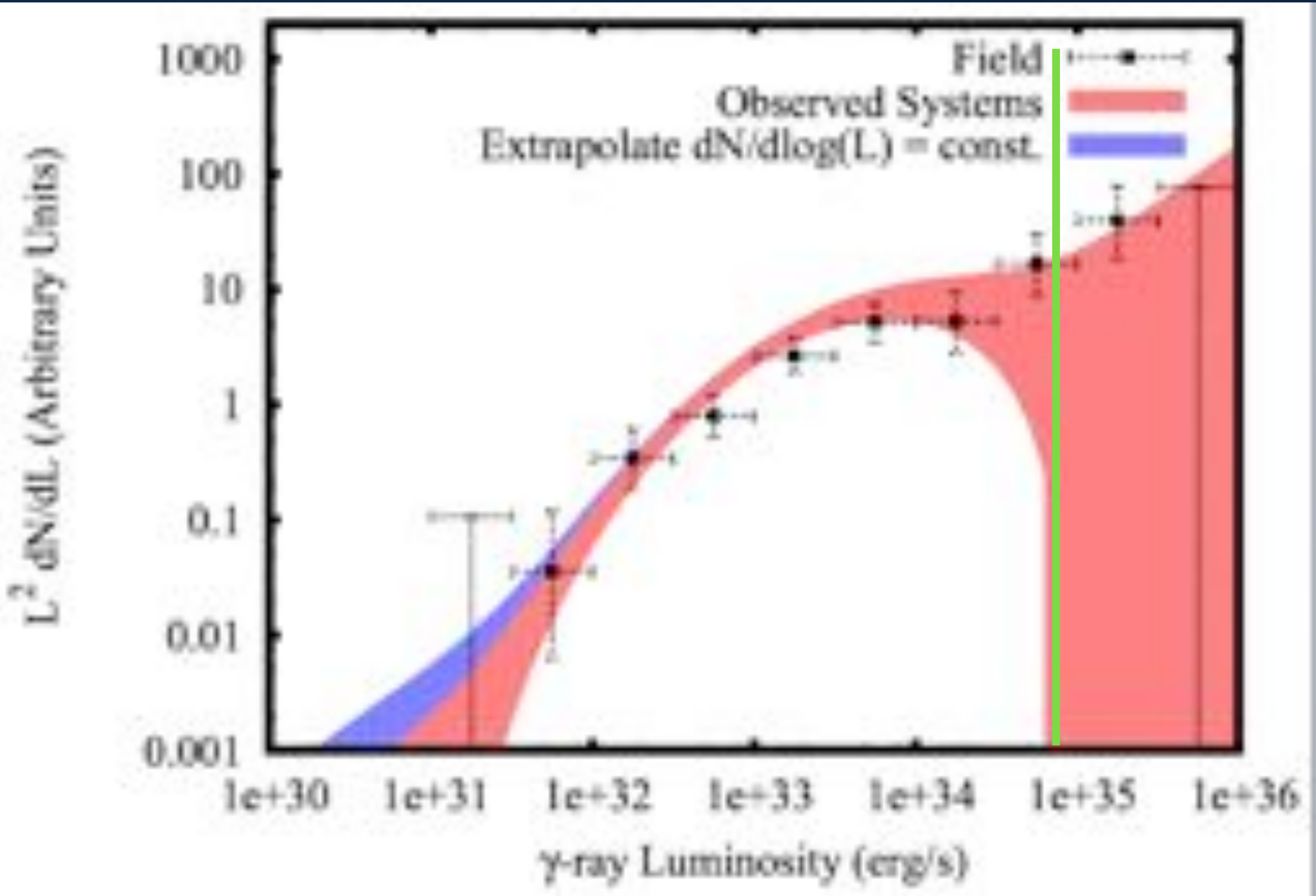

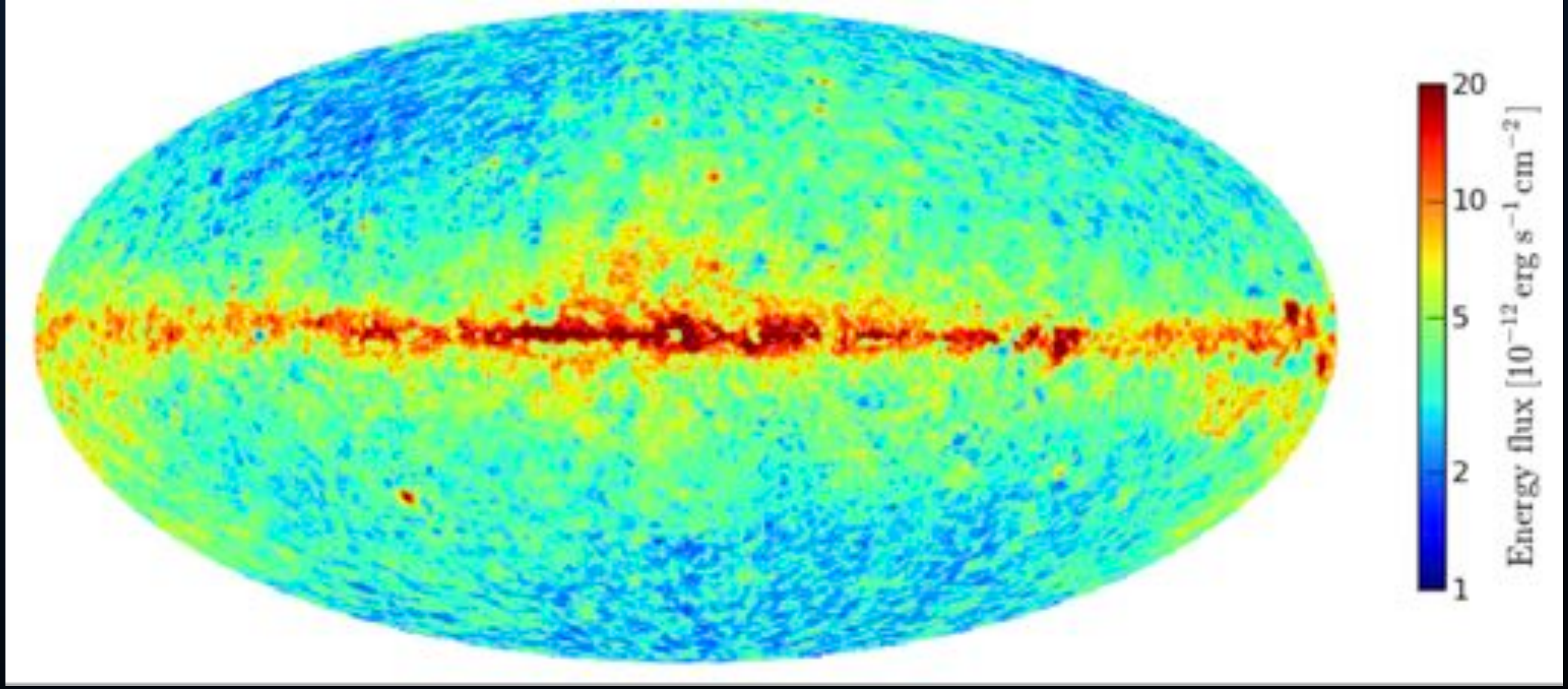

Cholis et al. (2014; 1407.5583)

Fermi-LAT Collaboration (2013; 1305.4385)

The Expected MSP Population

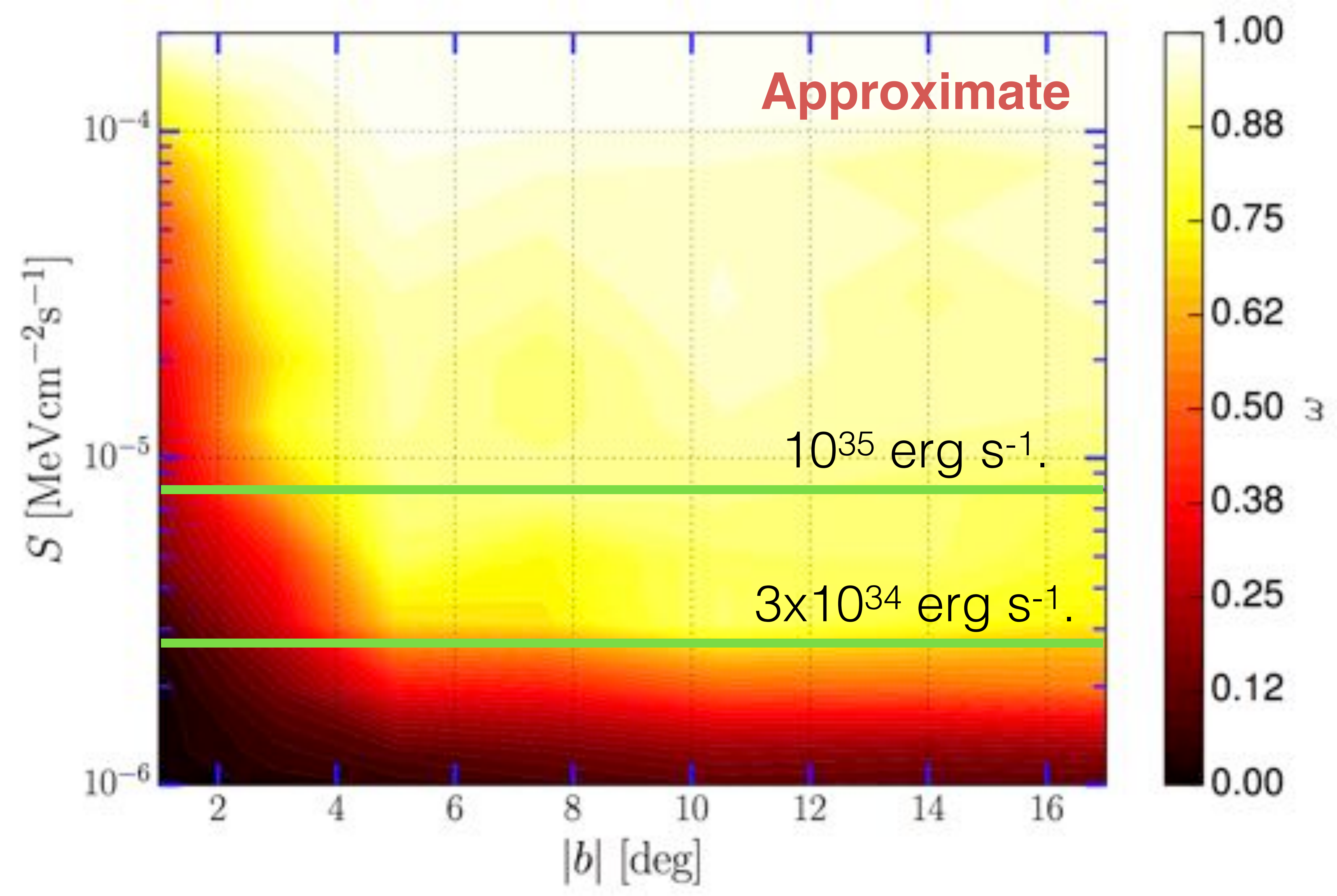

Fermi-LAT Collaboration (2017; 1705.00009v1)

The Expected MSP Population

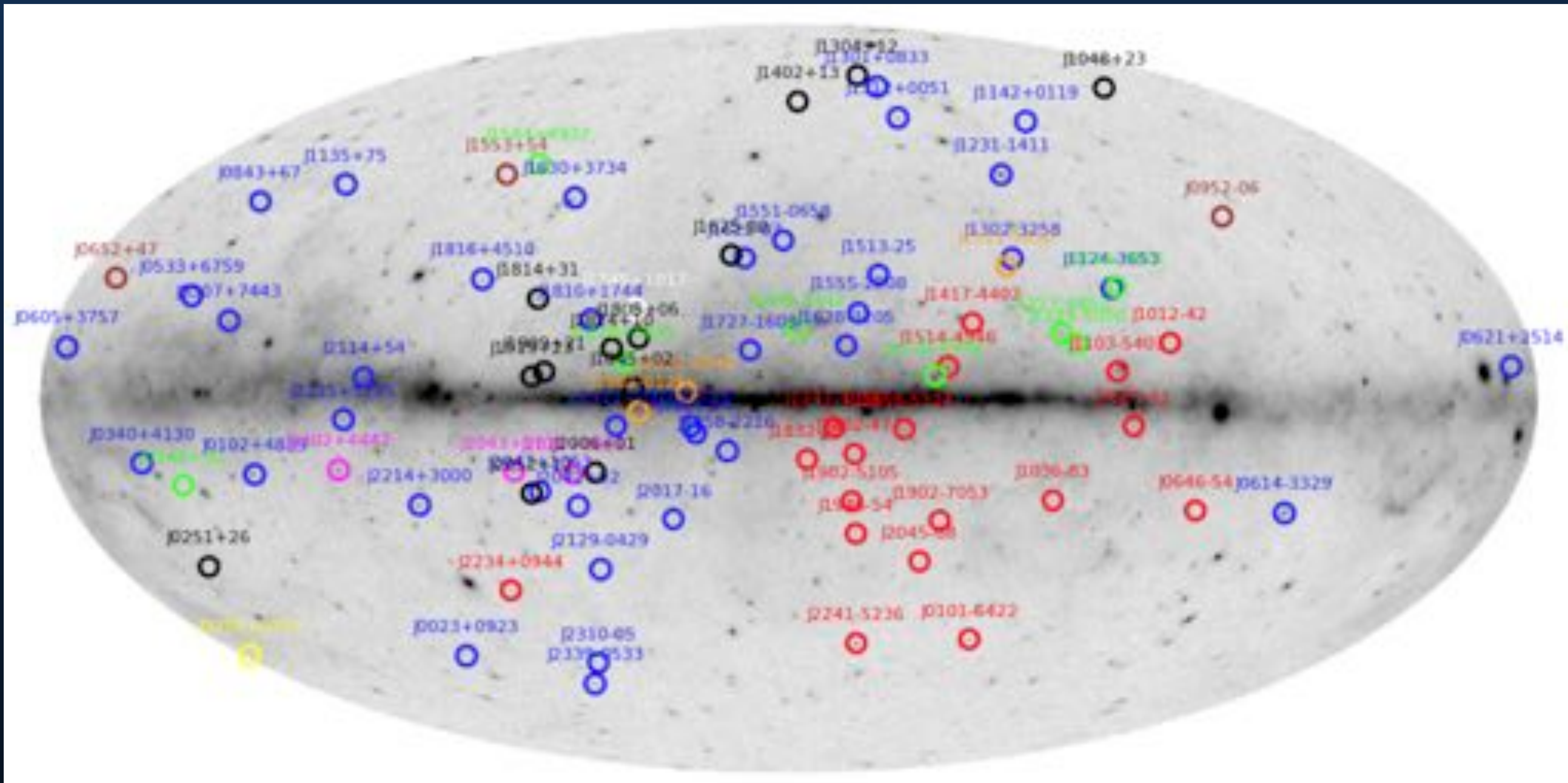

While these Fermi-LAT searches are difficult, radio follow ups have not confirmed these sources to be pulsars.

Paul Ray (Private Communication; see also 1205.3089)

The Missing ~~Satellites~~ Pulsar Problem

THE PECULIAR PULSAR POPULATION OF THE CENTRAL PARSEC

Jason Dexter
Department of Astronomy, University of California, Berkeley, CA 94720-3411, USA

Ryan M. O'Leary
Department of Astronomy, University of California, Berkeley, CA 94720-3411, USA

Draft version April 14, 2018

ABSTRACT

Pulsars orbiting the Galactic center black hole, Sgr A*, would be potential probes of its mass, distance and spin, and may even be used to test general relativity. Despite predictions of large populations of both ordinary and millisecond pulsars in the Galactic center, none have been detected within 25 pc by deep radio surveys. One explanation has been that hyperstrong temporal scattering prevents pulsar detections, but the recent discovery of radio pulsations from a highly magnetized neutron star (magnetar) within 0.1 pc shows that the temporal scattering is much weaker than predicted. We argue that an intrinsic deficit in the ordinary pulsar population is the most likely reason for the lack of detections to date: a "missing pulsar problem" in the Galactic center. In contrast, we show that the discovery of a single magnetar implies efficient magnetar formation in the region. If the massive stars in the central parsec form magnetars rather than ordinary pulsars, their short lifetimes could explain the missing pulsars. Efficient magnetar formation could be caused by strongly magnetized progenitors, or could be further evidence of a top-heavy initial mass function. Furthermore, current high-frequency surveys should already be able to detect bright millisecond pulsars, given the measured degree of temporal scattering.

Keywords: Galaxy: center — pulsars: general — pulsars: individual (SGR J1745-29) — stars: neutron

The Low-Mass X-Ray Binary Connection

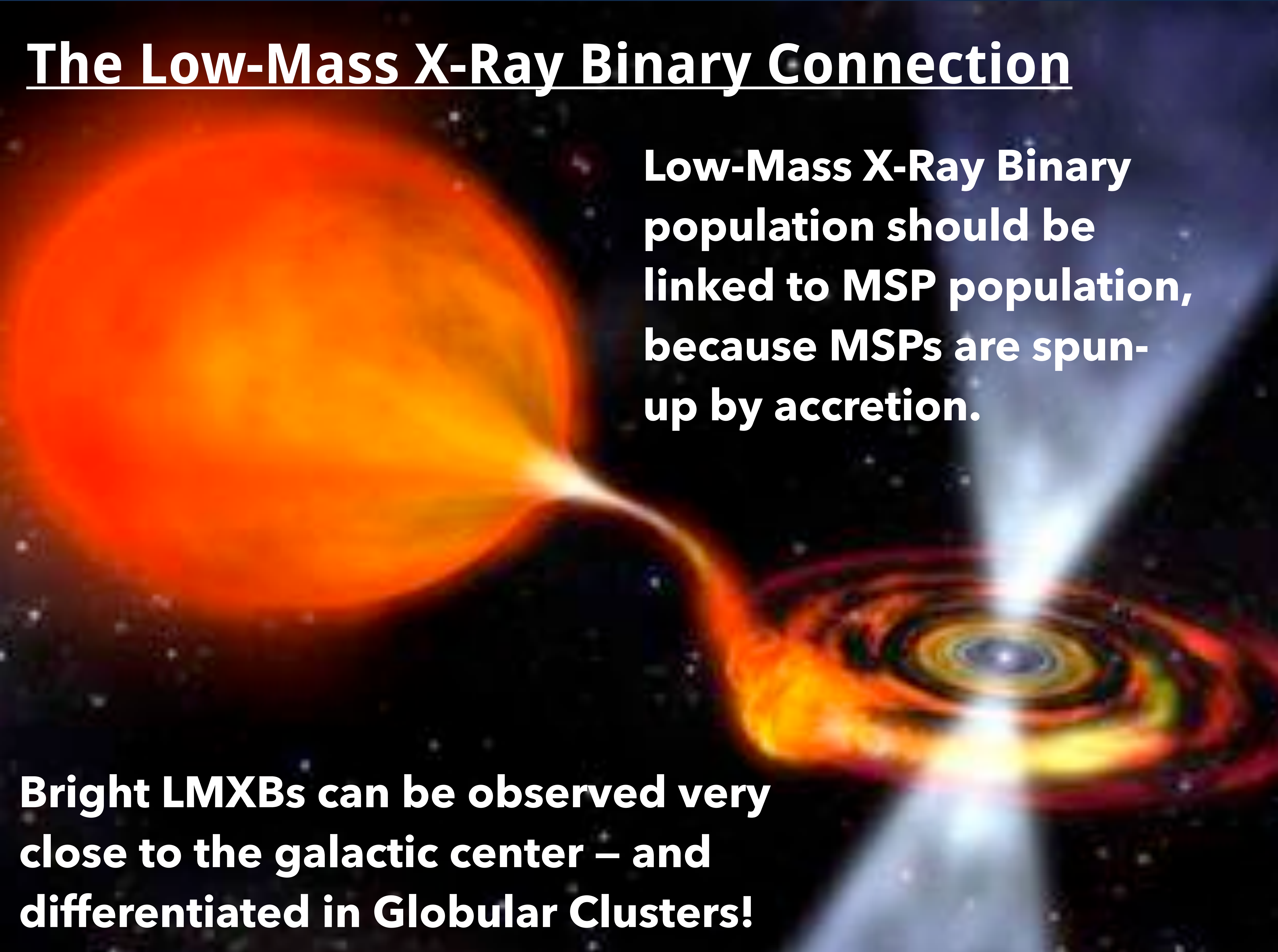

Low-Mass X-Ray Binary population should be linked to MSP population, because MSPs are spun-up by accretion.

Bright LMXBs can be observed very close to the galactic center – and differentiated in Globular Clusters!

The Low-Mass X-Ray Binary Connection

$$L_\gamma^{\rm IG} = L_\gamma^{\rm clusters} \times \left(\frac{N_{\rm LMXB}^{\rm IG}}{N_{\rm LMXB}} \right)$$

Globular Cluster	Flux (erg/cm^2/s)	Distance (kpc)	Stellar Encounter Rate	TS
NGC 104	$2.51^{+0.05}_{-0.06} \times 10^{-11}$	4.46	1.00	3995.9
NGC 362	$6.74^{+2.63}_{-2.46} \times 10^{-13}$	8.61	0.74	9.69
Palomar 2	$< 2.69 \times 10^{-13}$	27.11	0.93	0.0
NGC 6624	$1.14^{+0.10}_{-0.10} \times 10^{-11}$	7.91	1.15	455.8
NGC 1851	$9.05^{+2.92}_{-2.67} \times 10^{-13}$	12.1	1.53	14.4
NGC 5824	$< 4.78 \times 10^{-13}$	32.17	0.98	0.0
NGC 6093	$4.32^{+0.57}_{-0.53} \times 10^{-12}$	10.01	0.53	91.9
NGC 6266	$1.84^{+0.07}_{-0.10} \times 10^{-11}$	6.83	1.67	850.7
NGC 6284	$< 2.85 \times 10^{-13}$	15.29	0.67	0.0
NGC 6441	$1.00^{+0.09}_{-0.07} \times 10^{-11}$	11.6	2.30	210.9
NGC 6652	$4.84^{+0.51}_{-0.52} \times 10^{-12}$	10.0	0.70	128.3
NGC 7078/M15	$1.81^{+0.40}_{-0.39} \times 10^{-12}$	10.4	4.51	29.7
NGC 6440	$1.57^{+0.10}_{-0.11} \times 10^{-11}$	8.45	1.40	311.2
Terzan 6	$2.18^{+1.20}_{-0.90} \times 10^{-12}$	6.78	2.47	5.1
NGC 6388	$1.77^{+0.06}_{-0.09} \times 10^{-11}$	9.92	0.90	778.4
NGC 6626/M28	$1.95^{+0.13}_{-0.13} \times 10^{-11}$	5.52	0.65	749.8
Terzan 5	$6.61^{+0.17}_{-0.13} \times 10^{-11}$	5.98	6.80	2707.1
NGC 6293	$9.39^{+5.69}_{-5.45} \times 10^{-13}$	9.48	0.85	3.98
NGC 6681	$9.91^{+4.14}_{-3.86} \times 10^{-13}$	9.01	1.04	7.2
NGC 2808	$3.77^{+0.48}_{-0.48} \times 10^{-11}$	9.59	0.92	96.7
NGC 6715	$6.02^{+4.15}_{-3.77} \times 10^{-13}$	26.49	2.52	2.6
NGC 7089	$< 4.50 \times 10^{-13}$	11.56	0.52	0.0

LMXB	Notes	Globular Cluster	References
4U 1820-30	P	NGC 6624	[69–71]
4U 0513-40	P	NGC 1851	[72–74]
4U 1746-37	P	NGC 6441	[69, 75, 76]
XB 1832-330	P	NGC 6652	[75, 77, 78]
M15 X-2	P	NGC 7078/M15	[79–81]
AC 211	P	NGC 7078/M15	[69, 80, 82]
SAX J1748.9-2021	T, XP	NGC 6440	[75, 83, 84]
GRS 1747-312	T	Terzan 6	[85–87]
Terzan 6 X-2	T	Terzan 6	[88]
IGR J17361-4441	T	NGC 6388	[89, 90]
IGR J18245-2542	T, XP	NGC 6626/M28	[91, 92]
EXO 1745-248	T	Terzan 5	[93, 94]
IGR J17480-2446	T	Terzan 5	[95–97]
Terzan 5 X-3	T	Terzan 5	[98]
MAXI J0911-635	T	NGC 2808	[99]

Haggard et al. (2017; 1701.02726)

The Low-Mass X-Ray Binary Connection

$$L_\gamma^{\rm IG} = L_\gamma^{\rm clusters} \times \left(\frac{N_{\rm LMXB}^{\rm IG}}{N_{\rm LMXB}} \right)$$

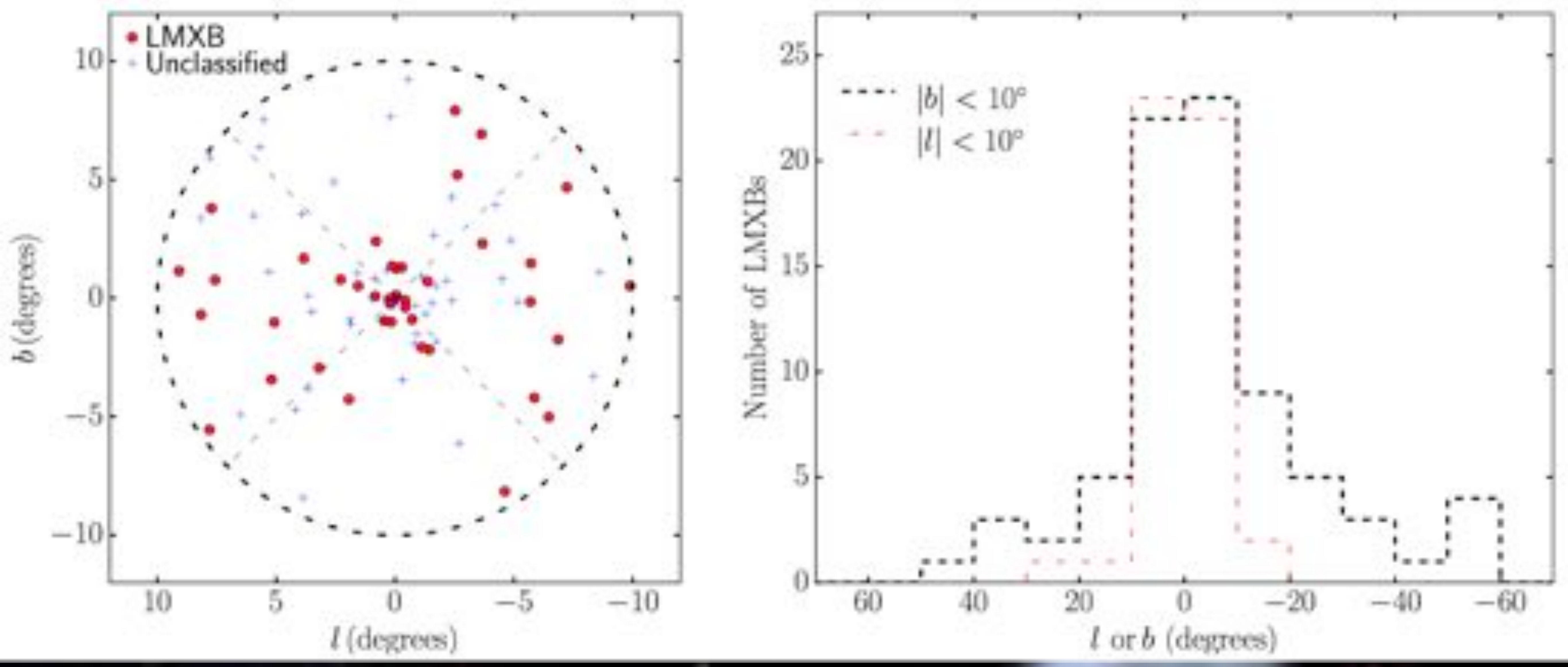

Haggard et al. (2017; 1701.02726)

The Low-Mass X-Ray Binary Connection

$$L_\gamma^{\mathrm{IG}} = L_\gamma^{\mathrm{clusters}} \times \left(\frac{N_{\mathrm{LMXB}}^{\mathrm{IG}}}{N_{\mathrm{LMXB}}} \right)$$

$$\begin{aligned} L_\gamma^{\mathrm{IG}} &= (2.09^{+0.86}_{-0.71}) \times 10^{36}\,\mathrm{erg/s}, && \text{Only Sources Classified as LMXBs} \\ L_\gamma^{\mathrm{IG}} &= (4.38^{+1.79}_{-1.48}) \times 10^{36}\,\mathrm{erg/s}, && \text{Including All Unclassified Sources} \end{aligned} \quad (4.2)$$

Comparing this result with the measured gamma-ray luminosity of gamma-ray excess, $L_\gamma = (2.0 \pm 0.4) \times 10^{37}$ erg/s integrated within 10° of the Galactic Center [8, 113], we estimate that $10.5^{+4.7}_{-4.1}\%$ (only LMXBs) or $21.9^{+9.9}_{-8.6}\%$ (LMXBs and unclassified) of the excess emission can be potentially attributed to an underlying MSP population. As mentioned above, however, this calculation almost certainly overestimates the fraction of the Galactic Center excess that arises from MSPs.

Haggard et al. (2017; 1701.02726)

The Low-Mass X-Ray Binary Connection

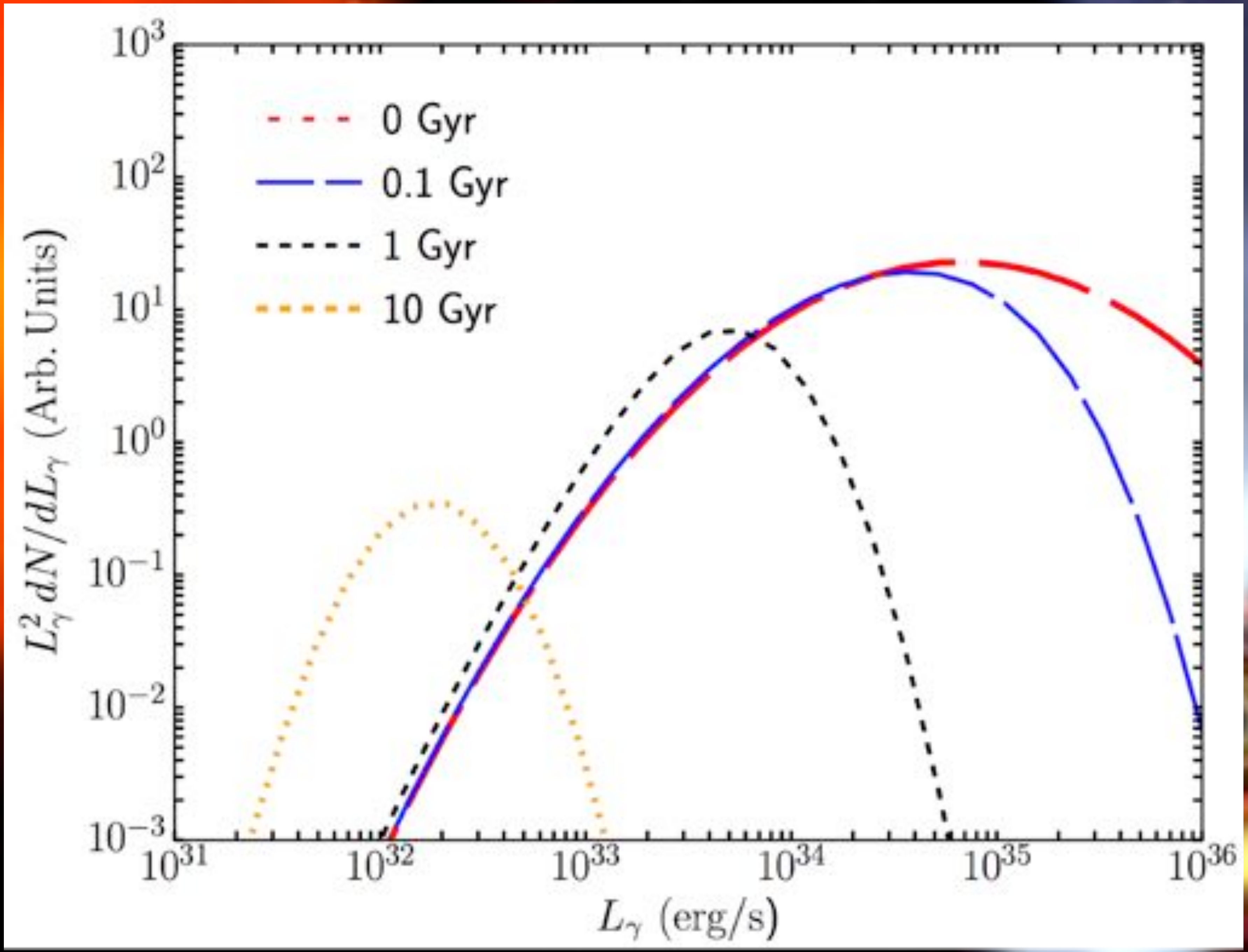

Hooper & Linden (2016; 1606.09250)

Leptonic Outbursts

Outbursts of relativistic electrons from Sgr A* can produce a radially symmetric diffuse component.

Hard to get leptons to high latitudes without cooling.

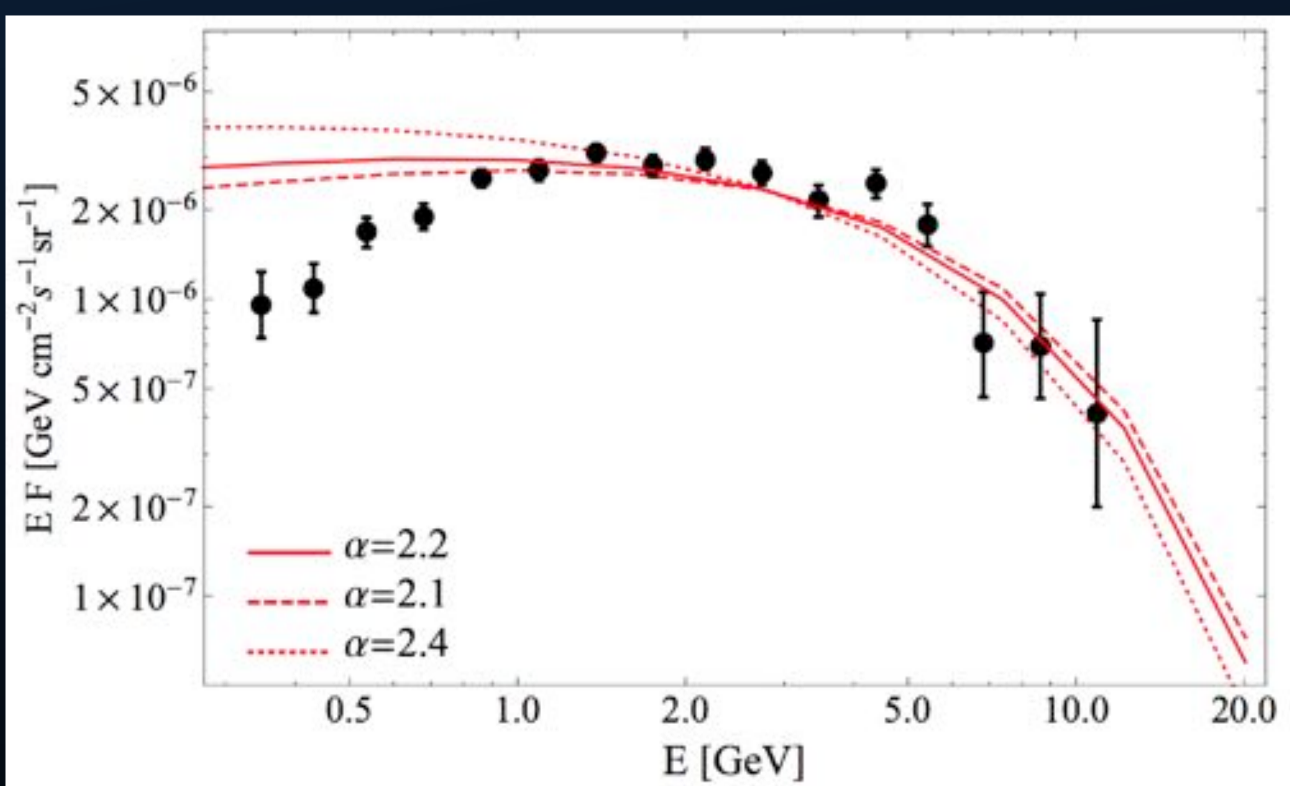

Petrovic et al. (2015; 1405.7928)

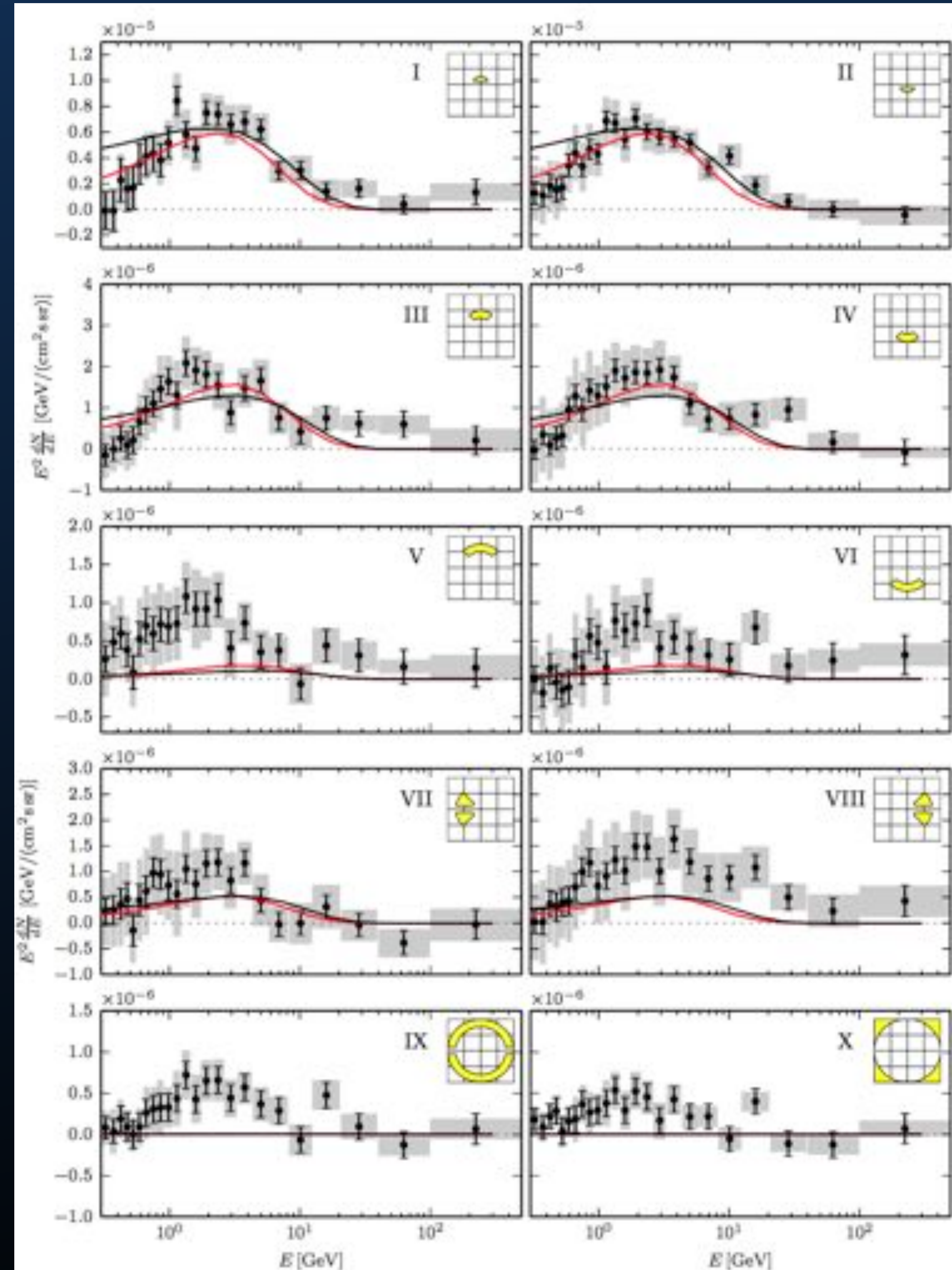

Cholis et al. (2015; 1506.05119)

Diffuse Emission Models

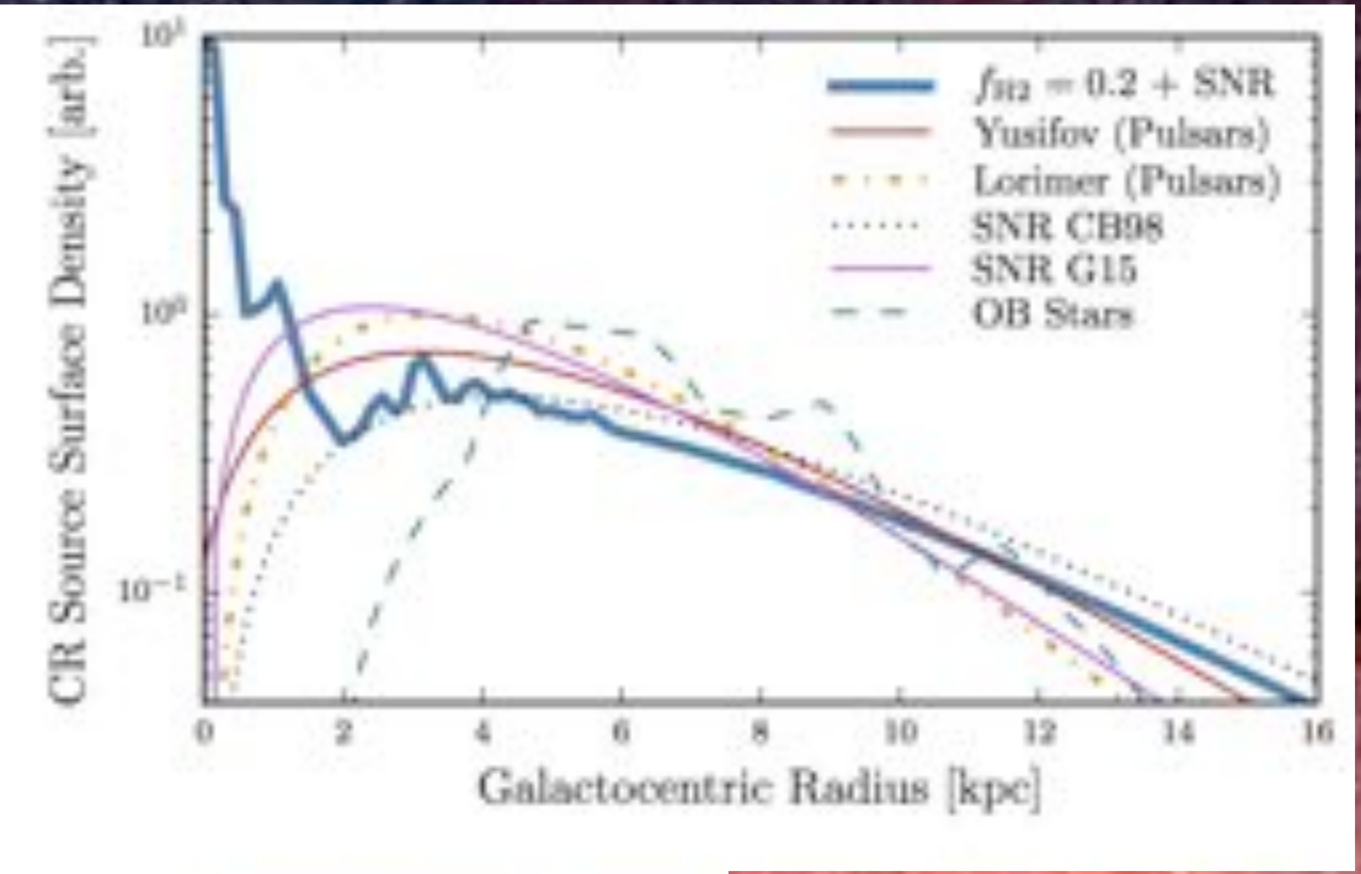

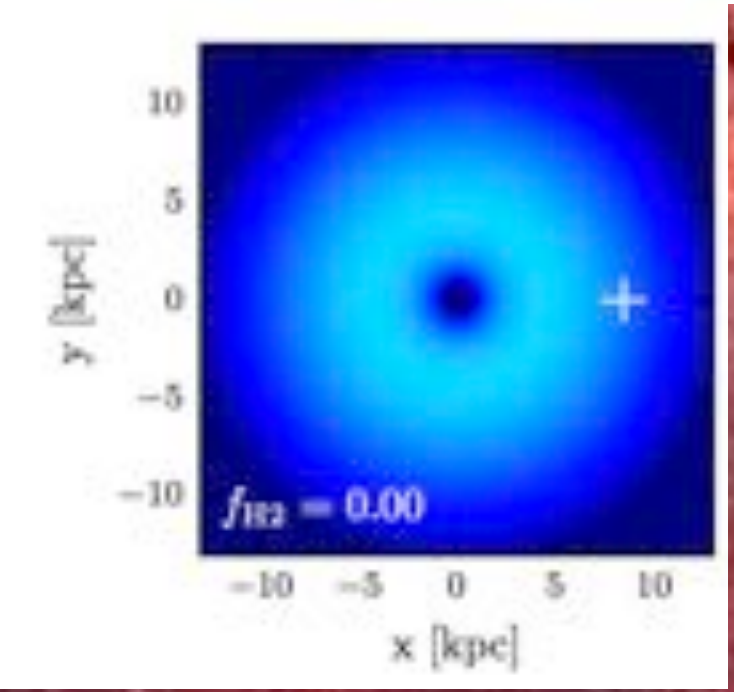

Typical Galprop models utilize cosmic-ray injection morphologies that include no injection near the Galactic center.

This is despite the fact that >10% of the Milky Way star formation is produced in the central molecular zone.

Diffuse Emission Models

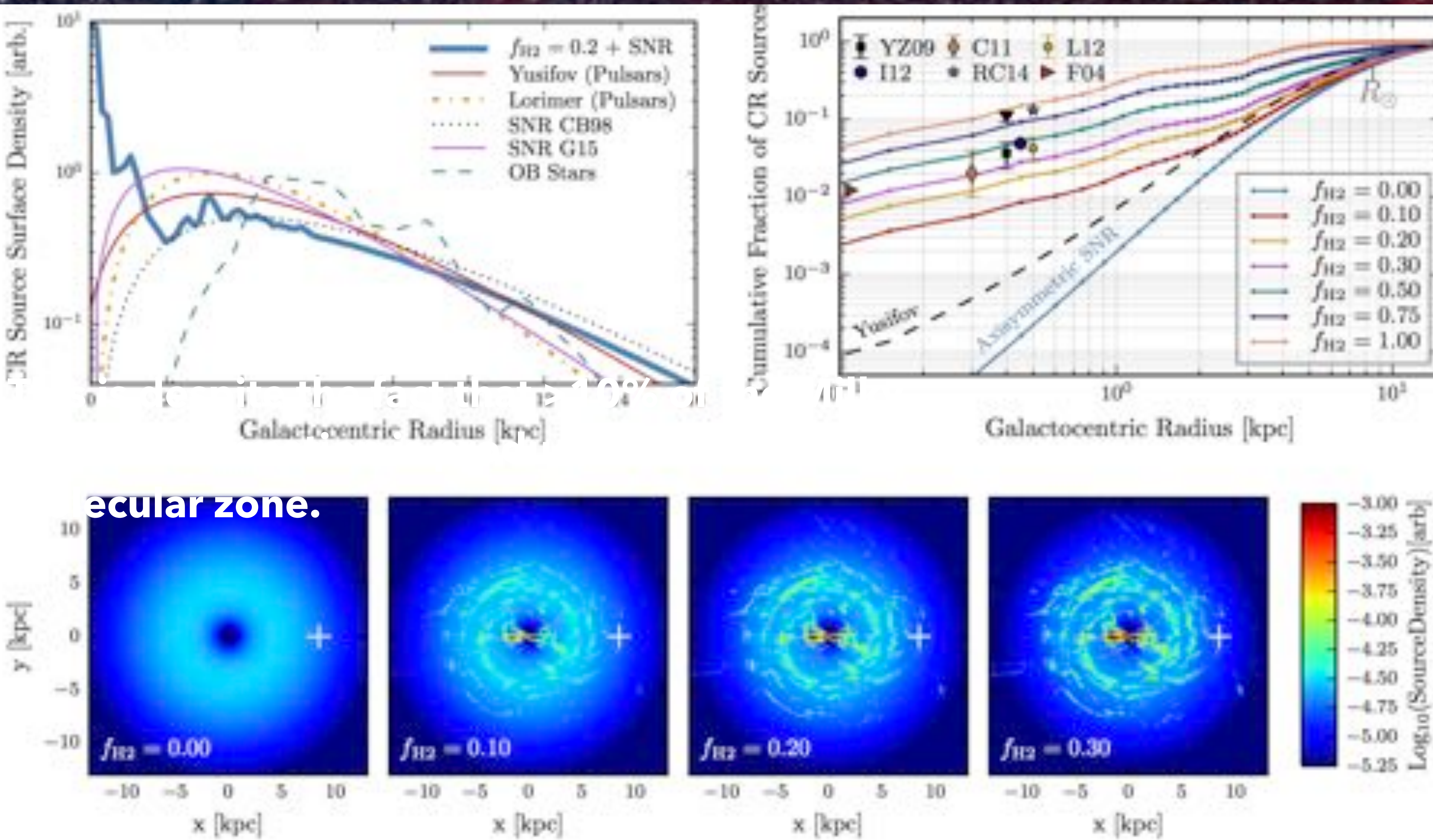

ecular zone.

Can build models that inject cosmic-rays tracing gas in the CMZ.

Diffuse Emission Models

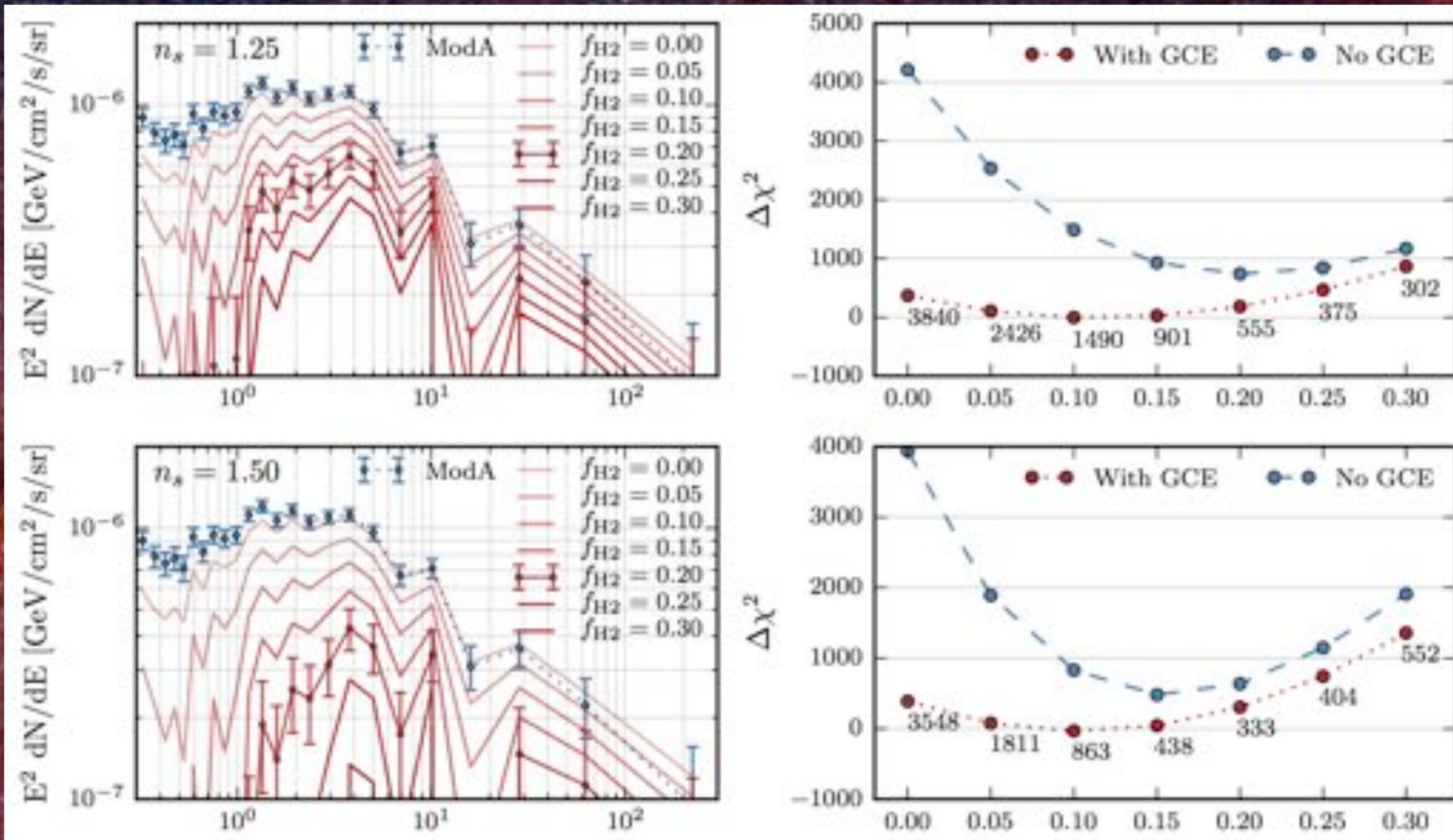

This decreases, the excess, by about a factor of 2 for best-fit models.

Diffuse Emission Models

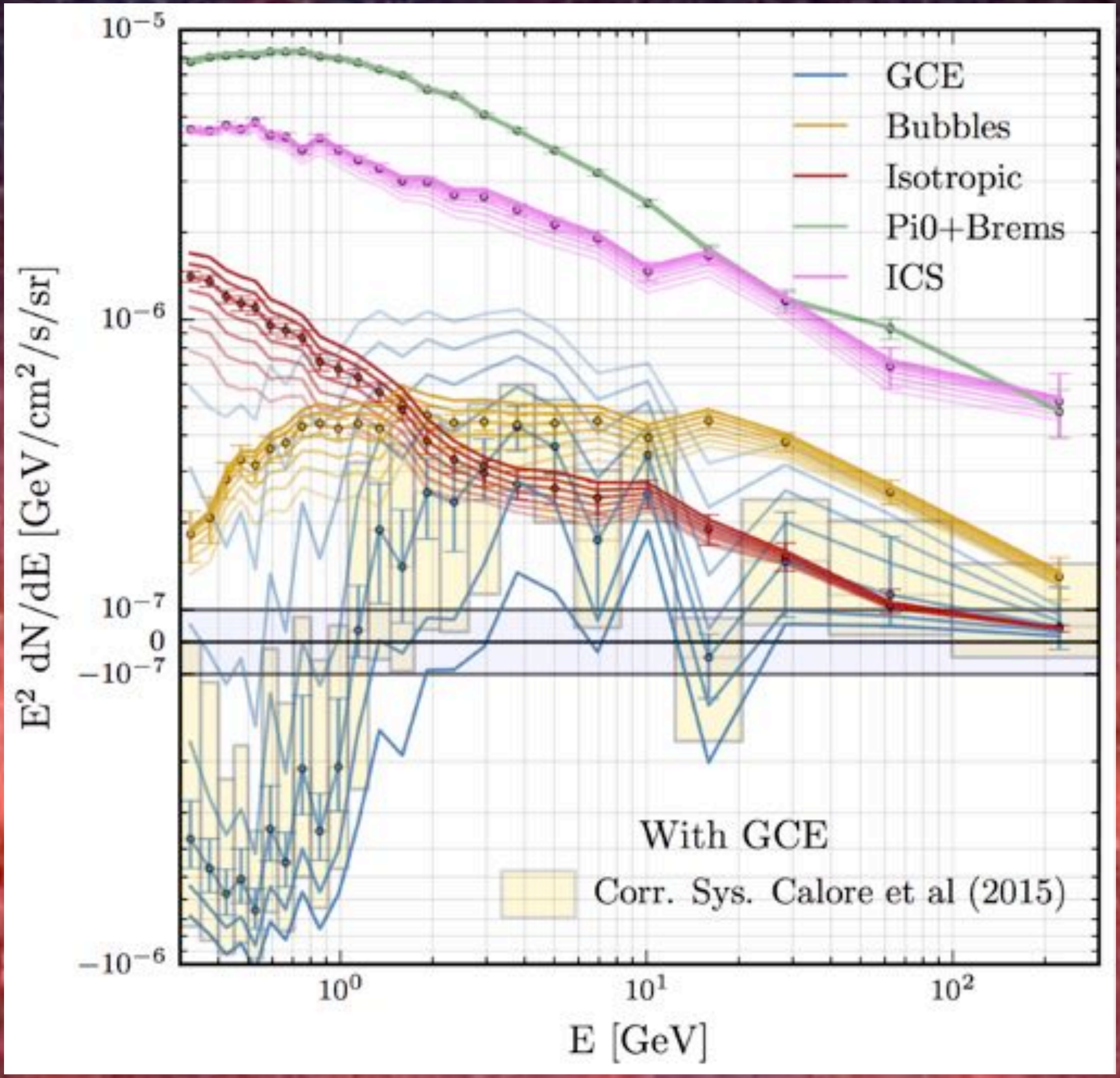

Cranking up the CR injection causes significant over subtraction at low energies. The GCE feature remains, but is zero-subtracted.

Diffuse Emission Models

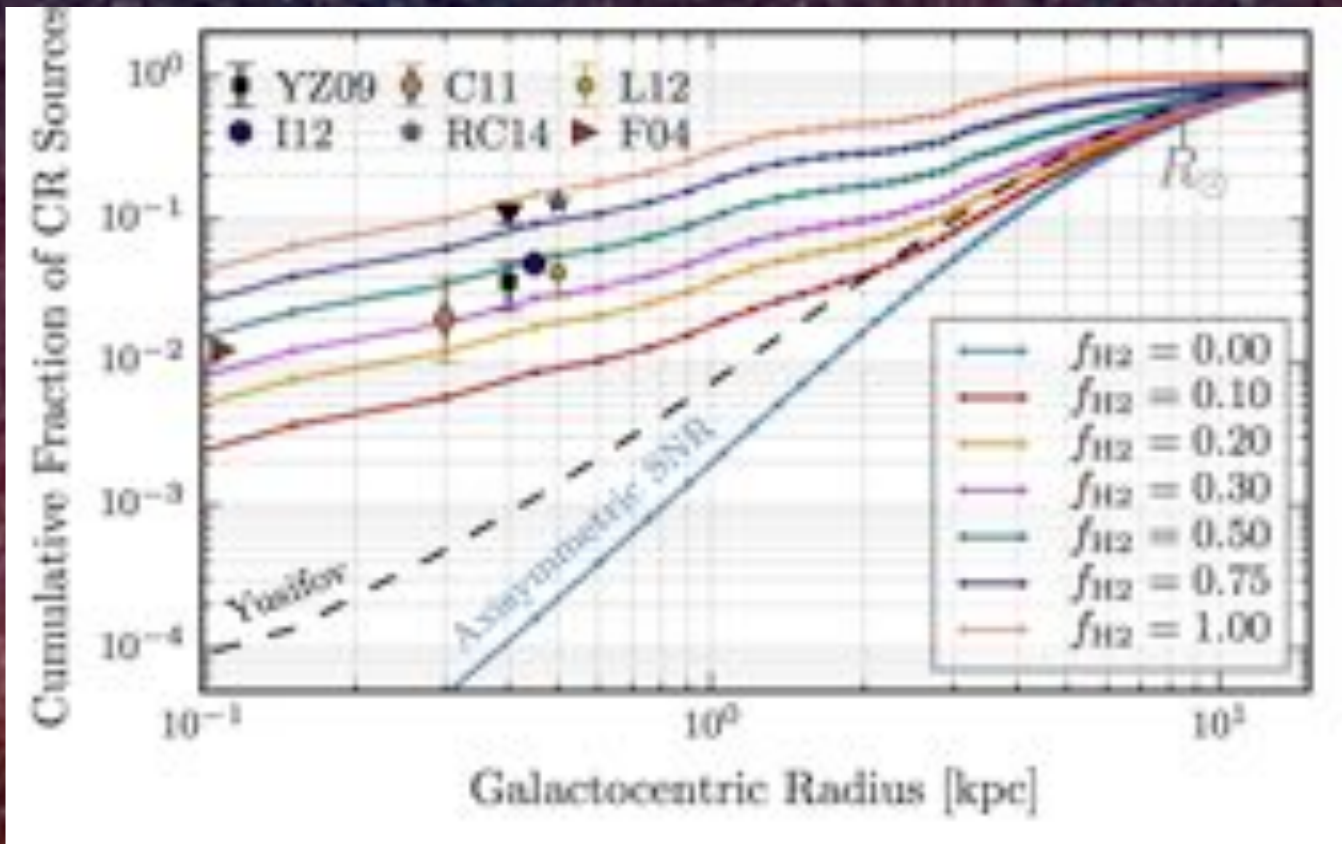

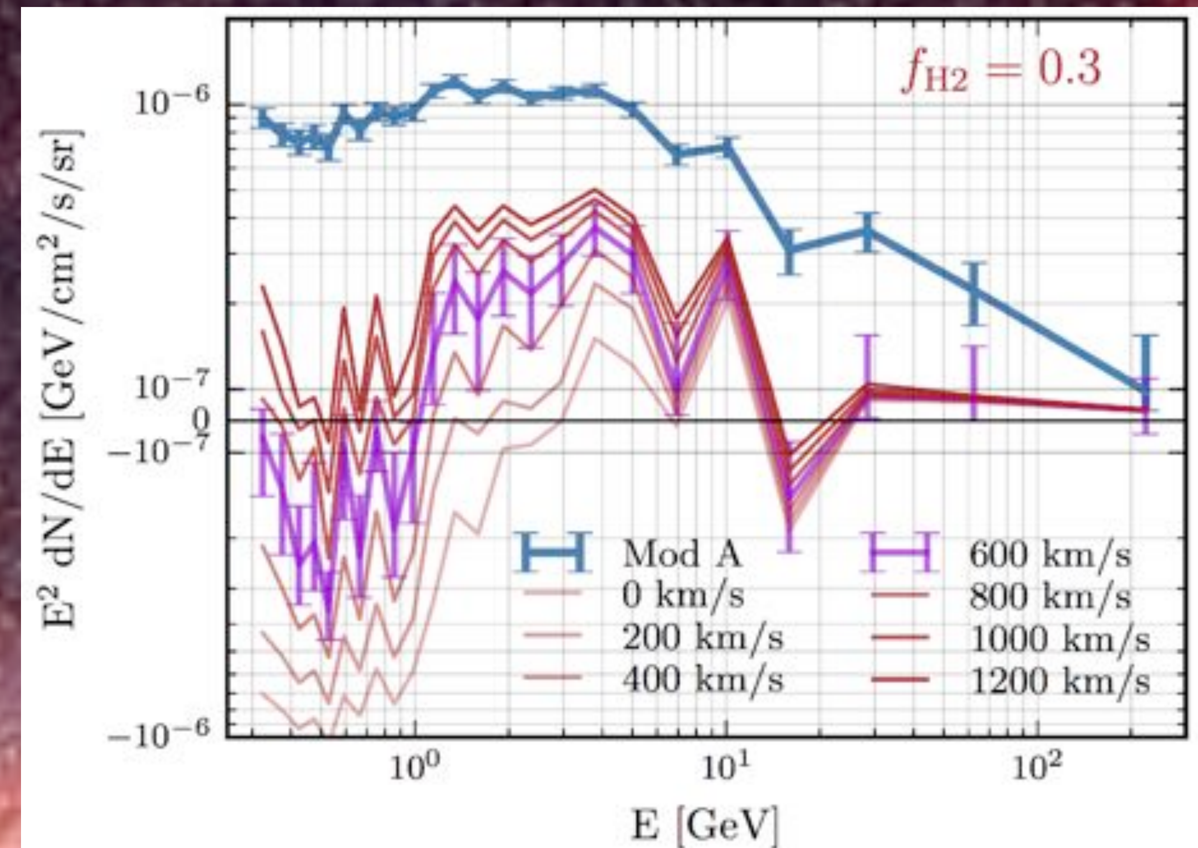

Can fix this by adding winds to remove low-energy cosmic-rays.

*** Better fit to data.**
*** Excess returns.**
*** Fits CMZ cosmic-ray injection**

Dark Matter Models

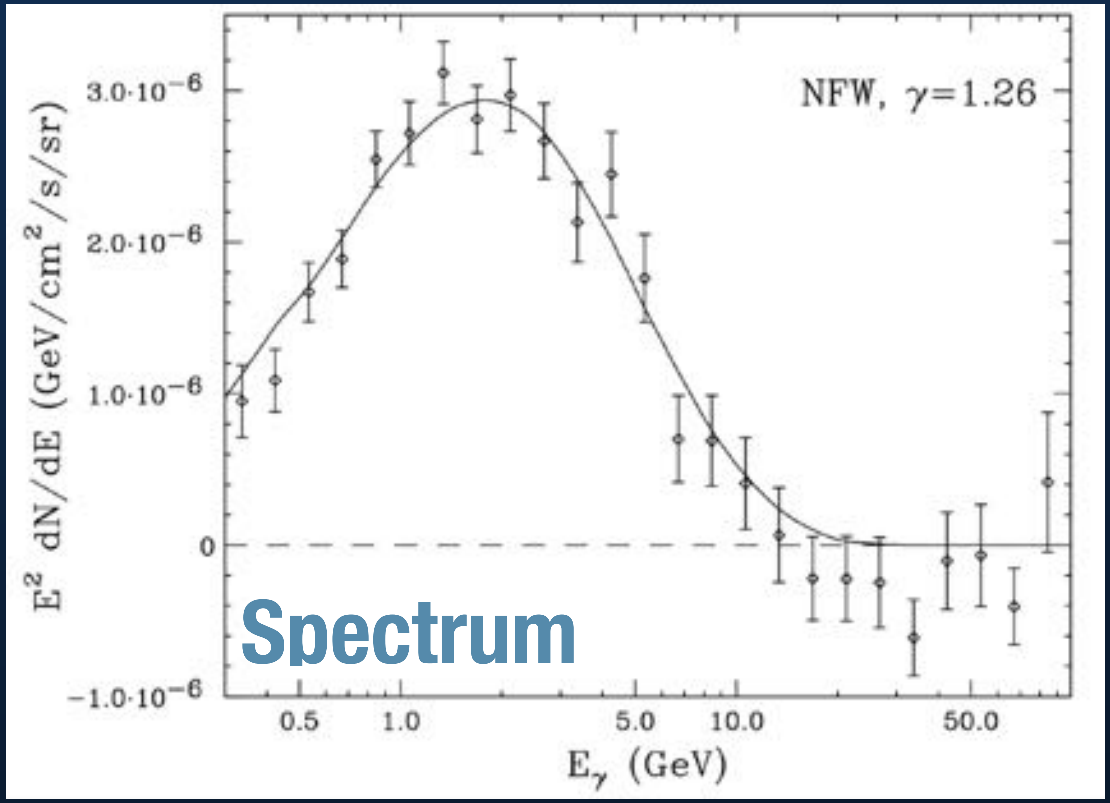

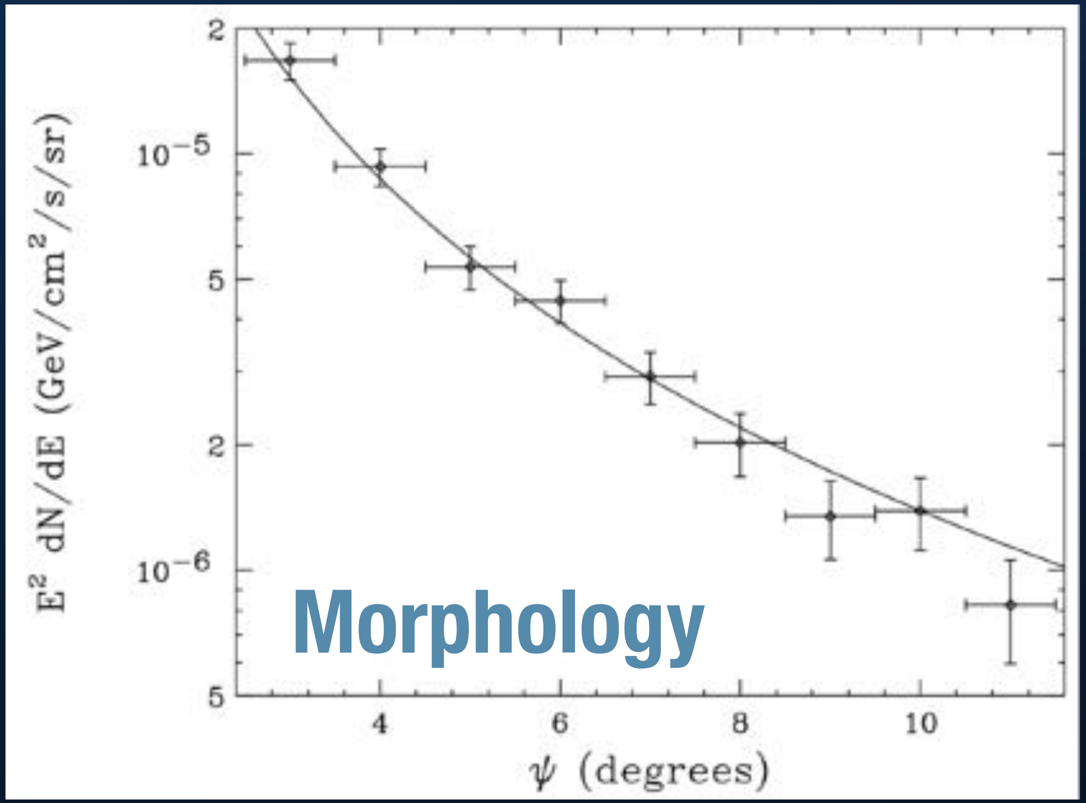

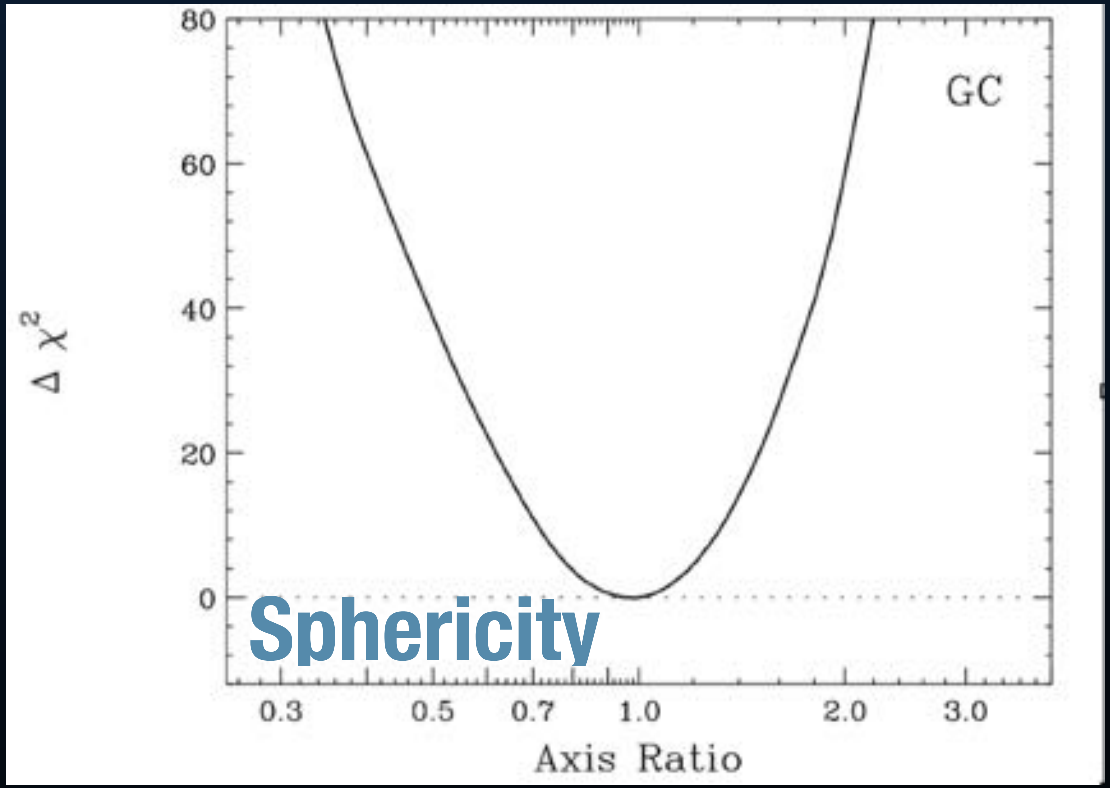

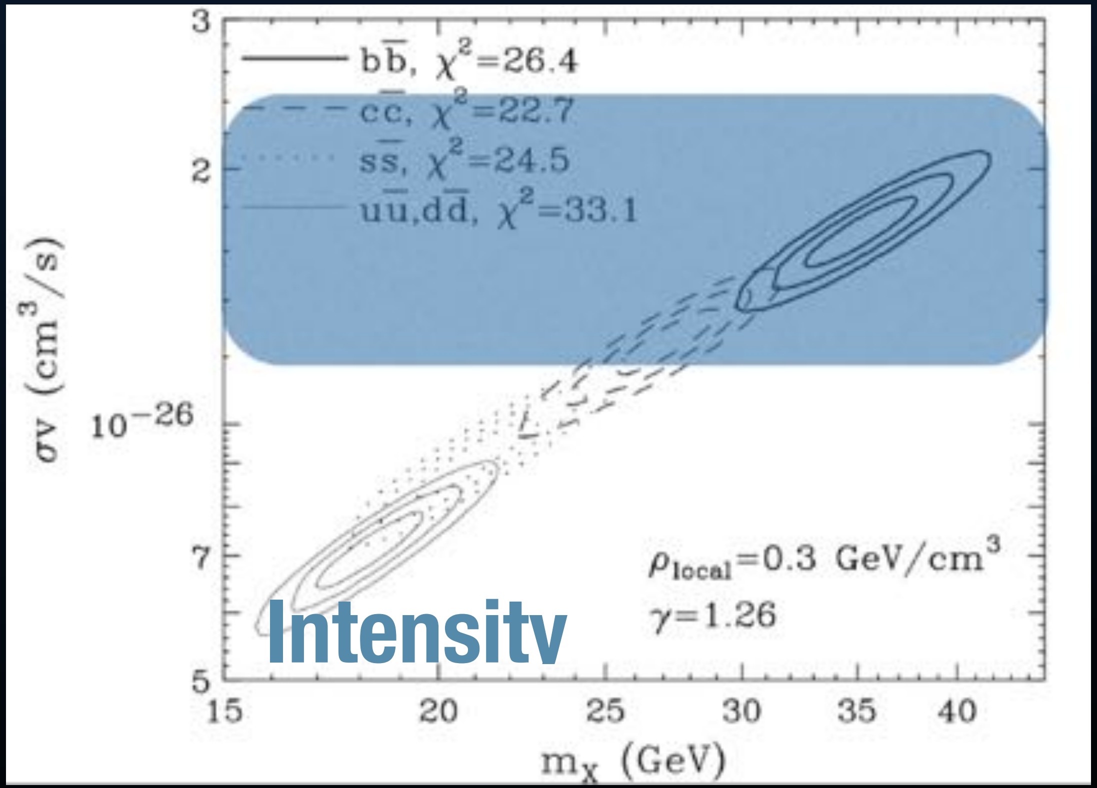

Dark Matter Models

Chan (1607.02246)
Jia (1607.00737)
Barrau et al. (1606.08031)
Huang et al. (1605.09018)
Cui et al. (1605.08138)
Krauss et al. (1605.05327)
Kumar et al. (1605.00611)
Biswas et al. (1604.06566)
Sage et al. (1604.04589)
Choquette et al. (1604.01039)
Cuoco et al. (1603.08228)
Chao et al. (1602.05192)
Horiuchi et al. (1602.04788)
Hektor et al. (1602.00004)
Freytsis et al. (1601.07556)
Kim et al. (1601.05089)
Huang et al. (1512.08992)
Kulkami et al. (1512.06836)
Tang et al. (1512.02899)
Cox et al. (1512.00471)
Cai et al. (1511.09247)
Agrawal et al. (1511.06293)
Duerr et al. (1510.07562)
Drozd et al. (1510.07053)
Arcadi et al. (1510.02297)
Williams (1510.00714)
Cai & Spray (1509.08481)
Freese et al. (1509.05076)
Bhattacharya et al. (1509.03665)
Algeri et al. (1509.01010)
Fox & Tucker-Smith (1509.00499)
Dutta et al. (1509.05989)
Liu et al. (1508.05716)
Berlin et al. (1508.05390)
Fan et al. (1507.06993)
Hektor et al. (1507.05096)
Achterbeg et al. (1507.04644)
Biswas et al. (1507.04543)
Butter et al. (1507.02288)
Mondal et al. (1507.01793)
Cao et al. (1506.06471)
Banik et al. (1506.05665)
Ipek (1505.07826)
Buchmueller et al. (1505.07826)
Balazs et al. (1505.06758)
Medina (1505.05565)
Kim et al. (1505.04620)
Ko et al. (1504.06944)
Ko & Tang (1504.03908)
Ghorbani & Ghorbani (1504.03610)
Fortes et al. (1503.08220)
Cline et al. (1503.08213)
Rajaraman et al. (1503.05919)
Bi et al. (1503.03749)
Kopp et al. (1503.02669)
Elor et al. (1503.01773)
Gherghetta et al. (1502.07173)
Berlin et al. (1502.06000)
Achterberg et al. (1502.05703)
Modak et al. (1502.05682)
Guo et al. (1502.00508)
Chen & Nomura (1501.07413)
Kozaczuk & Martin (1501.07275)
Berlin et al. (1501.03496)
Kaplinghat et al. (1501.03507)
Alves et al. (1501.03490)
Biswas et al. (1501.02666)
Biswas et al. (1501.02666)
Ghorbani & Ghorbani (1501.00206)
Cerdeno et al. (1501.01296)
Liu et al. (1412.1485)
Hooper (1411.4079)
Arcadi et al. (1411.2985)
Cheung et al. (1411.2619)
Agrawal et al. (1411.2592)
Kile et al. (1411.1407)
Buckley et al. (1410.6497)
Heikinheimo & Spethmann (1410.4842)
Freytsis et al. (1410.3818)
Yu et al. (1410.3347)
Cao et al. (1410.3239)
Guo et al. (1409.7864)
Yu (1409.3227)
Cahill-Rowley et al. (1409.1573)
Banik & Majumdar (1408.5795)
Bell et al. (1408.5142)
Ghorbani (1408.4929)
Okada & Seto (1408.2583)
Frank & Mondal (1408.2223)
Baek et al. (1407.6588)
Tang (1407.5492)
Balazs & Li (1407.0174)
Huang et al. (1407.0038)
McDermott (1406.6408)
Cheung et al. (1406.6372)
Arina et al. (1406.5542)
Chang & Ng (1406.4601)
Wang & Han (1406.3598)
Cline et al. (1405.7691)
Berlin et al. (1405.5204)
Mondal & Basak (1405.4877)
Martin et al. (1405.0272)
Ghosh et al. (1405.0206)
Abdullah et al. (1404.5503)
Park & Tang (1404.5257)
Cerdeno et al. (1404.2572)
Izaguirre et al. (1404.2018)
Agrawal et al. (1404.1373)
Berlin et al. (1404.0022)
Alves et al. (1403.5027)
Finkbeiner & Weiner (1402.6671)
Boehm et al. (1401.6458)
Kopp et al. (1401.6457)
Modak et al. (1312.7488)
Alves et al. (1312.5281)
Alves et al. (1312.5281)
Fortes et al. (1312.2837)
Banik et al. (1311.0126)
Arhrib et al. (1310.0358)
Kelso et al. (1308.6630)
Kozaczuk et al. (1308.5705)
Kumar (1308.4513)
Demir et al. (1308.1203)
Buckley et al. (1307.3561)
Cline et al. (1306.4710)
Cannoni et al. (1205.1709)
An et al. (1110.1366)
Buckley et al. (1106.3583)
Boucenna et al. (1106.3368)
Ellis et al. (1106.0768)
Cheung et al. (1104.5329)
Marshall et al. (1102.0492)
Abada et al. (1101.0365)
Tytgat (1012.0576)
Logan (1010.4214)
Barger et al. (1008.1796)
Raklev et al. (0911.1986)

Bigger Question: Are Dark Matter Models Ruled Out?

Ackermann et al. (2015; 1503.02641)

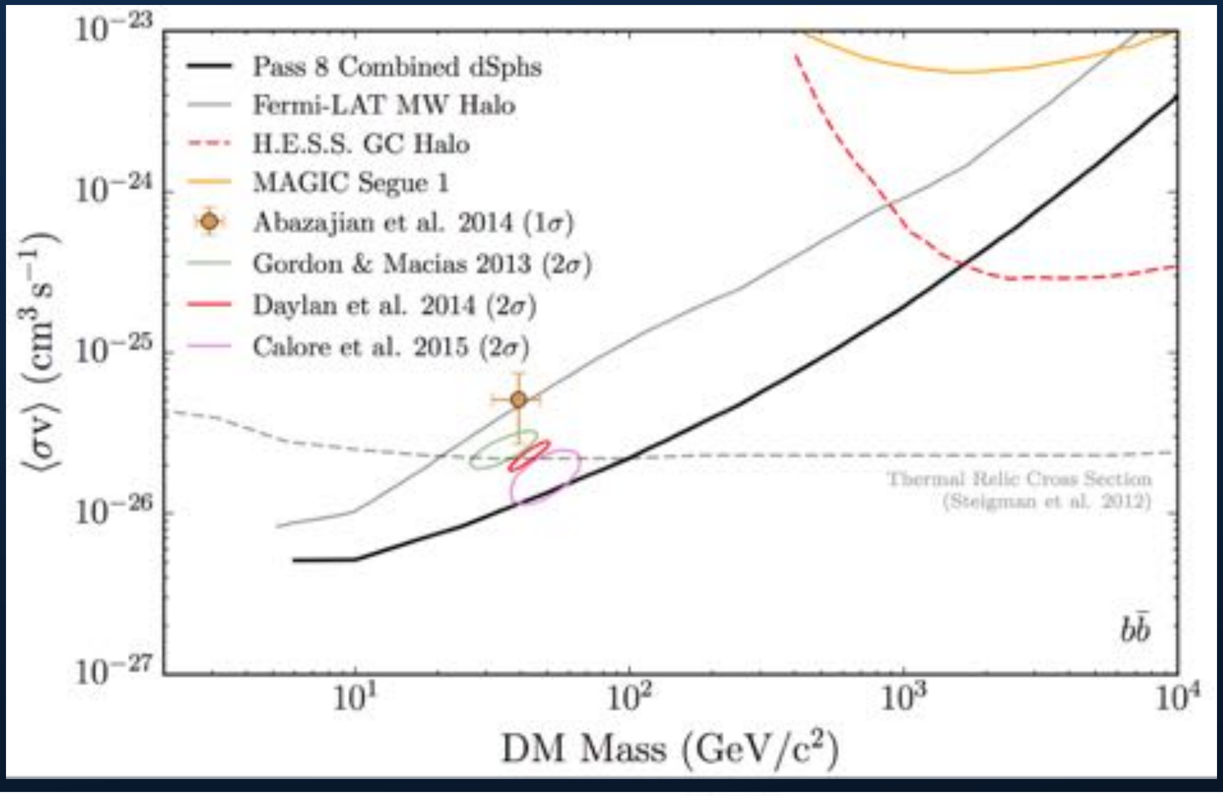

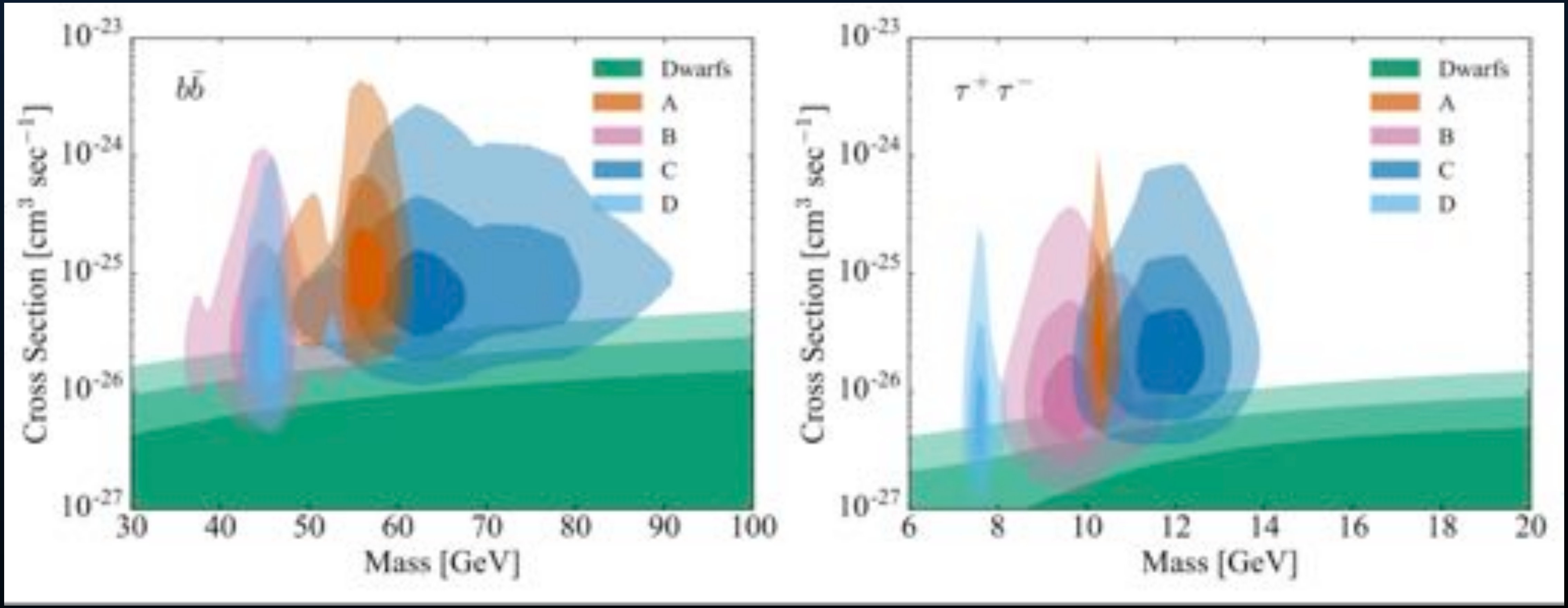

Keeley et al. (2017; 1710.03215)

Bigger Question: Are Dark Matter Models Ruled Out?

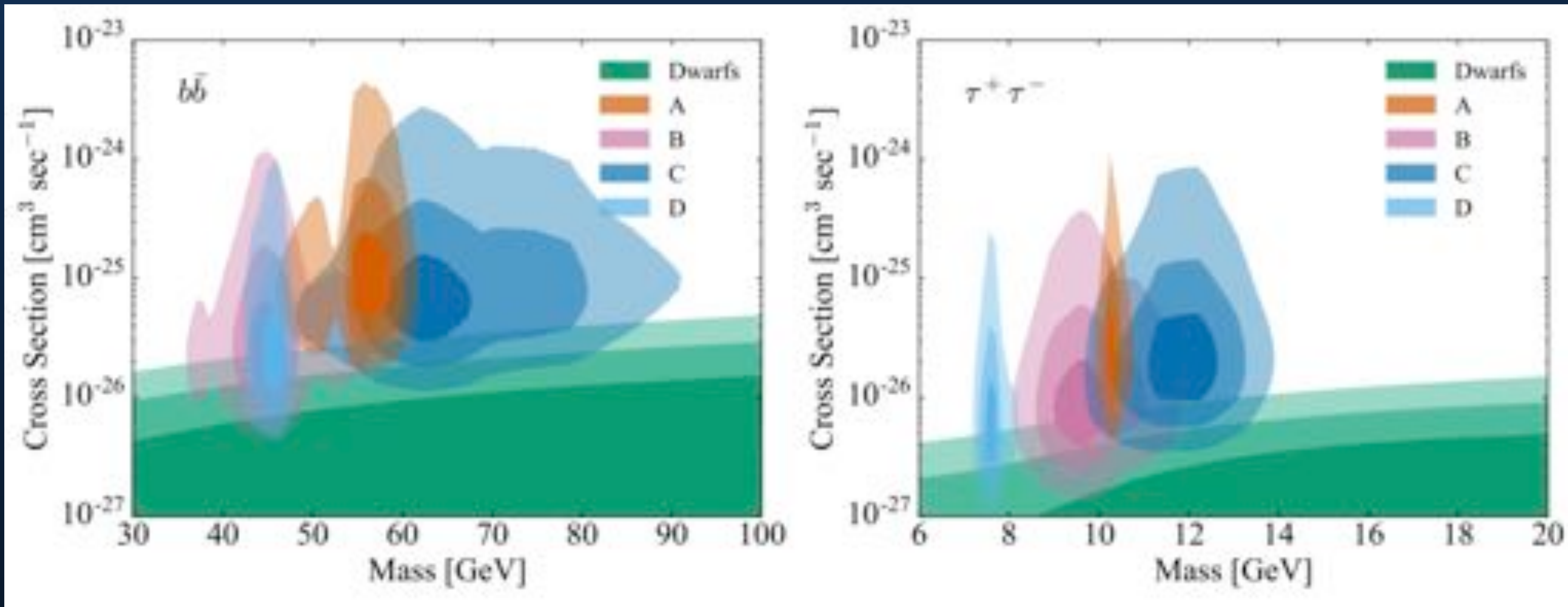

For the local density, we use the value determined by Zhang et al. (2012) [59]: $\rho_\odot = 0.28 \pm 0.08$ GeV cm^{-3}. This robust determination of the local DM density is derived from modeling the spatial and velocity distributions for a sample of 9000 K-Dwarf stars from the Sloan Digital Sky Survey (SDSS). The velocity distribution of these stars directly measures the local gravitational potential and, when combined with stellar density constraints, provides a measure of the local DM density.

		α-young		α-old		Combined analysis
		Tilt	No Tilt	Tilt	No Tilt	Tilt
95% CR upper	GeV cm^{-3}	**0.59**	0.57	0.85	0.51	0.48
	$M_\odot$ pc^{-3}	**0.016**	0.015	0.022	0.013	0.013
68% CR upper	GeV cm^{-3}	**0.53**	0.53	0.79	0.48	0.43
	$M_\odot$ pc^{-3}	**0.013**	0.014	0.021	0.013	0.012
Median	GeV cm^{-3}	**0.46**	0.48	0.73	0.46	0.40
	$M_\odot$ pc^{-3}	**0.012**	0.013	0.019	0.012	0.011
68% CR lower	GeV cm^{-3}	**0.37**	0.42	0.68	0.44	0.37
	$M_\odot$ pc^{-3}	**0.0098**	0.011	0.017	0.012	0.0097
95% CR lower	GeV cm^{-3}	**0.30**	0.35	0.60	0.42	0.34
	$M_\odot$ pc^{-3}	**0.0078**	0.0092	0.016	0.011	0.0091

Keeley et al. (2017; 1710.03215)

Sivertsson et al. (2017; 1708.07836)

Bigger Question: Are Dark Matter Models Ruled Out?

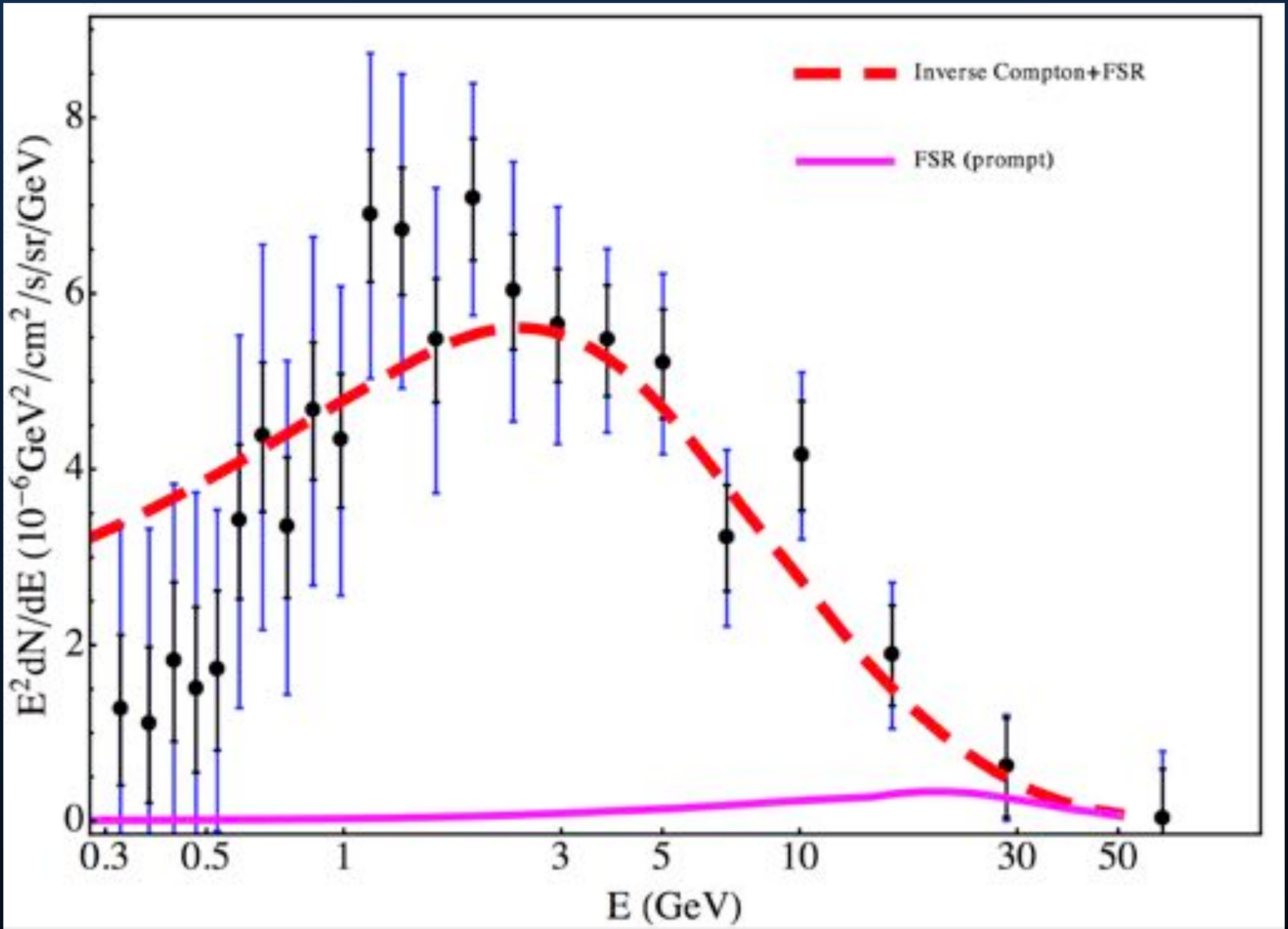

Can also model-build around constraints, for instance using SIDM to eliminate the signal from dwarfs.

Kaplinghat et al. (2015; 1501.03507)

Hints of Dark Matter Detection

Cuoco et al. (2017, 1711.06460)

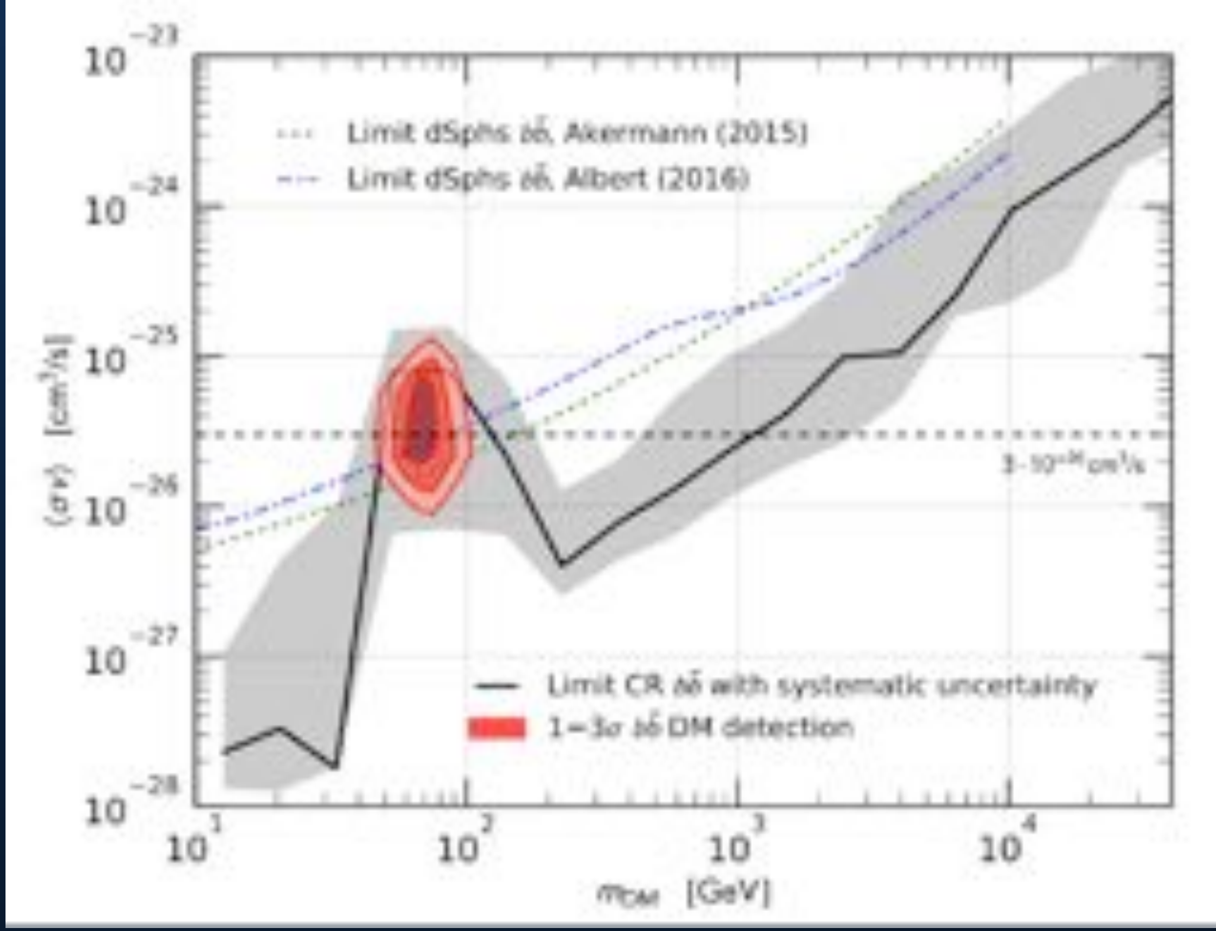

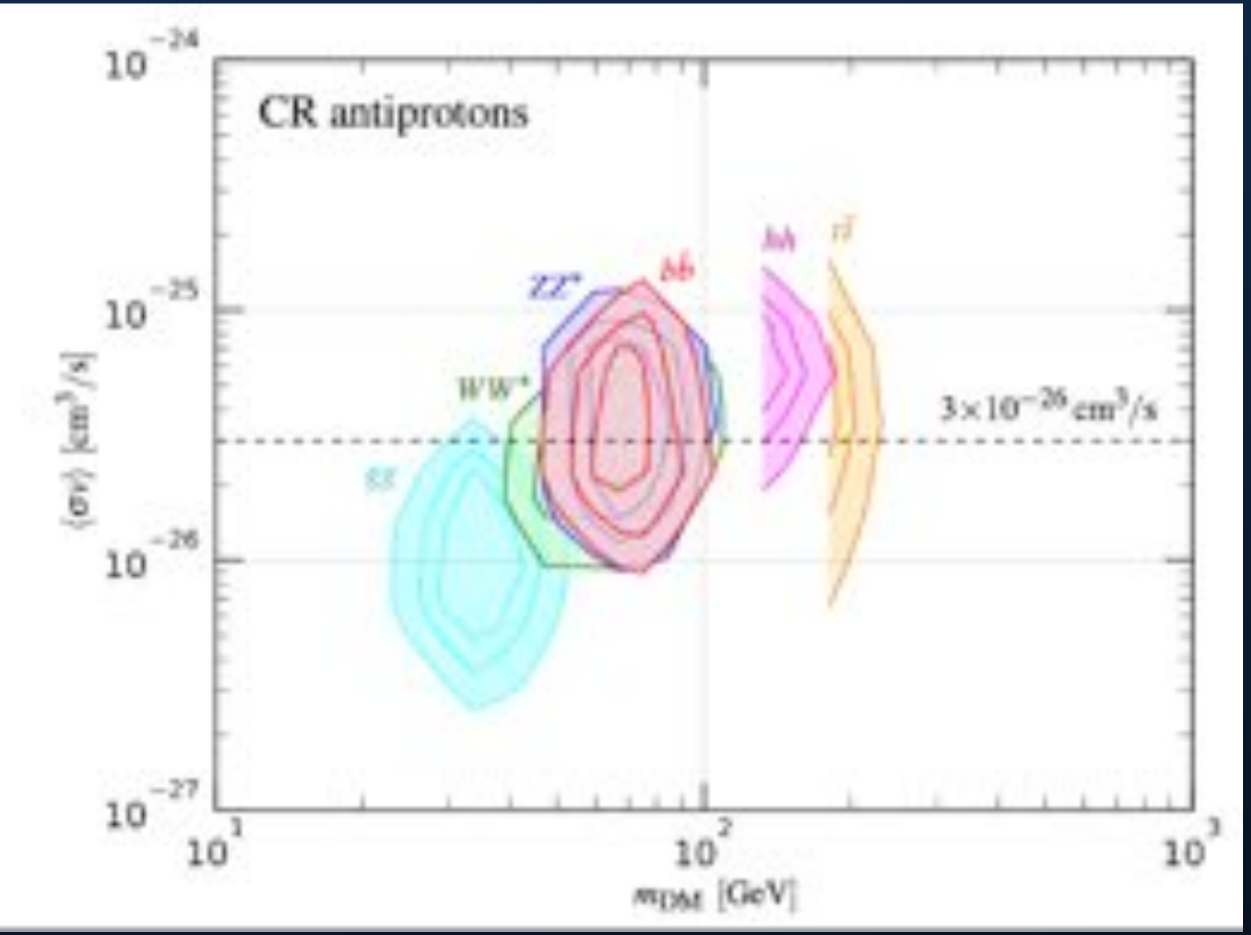

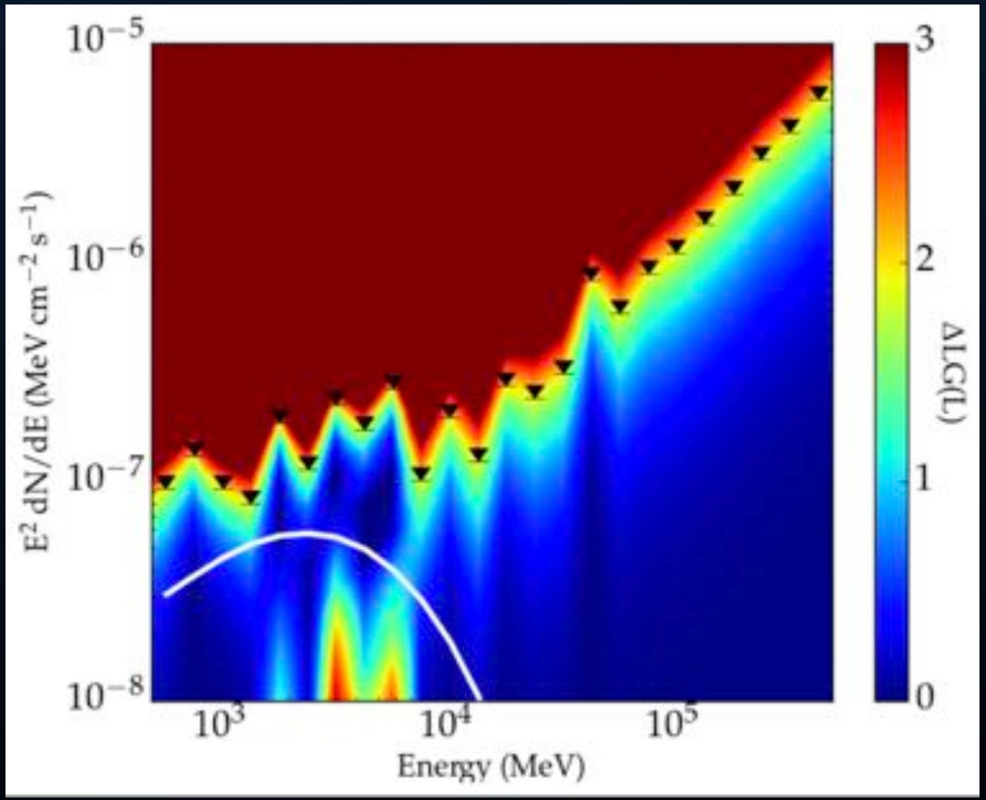

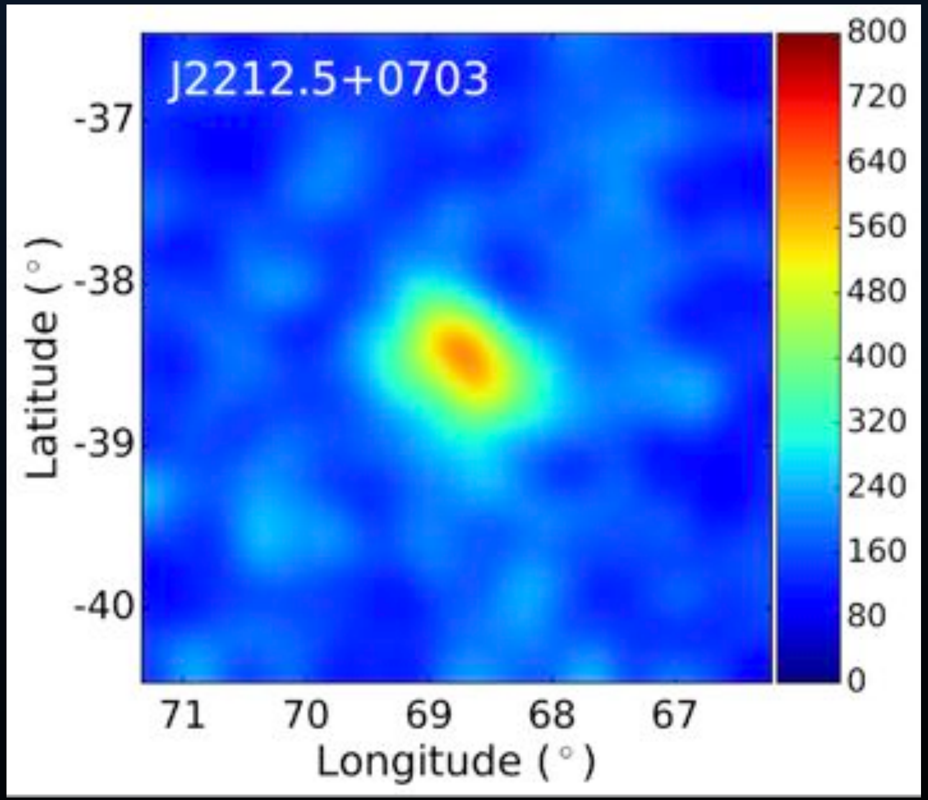

Hooper & Linden (2015, 1503.06029)

Bertoni et al. (2016; 1602.07303)

1. **Dark matter in its simplest form is being cornered**

2. **Recent results find difficulty in the dark matter hypothesis**

1. **Pulsar models are rich and have the flexibly to explain the GCE**

4. ASTROPHYSICAL EXPLANATIONS ARE BETTER THAN DARK MATTER EXPLANATIONS

(simple*) dark matter is cornered

Independent test regions are starting to show inconsistencies

*prompt two-body annihilating DM

vs Dwarfs

Posteriors for GCE-DM varying the MW J-factors, for 4 Galactic diffuse models

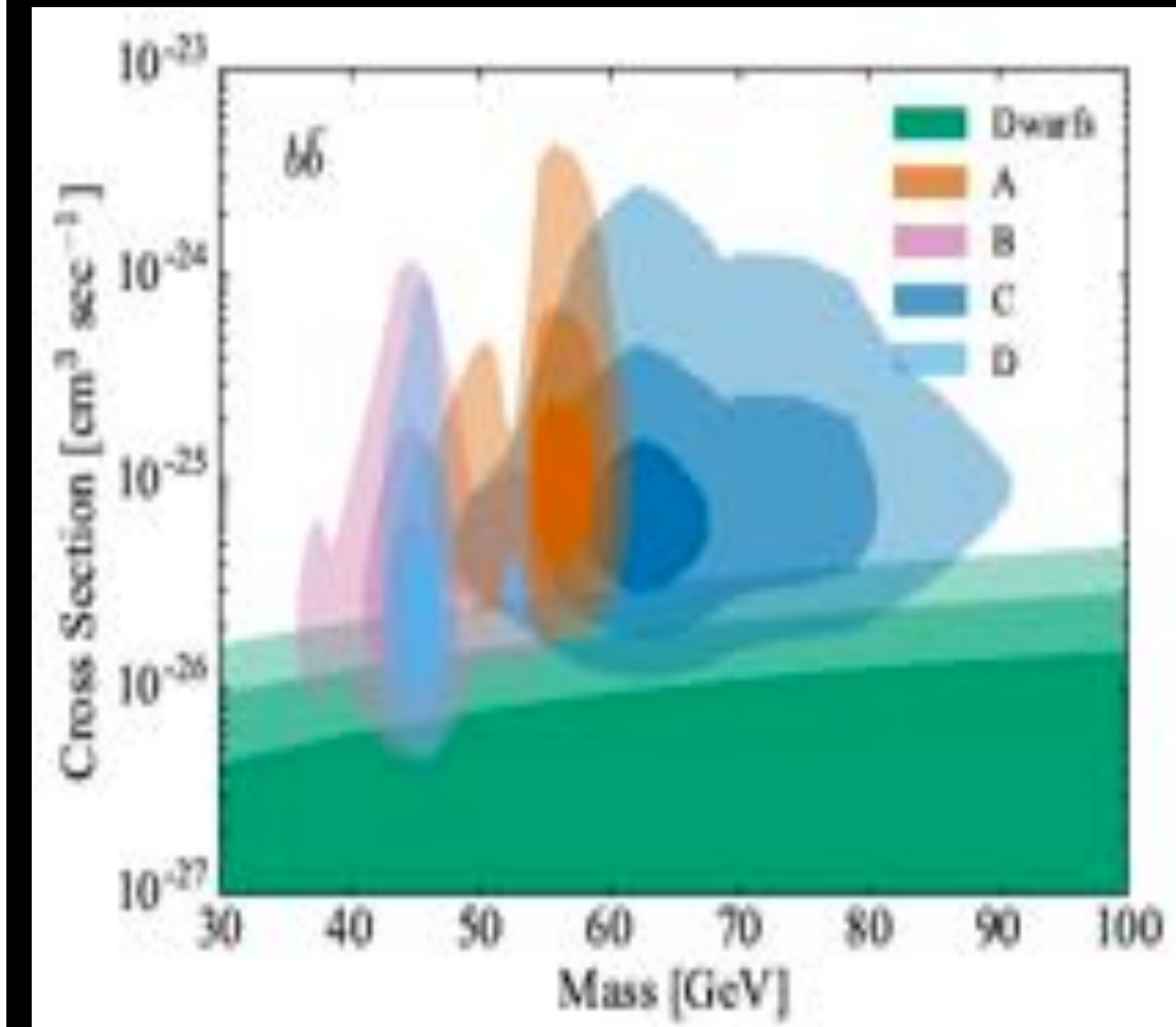

The parameter that the J-factor is most sensitive to is the local density of DM. As stated in a previous section, we use a value of 0.28±0.08 GeV/cm^3 taken from Zhang et al. (2012) [59]. Other groups including Pato et al. (2015) [65] and McKee et al. (2015) [66] tend to find higher values for the local density. To fully resolve the tension between the GCE and the dwarfs, the GCE J-factor needs to increase between 1 and 1.5 orders of magnitude, which translates into a local density of 3 to 6 times greater. As we show, none of these determinations of the local density relieve the GCE-dwarf evidence ratio to be unity.

Keeley et al (2017)

(simple*) dark matter is cornered

Independent test regions are starting to show inconsistencies

*prompt two-body annihilating DM

vs Milky Way halo

Milky Way Halo avoids the complex Galactic plane (here use |b| > 20 deg)

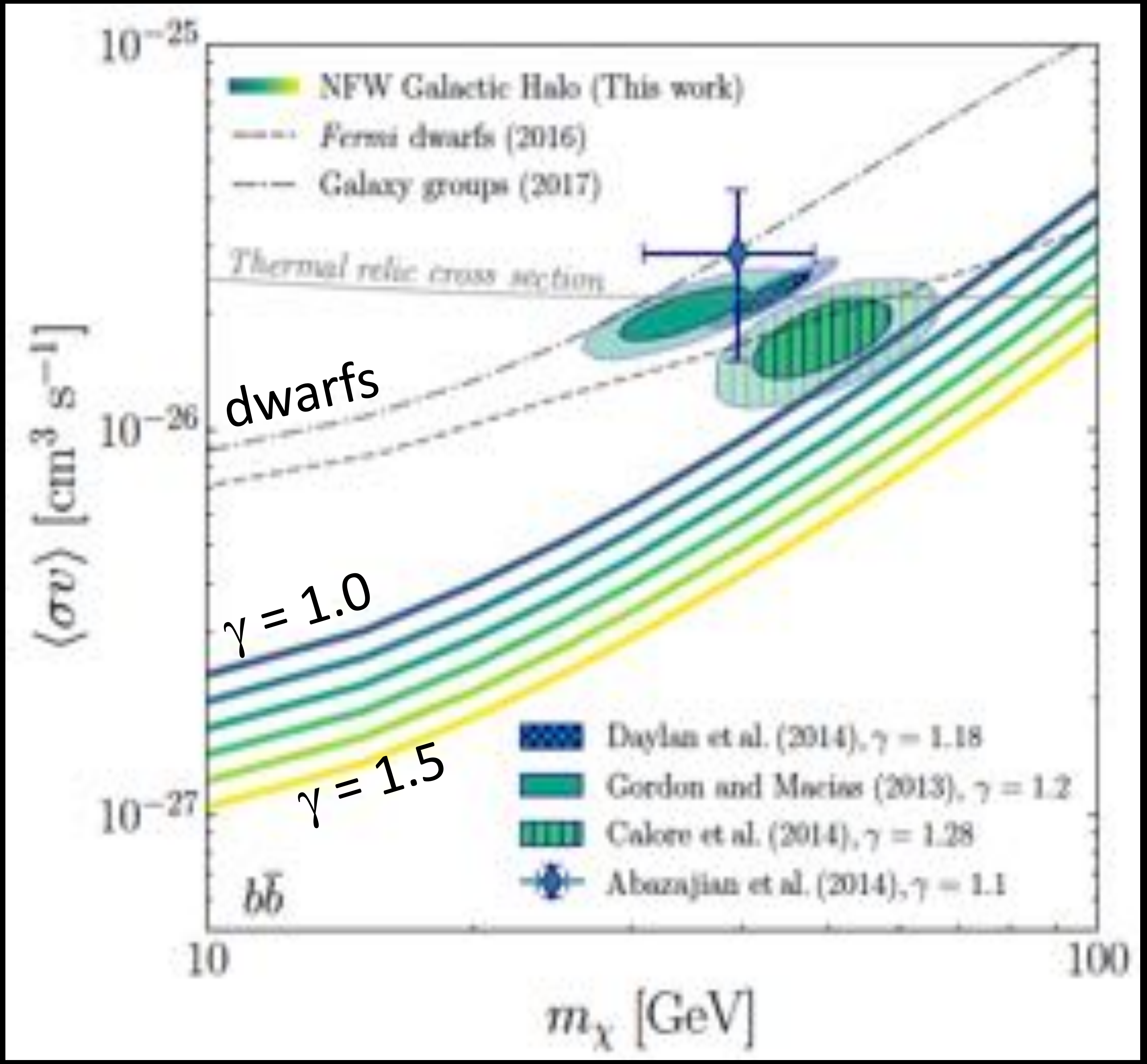

Chang et al (2018); see also Fermi (2012)

Difficulties of dark matter: morphology

Bulge over NFW

The data prefers an asymmetric excess outside of several degrees (the central few degrees are NFW-like)

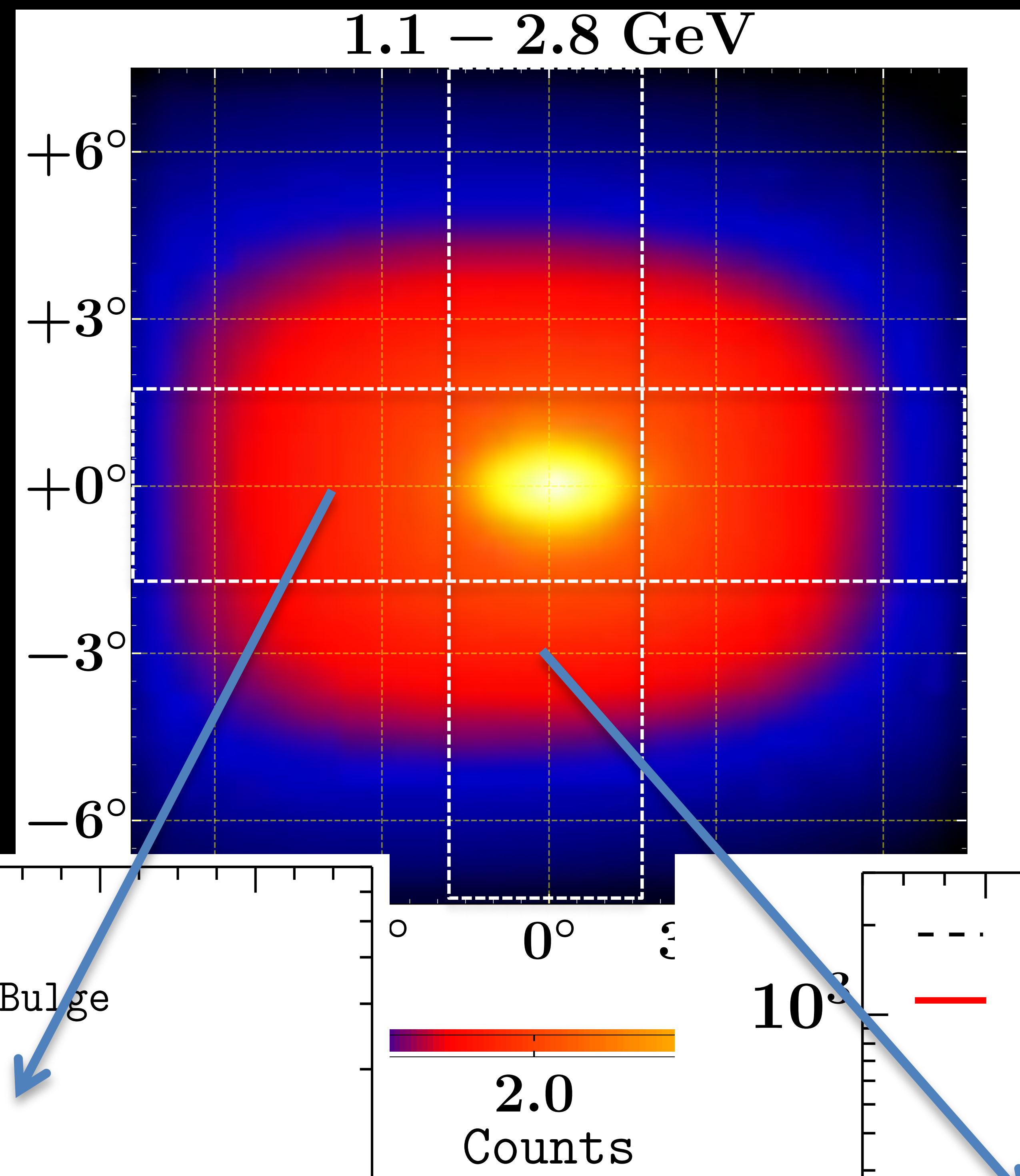

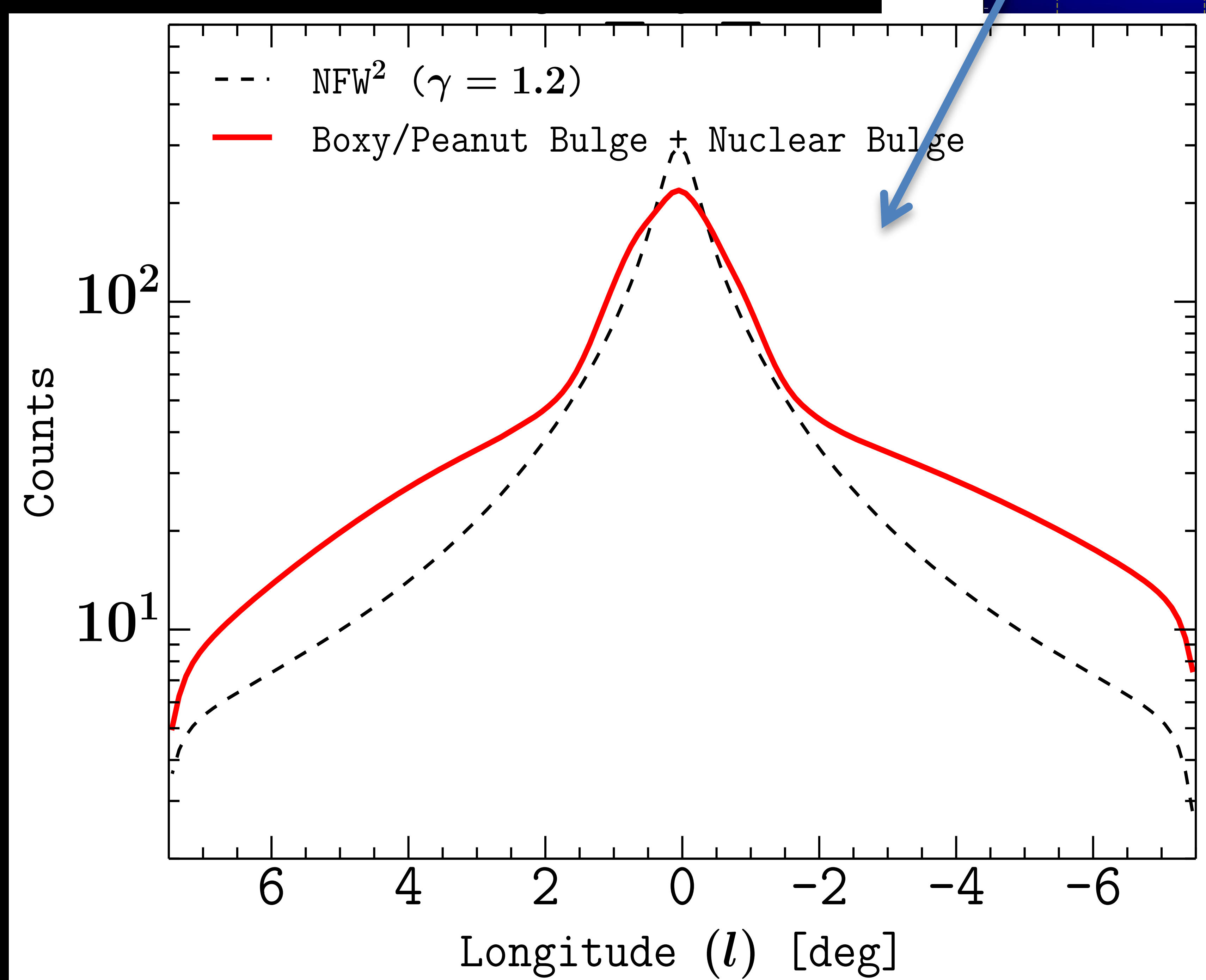

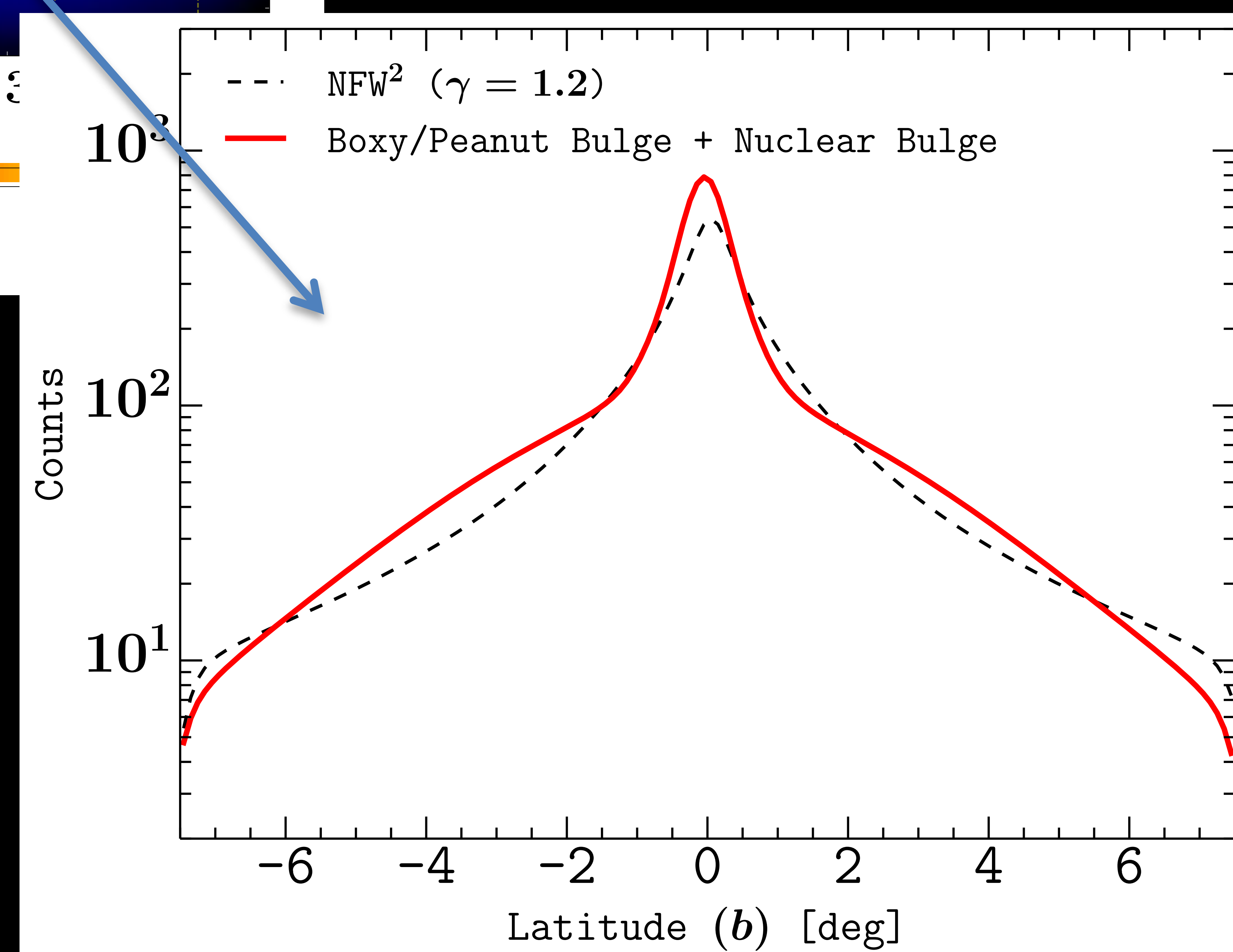

A dark matter bulge?

Can dark matter explain the bulge-correlated gamma-ray emission?

Co-evolution of dark matter and disk stars during bar formation:

Dark matter | Trapped component | Untrapped component

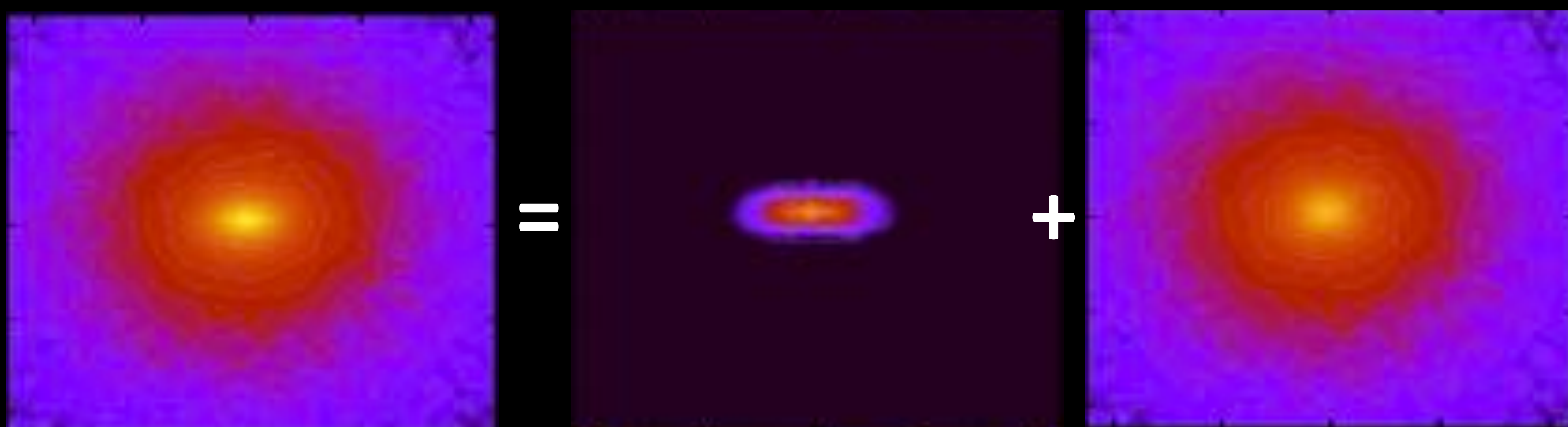

$\sim$12 % of dark matter within bar radius (3kpc) is trapped in the bar

Petersen et al (2016)

➔ **CDM can form a bulge-like feature, but appears to be subdominant**

Difficulties of dark matter: photon statistics

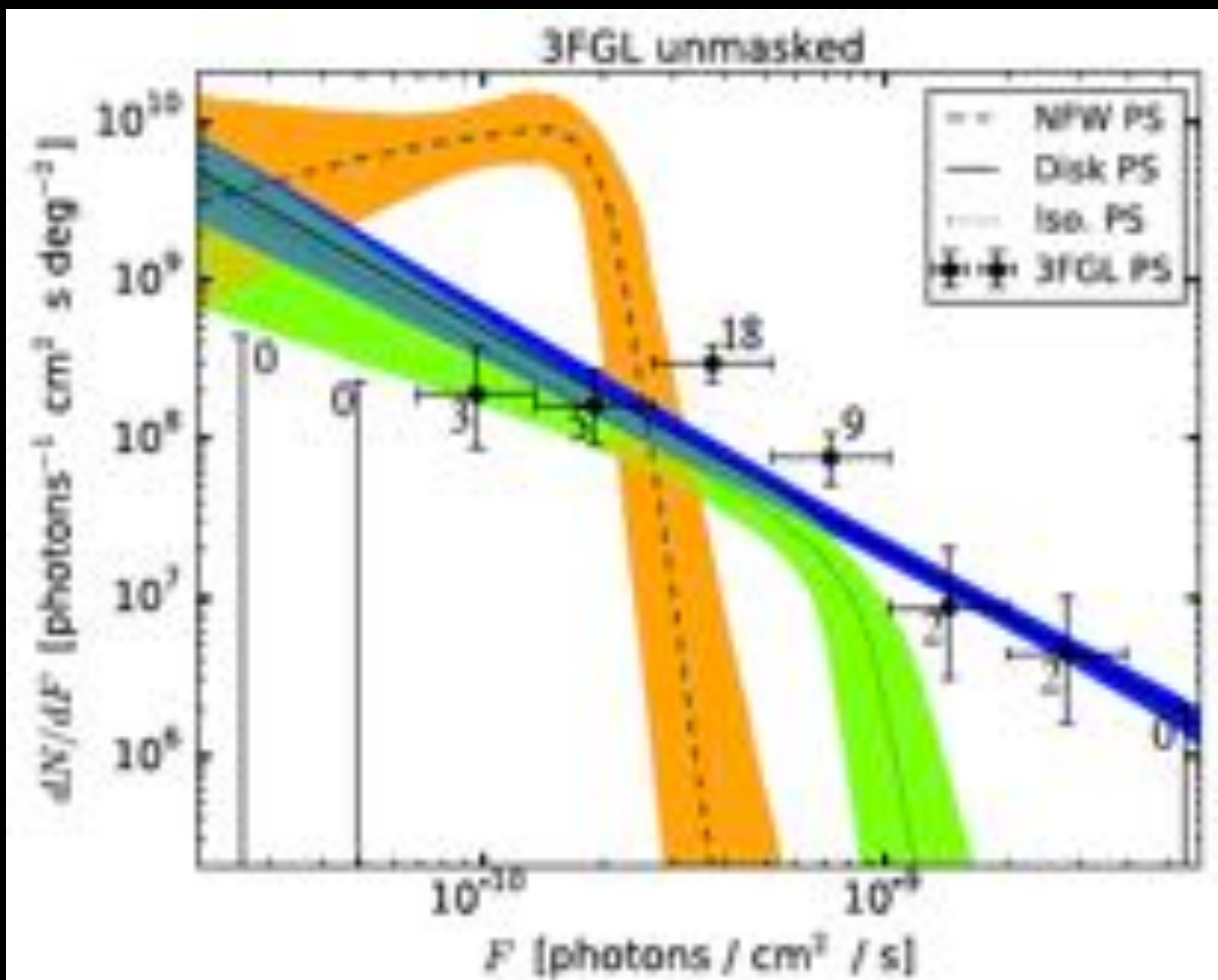

Lee et al (2016)

← This is <u>a lot</u> of substructure for dark matter in the Galactic Center region.

→ At least 80% of dark matter within 3 kpc need to be in subhalos. Too much compared to CDM simulations (which predict *f* of a few percent).

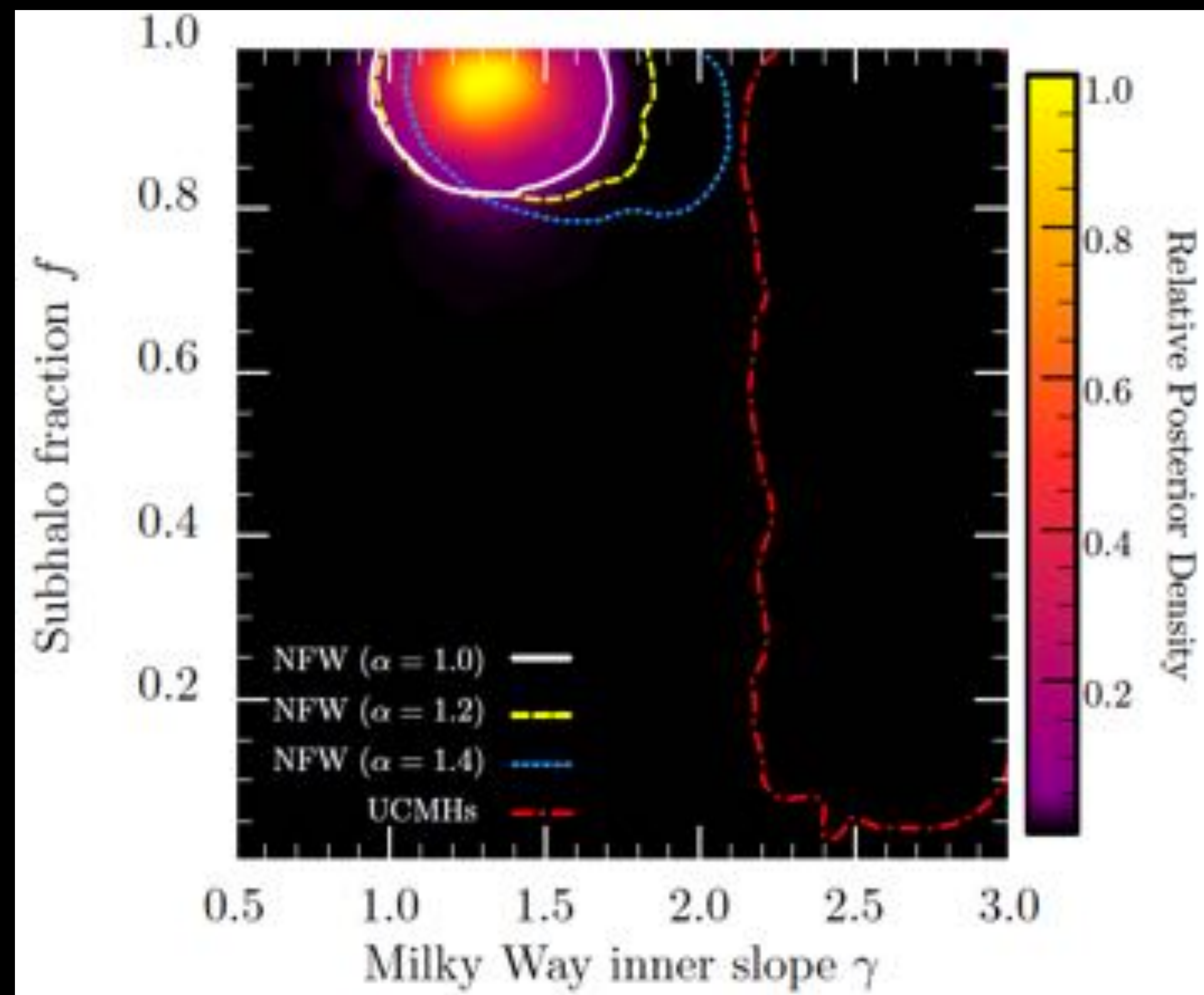

Clark et al (2016)

MSP constraint: large uncertainties

Uncertainties in MSP population constraints

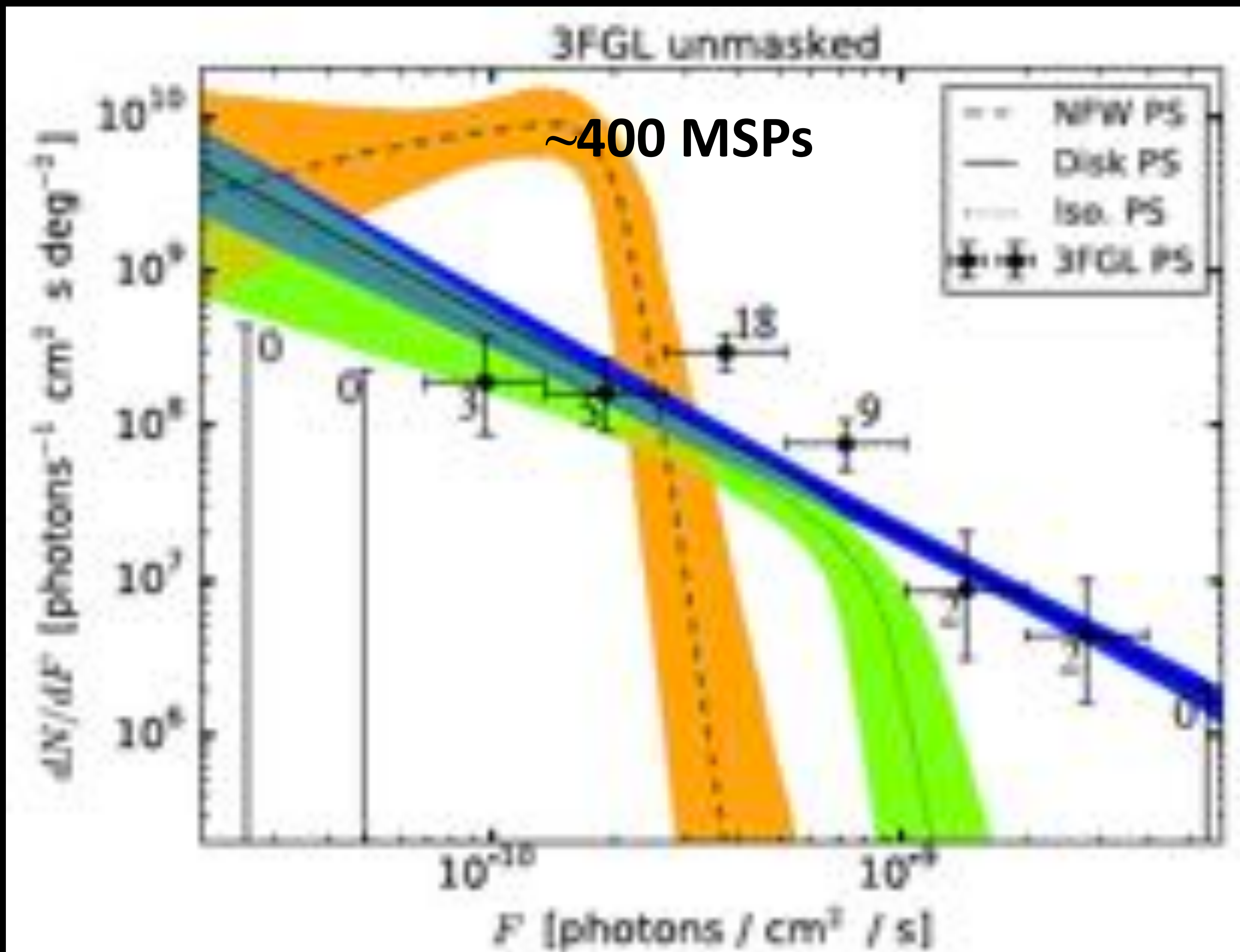

The luminosity function depends on the Galactic foreground and impacts the number of MSPs needed

Lee et al (2016)

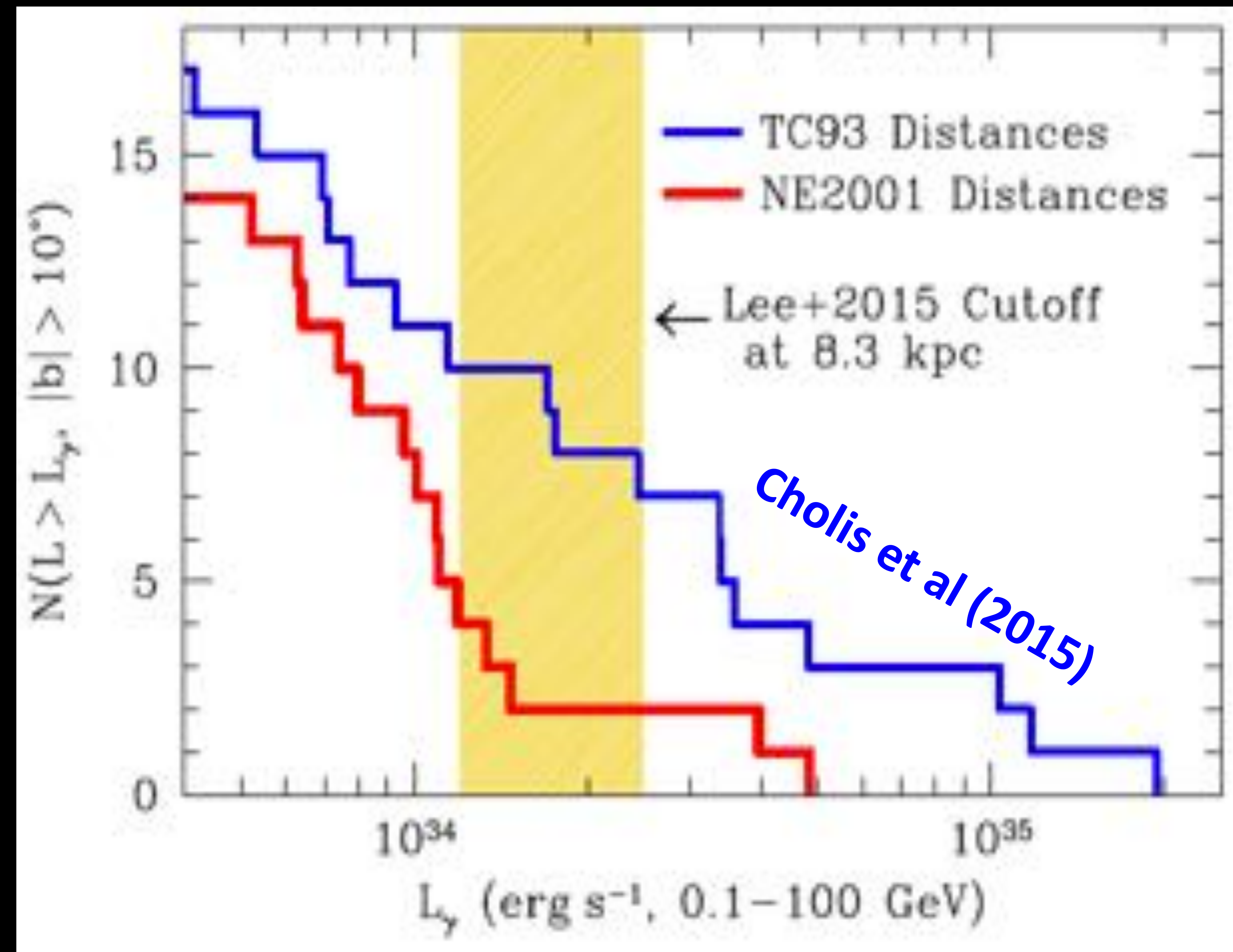

Distance systematics are also non-negligible; reduces number of MSP detection prediction by ~1/3 to 2.

Brandt & Kocsis (2015)

MSP constraint: large uncertainties

Uncertainties in MSP population constraints

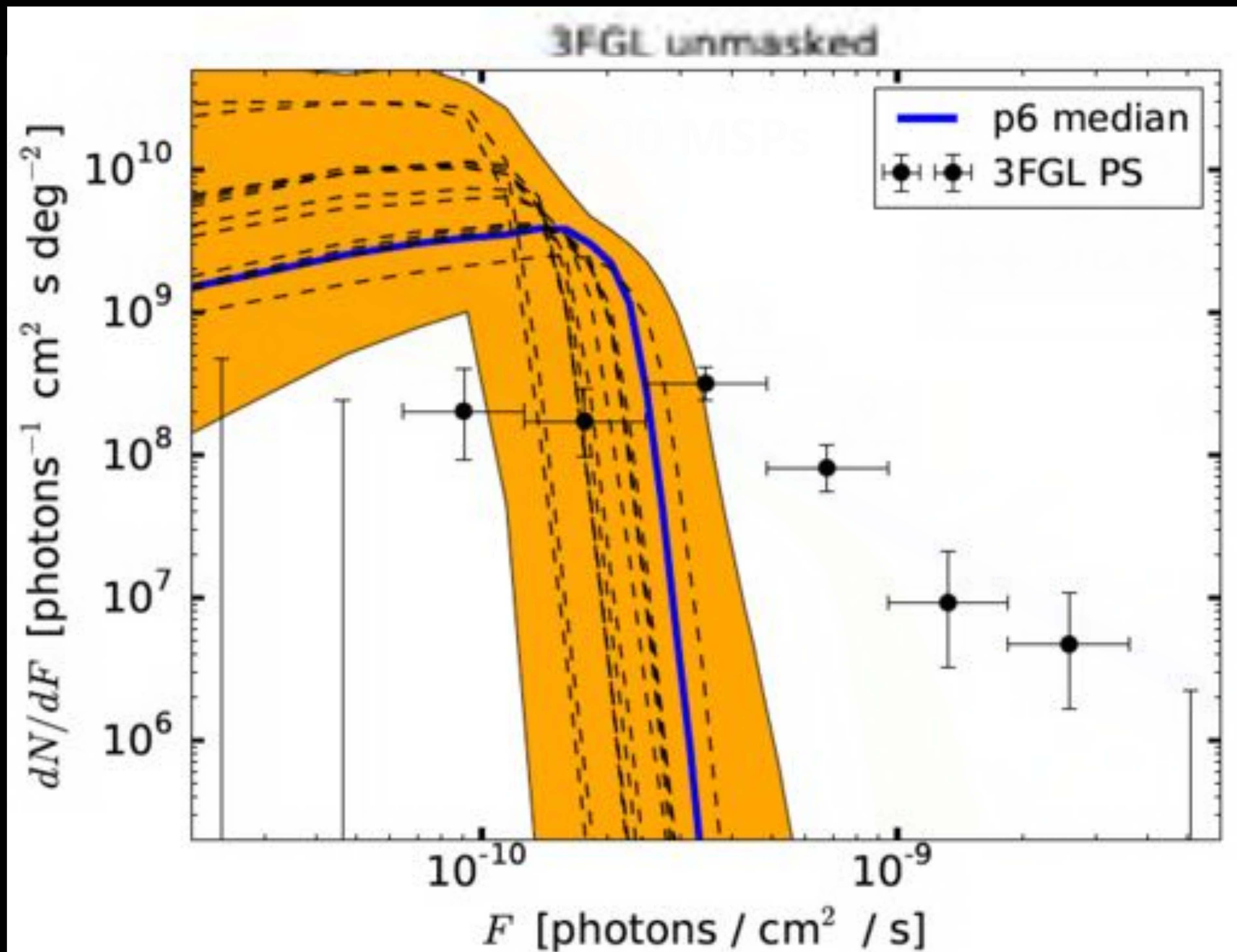

The luminosity function depends on the Galactic foreground and impacts the number of MSPs needed

Lee et al (2016)

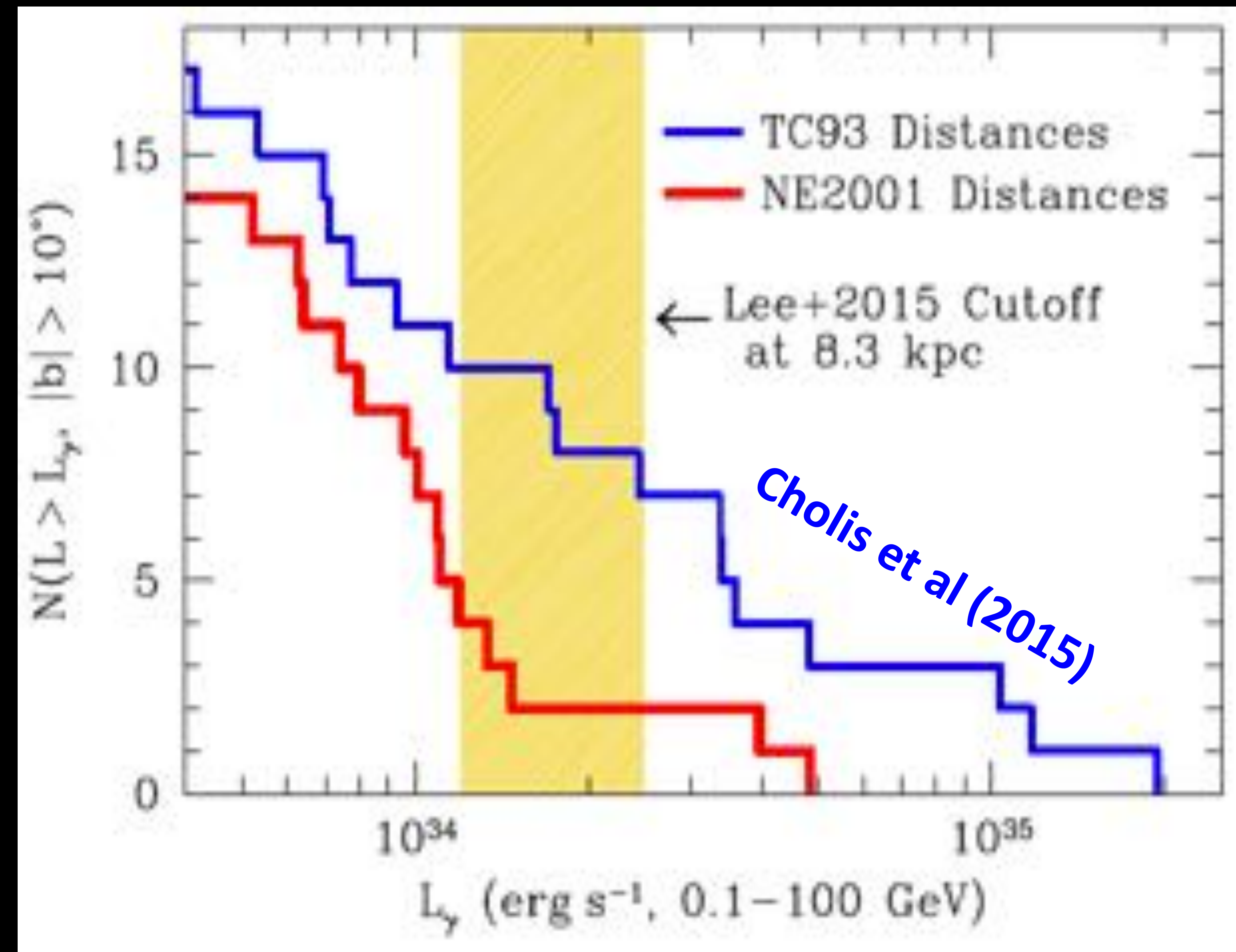

Distance systematics are also non-negligible; reduces number of MSP detection prediction by ~1/3 to 2.

Brandt & Kocsis (2015)

The MSP scenario is rich

Millisecond pulsars:

- Lower B fields than pulsars (~$10^{8\text{-}9}$ G vs ~$10^{11\text{-}13}$ G)
- Lower velocities than pulsars (~130 km/s vs ~400 km/s)
- Higher birth rate (~5×10^{-6} /yr) than X-ray binaries (~10^{-7} /yr)
- ~75% in binaries; eccentricities low, but some high ($e > 0.1$)

Recycling of old neutron stars:

✓ Initially a normal NS, but B-field decays or is buried in the superconducting core (resurface must be stopped)

? Lower velocities due to binary?

? Birth rate not enough, unless X-ray emitting phase is reduced, or population not in steady state

✗ X-ray binary phase causes tidal forces that reduce eccentricity

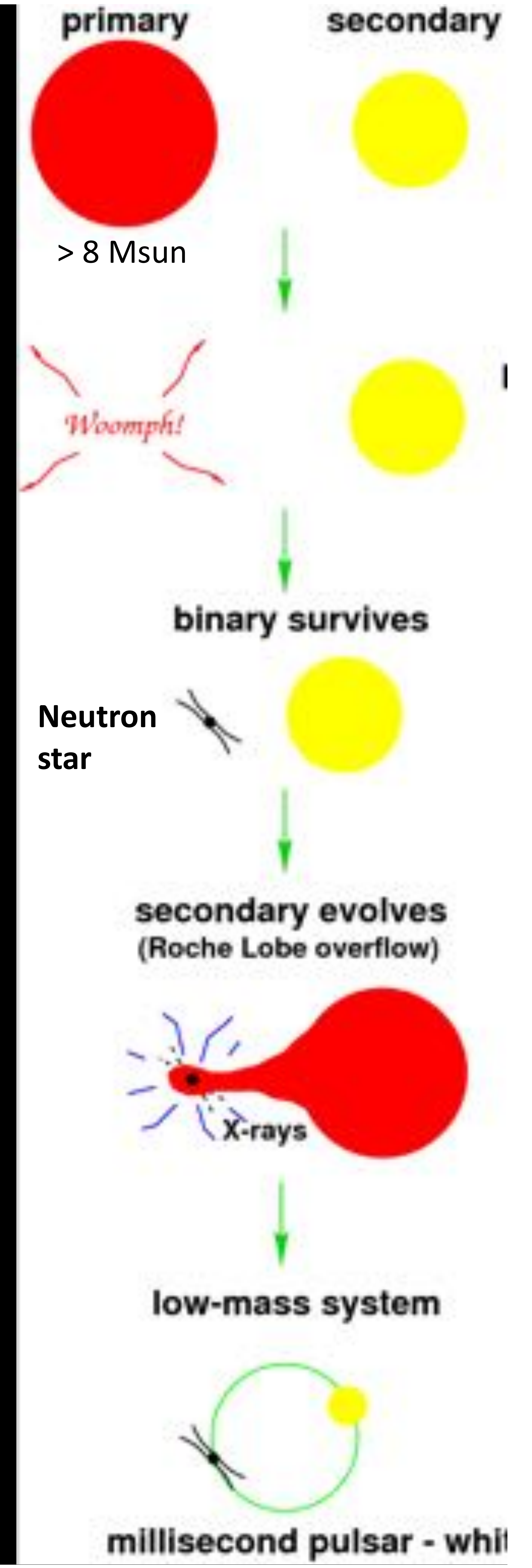

Shunsaku Horiuchi (Virginia Tech)

The MSP scenario is rich

Millisecond pulsars:

- Lower B fields than pulsars (~10^{8-9} G vs ~10^{11-13} G)
- Lower velocities than pulsars (~130 km/s vs ~400 km/s)
- Higher birth rate (~5×10^{-6} /yr) than X-ray binaries (~10^{-7} /yr)
- ~75% in binaries; eccentricities low, but some high (e > 0.1)

Accretion-induced collapse (AIC) of white dwarfs:

✓ Magnetic flux conservation yields the correct B-field.
✓ Very little external density makes natal kicks low.
? Provides an alternate channel*
✗ X-ray binary phase reduces eccentricity

*if mass accretion phase is short

AIC channel could be comparable to recycling channel in the disk.

Hurley et al (2010)

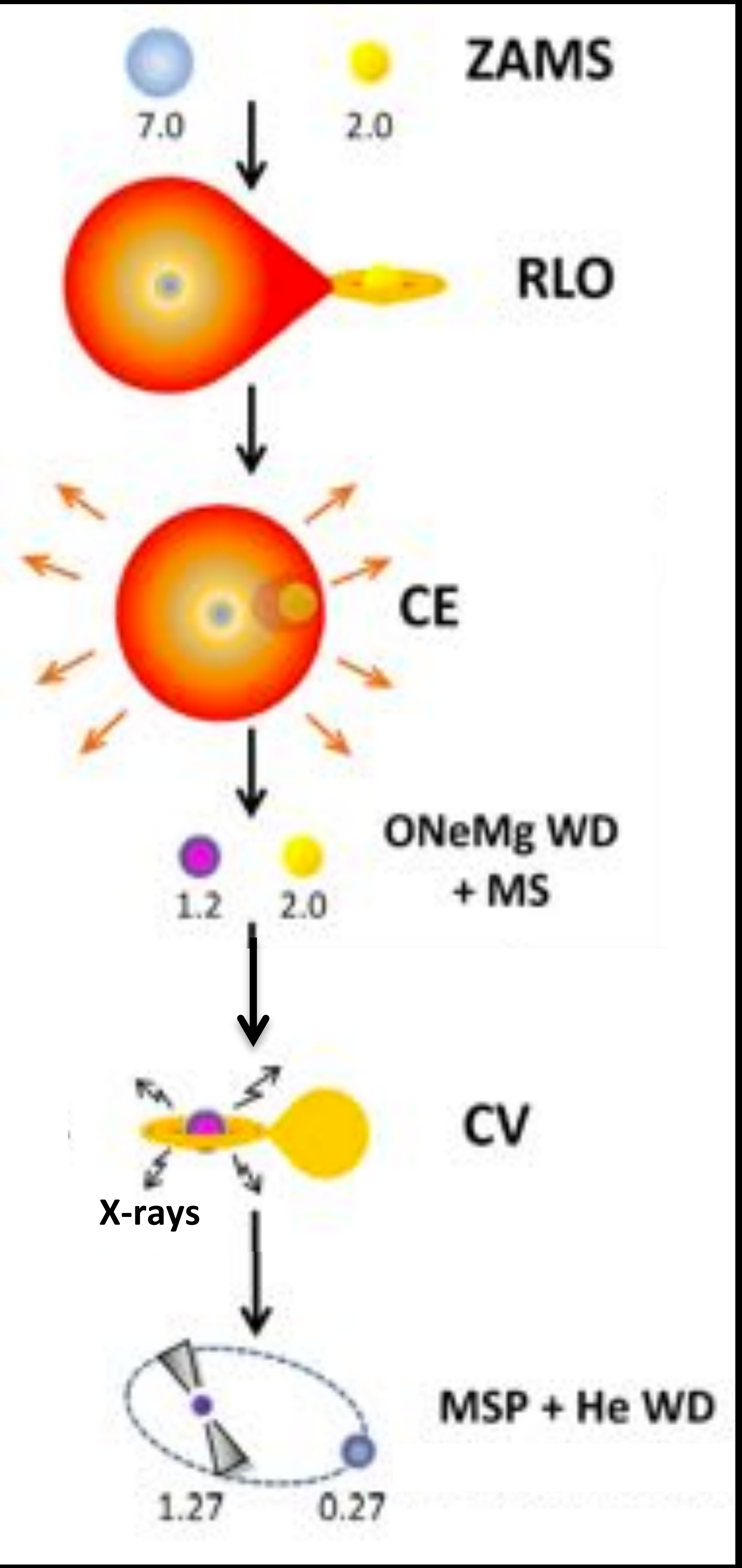

The MSP scenario is rich

Millisecond pulsars:

- Lower B fields than pulsars (~$10^{8\text{-}9}$ G vs ~$10^{11\text{-}13}$ G)
- Lower velocities than pulsars (~130 km/s vs ~400 km/s)
- Higher birth rate (~5×10^{-6} /yr) than X-ray binaries (~10^{-7} /yr)
- ~75% in binaries; eccentricities low, but some high ($e > 0.1$)

Accretion-induced collapse (AIC) of white dwarfs: DELAYED

✓ Magnetic flux conservation yields the correct B-field.
✓ Very little external density makes natal kicks low.
? Provides an alternate channel
✓ High eccentricities possible since no re-circularization after AIC event.

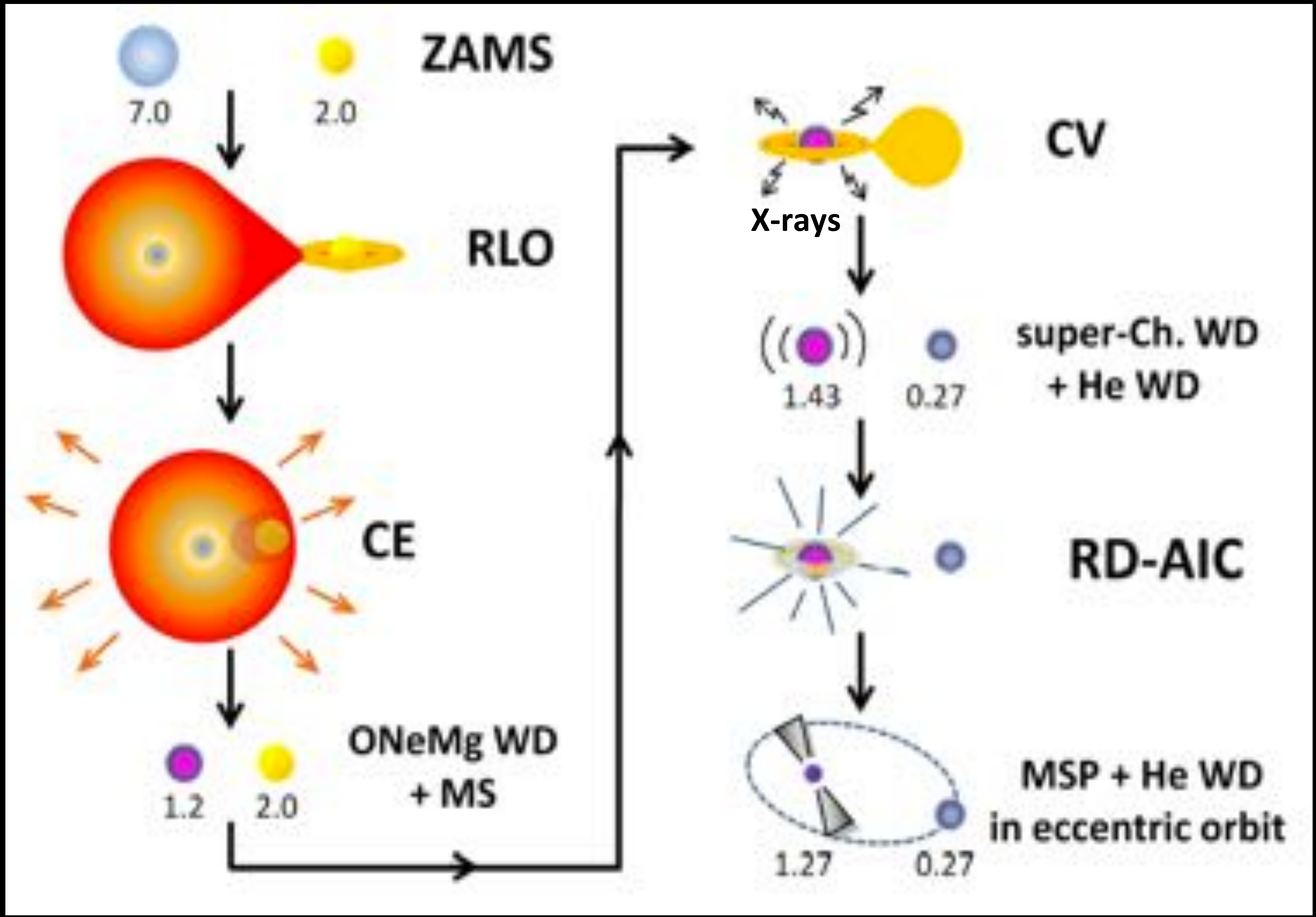

Freire & Tauris (2014)

The MSP scenario is rich

MSPs can be formed via a number of channels

- Recycling of old neutron stars
- Accretion induced collapse of O-Ne-Mg white dwarfs
- Merger induced collapse of two white dwarfs

All channels involve binary systems

- Primordial: stars born in binary systems
- Dynamical: captures a companion through encounters

Binary mass transfer and the X-ray connection will be different for different channels.

The relative importance of channels will be environmentally dependent

- Stellar age: active star forming (CMZ) to Gyrs old (bulge)
- Stellar density: low (bulge) to high (globular cluster)
- Stellar metallicity: low to solar populations

➔ **No a priori reason MSP population & their connection to LMXB are the same everywhere**

Comparison of regions

Gamma ray to mass ratios

Shows environmental dependence of MSP gamma rays

- Boxy bulge, nuclear bulge, Milky Way disk (from MSPs) consistent with each other

$$2 \times 10^{27}\,\mathrm{erg\,s^{-1}\,M_\odot^{-1}}$$

- Globular clusters higher by factor ~10-40, explained by large dynamical channel
- M31 also higher, consistent with its higher encounter rate; LMXB is also consistent with 20-25% dynamical origin (vs no such signs in the Milky Way LMXB)

Voss & Gilfanov (2007)

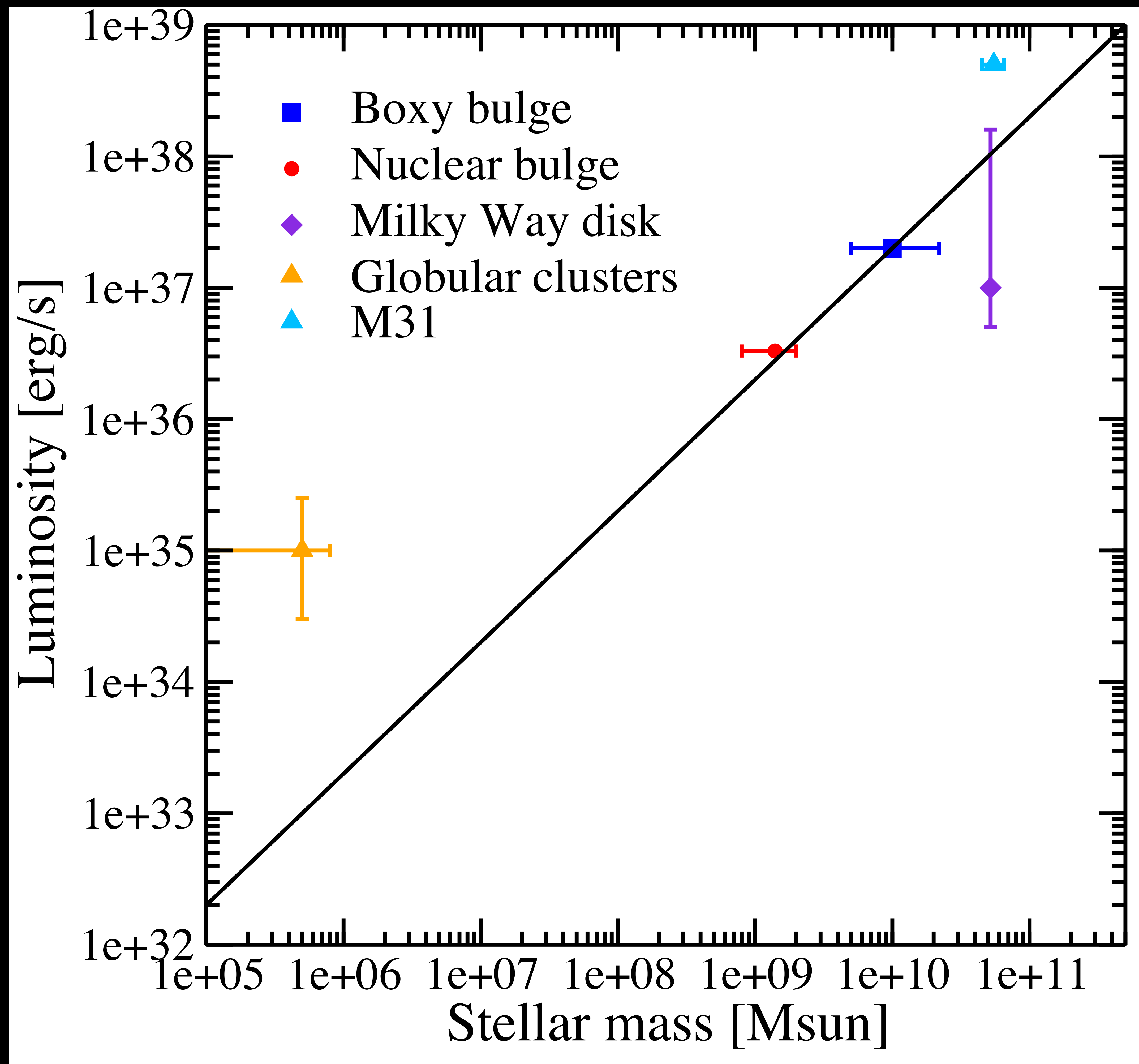

See also Bartels et al (2017)

Astrophysics consistent with observations

Furthermore, morphology no longer needs direct link to globular clusters

- **Accretion**: millisecond pulsars made in globular clusters that are subsequently disrupted by the Galactic Center. Models of dynamical friction and tidal stripping of globular clusters predict a centrally peaked NFW^2-like profile

- **In-situ formation**: millisecond pulsars formed out of bulge stellar population would follow the bulge morphology.

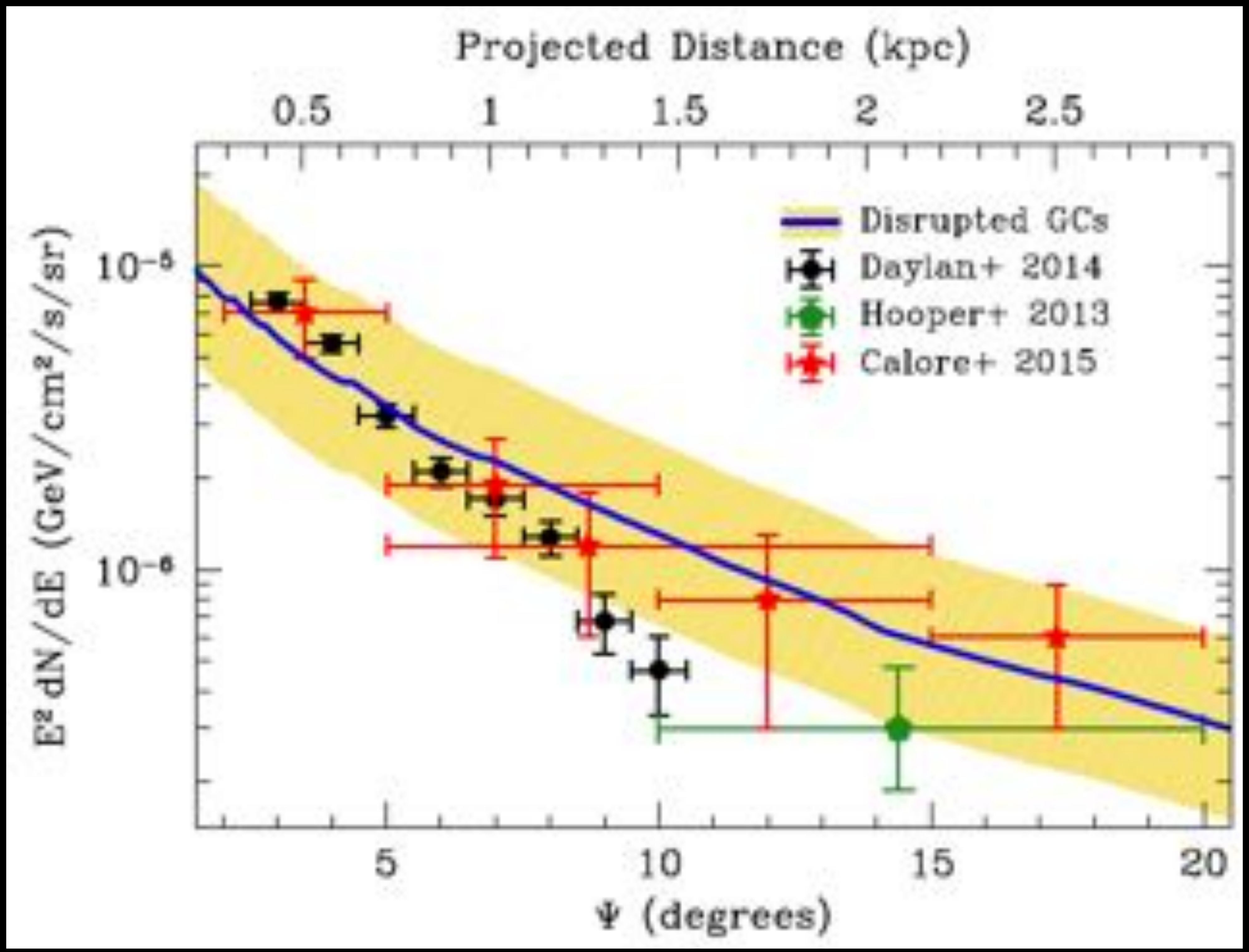

Brandt & Kocsis (2015)

Simple model of Galactic MSPs

MSP in the Galactic bulge

In-situ MSP modeling including primordial and dynamical formation.
Dynamical formation modeled after Globular clusters.

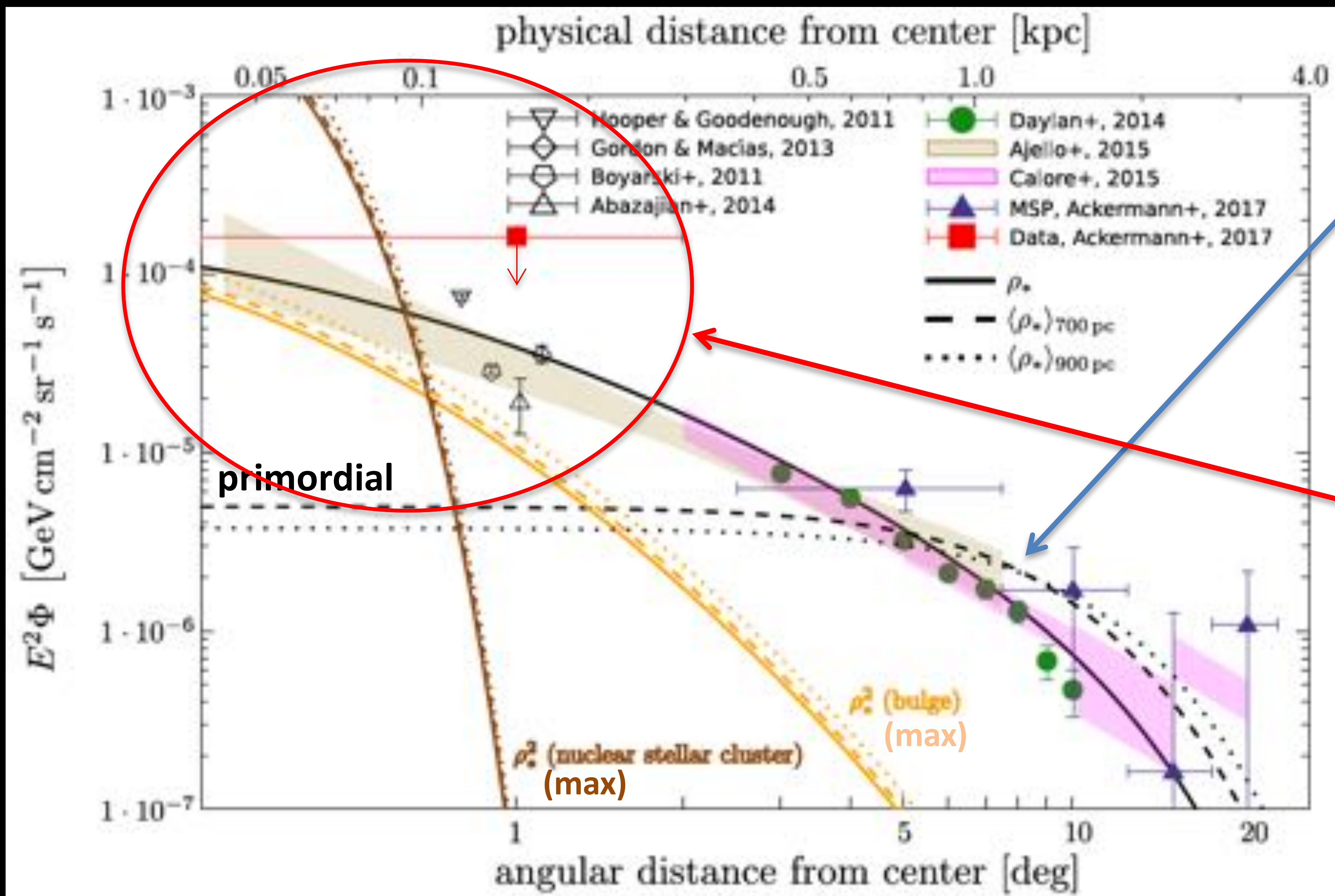

Primordial binaries explain most of the GCE outside a few degrees

While dynamical is a small overall (a few % of total), they will be prominent in the inner few degrees

Eckner et al (2016)

Millisecond pulsar – summary

The Galactic bulge is massive, old, and should host substantial millisecond pulsars produced in-situ, that can explain the bulge-correlated gamma rays, energy spectrum, and potentially photon statistics..

- ✓ **Spectrum is broadly consistent (but low energy systematics?)**
- ✓ **Spatial morphology expected to follow stars (but dark matter can too?)**
- ✓ **Formation scenarios are rich, allows considerable flexibility**
- ✓ **Multiple ways to test the hypothesis (next)**

The Future of the Galactic Center Excess

Tim Linden

CCAPP Postdoctoral Fellow
Center for Cosmology and Astro-Particle Physics
The Ohio State University

The Future:

1.) Finding MSPs

2.) Constraining the Dark Matter Density

3.) Understanding Cosmic-Ray Propagation in the CMZ.

4.) New Constraints on Indirect Detection

Future Radio Surveys

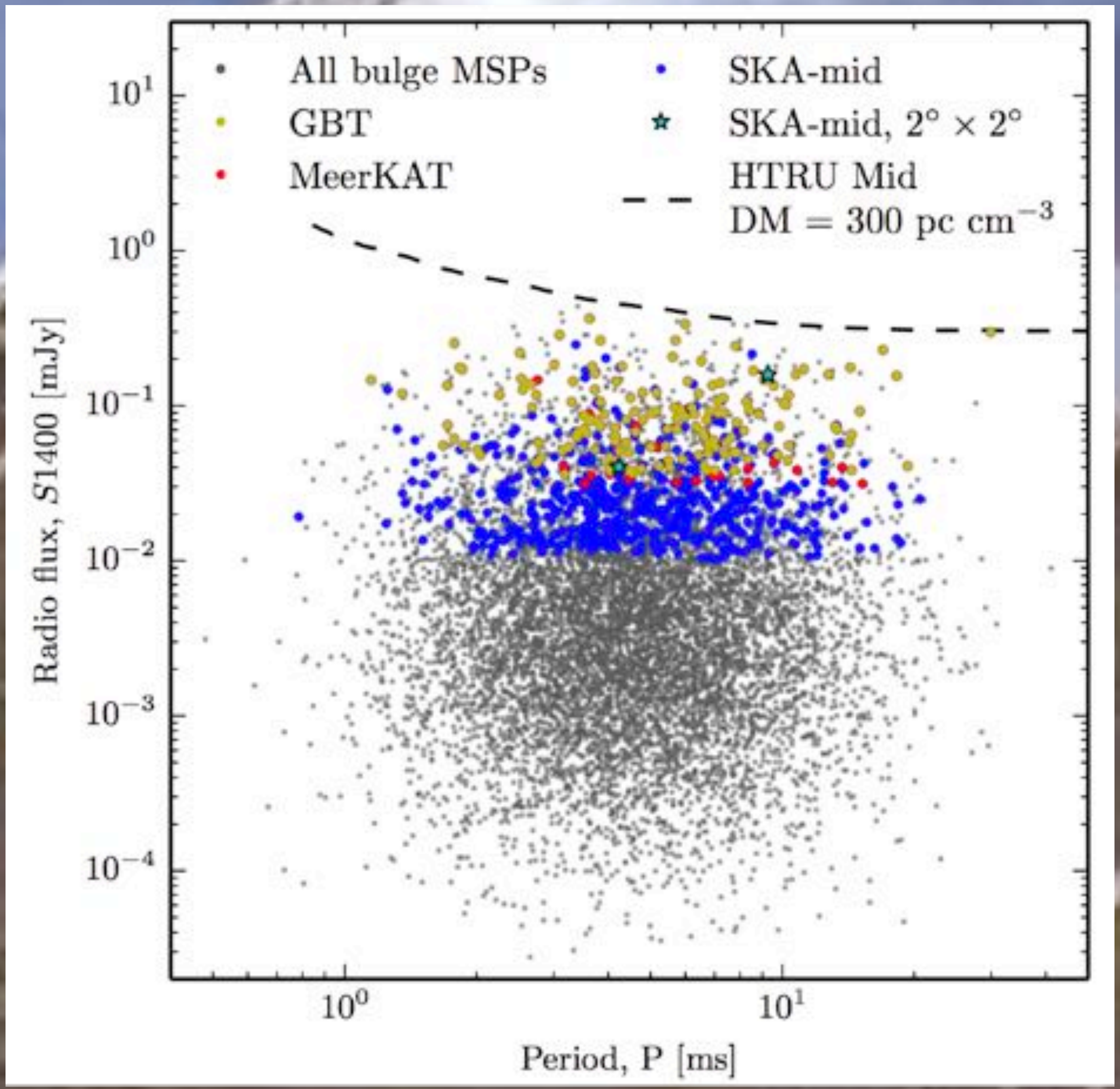

MeerKat and SKA will be extremely sensitive to Galactic center radio pulsars.

Calore et al. (2016; 1512.06825)

Future Radio Surveys

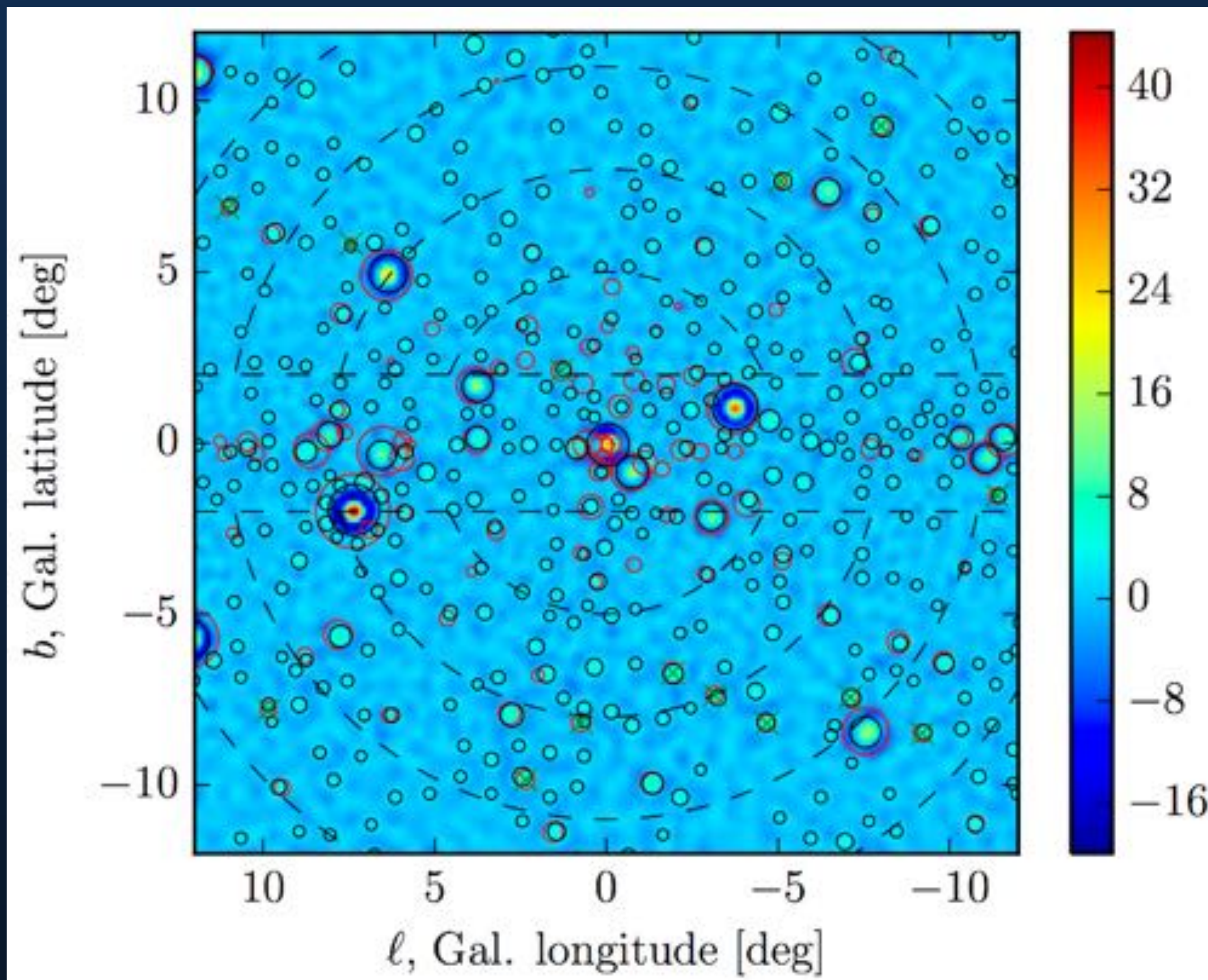

Radio surveys can find pulsars coincident with the positions of known gamma-ray hotspots.

Only a handful of sources necessary to provide definitive evidence.

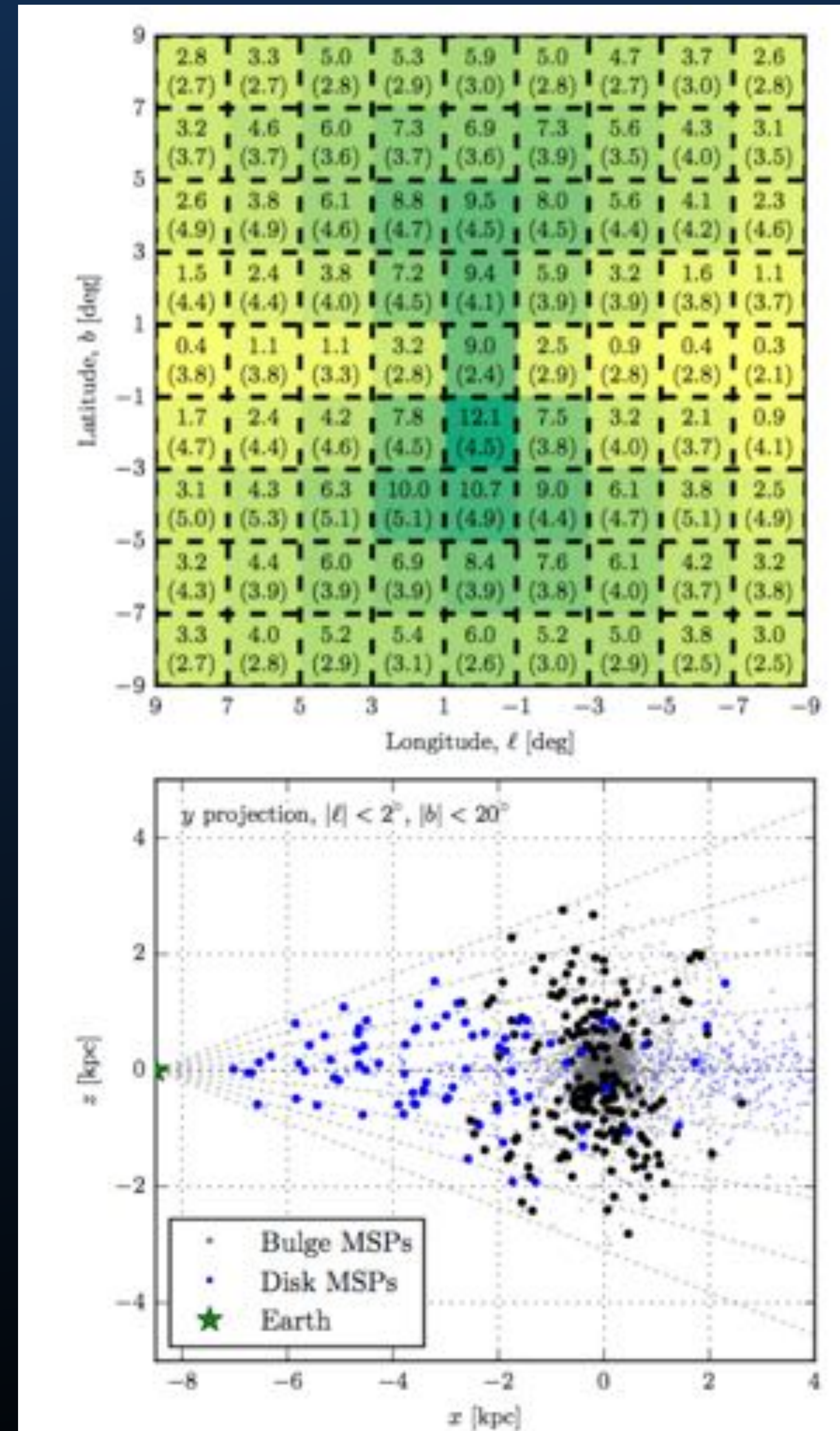

Calore et al. (2016; 1512.06825)

The Local Dark Matter Density

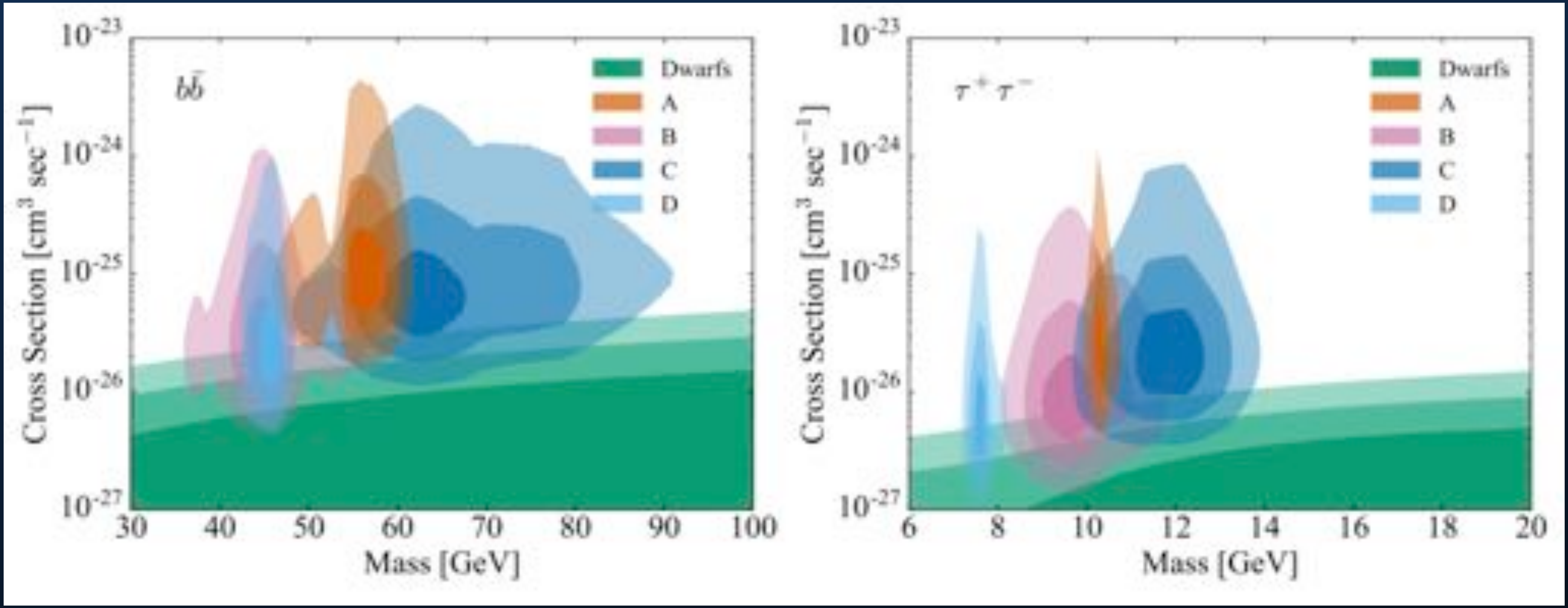

The major uncertainty in correlating the GCE and dwarf spheroidal galaxies is the local dark matter density.

Keeley et al. (2017; 1710.03215)

The Local Dark Matter Density

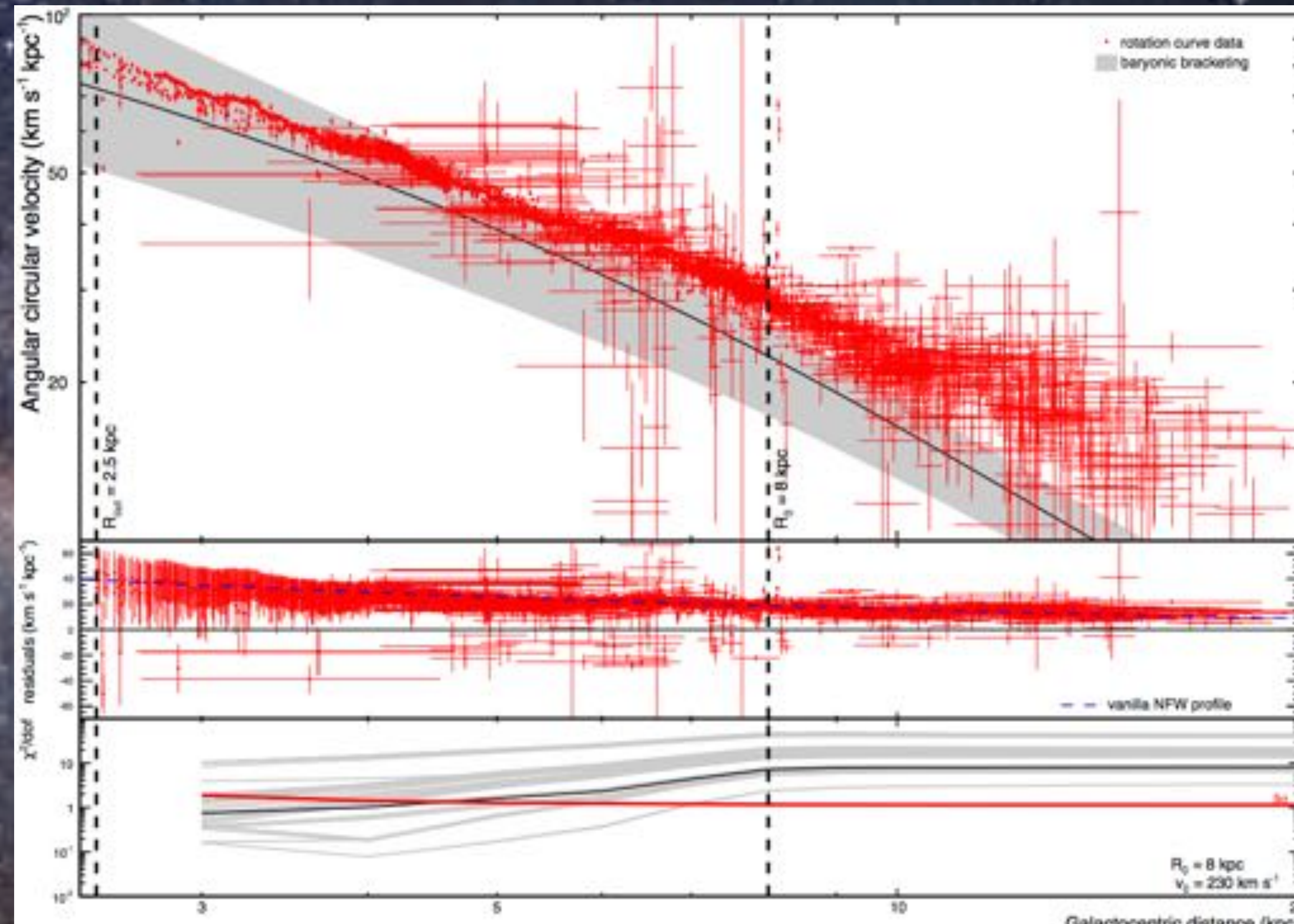

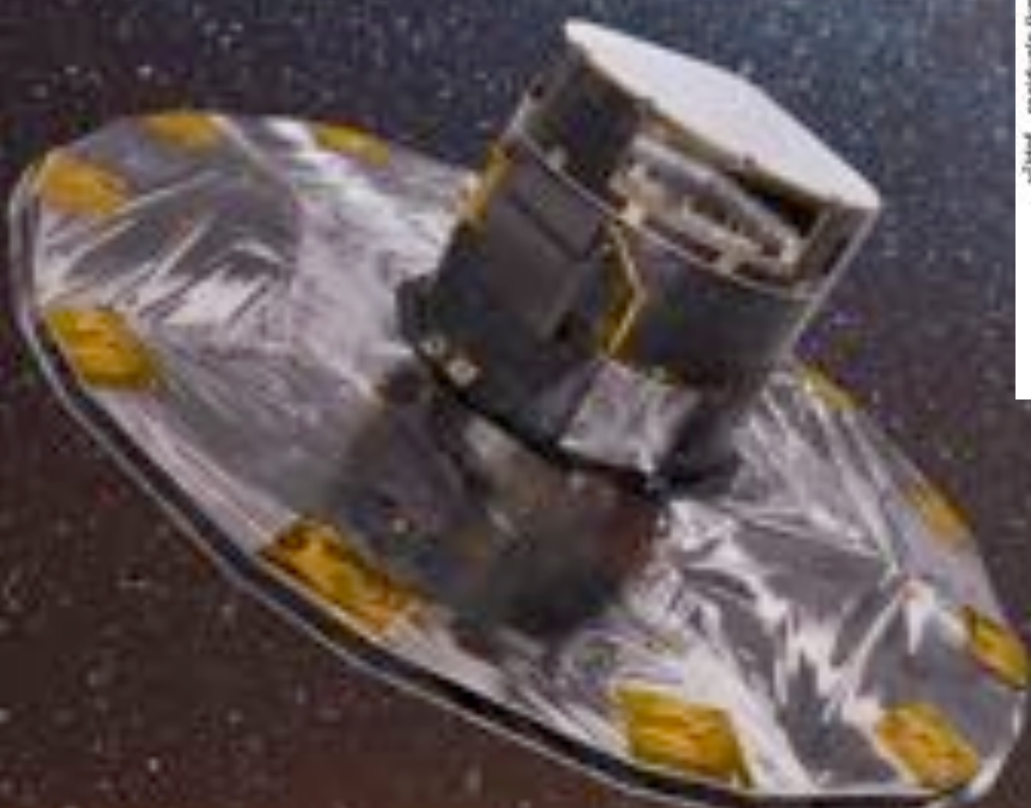

Iocco et al. (2015; 1502.03821)

New Insights into Cosmic-Ray Diffusion

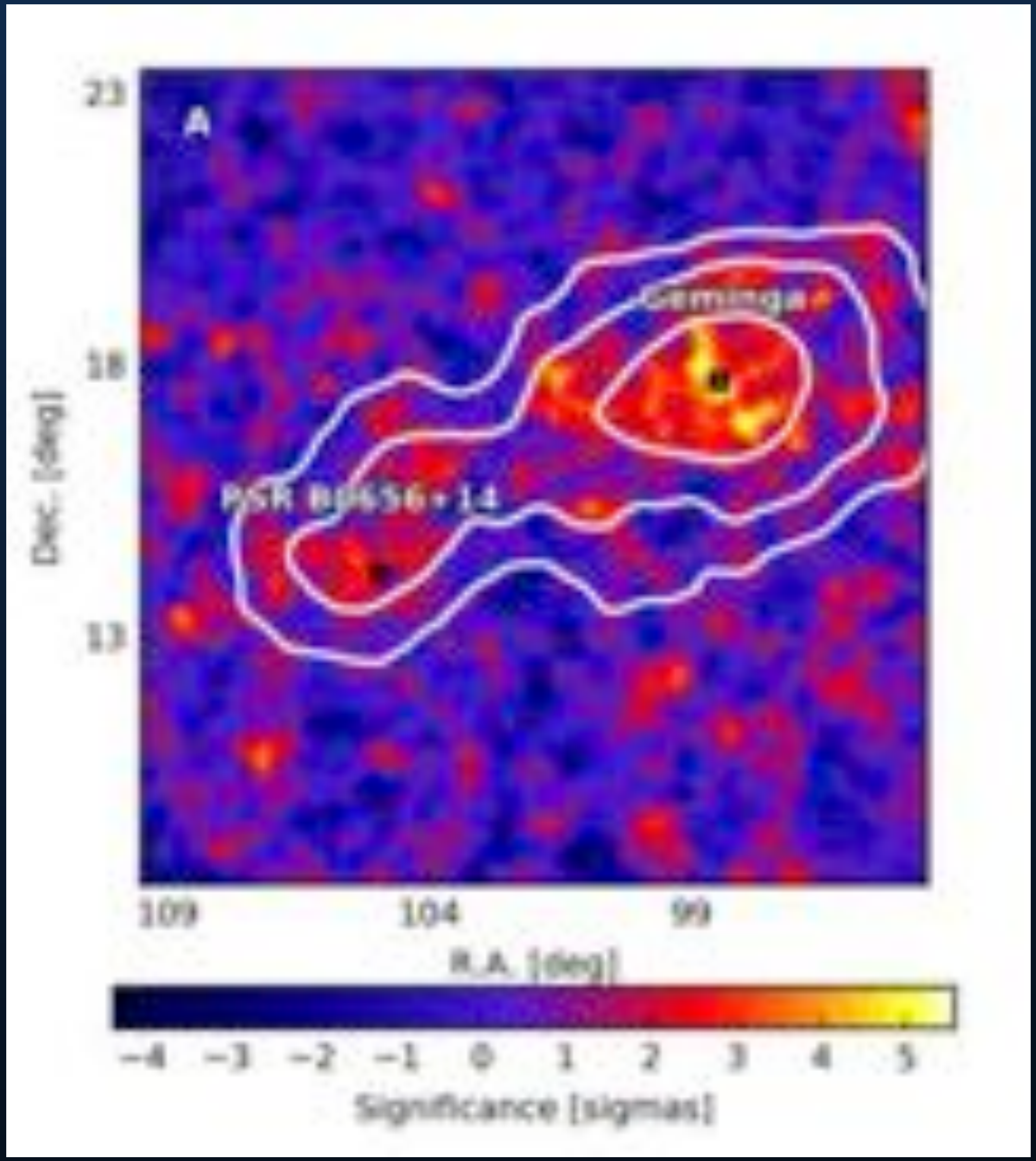

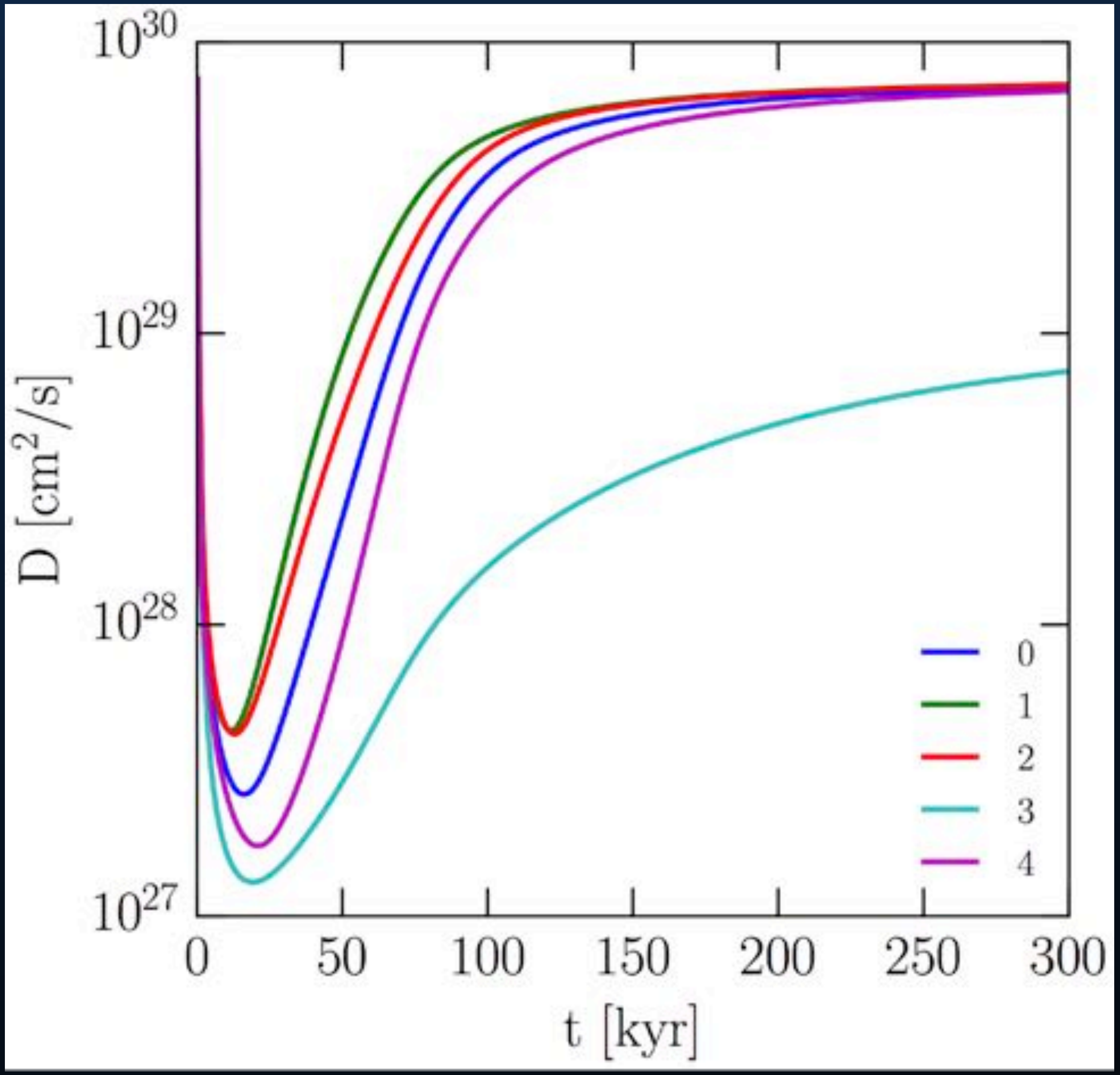

HAWC Collaboration (2017; 1711.06223)

Evoli et al. (2018; TBS)

New Insights into Cosmic-Ray Diffusion

H.E.S.S. Collaboration (2016; 1603.07730)

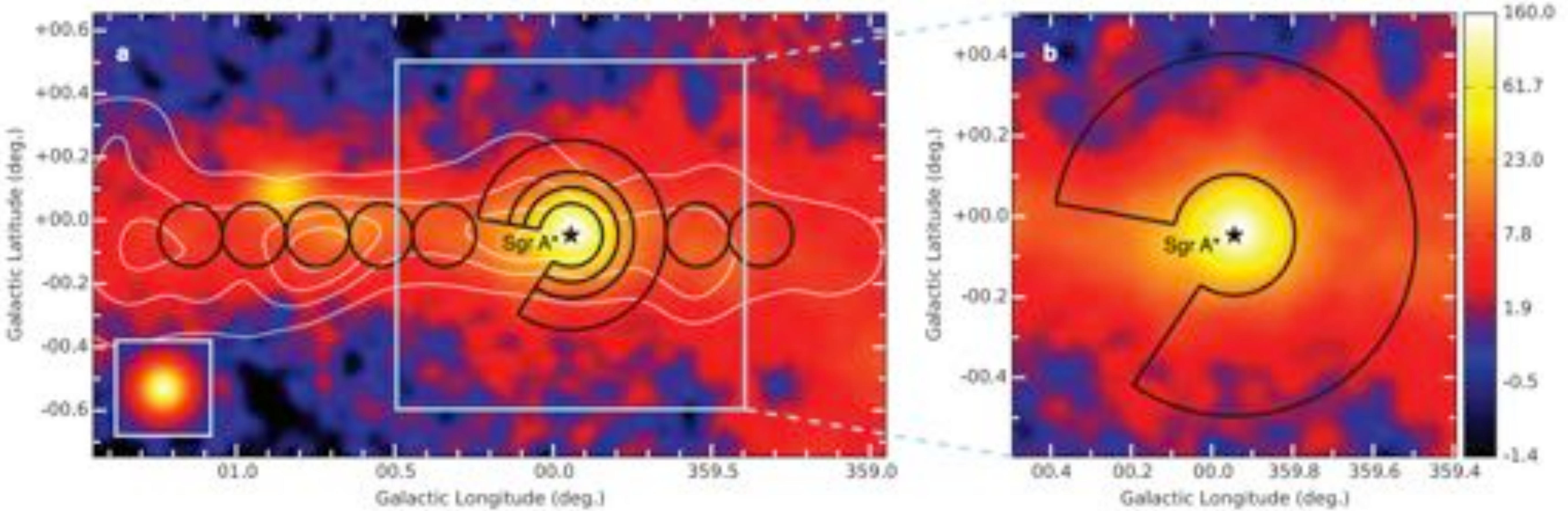

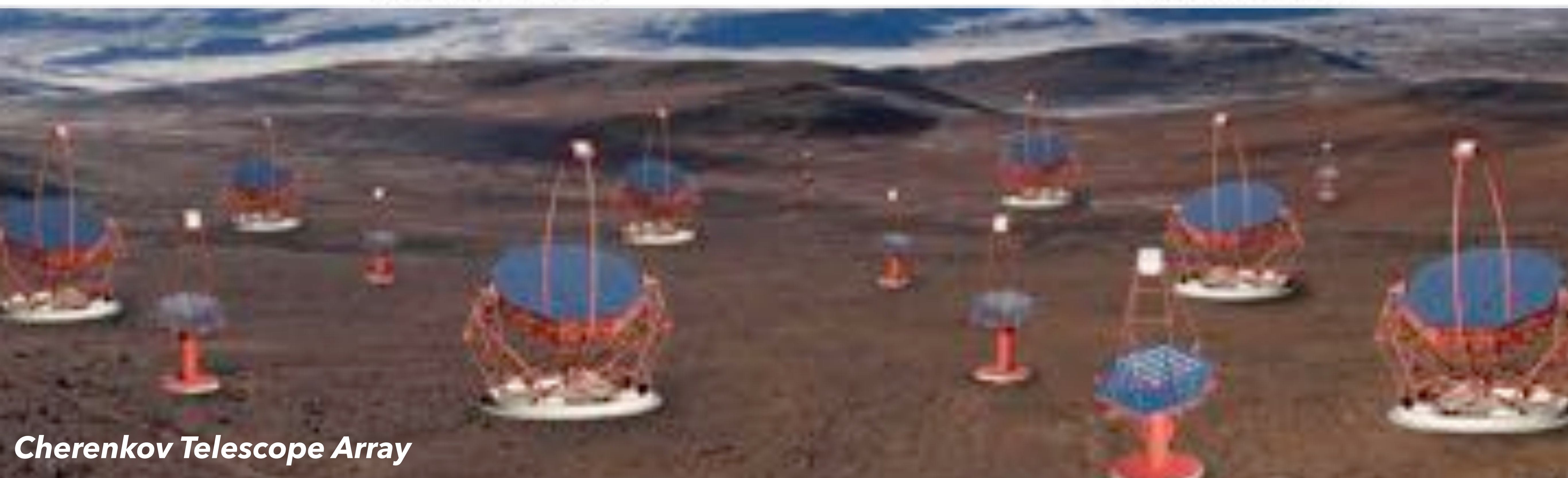

New Insights into Cosmic-Ray Diffusion

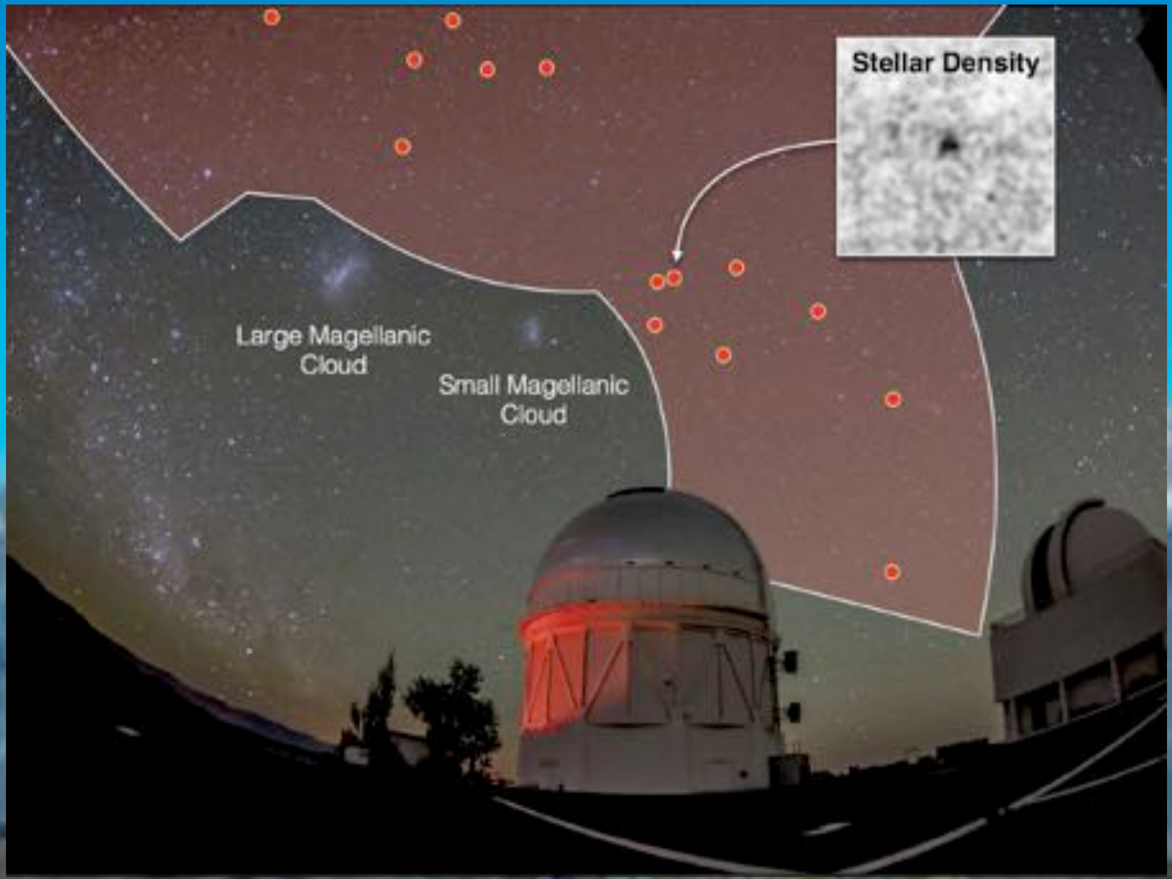

Continued DES observations, and upcoming LSST observations will find more (and smaller) dwarfs.

LSST

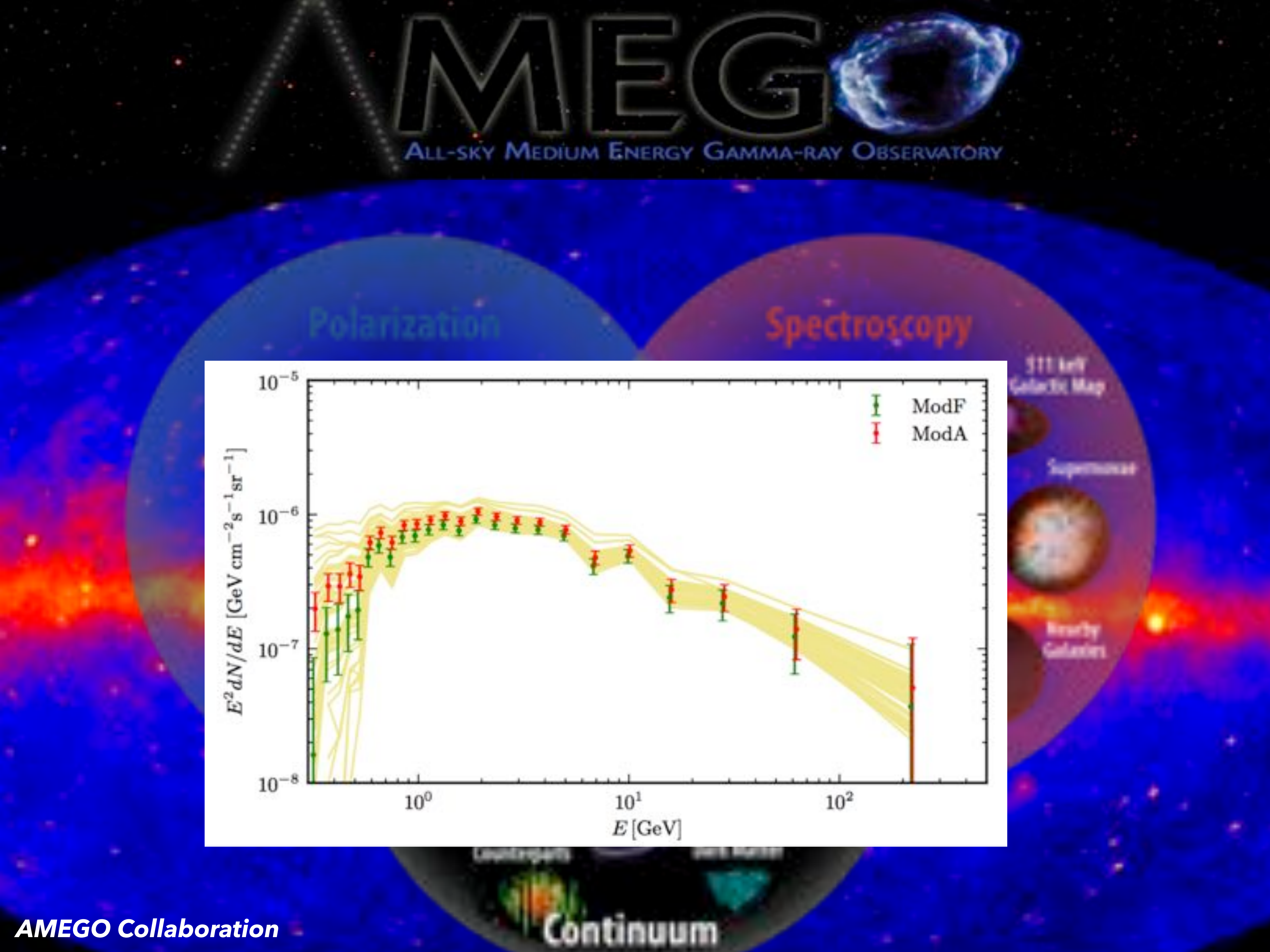

AMEGO Collaboration

Continued Operation of Fermi-LAT

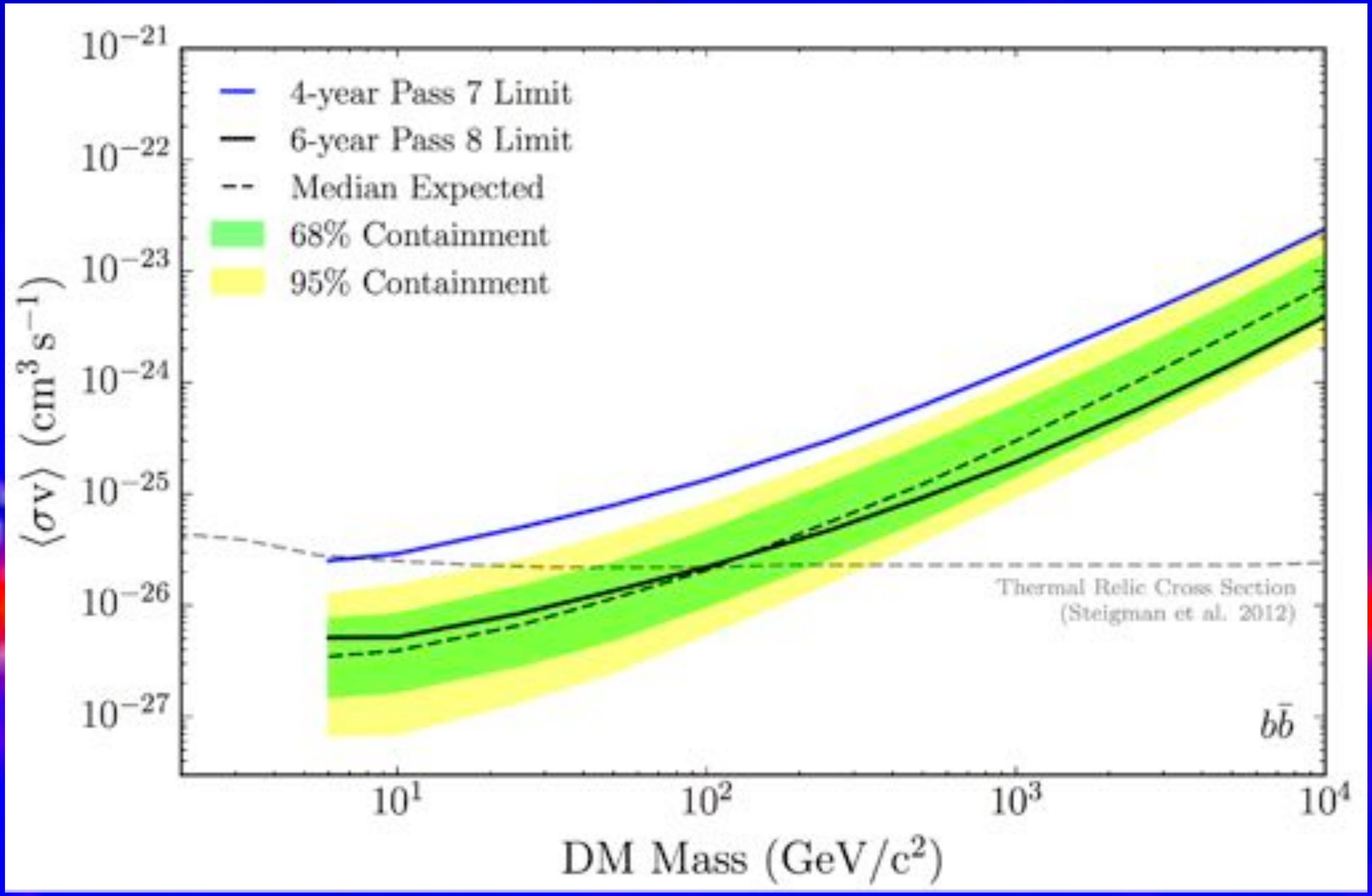

Fermi-LAT observations will continue for up to another decade.

Fermi-LAT Collaboration

Continued Operation of Fermi-LAT

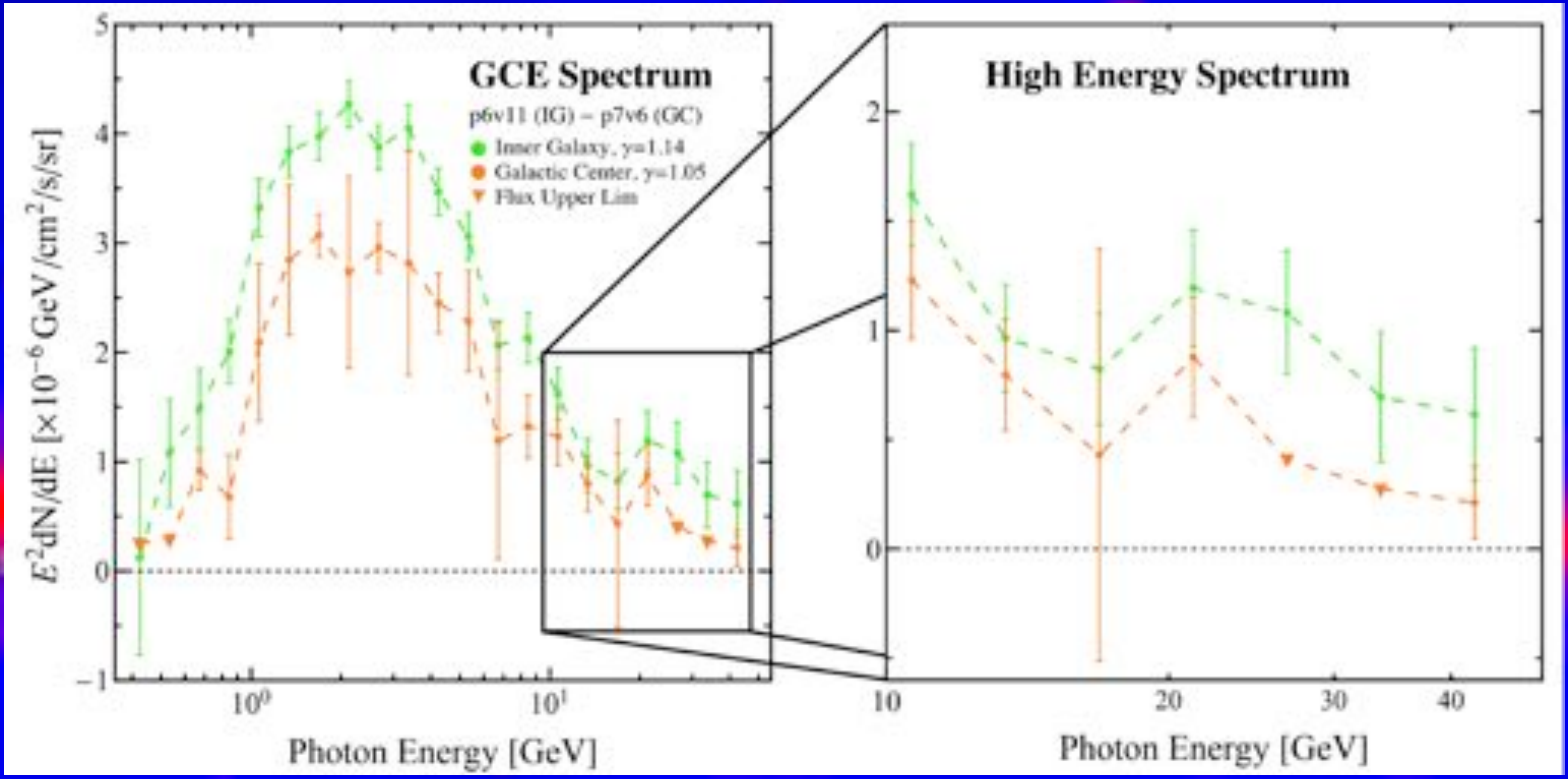

Fermi-LAT observations will continue for up to another decade.

Linden et al. (2016; 1604.01026)

Continued Operation of Fermi-LAT

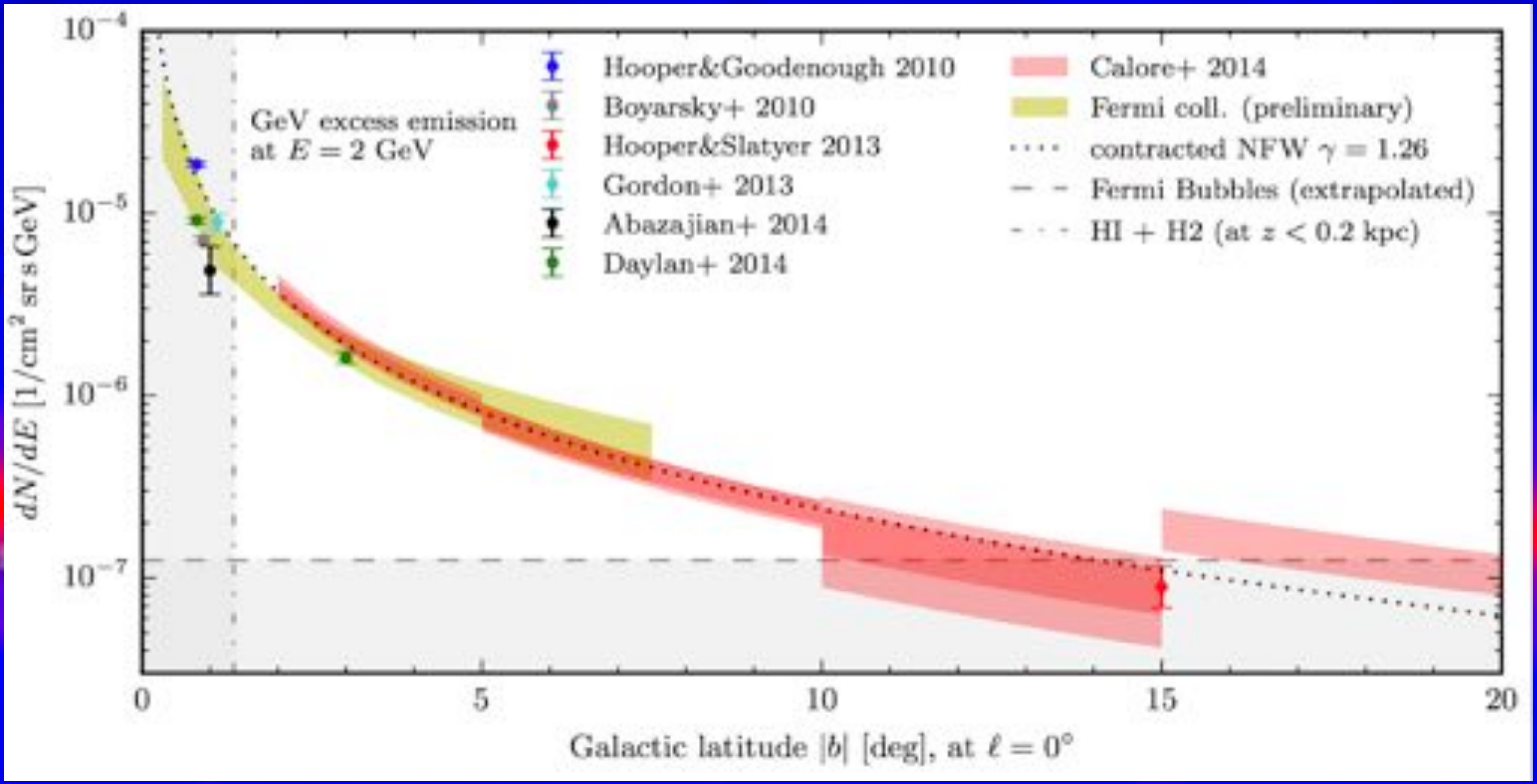

Fermi-LAT observations will continue for up to another decade.

Linden et al. (2016; 1604.01026)

Continued Operation of Fermi-LAT

Fermi-LAT observations will continue for up to another decade.

Linden et al. (2016; 1604.01026)

Conclusions

1.) The Galactic Center Excess (compared to any standard model of astrophysical emission) is real.

2.) Models including dark matter, pulsars, leptonic outbursts, and changes in galactic cosmic-ray diffusion exist.

3.) New observations and models over the next decade offer the potential to understand the galactic center at GeV energies.